NEW STRATEGIES FOR DEVELOPING RECEPTORS BASED ON MOLECULAR IMPRINTING FOR ANALYTICAL APPLICATIONS

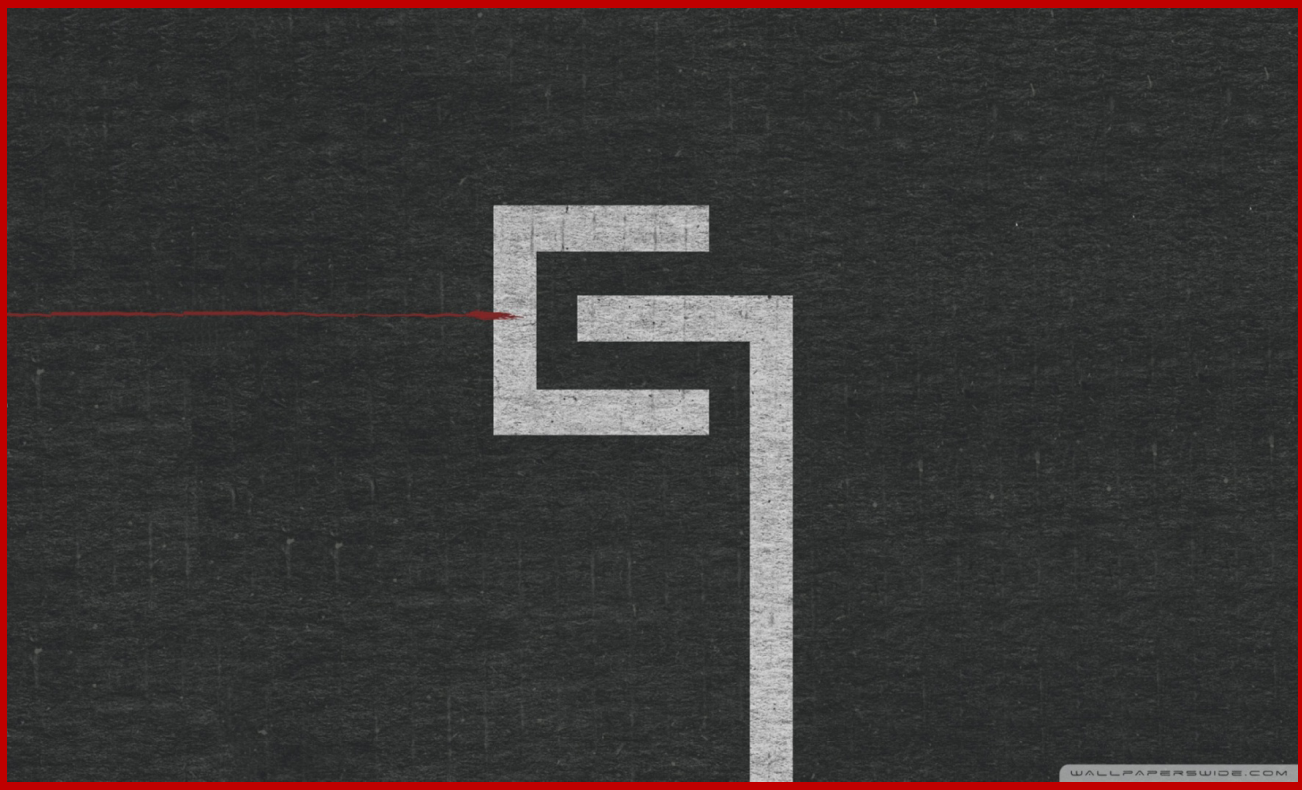

Deiene Garcia Mutio

2016

eman ta zabal zazu

Universidad del País Vasco

Euskal Herriko Unibertsitatea

eman ta zabal zazu
Universidad del País Vasco
Euskal Herriko Unibertsitatea

NEW STRATEGIES FOR DEVELOPING RECEPTORS BASED ON MOLECULAR IMPRINTING FOR ANALYTICAL APPLICATIONS

NUEVAS ESTRATEGIAS DE DESARROLLO DE RECEPTORES BASADOS EN IMPRESIÓN MOLECULAR PARA APLICACIONES ANALÍTICAS

This Doctoral Thesis has been carried out in Forensic Analysis Doctorate Programme at the University of the Basque Country, UPV/EHU

Faculty of Pharmacy, Vitoria-Gasteiz

DEIENE GARCIA MUTIO

2016

Esta tesis ha sido realizada, y consecuentemente será defendida, con el propósito de obtener el título de Doctorado Internacional por la Universidad del País Vasco/Euskal Herriko Unibertsitatea (UPV-EHU).

Previamente a la defensa de esta Tesis Doctoral, este trabajo ha sido evaluado por dos expertos pertenecientes a Instituciones de Educación Superior directamente relacionados con el área de Investigación:

- **Dr. Antonio Guerreiro**, research fellow in Chemical Engineering at the University of Leicester, Leicester (UK).
- **Dra. Ana Soares**, Senior lecturer in Biological Engineering at Cranfield Water Sciences Institute (Cranfield University), Cranfield (UK).

Nire gurasoei,

Esta tesis ha sido posible gracias a la ayuda de varias personas y organismos que me han brindado su apoyo. En primer lugar me gustaría agradecer a mis directores, la Dra. Arantxa Goicolea y el Dr. Alberto Gomez, por todo lo que me han enseñado y ayudado a lo largo de esta tesis.

Del mismo modo, quiero agradecer al Dr. Ramon Barrio mi admisión en el programa de doctorado y en el grupo de investigación en el que se ha llevado a cabo esta investigación.

Gracias a la Universidad del País Vasco (EHU/UPV), al Servicio Central de Análisis SGIker y al departamento de Química Analítica por las instalaciones, equipamiento y medios ofrecidos sin los cuales este trabajo no hubiera sido posible. Por otro lado, quisiera agradecer a BIOLAN la financiación para la consecución de la tesis.

I gratefully acknowledge Dr. Sergey Piletsky who accepted me in his research group in the University of Leicester, where I had a really fruitful stay. También me gustaría agradecer a la Unidad de Formación e Investigación en Neuroquímica, Neuropsicofarmacología y Psiquiatría de la UPV/EHU (UFI 11/35) la financiación de esta estancia.

Last but not least, me gustaría agradecer a mis compañeras de laboratorio la ayuda y los ánimos que me han dado durante toda la tesis. A mis amigos fuera del círculo científico por ayudarme a mantener un estado de ánimo lo mejor posible durante estos largos años de alegrías y penas. A ti Alar, por todo tu apoyo y comprensión. Finalmente, a mi familia por animarme a realizar esta tesis y ayudarme en todo lo que han podido a finalizarla, sin vosotros no hubiera sido posible.

ESKERRIK ASKO!

“There will always be rocks in the road ahead of us. They will be stumbling blocks or stepping stones; it all depends on how you use them.”

Friedrich Nietzsche

CONTENTS

Resumen

Los fenoles volátiles como 4-vinilfenol, 4-vinilguayacol, 4-etilfenol y 4-etilguayacol afectan a las características organolépticas del vino, siendo perjudiciales en altas concentraciones. Estos fenoles volátiles se generan en los vinos debido a una contaminación por levaduras del género *Brettanomyces.* El nivel de 4-etilfenol es proporcional a la concentración y la actividad de la levadura, y por lo tanto puede ser utilizado como un indicador de su presencia.

El objetivo principal de esta tesis, consiste en avanzar en el conocimiento y las posibilidades de los polímeros de huella molecular para su aplicación en el análisis de 4-etilfenol y compuestos pertenecientes a su ruta metabólica. Para ello, el trabajo experimental ha sido divido en dos secciones principales, en función de la técnica analítica en la que ha sido implementado el material impreso desarrollado.

Inicialmente, se presenta una metodología para el desarrollo y aplicación de fases estacionarias basadas en MIP. Los materiales desarrollados han sido evaluados como fases estacionarias en extracción en fase sólida y cromatografía líquida. Como segundo apartado del trabajo, se describen distintas técnicas de impresión molecular para su implementación en sensores voltamperométricos, por un lado, la síntesis de películas MIP sobre electrodos de oro y por otro, la síntesis de nanopartículas

MIP y su posterior inmovilización en la superficie de electrodos de oro.

Se estableció como principal objetivo de la primera etapa experimental, el diseño de un método de extracción en fase sólida basado en polímeros MIP para los compuestos pertenecientes a la ruta metabólica del 4-etilfenol y para su posterior separación por cromatografía líquida de forma que fuera posible su cuantificación en vino. Como primer paso, se optimizó la composición del MIP utilizando como *template* el 4-etilfenol. Posteriormente se evaluaron las propiedades de unión del MIP como receptor macromolecular sintético, a partir de ensayos de unión ligando-receptor realizados en estático.

El MIP sintetizado para el 4-etilfenol fue utilizado como fase estacionaria en extracción en fase sólida y se optimizaron las etapas de acondicionamiento, lavado y elución del 4-etilfenol y los compuestos pertenecientes a su ruta metabólica en vino.

A pesar de su capacidad para la extracción de los compuestos objetivo de muestras de vino, este polímero no permitía su correcta separación cromatográfica cuando era utilizado como fase estacionaria en cromatografía líquida. Por ello, se sintetizó un nuevo MIP, en este caso utilizando como *template* ácido cumárico, compuesto perteneciente a la ruta metábolica del 4-etilfenol, que presenta mayor tamaño y funcionalidad.

El polímero impreso para el ácido cumárico fue optimizado con el objetivo de obtener una fase estacionaria capaz de separar

los compuestos de la ruta metabólica del 4-etilfenol. Una vez optimizada la fase estacionaria, ésta también se evaluó por ensayos de unión ligando-receptor realizados en estático. Finalmente, la metodología desarrollada con el MIP para el 4-etilfenol como fase estacionaria en extracción en fase sólida y el MIP para el ácido cumárico como fase estacionaria en cromatografía líquida se aplicó al análisis del 4-etilfenol, 4-vinilfenol, ácido cumárico y el ester etílico del ácido cumárico en muestras de vino.

El segundo objetivo establecido fue el desarrollo de receptores sintéticos basados en MIP implementados en superficies de oro mediante estrategias de polimerización radical por desactivación reversible y su utilización como sensores voltamperométricos para la medida de 4-etilfenol.

Inicialmente, se sintetizaron capas de polímero impresas para el 4-etilfenol en la superficie de electrodos de oro. Para ello, se siguió la estrategia de injerto conocida como *grafting from*, utilizando un iniferter inmovilizado en el oro para la iniciación de la polimerización. El iniferter (initiator, transfer agent, terminator), además de actuar como iniciador, actúa como agente de transferencia de cadena y permite la terminación de la reacción. Esta técnica es adecuada para la síntesis de capas finas y controladas en una superficie. En este caso, para que la polimerización se iniciara desde la superficie del electrodo, se sintetizó un iniferter con un grupo funcional tiol para su fácil

inmovilización en esta superficie. Finalmente, se optimizaron las mejores condiciones de síntesis para la obtención de un sensor voltamperométrico selectivo para el 4-etilfenol. El seguimiento del recubrimiento polimérico de la superficie electródica se realizó por Voltamperometría Cíclica y por Espectroscopía de Impedancia Electroquímica y su morfología fue caracterizada por Microscopía Electrónica de Barrido.

Por otro lado, se sintetizaron nanopartículas MIP por medio de la estrategia de síntesis en fase sólida. Esta técnica de síntesis de nanopartículas MIP ha sido recientemente desarrollada. Su principal diferencia, frente a otras estrategias de síntesis MIP, radica en que el *template* se encuentra inmovilizado en una fase estacionaria (esferas de vidrio). Las esferas de vidrio con el *template* inmovilizado se mezclan con el resto de la mezcla de polimerización y las nanopartículas con alta afinidad se sintetizan alrededor del *template*. Una vez sintetizadas, las nanoparticulas permaneceran inmovilizadas en las esferas de vidrio por medio del *template*, pudiendo ser utilizadas como fase estacionaria para la purificación de las nanopartículas por afinidad. En primer lugar, los monómeros que no han reaccionado y las nanopartículas de poca afinidad se eliminan mediante un lavado a baja temperatura. Finalmente, las nanopartículas MIP de elevada afinidad se eluyen rompiendo la unión nanopartícula-*template,* mediante un lavado a alta temperatura. En la mezcla de polimerización se añadió un monómero que dotó a las nanopartículas sintetizadas con un grupo

amino, clave para su posterior inmovilización en la superficie electrodica de oro, llevando a cabo la estrategia de injerto *grafting to*.

Los sensores desarrollados por medio de la inmovilización de nanopartículas MIP sobre la superficie de electrodos de oro se caracterizaron también por Voltamperometría Cíclica, Espectroscopía de Impedancia Electroquímica y Microscopía Electrónica de Barrido. En este caso, para la obtención de un sensor para el 4-etilfenol sensible y selectivo se optimizaron las posibles configuraciones para la correcta inmovilización de las nanopartículas MIP. Para ello, se ensayaron diferentes compuestos para la inmovilización de las nanopartículas y su síntesis con diferentes monómeros funcionales.

Los sensores desarrollados por medio de la técnica *grafting to*, resultaron ser más selectivos que los desarrollados por la técnica *grafting from*. Además, mientras que los sensores desarrollados por medio de capas MIP en la superficie de oro mostraban sensibilidad menor que el electrodo de oro no modificado, el hecho de inmovilizar nanopartículas de alta afinidad mejoraba la sensibilidad del electrodo de oro para la medida de 4-etilfenol.

LIST OF ACRONYMS

4EG	4-ethylguayacol
4EP	4-ethylphenol
4VP	4-vinylpiridine
4VPh	4-vinylphenol
AA	Acrilamide
ABCN	1-1’-azo-bis-(cyclohexanecarbonitrile)
ABDV	2-2’-azo-bis-(2,4-dimethylvaleronitrile)
ACN	Acetonitrile
AIBN	Azo-bis-isobutyronitrile
AMPSA	2-acrylamido-2-methyl-1-propanesulfonic acid
APMA	N-(3-aminopropyl) methacrylamide hydrochloride
APS	Ammonium persulphate
ATRP	Atom transfer radical polymerisation
B-R	Britton-Robinson
CA	Coumaric acid
CAEE	Coumaric acid ethyl ester
CE	Capillary ectrophoresis
CEC	Capillary electrochromatography
CHEMFET	Chemical Field Effect Transistors
CL	Cross linking monomer
CPE	Carbon paste electrode
CRP	Controlled "living" radical polymerisation
CV	Cyclic voltammetry
DABE	N,N,-diethyldithiocarbamic acid benzyl ester
DAD	Diode array detector
DCM	Dicloromethane
DEAM	N,N-diethylaminoethyl methacrylate
DLS	Dynamic light scattering
DMAPMA	3-dimethylaminopropyl methacrilamide
DMF	Dimethylformamide
DMSO	Dimethyl sulfoxide
DP-MISPE	Differential pulse molecularly imprinted solid phase extraction
DPV	Differential pulse voltammetry

DVB	Divinylbenzene
EA	Ethanolamine
EDC	1-ethyl-3-[dimethylaminopropyl]carbodiimide
EDMA	Ethylene dimethacrylate
EGMP	Ethylene glycol methacrylate phosphate
EIS	Electrochemical impedance spectroscopy
ELISA	Enzyme-like immunosorbent assay
FD	Flurorescence detector
FER	Ferrocenylmethyl methacrylate
FM	Functional monomer
FT-IR	Fourie trasnform infrared spectroscopy
GCE	Glassy carbon electrode
GE	Gold electrode
GWM	Gold wire microelectrode
HEMA	2-hydroxyethyl methacrylate
HPLC	High resolution liquid cromatography
IA	Itaconic acid
IF	Imprinting Factor
IIT	Ion imprinting technology
ISE	Ion selective electrode
ISFET	Ion Selective Field Effect Transistors
KPS	Potassium persulphate
LA	Lipoic acid
LC	Liquid chromatography
LOD	Detection limit
LOQ	Quantification limit
LPME	Liquid phase microextraction
LSV	Linear sweep voltammetry
MA	Methacrylic acid
MBA	Methylene-bis-acrylamide
MeOH	Methanol
MI-MSPE	Moleclarly imprinted micro solid phase extraction
min	Minutes
MIN	Molecularly imprinted nanoparticles
MIP	Molecularly imprinted polymer
MISPE	Molecularly imprinted solid phase extraction

MS	Mass spectrometry
MSPD	Matrix solid phase extraction
MSPE	Micro solid phase extraction
MUA	Mercaptoundecanoic acid
MWCNT	Multiwall carbon nanotubes
NHS	N-hydroxysuccinimide
NP	Nanoparticle
NTP	Nitroxide mediated polymerisation
PDI	Polidispersity index
PE-MISPE	Pulsed elution molecularly imprinted solid phase extraction
PETEA	Pentaerythritol tetracrylate
PETRA	Pentaerythritol triacrylate
PVC	Polyvinyl chloride
R.T.	Room temperature
RAFT	Reversible addition-fragmentation chain transfer
RAFT	Reversible addition-fragmentation chain transfer
RDRP	Reversible deactivation radical polymerisation
RSD	Relative standard deviation
SAM	Self-assembled monolayer
SBSE	Stir bar sorptive extraction
SD	Standard deviation
SEM	Scanning electron microscopy
SPE	Solid phase extraction
SPME	Solid phase microextraction
SPR	Surface plasmon resonance
Sty	Styrene
SWV	Square wave voltammetry
TEMED	N,N,N’,N’-tetramethylenediamine
TFMAA	2-(trifluoromethyl)acrylic acid
TRIM	Trimethylpropane trimethacrylate
UV	Ultraviolet

Chapter 1

INTRODUCTION

Introduction

Lately, molecular imprinting has become a common technique for the development of synthetic receptors. These polymers have the potential of replacing natural occurring compounds used as molecular receptors. These receptors include, among others, nucleic acids, enzymes, antibodies or aptamers. The main drawbacks they present come from their natural character, as low stability, low abundance and the fact that for some target molecules do not exist natural receptors capable of selective recognition and binding. In this sense, molecularly imprinted polymers can be helpful, as imprinted polymers are usually stable in extreme conditions and for long periods of time and can be designed for a wide range of target compounds.

The selectivity of these polymers relies on their specific binding sites created during polymer synthesis. Molecularly imprinted polymers (MIP) are synthesised in the presence of a template or target molecule creating binding sites that are complementary to the molecule in shape, size and functional groups. For this purpose, three main components are necessary, a template –which will model the binding site-, a functional monomer -which will interact with the template for the creation of the binding sites-, and a crosslinker monomer -which will form the three-dimensional polymeric structure -.

As a general procedure, template and functional monomer(s) are dissolved on a solvent and let interact, forming a prepolymerisation adduct. Later, the crosslinker monomer is added followed by an initiator and subsequently, polymerisation will be started. Once the polymer is synthesised, the template must be cleaned in order to release the created binding sites. For the obtainment of a polymer with the optimum properties, it is important to choose the adequate components and their proportion on the polymerisation mixture. For years, the most popular polymerisation method has been free radical polymerisation, due to its simplicity. However, on last years, Reversible Deactivation Radical Polymerisation methods have gained importance. The main improvement achieved with these polymerisation methods is the higher control on the polymerisation process.

Although in the first stages of MIP development these polymers were synthesised on bulk format, nowadays, different formats have been used depending on the purpose. Bulk form polymers, usually have to be grounded and sieved to obtain MIP particles for their application. However, other approaches allow the direct MIP particle synthesis using different methods such as precipitation polymerisation, emulsion polymerisation or solid-phase synthesis. These methods, avoid grounding and sieving and improve particle homogeneity, improving MIP performance. Further improve has been achieved with the emergence of

nanoscale molecularly imprinted polymers. Due to the nano size of these particles, the volume to surface ratio is increased, and in consequence, the binding site accessibility.

Once the imprinted polymer particles are synthesised they can be implemented on different supports or surfaces depending on the final application. First, surface must be functionalised for the latter immobilisation of the polymer. This technique is called the grafting to technique. On the other hand, imprinted polymers can be directly synthesised on the surface. For this approach, the surface must be functionalised with a polymerisation initiator. This approach is called grafting from approach. Finally, surfaces can be functionalised with a reacting monomer, which will be part of the polymer grafted on the surface when polymerisation is performed. This last approach is called grafting through.

Due to their ability for selectively binding the template compound, the major application of MIP over the years has been its use as sorbent in affinity separation techniques. MIP can bind the analyte discriminating from its structural analogues or enantiomers. On the other hand, MIP developed with a proper design can be selective for a group of similar compounds, due to their resemblance in shape and functional groups. These features, make them proper sorbents to be used in different sample preparation techniques such as solid phase extraction, solid phase microextraction or stir bar sorptive extraction. Following the same

principle, MIP can be used in affinity chromatography (liquid or capillary electrochromatography) as solid phase.

On the other hand, MIP have been widely used in sensor development. Usually, in the construction of selective chemical or physical sensors, there is a need to use a recognition element to achieve a selective measurement, as the chemical of physical properties used for detection are not selective enough. Due to the intrinsic properties of MIP, they are very suitable candidates to use as recognition elements. When the target molecule binds the MIP selectively it will produce a chemical and/or physical change on the polymer. If the polymer is selective enough, the produced change will be only attributable to the target analyte. The change on the properties can be measured with the proper transducer and could be related to analyte concentration. The most used transducers for the construction of sensors based on MIP, have been optical, mass/acoustic and electrochemical transducers.

Chapter 2

OBJECTIVES

Objectives

Molecular recognition is the main principle of many receptors used in analytical chemistry. Natural receptors such as antibodies or enzymes have been widely used, however, due to the drawbacks they present, such as, low stability in laboratory conditions, synthetic receptors have gained great attention. Among synthetic receptors molecularly imprinted polymers have resulted a simple way to imitate natural molecular receptors. Taking this into account the main objective of this work was set as:

Development of polymeric receptors based on molecular imprinting techniques for the separation and sensing of 4-ethylphenol and the compounds belonging to its metabolic pathway.

In order to achieve this general objective this work has been structured in two sections. The main objective of the first section, explained on chapter 3, was the following:

- **The design of a solid phase extraction method based on molecularly imprinted polymers for 4-ethylphenol and the compounds that belong to its metabolic pathway and their latter separation by liquid chromatography for their quantification in wine.**

On the other hand, the second section of this work is explained on chapter 4, the main objective set for this part of the work was:

- **The development of MIP-based synthetic receptors on gold substrates, through different Reversible Deactivation Radical Polymerisation strategies, and the use thereof as sensing elements for voltammetric measurements of 4-ethylphenol.**

Capítulo 3

DESARROLLO DE POLÍMEROS DE HUELLA MOLECULAR PARA EL ESTUDIO DE LA RUTA METABÓLICA DEL 4-ETILFENOL EN VINO

Índice

1. Introducción

Los polímeros de huella molecular (MIP) han sido definidos como la construcción de sitios de reconocimiento selectivo en polímeros sintéticos, donde una molécula molde o *template* (átomo, ión, molécula, complejo o grupo molecular, iónico o macromolecular, incluyendo microorganismos), facilita durante el ensamblaje del polímero, la construcción a medida de un receptor de sitios de enlace (*1*).

Para la síntesis de estos polímeros, la molécula molde interactúa con los monómeros funcionales (FM) formando un complejo estable mediante interacciones covalentes o no covalentes. Posteriormente a la formación de este enlace, comienza la polimerización de los monómeros funcionales y entrecruzadores (CL) formándose una malla polimérica, que después de la eliminación del *template*, presenta cavidades que son estructuralmente complementarias a éste en tamaño, forma y disposición de los grupos funcionales. Los monómeros funcionales deben de interaccionar fuertemente con el *template* antes y durante la polimerización para conseguir un gran número de sitios de enlace. El aumento de la selectividad del polímero se debe, principalmente, a la rigidez de la huella impresa ocasionada por la preservación de la unión monómero-*template* durante la polimerización.

La técnica de huella molecular permite la construcción a medida de receptores sintéticos que imiten el reconocimiento biomolecular de procesos biológicos como la replicación de DNA, la interacción antígeno-anticuerpo o enzima-sustrato, pero con la ventaja de poder ser sintetizados para una gran variedad de moléculas orgánicas y en diferentes formas físicas (2,3). La impresión molecular se engloba dentro de la química supramolecular y más concretamente en la química biomimética, que estudia la síntesis y caracterización de materiales en los que participan fundamentalmente interacciones huésped-receptor.

Para describir este concepto se han utilizado diferentes expresiones, como "polímeros construidos como análogos enzimáticos" (*4*), "polimerización hospedador-huésped" (*5*) o "síntesis con plantilla" (*6*). Aunque el concepto huella (*imprints*) aparece por primera vez en 1957 (*7*), el término "*molecular imprinting*", fue utilizado por primera vez en los años 80 (*8*), convirtiéndose posteriormente en el término estándar *"molecularly imprinted polymer"* o polímeros de huella molecular (*9*).

1.1. Evolución histórica de la Impresión Molecular

En 1931 Polyakov *et al*. investigando en el desarrollo de nuevos materiales para su aplicación en cromatografía, observaron que las partículas de sílice presentaban memoria hacia algunos aditivos (*10*). Cuando añadieron moléculas aromáticas como benceno, tolueno o xileno en la etapa de secado, después de la síntesis de la sílice, observaron que posteriormente en ensayos de adsorción, la sílice presentaba mayores capacidades para la captación de estos aditivos. Años después se concluyó que la selectividad mostrada para los aditivos era debida a los cambios estructurales originados en la matriz de la sílice y en consecuencia a la naturaleza química de los aditivos (11,12).

Contemporáneamente, se discutían diferentes hipótesis para explicar la selectividad de los anticuerpos del sistema inmune. En 1940, Pauling propuso que la formación de los anticuerpos se daba por la presencia de un antígeno que actuaba como *template* (*13*). Intentando aplicar esta teoría en un sistema inorgánico como la sílice, Dickey, utilizó un procedimiento similar al de Polyakov utilizando naranja de metilo como molécula molde (14,15). A diferencia del procedimiento anterior, en este caso el *template* se mezcló con el silicato de sodio antes de la formación de la estructura de la sílice. Este nuevo procedimiento pareció influir en mayor medida en la estructura formada (*14*). Más tarde, profundizaron en la investigación de este sistema (*16*) al igual que

lo hicieron otros grupos que sintetizaron geles de sílice en presencia de tintes del tipo naranja de alquilo obteniendo resultados similares (17,18).

Después de dos décadas de investigación sobre la impresión en sílice, Wulff y Klotz de forma independiente, introdujeron la impresión molecular en polímeros orgánicos sintéticos (4,19). Para entonces, Blow *et al.* habían elucidado la estructura completa y el mecanismo de acción de la primera enzima natural, describiendo que la forma y orientación de los sitios activos de la enzima era complementaria a la estructura química del sustrato (*20*).

La aparición de la impresión en polímeros orgánicos trajo consigo el decaimiento de la impresión molecular en sílice. Sin embargo, Sagiv (*21-24*) introdujo una nueva manera para la impresión en matrices inorgánicas. La molécula molde era adsorbida por las partículas de sílice y a continuación grupos octametilsilanos se unían químicamente a grupos hidroxilo no unidos al template, de forma que después de eliminado este se generaban parches de sílice no derivatizada complementarios a la molécula molde. Posteriormente, esta técnica fue utilizada por otros grupos para la impresión de la vitamina K1 para su aplicación en la medida por elipsometría (*25*), porfirinas y clorofilas para la medida por Espectroscopía Raman Resonante intensificada en superficie (*26*) y colesterol (*27*) o catecol (*28*) para su aplicación en sensores voltamperométricos.

La mayor desventaja de esta primera generación de MIP inórganicos en bloque mediante síntesis sol-gel, era el número limitado de grupos funcionales disponibles, reduciendo los tipos de moléculas molde que podían ser impresas. Mosbach y colaboradores utilizaron para la impresión de tintes en la superficie de partículas de sílice porosa, nuevos monómeros orgánicos conteniendo grupos funcionales como amino, fenilo, dodecilo y glicidoxilo (*29*).

En las últimas décadas, se han desarrollado nuevas matrices inorgánicas disponibles para la impresión molecular, como polímeros de cristal líquido de polisiloxano (*30*) o las zeolitas (*31*).

En la impresión molecular en sílice solamente pueden darse interacciones hidrofóbicas a partir de los grupos siloxano e interacciones hidrofílicas para los grupos silanol, por otro lado las cavidades de unión presentan poca estabilidad y además no hay posibilidad de variar su estructura de forma sistemática (*32*).

Estas desventajas hicieron pensar en el interés de poder introducir en los sitios de unión grupos funcionales con orientación. Los monómeros sintéticos orgánicos, estaban altamente estudiados y su polimerización podía ser fácilmente controlable. Los primeros resultados de los polímeros orgánicos de huella molecular fueron presentados por Ali Sarhan en 1971 (4,33), uniendo grupos funcionales polimerizables al *template* mediante uniones covalentes y no covalentes. En 1974 Wullf *et al*. patentaron este procedimiento (*34*).

Al mismo tiempo, Klotz y colaboradores publicaron un trabajo donde entrecruzaban grupos tiol en presencia y ausencia de una molécula objetivo (*19*). Observaron que el polímero sintetizado en presencia de la molécula mostraba una unión más fuerte.

En la década siguiente Shea (*6*) y Neckers (*35*) estudiaron las reacciones estéreoselectivas usando polímeros de huella molecular. Tsuchida (*36*) y Kabanov (*37*) estudiaron los polímeros impresos con metales iónicos y el grupo de Mosbach sintetizó en 1981 el primer MIP totalmente no covalente (5,8). Este último método, ha resultado una manera simple y eficiente de imprimir polímeros para una gran variedad de aplicaciones.

Desde los primeros trabajos de Wulff y Klotz en la síntesis de MIP orgánicos, la mayoría de polímeros impresos se preparaban en forma de bloque. A pesar de los avances realizados en el conocimiento de la influencia de los diferentes factores químicos y físicos en las propiedades de reconocimiento del polímero, no se realizaron grandes avances en las técnicas experimentales básicas para la síntesis de polímeros en bloque (38,39). Además, los MIP preparados de forma tradicional (como monolitos, membranas, capas o partículas) pueden presentar una serie de desventajas como la heterogeneidad de los sitios de unión (*40*), el sangrado del *template* residual en el polímero (*41*) y dificultades para su aplicación en sensores y ensayos biológicos. En este sentido, en los últimos años se ha avanzado en la síntesis de nanopartículas

molecularmente impresas, debido a las mejoras significativas que presentan estos materiales frente a los MIP convencionales. La relación superficie-volumen es mayor, lo que favorece la accesibilidad del compuesto objetivo a las cavidades impresas, mejorándose la reactividad química, la capacidad y las cinéticas de unión, típicamente lentas en los MIP sintetizados de forma tradicional. Sin embargo, las diferentes estrategias para la síntesis de nanomateriales impresos, como la polimerización por precipitación (*42-44*), por emulsión (45,46) o miniemulsión (47,48), se basan en las mismas pautas que la síntesis en bloque, empleando *templates* solubilizados en un disolvente. Muchas de las desventajas de los polímeros en bloque residen precisamente en el hecho de que el *template* se encuentre disuelto, y por lo tanto, en movimiento durante las etapas críticas de formación de los sitios de unión. Para solventar esta circunstancia recientemente, Poma *et al.* han propuesto un método de síntesis de nanopartículas MIP en fase sólida, donde el *template* se encuentra inmovilizado en partículas de vidrio obteniendo nanoparticulas con alta afinidad para la molécula objetivo (*49*). Esta nueva estrategia supone un avance muy prometedor en el desarrollo de nanomateriales MIP.

En los últimos años, un gran número de grupos de investigación se han unido al campo de la impresión molecular (*32*). Según la base de datos MIPdatabase (http://www.mipdatabase.com) (50) desde 1930 hasta 2015 se han

publicado 11673 artículos sobre este tema y para una gran cantidad de moléculas *template* (*51*). Estas moléculas pueden clasificarse en moléculas pequeñas con pesos moleculares menores a 1000 Da como es el caso de ciertos contaminantes ambientales (*52-54*) aditivos y compuestos naturales en alimentos (*55-58*), fármacos y drogas (*59-61*) u otros compuestos biológicos (62,63); y otro grupo constituido por moléculas de hasta los 10000 Da como péptidos y proteínas (*64-66*). La mayoría de las publicaciones se centran en el primer grupo de moléculas, ya que estas tienen una forma definida, funcionalidad más reducida y son estables, propiedades que las hacen ideales para la impresión molecular.

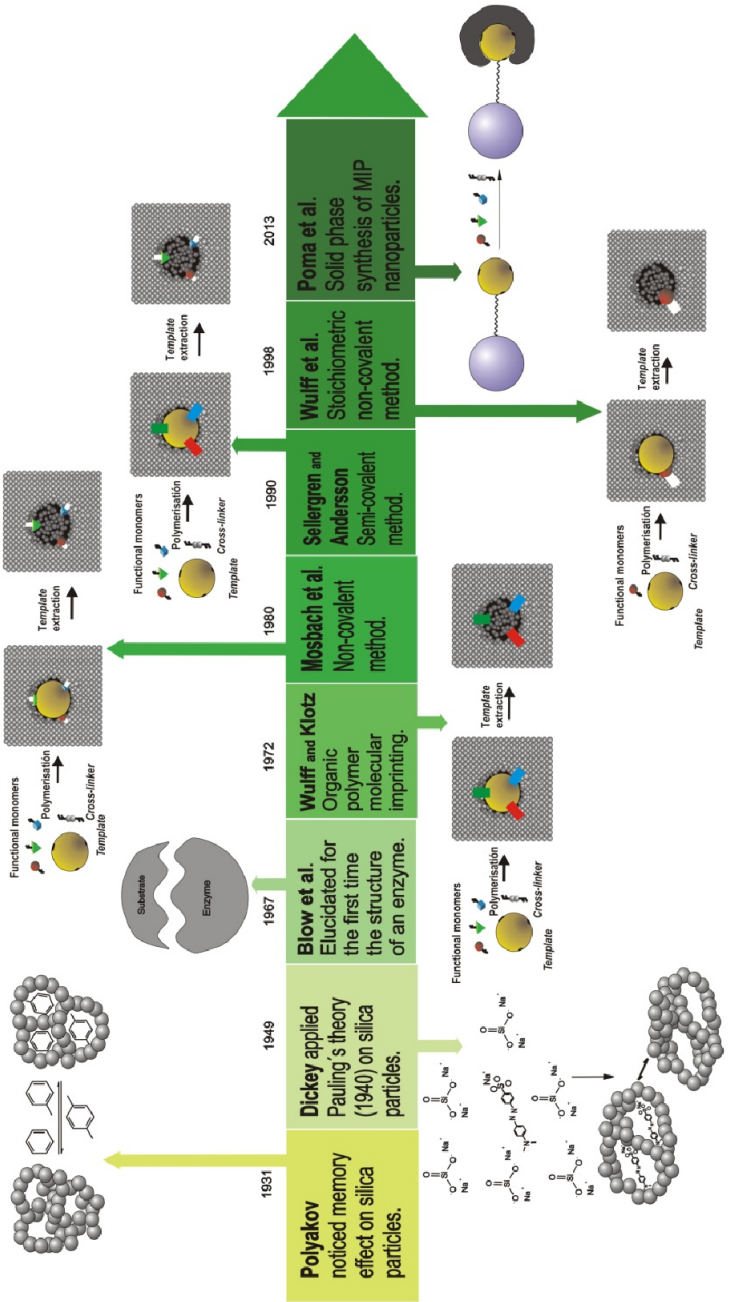

Figura 3. 1. Evolución de la impresión molecular.

1.2. Métodos para la impresión molecular de polímeros

El punto crítico en la síntesis de los polímeros de huella molecular es la unión de la molécula *template* con el monómero funcional. Dependiendo del método utilizado, estas uniones pueden ser covalentes, no covalentes o iónicas.

1.2.1. Método covalente

Este método de impresión molecular se basa en la unión covalente del *template* a uno o más grupos funcionales polimerizables. Después de la síntesis del polímero, el *template* se elimina creando cavidades de unión con funcionalidad capaces de volver a establecer las uniones covalentes con el *template* (*1*). El método covalente fue usado en las primeras etapas de desarrollo del concepto y optimización de las estructuras MIP (67). Sin embargo, hoy en día ha sido sustituido por el método no covalente (68,69).

La mayor ventaja del método covalente radica en que al realizarse la síntesis en condiciones estequiométricas, los grupos funcionales siempre se encuentran en las cavidades de unión, lo que minimiza la presencia de interacciones inespecíficas. Sin embargo, su mayor desventaja es el limitado número de compuestos que pueden ser empleados como *template* (dioles, aldehídos, cetonas, aminas y ácidos carboxílicos) (*1*).

El método covalente más extensamente utilizado, se basa en la utilización de monómeros funcionales con el grupo ácido borónico (*1*). Este método fue desarrollado y profundamente estudiado por Wulff *et al*. (70,71). Normalmente, se utiliza para la impresión de *templates* que poseen grupos diol (67,72). Sin embargo, también han sido impresos ácido glicérico (*4*), aminoácidos (73,74), ácido siálico (75), derivados de la manosa (76,77), galactosa y fructosa (78,79). Hoy en día este método sigue siendo el más utilizado dentro de los métodos covalentes (80-83).

Las bases de Schiff resultan útiles para la impresión molecular de aminas o aldehídos y además, estos enlaces covalentes son totalmente reversibles sin activación adicional (1,84-87). La posición en el equilibrio para la formación del enlace imino es favorable a la unión, sin embargo, la velocidad de formación/ruptura del enlace puede ser muy lenta, razón por la que estos polímeros no son adecuados para aplicaciones como la cromatografía (84,88).

Shea *et al.* y Marty *et al.* emplearon el método covalente para la impresión de cetonas, generando cetales reversibles (89-92). Estos enlaces se forman lentamente y la recaptación del *template*, a diferencia del resto de enlaces explicados hasta el momento, está controlada cinéticamente (67). Cuando la disposición de las moléculas es la misma, el tamaño y la forma de éstas resultan de gran importancia en la recaptación selectiva.

Otros autores plantean uniones entre los grupos éster y los grupos carboxilo para la impresión covalente de ácidos carboxílicos (35,93-95). Sin embargo, esta impresión presenta cinéticas lentas por lo que sus aplicaciones resultan limitadas (*6*).

1.2.2. Método no-covalente

Este método fue desarrollado por el grupo de Mosbach a principios de los años 1980, sin embargo, actualmente sigue siendo el método más empleado para la síntesis de MIP (96). Este método conlleva el autoensamblaje mediante enlaces no-covalentes del *template* con el monómero funcional, la polimerización radical con un monómero entrecruzador y finalmente el lavado del *template* y su recaptación por enlaces no-covalentes (97). Este tipo de interacciones no covalentes *template*-monómero funcional incluyen enlaces por fuerzas de Van der Waals, enlaces iónicos, uniones por puentes de hidrógeno o interacciones electrostáticas entre otras.

En los sistemas bioquímicos las interacciones no-covalentes son las responsables de las uniones reversibles y de los fenómenos de reconocimiento. Estos enlaces son más débiles que los covalentes, sin embargo, cuando varios enlaces no covalentes participan en la misma cavidad de unión se pueden conseguir uniones suficientemente fuertes (98).

Los monómeros funcionales que participan en este tipo de unión suelen estar disponibles comercialmente, sin embargo, también se han desarrollado MIP no covalentes con monómeros funcionales diseñados a medida del *template* (*1*).

Entre los monómeros funcionales ácidos, el metacrílico es el más utilizado (99,100). Otros ejemplos de monómeros ácidos son el ácido 4-vinilbenzoico (101), ácido acrílico (102), ácido 2-acrilamido-2-metil-1-propanosulfónico (AMPSA) (103), ácido (2-trifluorometil) acrílico (TFMAA) (104), ácido itacónico (61,105) o 2-(metacriloiloxi) etil fosfato (106).

Para los monómeros básicos el más empleado es la 4-vinilpiridina (107,108), en este grupo también se pueden encontrar monómeros funcionales como N,N-dietilaminoetil metacrilato (DEAM) (109), aminoestireno (110), vinilimidazol (111,112) o 3-dimetilaminopropil metacrilamida (DMAPMA) (113).

Finalmente, entre los monómeros funcionales neutros más utilizados se encuentran la acrilamida (114), la vinilpirrolidona (115) y el 2-hidroxietil metacrilato (HEMA) (116,117).

En la tabla 3.1 se recogen algunos ejemplos de polímeros de huella molecular sintetizados con monómeros funcionales ácidos, básicos o neutros.

En algunos casos, la combinación de varios monómeros funcionales permite obtener mejores resultados en comparación con los obtenidos para un MIP sintetizado a partir de sólo un monómero funcional (1,111,117).

Tabla 3. 1. Ejemplos de MIP sintetizados con diferentes monómeros funcionales.

Monómero	*Template*	Aplicación	Ref.	Año
Monómeros Ácidos				
Ácido metacrílico	Cotinina	SPE	Martins et al. (99)	2015
	Tetraciclina	SPE	Lv et al. (100)	2015
Ácido 4-vinilbenzoico	Feniletanola-mina A	SPE	Wang et al. (101)	2015
Ácido acrílico	Ácido úrico	Sensor	Motghare et al. (102)	2015
AMPSA	Bisfenol A	SPE	Duan et al. (103)	2014
TFMAA	Cefalexina	SPE	Lata et al. (104)	2015
Ácido itacónico	S-citalopram	LC	Gutierrez-Climente et al. (*61*)	2015
	Microcistina-LR	SPE	Krupdam et al. (105)	2014
2-(metacriloiloxi) etil fosfato	Colesterol	LC	Kugimiya et al. (106)	2001

Tabla 3.1. cont. Ejemplos de MIP sintetizados con diferentes monómeros funcionales.

Monómero	*Template*	Aplicación	Ref.	Año
Monómeros básicos				
4-vinilpiridina	Quercetina	SPE	Piacham *et al.* (107)	2015
	Tolueno	SPE	Egli *et al.* (108)	2015
DEAM	Ácido 2-quinoxalina-carboxílico	SPE	Duan *et al.* (109)	2013
Aminoestireno	Dietilclorofosfato	Sensor	Vishnuvardhan *et al.* (110)	2011
Vinilimidazol	4-nitrofenol	SPE	Muhammad *et al.* (112)	2014
Vinilimidazol + 4-Vinilpiridina	Selenio	SPE	De Lima *et al.* (111)	2015
DMAPMA	Albumina de suero bovino	SPE	Gai *et al.* (113)	2011

Tabla 3.1. cont. Ejemplos de MIP sintetizados con diferentes monómeros funcionales.

Monómero	*Template*	Aplicación	Ref.	Año
Monómeros neutro				
Acrilamida	Teofilina	SPE	Cela-Perez *et al.* (114)	2015
4-vinilpirrolidona	Acetato de etilo	Sensor	Iqbal *et al.* (115)	2013
HEMA	Gatifloxacina	Administración de fármacos	Lu *et al.* (116)	2014

1.2.3. Método no-covalente estequiométrico

En el método no covalente ordinario, las interacciones entre el monómero funcional y el *template* suelen ser débiles. Por ello, es necesaria la utilización de una gran cantidad de monómero funcional para asegurar un grado suficiente de complejación con el *template.* Consecuentemente, se forman un gran número de sitios de unión no específicos.

Teniendo en cuenta las ventajas de los métodos covalente y no covalente, muchos grupos de investigación han planteado para la síntesis de MIP el modelo no covalente estequiométrico. En este tipo de interacciones, el complejo que se forma entre el monómero funcional y el *template* es suficientemente fuerte para asegurar que el equilibrio se desplaza hacia la formación del complejo. Cuando la constante de asociación es suficientemente alta ($K_a \geq 10^3\ M^{-1}$) el monómero funcional y el *template* se unirán completamente para una relación molar 1:1 evitando la formación de sitios de unión no específicos (*3*). En consecuencia, los altos rendimientos de ruptura y rápidas cinéticas observadas habitualmente en los enlaces no covalentes se combinan con la precisa localización de los monómeros funcionales en las cavidades de unión y la alta accesibilidad de las cavidades de reconocimiento libres típicas de la impresión no covalente (67).

Este método fue utilizado por primera vez por Wulff *et al*. (118) para el diseño y la síntesis de MIP, utilizando monómeros con

grupos amidina. Estos grupos forman enlaces muy fuertes con los grupos carboxilato, fosfonato y fosfato ($5 \cdot 10^3$ M^{-1} < K_a < 10^6 M^{-1}). Desde entonces, han sido desarrollados otros monómeros como quinonas o derivados conteniendo boro (119), o monómeros de urea (120,121) que han demostrado un alto potencial para la impresión de compuestos bioactivos y para generar polímeros que podrían ser utilizados en medios acuosos.

1.2.4. Método semi-covalente

Este método de impresión molecular combina las ventajas del método covalente con las del método no covalente. En este caso, el *template* se une covalentemente al monómero funcional para la síntesis del polímero, consecuentemente, la funcionalidad unida al *template* se encontrará únicamente en las cavidades de unión. Por otro lado, la recaptación del *template* por el polímero se da mediante enlaces no covalentes y no sufre restricciones cinéticas diferentes a las propias de la difusión.

Este método fue publicado por primera vez por Sellergren y Andersson (122). El *template* que utilizaron fue el éster etílico de p-aminofenilalanina, utilizando como análogo estructural una molécula con grupos polimerizables unidos por enlaces éster. Una vez eliminado el *template* por hidrólisis, los grupos carboxílo

quedaron libres en las cavidades de unión, por los que el *template* se unía no covalentemente en la recaptación.

Whitcombe *et al*. introdujeron espaciadores de sacrificio en las cavidades de unión para evitar la agrupación de moléculas de *template* y facilitar la recaptación no covalente (123). El *template* se unía a espaciadores con grupos carbonilos, finalizada la polimerización y la eliminación del *template* de las cavidades, los grupos carbonilo se disipaban como CO_2 dejando espacio suficiente entre los grupos funcionales para la recaptación.

1.2.5. Método para la impresión de especies iónicas

La tecnología de impresión de iones (IIT) combina los ligandos o monómeros funcionales, para formar quelatos o compuestos por enlaces de coordinación, enlaces metálicos o puentes de hidrógeno (124).

En la tecnología IIT, los iones pueden actuar como *template* o pueden ser parte del monómero funcional para ayudar a imprimir macromoléculas resolviendo los problemas de la impresión de éstas en sistemas acuosos (124). El papel del ligando en la impresión de iones es fundamental, ya que la formación del quelato que implica el proceso de reconocimiento del *template,* favorece la especificidad de la unión (124,125).

Los primeros en emplear esta tecnología fueron Nishide *et al*., entrecruzando poli(4-vinilpiridina) con 1.4-dibromobutano para metales iónicos como Cu(II), Fe(III), Co(II), Zn(II), Ni(II) o Hg(II) (*36*).

1.3. Factores que influyen en la síntesis de los polímeros de huella molecular

Entre los parámetros a optimizar en la síntesis de los MIP se encuentran la naturaleza y cantidad de los reactivos, la forma de iniciar la polimerización y la metodología empleada.

1.3.1. Reactivos en la mezcla de polimerización

Entre los reactivos que más comúnmente se utilizan en la síntesis de los MIP se encuentran los monómeros funcionales y entrecruzador, el disolvente y el iniciador de la polimerización. Una buena elección de cada uno de estos reactivos es indispensable para la síntesis de un polímero impreso óptimo y específico para el objetivo deseado.

1.3.1.1. Selección del monómero funcional

El papel del monómero funcional es el de proveer al polímero de grupos funcionales que puedan formar complejos con el *template*

mediante uniones covalentes o no covalentes (126). La elección de este monómero es clave para la impresión molecular, por ello, el monómero funcional debería formar uno o más enlaces con alta fuerza de unión, de forma que además estas interacciones fueran direccionales para generar cavidades más selectivas (127).

Teniendo en cuenta el principio de Le Chatelier, aumentando la cantidad de *template* o monómero funcional en la mezcla de prepolimerización, aumentará el número de complejos formados entre ellos. Estos complejos son los responsables de la creación de las cavidades de unión, en consecuencia, bajas relaciones molares monómero funcional:*template*, propiciaran polímeros con baja selectividad. A medida que la relación aumenta, la selectividad aumentará hasta alcanzar el valor óptimo, específico para cada sistema. Por otra parte al aumentar la relación molar por encima del valor óptimo podrían originarse cavidades de unión no específicas (127). En la práctica, se deben optimizar las condiciones experimentales que garanticen la máxima selectividad para la interacción del MIP y el analito.

1.3.1.2. Monómero entrecruzador

El monómero entrecruzador es el responsable de controlar la morfología del polímero, permitiendo la obtención de cavidades de unión bien definidas y proporcionando estabilidad mecánica a la

matriz polimérica de manera que la capacidad de reconocimiento sea fija (128). Cuando la concentración de este monómero es muy baja, el grado de entrecruzamiento del polímero será bajo y las cavidades de unión no serán capaces de permanecer estables. Por otro lado, si la concentración es demasiado alta la concentración de cavidades de unión por masa de polímero decrecerá (126). El monómero entrecruzador hace que los polímeros sean insolubles (129), resultando esta una ventaja o una desventaja dependiendo de las aplicaciones. El monómero entrecruzador afecta directamente a las características físicas del MIP y en cambio, tiene un efecto menor en las interacciones entre el *template* y el monómero funcional (130-132).

El divinilbenceno (DVB) fue el primer monómero entrecruzador utilizado para la impresión molecular de polímeros orgánicos (127) y actualmente sigue siendo ampliamente empleado (133-135) junto con el dimetacrilato de etilenglicol (EDMA) (77,136-139) y el trimetilpropano trimetacrilato (140,141) (TRIM). Ha sido demostrado que en algunos casos, para los monómeros entrecruzadores con más de dos grupos (met)acrilato como el TRIM, triacrilato de pentaeritritol (PETRA) o tetracrilato de pentaeritritol (PETEA) se obtienen mejores resultados que al utilizar el EDMA (*1*). Para el caso de la impresión molecular en sistemas acuosos el monómero entrecruzador más habitual es el N,N'-metilen-bis-acrilamida (MBA) (142-144).

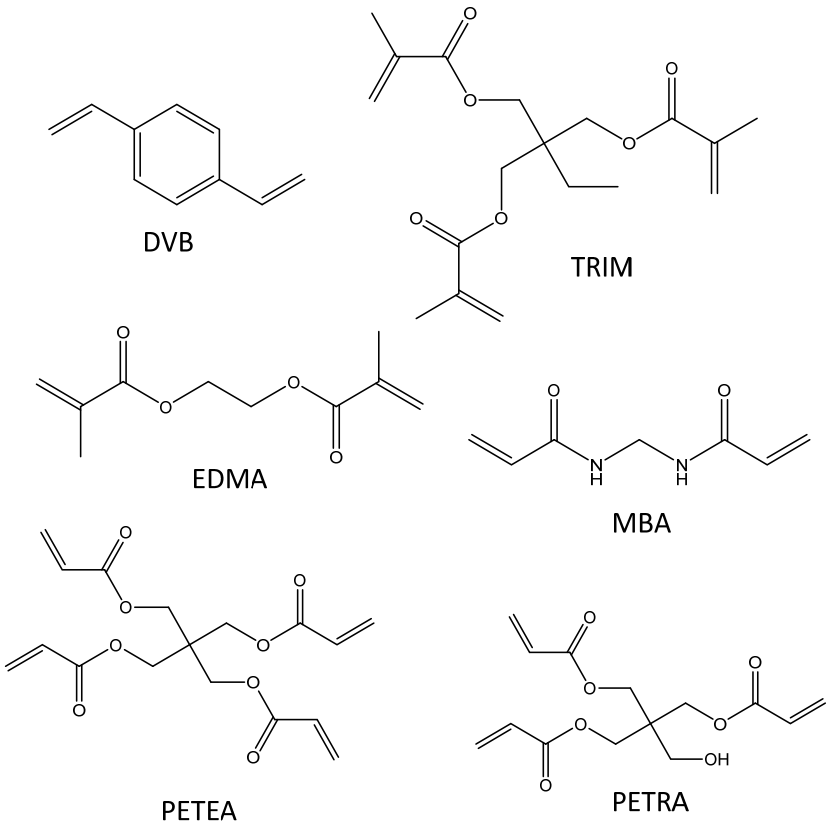

Figura 3. 2. Estructuras de los monómeros entrecruzadores más comunes.

1.3.1.3. Medio de polimerización

El disolvente en el que tiene lugar la polimerización debe solubilizar la totalidad de los componentes de la mezcla, no afectando a la estabilidad del complejo de prepolimerización monómero funcional-*template*. Debido a que la estabilidad de este

complejo se da fundamentalmente por interacciones intermoleculares polares, a medida que desciende la polaridad del disolvente mejoran las propiedades de impresión del polímero.

Cuando los monómeros funcionales forman pares iónicos con el *template,* durante la polimerización se forma un polielectrolito, de forma que las propiedades de los grupos funcionales se ven afectadas por su entorno (*39*). En un medio apolar representado por el disolvente, los monómeros, las cadenas oligoméricas y las cadenas poliméricas parcialmente formadas, estos pares iónicos tienden a agregarse por medio de interacciones dipolo-dipolo (145), proporcionando un mayor grado de entrecruzamiento (146). En los MIP, las constantes dieléctricas de la mezcla de monómeros y de sus componentes pueden afectar a la morfología del polímero sintetizado y a la ionización de los grupos funcionales.

En un estudio realizado por Piletska *et al*. sobre el efecto del disolvente en la formación del MIP, se comprobó que la inclusión y disponibilidad de los monómeros funcionales dependía de la constante dieléctrica del disolvente utilizado en la síntesis polimérica. Los disolventes hidrofóbicos producían polímeros con un mayor número de grupos ionizables, demostrando una mejor inclusión de los monómeros funcionales (*39*). Además, en un estudio anterior habían demostrado que los polímeros sintetizados en disolventes con constantes dieléctricas bajas mostraban mayor especificidad y afinidad (147).

Por otro lado, el disolvente o porógeno utilizado para la polimerización es muy importante en la formación de poros a lo largo de la estructura polimérica (127). Durante la polimerización, los espacios ocupados por el disolvente se convierten en poros al final del proceso (129). Los polímeros preparados con un mayor volumen de porógeno son más (macro)porosos, mientras que los MIP preparados con menores volúmenes de porógeno presentaran una morfología más compacta (148).

Una vez sintetizado el polímero, también se utilizan disolventes para la recaptación de *template*. Kempe y Mosbach comprobaron que usando el mismo disolvente en la síntesis y en la recaptación, las interacciones antes y durante la síntesis eran similares (149). Los polímeros poseen diferentes propiedades de hinchamiento dependiendo del disolvente utilizado, por lo que este puede jugar un papel importante en la determinación de los parámetros de forma y distancia fijadas en el polímero, por ello, para la óptima recaptación es necesario poder lograr propiedades de hinchamiento iguales o muy similares a las que se dan durante la polimerización (127).

1.3.1.4. Iniciador de la polimerización

La polimerización radical libre es el método más extendido en la síntesis de MIP, debido a que elimina cualquier interferencia con complejos de prepolimerización no covalentes, a partir de intermediarios polares que podrían originarse en otros procesos de polimerización. Además, las cinéticas de la polimerización radical siguen un mecanismo de crecimiento en cadena a diferencia de las polimerizaciones por condensación que siguen cinéticas de crecimiento por pasos (127). La reacción de polimerización es rápida y comienza por la acción de un iniciador que se descompone por radiación ultravioleta (iniciadores fotoquímicos) o por calor (iniciadores térmicos), liberando radicales libres que reaccionan con el grupo vinilo de los monómeros, formando especies temporales con una duración suficiente para sumarse a otra molécula con doble enlace (150). Este proceso (figura 3.3) genera constantemente centros activos y la repetición de procesos de adición lleva a la formación de polímeros, hasta que los mecanismos de terminación paran el crecimiento de la cadena.

La propagación se detendrá cuando el radical libre reaccione para formar un enlace covalente inactivo. La terminación puede ocurrir por la interacción de dos cadenas activas, por la reacción de una cadena activa con un iniciador radical, por la transferencia del centro activo o por la interacción con otras impurezas como el oxígeno u otros inhibidores (97).

Iniciación

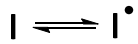

Propagación

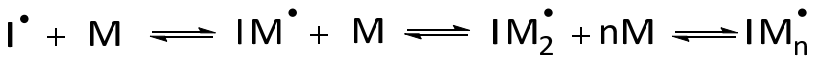

Terminación

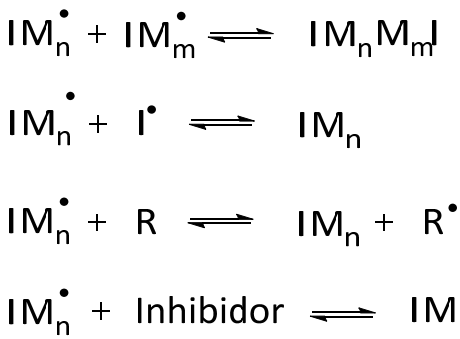

Figura 3. 3. Mecanismo en la polimerización radical libre.

I: iniciador, M: monómero, Mn y Mm: cadenas poliméricas, n y m: número promedio de monómeros en las cadenas poliméricas.

La descomposición térmica o fotodescomposición de los iniciadores del tipo azo (tabla 3.2) es muy empleada como fuente de radicales en MIP basados en DVB o acrilatos (*1*). Los iniciadores azo (R-N=N-R), normalmente tienen grupos R terciarios que estabilizan el radical incipiente. El iniciador más utilizado hasta el momento ha sido azo-bis-isobutironitrilo (AIBN) (137,151,152).

Otro iniciador azo como el 2-2'-azo-bis-(2,4-dimetilvaleronitrilo) (ABDV), requiere una baja temperatura para una vida media de 10 horas (tabla 3.2), por lo que la polimerización puede iniciarse a temperaturas más bajas (153). Por otro lado, la ventaja del iniciador 1-1'-azo-bis-(ciclohexanocarbonitrilo) (ABCN) (58,154,155) en comparación a AIBN, es que es más soluble en disolventes orgánicos a bajas temperaturas mejorando la condiciones de la polimerización fotoquímica (*1*). Además, este iniciador necesita una temperatura más alta para la termodescomposición, por lo que, en sistemas fotoquímicos con control de temperatura se puede asegurar que la iniciación sólo se de por descomposición fotoquímica.

Tabla 3. 2. Características de los iniciadores de tipo azo más comunes en la síntesis de MIP.

Iniciador	LogP	Temperatura para una vida media de 10 horas	Estructura molecular
AIBN	1.66	65 ºC	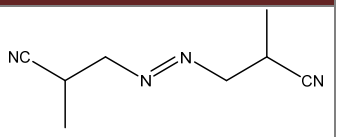
ABDV	4.40	51 ºC	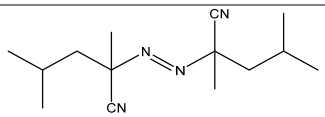
ABCN	2.99	88ºC	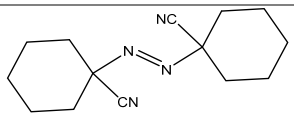

Mijangos *et al.* estudiaron la influencia de las condiciones de iniciación y la cantidad de iniciador en el funcionamiento del polímero (156). Debido a los efectos negativos del aumento de la temperatura en la formación de complejos entre el *template* y el monómero funcional (157), es lógico que se observaran mejores propiedades en los MIP fotoiniciados en comparación con los iniciados térmicamente. En la mayoría de los casos, altas concentraciones de iniciador afectaban negativamente a las

propiedades de reconocimiento de los polímeros. Probablemente este hecho esté relacionado con que grandes concentraciones de iniciador añadido a la mezcla de monómeros incrementa la velocidad de polimerización y en consecuencia aumenta el calor de la reacción (158). La conclusión general del estudio es que los polímeros se deben sintetizar en un amplio periodo de tiempo con bajas concentraciones de iniciador y a bajas temperaturas para conseguir el mejor comportamiento del MIP.

Cuando la polimerización tienen lugar en agua, se emplean iniciadores inorgánicos como el persulfato de amonio (APS) y persulfato de potasio (KPS) (159,160), estos se pueden utilizar en combinación con N,N,N',N'-tetrametilenediamina (TEMED) como catalizador de la reacción de iniciación.

1.3.2. Condiciones de polimerización

Además de los reactivos utilizados en la síntesis del polímero las condiciones en las que se da la polimerización son clave para la obtención del MIP deseado.

1.3.2.1. Temperatura de polimerización

La estabilidad de los complejos formados entre el *template* y el monómero funcional depende de las condiciones de polimerización. La fase de formación del complejo también se encuentra bajo control termodinámico y su energía se puede describir con la siguiente ecuación (161):

$$\Delta G_{bind} = \Delta G_{t+r} + \Delta G_r + \Delta G_h + \Delta G_{vib} + \Sigma \Delta G_p + \Delta G_{conf} + \Delta G_{VdW} \quad \textbf{3. 1}$$

Donde los cambios en la energía libre de Gibbs para la formación del complejo (ΔG_{bind}) dependerán de la energía de traslación y rotación (ΔG_{t+r}), de la restricción del rotor sobre la complejación (ΔG_r), de las interacciones hidrofóbicas (ΔG_h), de los modos residuales de vibración (ΔG_{vib}), de la suma de las contribuciones de los grupos polares que interaccionan ($\Sigma \Delta G_p$), de los cambios conformacionales (ΔG_{conf}) y de las interacciones de Van der Waals (ΔG_{vdW}).

La afinidad y especificidad del polímero, dependen significativamente en la elección de los monómeros (funcional y entrecruzador), del disolvente y de la temperatura de polimerización. Los monómeros funcionales se seleccionan por la fuerza de sus interacciones con el *template* afectando a los términos $\Sigma \Delta G_p$, ΔG_h y ΔG_{t+r}. El monómero entrecruzador en la

impresión covalente y no covalente conserva la estructura de las cavidades de impresión formadas (ΔG_r) (162,163). El disolvente puede variar la entropía y la entalpia de la complejación ($\Sigma\Delta G_p$, ΔG_h) y puede mejorar las interacciones de Van der Waals (ΔG_{vdW}) si tiene lugar un buen proceso de solvatación. Además de la contribución termodinámica, el disolvente puede influir en la transferencia de masa debido a su efecto en la morfología del polímero (164). La temperatura afecta a las interacciones monómero-*template* y polímero-*template*. Temperaturas más bajas reducen los modos residuales de vibración (ΔG_{vib}) y aumentan las fuerzas de las interacciones polares ($\Sigma\Delta G_p$) (165,166). Sin embargo, en los complejos formados a bajas temperaturas pueden aumentar los cambios conformacionales (ΔG_{conf}) y las interacciones por fuerzas de Van der Waals (ΔG_{vdW}) (157).

O'Shannesy *et al.* compararon diferentes MIP sintetizados a diferentes temperaturas, comprendidas entre 0ºC y 60ºC, usando también diferentes iniciadores. Los polímeros sintetizados a bajas temperaturas demostraban mayor selectividad que los sintetizados a temperaturas altas (153). Piletsky et al. también realizaron un estudio similar de la influencia de la temperatura en la capacidad del polímero para reconocer el *template*, esta vez las temperaturas estudiadas variaban desde -30ºC a 80ºC, realizándose todos los experimentos con el mismo iniciador (157). Llegaron a la conclusión de que la temperatura juega un papel crucial en la síntesis del MIP, mejorando significativamente la afinidad y

especificidad del polímero con el descenso de la temperatura de polimerización. Asimismo, demostraron que los MIP pueden tener efecto memoria para la temperatura empleada en la síntesis, de la misma manera que se habían observado efectos memoria para el *template* o el disolvente de polimerización.

1.3.2.2. Presión de polimerización

La influencia de la presión en la etapa de polimerización ha sido estudiada por pocos grupos con resultados poco concluentes (*39*). El grupo de Sellergren estudió el efecto de la presión sobre la efectividad de los MIP modificando esta variable entre 1 y 1000 bar utilizando como medio en la polimerización tres disolventes distintos y para dos *templates*. Los resultados demostraron que los MIP polimerizados a presiones más altas presentaban mayor afinidad por el *template* (167). Este fenómeno lo asociaron con el efecto positivo de las altas presiones en las asociaciones intramoleculares de la mezcla de monómeros. La respuesta a la presión de las asociaciones intramoleculares en solución depende del cambio del volumen libre (ΔV^0) para la asociación (167):

$$\left[\frac{dRTlnK}{dP}\right]T=-\Delta V^0 \qquad \textbf{3. 2}$$

Donde K es la constante de asociación del complejo, R la constante de los gases, T la temperatura absoluta, P la presión y ΔV^0 la diferencia en el volumen ocupado por los productos y reactivos (volumen de reacción). Si la asociación intramolecular conduce a una pérdida de volumen ($\Delta V^0 < 0$), la constante de asociación (K) aumentará con la presión. Concluyeron el estudio calculando que el factor de capacidad del MIP aumentaría entre 1.1 y 2.2 veces cuando se aumentaba la presión de polimerización 1000 bar.

Por otro lado, Beuermann y Buback analizaron los coeficientes de propagación para diferentes sistemas poliméricos (168). La presión no sólo afecta a la asociación intramolecular sino que también afecta junto con la temperatura a los coeficientes de velocidad de la polimerización radical libre, descrita por la ecuación 3.3:

$$\frac{d(\ln k_p)}{dP} = \frac{\Delta V^{\#}}{RT} \qquad \textbf{3. 3}$$

Donde k_p es el coeficiente de la velocidad de propagación y $\Delta V^{\#}$ el cambio en el volumen de activación (168). Observaron que para acrilatos y metacrilatos un aumento de 1000 bar en la presión aumentaría la velocidad de propagación en un factor de 1.1, este mismo resultado se conseguiría con un aumento de la temperatura

de 30º K. Finalmente, se puede concluir que el comportamiento de asociación, las cinéticas de la reacción de polimerización o la morfología del polímero no van a ser afectadas significativamente por cambios en la presión por debajo de 100 bar (*39*).

Piletsky *et al.* también estudiaron el efecto de la presión, para ello, sintetizaron dos polímeros a 0ºC, uno a presión atmosférica y otro a 10 bar (169). Teniendo en cuenta las conclusiones de los anteriores estudios no deberían observarse diferencias entre los dos MIP, sin embargo, observaron que el polímero sintetizado a presión atmosférica contenía más enlaces dobles sin polimerizar. Además, la presión a 10 bar ayudó en la síntesis de un material transparente tipo gel. Concluyeron que la presión parece ser un parámetro importante en la polimerización, pero de forma indirecta, su influencia parece estar más unida al efecto de la presión en el punto de ebullición del disolvente.

1.3.2.3. Tiempo de polimerización

Al igual que hicieron para otros parámetros que condicionan la síntesis de los MIP y su comportamiento, Piletsky et *al*. estudiaron el efecto del tiempo de polimerización. La conclusión del estudio fue que el tiempo de polimerización es importante en la síntesis de los MIP porque determina el rendimiento y la morfología del polímero. Cuando los tiempos de polimerización son mayores, los

polímeros son más rígidos y las cavidades de unión más definidas. La etapa más crítica en la impresión y en la selectividad del MIP es la formación de las cavidades en el inicio de la polimerización (170).

Posteriormente, Mijangos et al. en un trabajo donde observaban la influencia de los parámetros de polimerización y la relación entre ellos, comprobaron que la rigidez del polímero no era favorable para la selectividad del MIP, si esta se obtiene para tiempos de polimerización cortos y altas concentraciones de iniciador. Dada la naturaleza exotérmica de la reacción, altas concentraciones de iniciador producirán altas temperaturas, no favoreciendo la selectividad (156).

1.4. Aplicaciones de los polímeros de huella molecular en técnicas de separación por afinidad

Las propiedades de los MIP los convierten en herramientas de interés para su aplicación en diferentes áreas como es el caso de las técnicas de separación y purificación, la catálisis, su implementación en sensores y biosensores y la administración de fármacos.

Las muestras cada vez más complejas en combinación con la necesidad de disminuir los límites de detección, ha incrementado la demanda de una mayor selectividad en la etapa

de pretratamiento dentro del proceso general de análisis. Los MIP proporcionan una alta afinidad, capacidad para la discriminación molecular y además estos materiales no dependen de la matriz y pueden ser aplicables en muestras acuosas y apolares. Por este motivo, los MIP son especialmente adecuados para la separación por afinidad (tabla 3.3), permitiendo la elaboración de soportes con determinada selectividad, siendo una de las áreas de aplicación de los MIP más extensamente estudiada (171). El ámbito en el que más éxito han obtenido estos materiales es en la preparación de muestra y más concretamente en la extracción en fase sólida (SPE) (172).

La impresión no covalente es el método más utilizado para los MIP utilizados en separación, debido a que facilita una síntesis adaptable y rápida, se asemeja a los mecanismos de reconocimiento molecular de receptores naturales, y además se dispone de una amplia variedad de monómeros funcionales (173).

Tabla 3. 3. Ejemplos de aplicaciones de MIP en separación por afinidad.

Aplicación	*Template*	Matriz	Ref.	Año
MIP como fase estacionaria en LC	S-naproxeno	----------	Kadhirvel *et al*. (174)	2015
	Metromidazol	Pescado	Liu *et al*. (175)	2015
	Ácido clorogénico	Madreselva	Niu *et al*. (176)	2014
	Hidrocloruro de berberina	Raiz de coptis	Li *et al*. (177)	2014
	S-DABN	----------	Dong *et al*. (178)	2014
MIP como fase estacionaria en CEC	Metil-mercurio	Agua de mar	Rodriguez-Reino *et al.* (179)	2015
	Trietacina	----------	Asir *et al*. (180)	2015
	4-Nitrofenol	----------	Wu *et al*. (181)	2015
	α-Zoplicona	----------	Zong *et al.* (182)	2015
	Bisfenol A	----------	Derazshamshir *et al.* (183)	2015
MISPE *Off-line*	Alfa cipermetrina	Suelo	Zhao *et al.* (184)	2016
	Cefalexina	Leche	Lata *et al.* (104)	2015
	Baicaileina	Plasma	He *et al.* (185)	2015

Tabla 3.3. cont. Ejemplos de aplicaciones de MIP en separación por afinidad.

Aplicación	*Template*	Matriz	Ref.	Año
MISPE *On-line*	Ion uranilo	Aguas	Fasihi *et al*. (186)	2016
	Lactato	Leche	Divya *et al*. (187)	2015
	Rosa de bengala	Azúcar	Yuan *et al.* (188)	2015
	Oxpranolol	Orina	Santos *et al*. (189)	2015
MISPE en estático	Salbutamol	Suero	Alizadeh *et al.* (190)	2016
	Cu^{2+}	Sangre bovina	Gao *et al.* (191)	2016
PE-MISPE	Cefalexina	Suero	Wu *et al.* (192)	2004
	2-Aminopiridina	Suero	Mullet *et al*. (193)	2000
DP-MISPE	Teofilina	----------	Mullet *et al.* (194)	1999
	Nicotina	Tabaco	Mullet *et al.* (195)	1999
MIP como adsorbente en SPME	Pirrol	Atún	Hashemi-Maghaddam *et al*. (196)	2016
	Colecistoquinina	Fluido cerebro-espinal	Ji *et a*l. (197)	2015
	Epinefedrina	Suero y orina	Zhang *et al.* (198)	2012
	Metil paratión	Frutas	Li *et al.* (199)	2016
	Acesulfamo	Bebidas	Moein *et al.* (200)	2015

Tabla 3.3. cont. Ejemplos de aplicaciones de MIP en separación por afinidad.

Aplicación	*Template*	Matriz	Ref.	Año
MIP como adsorbente en MSPD	Tolcoflos metil	Aguas naturales	Zhou *et al.* (201)	2015
	Quinolona	Aguas naturales	Chen *et al.* (202)	2015
	Verde malaquita	Pescado	Wang *et al.* (203)	2015
	Teofilina	Pescado	Cela-Perez *et al.* (114)	2015
	Estradiol	Leche de cabra	Ganan *et al*. (204)	2014
MIP como adsorbente en SBSE	Criomacina	Comida y leche animal	Fan *et al.* (205)	2015
	S-citalopram	Orina	Unceta *et al.* (206)	2013
	Ractopamina	Carne de cerdo	Wang *et al.* (207)	2012
	Terbutilacina	Alimentos y suelo	Hu *et al*. (208)	2010
	Nicosulfurón	Agua y suelo	Yang *et al.* (209)	2010
	L-glutamina	----------	Zhu *et al.* (210)	2008
	Monocrotofós	Suelo	Zhu *et al*. (211)	2006

1.4.1. Cromatografía líquida

La cromatografía líquida (LC) es una etapa de separación analítica en la que tiene lugar la partición de los analitos entre una fase móvil líquida y una fase estacionaria. El soporte más comúnmente utilizado como fase estacionaria son partículas microporosas de sílice permeables a la fase móvil, pudiendo también utilizar polímeros orgánicos (171).

La aplicación de los MIP en las áreas de separación por afinidad y ensayos de unión se están expandiendo gracias a su bajo coste, mayor estabilidad y la mejora en el funcionamiento. Se consideran los MIP como una alternativa a las tradicionales fases estacionarias en separación por afinidad, especialmente en cromatografía líquida (173).

El primer estudio en utilizar un adsorbente MIP como fase estacionaria en LC fue publicado por Mosbach *et al.* para la separación de derivados de aminoácidos (212). Los MIP para poder ser utilizados como fases estacionarias en cromatografía líquida, han de presentar una alta selectividad, un buen comportamiento hidrodinámico y una alta capacidad, pudiendo además mejorar la separación con la homogeneidad de las partículas MIP (213). MIP para S-naproxeno (174), metromidazol (175), hidrocloruro de berberina (176) o S-(-)-1-1'-dinaftaleno-2,2'-diamina (S-DABN) (178), entre otros, han sido utilizados satisfactoriamente como fases estacionarias en cromatografía líquida.

Una de las mayores desventajas de los MIP para su utilización como fases estacionarias en cromatografía líquida, es la excesiva anchura de los picos cromatográficos y la obtención de picos poco simétricos. Estos fenómenos son atribuidos a los altos valores de las constantes de asociación del polímero (172) y a la heterogeneidad de las cavidades de unión en los materiales impresos utilizados como fases estacionarias (214).

Por otro lado, la LC se utiliza extensamente para la evaluación y caracterización de los MIP, proporcionando un método fácil y rápido para analizar el funcionamiento de la unión de los MIP con sus correspondientes moléculas molde. A partir del comportamiento cromatográfico experimentado por el *template* respecto de las fases estacionarias impresas y no impresas es posible calcular el factor de impresión (IF), parámetro que da una idea de la selectividad del MIP (172).

1.4.2. Electrocromatografía capilar

La electrocromatografía capilar (CEC) es una técnica híbrida que combina la selectividad de la LC de partición, y la alta eficacia en la separación de la electroforesis (CE) (215). A diferencia de la cromatografía, que utiliza la presión para movilizar la fase móvil, la electrocromatografía capilar utiliza un campo eléctrico. En CE y electrocromatografía capilar (CEC) el campo eléctrico conduce un

líquido por electroósmosis a través de un capilar que contiene la fase estacionaria (216).

El pequeño volumen de los capilares y, en consecuencia, la poca cantidad de MIP necesaria, ha facilitado la aparición de diferentes aplicaciones de materiales MIP en CEC (179-183). Sin embargo, en los últimos años el uso de MIP para CEC ha sufrido un descenso, probablemente debido a la limitada reproducibilidad del empaquetamiento de la fase estacionaria o de los polímeros sintetizados como monolitos en el interior de los capilares.

1.4.3. Pretratamiento de muestra

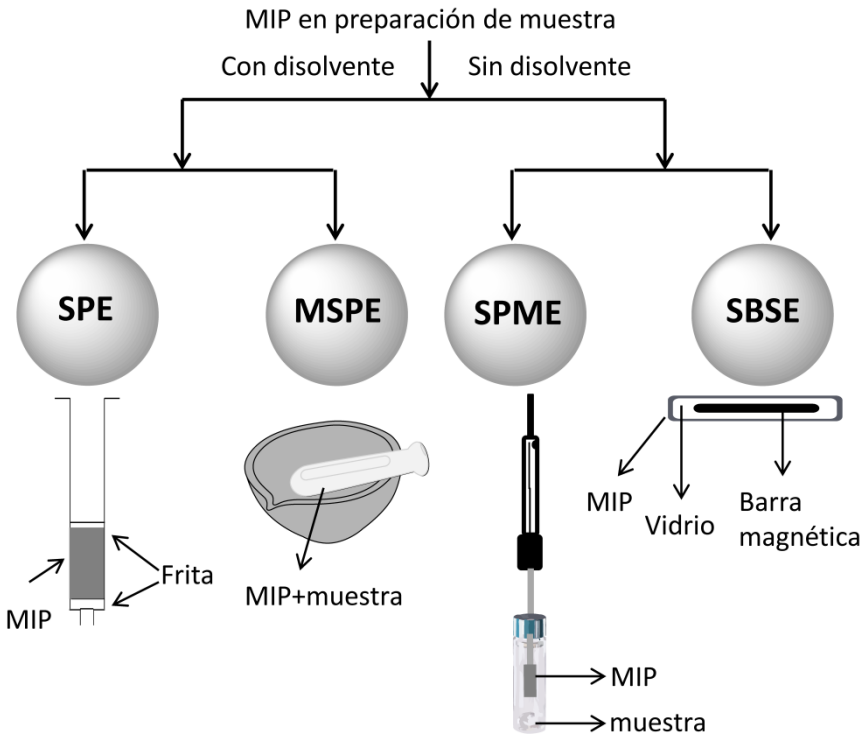

Figura 3. 4. Aplicaciones de MIP en métodos de tratamiento de muestras.

SPE: extracción en fase sólida; MSPD: dispersión de la matriz en fase sólida; SPME: microextracción en fase sólida; SBSE: Extracción por adsorción con barras magnéticas.

En los últimos años la instrumentación analítica ha sufrido un gran desarrollo permitiendo finalmente, la determinación de prácticamente cualquier compuesto en muestras ambientales, alimentarias o biológicas. Normalmente, los analitos objetivo se determinan por técnicas cromatográficas acopladas a detectores habituales como espectroscopía ultravioleta, fluorescencia o espectrometría de masas. Sin embargo, incluso cuando se utilizan detectores selectivos como el de espectrometría de masas, la inyección directa de los extractos de las muestras no está recomendada ya que los diferentes componentes de la matriz podrían inhibir o aumentar la ionización de los analitos. Por ello, la preparación de la muestra sigue siendo la etapa clave en el proceso analítico (217).

Los objetivos principales de la preparación de la muestra son la eliminación de potenciales interferentes, la preconcentración del analito, la conversión de este, si fuera necesario, en una especie más adecuada para la detección o separación y plantear un método robusto y reproducible independiente de la matriz de la muestra. En los últimos años, se vienen planteando otros objetivos secundarios, como la utilización de menores cantidades de muestra, la mejora de la selectividad en la extracción, la automatización del proceso y minimizar la cantidad de materiales y de disolventes orgánicos utilizados (218). Es evidente que la tradicional extracción líquido-líquido no cumple la mayoría de los objetivos mencionados, por ello se han

desarrollado nuevas técnicas como la extracción en fase sólida (SPE), la microextracción en fase sólida (SPME), la extracción por adsorción con barras magnéticas agitadoras (SBSE), y más recientemente la extracción por dispersión de la matriz en fase sólida (MSPD), extracción en microfase sólida (MSPE) o microextracción en fase líquida (LPME) entre otras (217).

No se ha demostrado que ninguna de estas técnicas sea mejor que las otras, sin embargo, gracias a la disponibilidad de una gran variedad de fases, SPE y SPME son las técnicas más utilizadas en los laboratorios analíticos. La mayor desventaja de estas técnicas es la falta de adsorbentes selectivos, obligando a un desarrollo exhaustivo del proceso de extracción y limpieza, que no siempre consigue evitar que algunos componentes de la matriz coeluyan con los analitos objetivo, haciendo difícil la obtención de límites de detección acordes con la exigencias actuales. Una de las alternativas propuestas a estos adsorbentes han sido los inmunoadsorbentes, anticuerpos unidos a un soporte adecuado (219). Estos inmunoadsorbentes han sido utilizados para la determinación de pesticidas (220), fármacos (221) o toxinas (222) entre otros. No obstante, la obtención de anticuerpos es difícil, lenta y cara, y además no siempre está asegurado su éxito. A esto se le añade además el hecho de que los anticuerpos se deben fijar en un soporte adecuado pudiendo acabar con una mala orientación de los mismos o con su total desnaturalización (217).

El uso de MIP como materiales adsorbentes permite desarrollar un tratamiento de la muestra más personalizado, siendo su uso en SPE (MISPE) la técnica de extracción más avanzada (223-227), aumentando en los últimos años su aplicación a otras técnicas de extracción como SPME o SBSE.

1.4.3.1. Extracción en fase sólida con adsorbente MIP

La técnica de extracción utilizando como fases sólidas materiales MIP (MISPE), ha tenido un gran desarrollo. De hecho, se pueden encontrar comercializadas fases sólidas SPE basadas en materiales impresos para su aplicación a la separación de diversos compuestos en diferentes matrices (228,229). Al mismo tiempo, la investigación sobre esta técnica de extracción sigue avanzando con un gran número de artículos dedicados a la síntesis y aplicación de MIP en SPE (227).

Sellergren en 1994 publicó por primera vez la utilización de un MIP como adsorbente SPE, para el pretratamiento de muestras de orina en la determinación del fármaco pentamidina (230). Dado que los MIP pueden mostrar reactividad cruzada con los compuestos relacionados estructuralmente con la molécula molde, estos polímeros podrían ser utilizados como adsorbentes SPE específicos para un compuesto o para un grupo de compuestos (231,232).

Diferentes modos de MISPE han sido desarrollados incluyendo SPE en estático, donde el MIP es incubado con la muestra, SPE convencional *off-line*, donde el MIP es empaquetado en cartuchos, y diferentes modos de SPE *on-line.*

Protocolo MISPE off-line:

En los métodos *off-line*, una pequeña cantidad de material impreso (15-500 mg) se empaqueta en cartuchos de poliestireno o de vidrio dependiendo de las propiedades de los analitos. Después de acondicionar el polímero, cargar la muestra y lavar los interferentes, se lleva a cabo la elución de los analitos.

En los últimos años la técnica MISPE *off-line* ha sufrido un gran desarrollo para la determinación de una gran variedad de analitos en muestras ambientales (184), muestras alimentarias (104) y fluidos biológicos (185).

Los adsorbentes MIP pueden actuar como fase normal o como fase reversa. Generalmente, la carga de la muestra se realiza en un disolvente de baja polaridad, puesto que la eficiencia de los MIP no covalentes más habituales aumenta en disolventes apolares. Después del lavado de interferencias, los analitos se eluyen en un disolvente capaz de evitar las interacciones típicas en estos materiales. Por otro lado, las muestras acuosas también se pueden cargar directamente en el cartucho, actuando esta vez como fase reversa. En principio, tanto el analito como otros

compuestos de la matriz quedaran retenidos en el polímero por interacciones no específicas con el monómero entrecruzador. Posteriormente, se usará un disolvente de lavado capaz de eluir los compuestos no deseados y de redistribuir los analitos en las cavidades específicas de unión.

Protocolo MISPE *on-line*:

Este protocolo trata de automatizar todo el proceso de análisis realizando en el mismo equipo, la preparación de la muestra, la separación cromatográfica y finalmente la detección y cuantificación. Para ello, una pequeña columna empaquetada con un material MIP (50 mg) se coloca en el *loop* de una válvula de inyección de seis puertos. Después de cargar la muestra y lavar los interferentes, los analitos se eluyen con la fase móvil y son separados cromatograficamente para su llegada al detector de manera ordenada.

Aunque este protocolo tiene ventajas claras frente al protocolo *off-line,* como son el ahorro de tiempo y disolvente, no hay muchos trabajos publicados. Probablemente debido a una mayor dificultad técnica para poder incluir la columna en el sistema de LC y por la no coincidencia del disolvente de elución con la fase móvil necesaria para su posterior separación cromatográfica (217).

Protocolo MISPE in-line:

Una alternativa a los sistemas *off-line* es el acoplamiento directo de la columna MIP al sistema de detección. De esta manera, gracias a la selectividad de los MIPs, teóricamente sería posible la extracción, preconcentración, separación y determinación en simultáneo de los analitos en matrices complejas (230). La mayor desventaja de este método es la cantidad de disolución de lavado necesaria para eliminar todos los compuestos de la matriz unidos no especificamente, lo que origina largos tiempos de análisis.

Como alternativa, Mullet y Lai propusieron un método similar con menor volumen de disolvente de elución (233), el llamado MISPE con elución pulsada (PE-MISPE). Esta metodología ha sido mejorada aplicando sucesivos pulsos de diferentes disolventes, MISPE con elución de pulso diferencial (DP-MISPE). Este proceso es más eficiente eliminando compuestos interferentes y la fracción de analito unida al adsorbente no específicamente. Tanto PE-MISPE como DP-MISPE permiten la preconcentración de analito a partir de la inyección de grandes volúmenes de muestra y proporcionan gran sensibilidad analítica gracias al pequeño volumen de elución de los analitos y la consecuente concentración de estos (234).

Protocolos MISPE en estático:

Los protocolos MISPE en estático consisten en incubar el adsorbente MIP por un tiempo en la muestra, una vez finalizado el tiempo de adsorción el material es separado por filtración y/o centrifugación y es incubado en un disolvente para la desorción de los compuestos objetivo. Desde los primeros trabajos de MISPE en estático (235), esta técnica fue desplazada por los modos *off-line*, *on-line* e *in-line*. Sin embargo, actualmente ha resurgido gracias a la utilización de partículas MIP sintetizadas en la superficie de partículas de Fe_3O_4 (MIP magnéticas) (236-239) y a la facilidad de poder separar el material de la muestra mediante un imán, evitando las laboriosas etapas de filtración y centrifugación.

Además recientemente, se ha desarrollado la técnica de extracción en microfase sólida MIP (MI-MSPE). Se trata de una técnica de extracción en estático, en la que el dispositivo utilizado consiste en una membrana porosa que sirve de soporte de las partículas del material impreso. Una vez acondicionado el material MIP implementado en la membrana, el dispositivo se coloca en la muestra en agitación durante un tiempo optimizado. Como último paso, el dispositivo se extrae de la muestra con ayuda de unas pinzas y se coloca en un vial para la elución de los analitos adsorbidos (240).

1.4.3.2. Microextracción en fase sólida con adsorbente MIP

La técnica de microextracción en fase sólida (SPME) se basa en la partición de los analitos entre la muestra y una fase estacionaria, que normalmente se trata de un recubrimiento polimérico sobre una fibra de sílice. En su origen los analitos eran desorbidos directamente en el inyector de GC, pero hoy en día a esta se le suma la posible desorción de los analitos con un disolvente para su inyección en LC (241). Al igual que pasaba en SPE, esta técnica es poco selectiva debido a que comercialmente no hay disponibilidad de gran variedad de fibras SPME. Por ello, recientemente existe un interés creciente en la síntesis de adsorbentes a medida que favorezcan la adsorción selectiva de los compuestos a analizar. En este sentido, la combinación de SPME con adsorbentes MIP proporciona una herramienta analítica de gran aplicabilidad (217).

Para la fabricación de fibras SPME con adsorbente MIP se han utilizado diferentes estrategias. En el primer trabajo que utilizaban un MIP para SPME se cubrió una fibra de sílice con el MIP (242), esta técnica no ha tenido mucho éxito, probablemente por la dificultad de controlar el grosor del polímero. Otra técnica utilizada ha sido la fabricación del polímero dentro del capilar de sílice y posteriormente esta era eliminada, obteniéndose un polímero con un grosor fijado por el molde (243). Por otro lado también se han utilizado para SPME, partículas MIP encapsuladas en un capilar de poliéter éter cetona (PEEK) (244). Yu y Lai (245)

han utilizado como fibras para SPME, un MIP electropolimerizado sobre acero inoxidable. En los últimos años se han utilizado también MIP monolíticos (196-198) y MIP preparados mediante la técnica sol-gel (199,200).

1.4.3.3. Dispersión de la matriz en fase sólida con adsorbente MIP

La técnica de extracción por dispersión de la matriz en fase sólida (MSPD) se basa en la completa ruptura de la muestra viscosa (líquida, semi-sólida o sólida), permitiendo su dispersión en el adsorbente sólido. La muestra es disgregada o molida y mezclada en un mortero con el polímero impreso hasta que se obtiene su completa dispersión. La mezcla es posteriormente empaquetada en un cartucho vacío para SPE. Después del lavado de interferencias se eluyen los analitos adsorbidos. Este método ha sido utilizado entre otros, para la extracción de pesticidas organofosforados (201) y fluoroquinonas (202) en aguas, el colorante verde malaquita (203) y productos de degradación de ATP (114) en diferentes animales acuáticos o esteroides en leche de cabra (204).

1.4.3.4. Extracción por adsorción con barras magnéticas agitadoras con adsorbentes MIP

Esta técnica también se basa en la partición de los compuestos entre la muestra y el polímero que recubre la barra magnética. En general, el rendimiento del proceso de extracción por SBSE es mayor en comparación a SPME, gracias a la mayor superficie polímerica. Por otro lado, esta mayor superficie conlleva cinéticas de extracción más lentas y como consecuencia de ello, la extracción junto con los analitos objetivo, de compuestos no deseados. Durante muchos años solo se podían encontrar barras magnéticas recubiertas por polidimetilsiloxano (PDMS), restringiendo el uso de estas barras al análisis de compuestos apolares, hoy en día, también se comercializan barras magnéticas recubiertas por un copolímero de PDMS y etilenglicol, ampliando el rango de compuestos a aquellos que pueden dar uniones por formación de puentes de hidrógeno. Estos recubrimientos se basan en todos los casos en la adsorción inespecífica y no selectiva, por lo que vuelve a resultar de interés la unión de esta técnica con polímeros específicos y selectivos como los materiales MIP.

El uso de polímeros MIP como recubrimiento de barras magnéticas, puede mejorar la capacidad selectiva de extracción del analito y minimizar la presencia de interferencias provenientes de la matriz. Se han desarrollado barras magnéticas recubiertas con polímero MIP para la extracción de melamina en alimentos para

animales y leche (205), para la extracción enantioselectiva de S-citalopram y sus metabolitos de la orina (206), para la extracción de ractopamina de carne de cerdo (207), para la extracción de herbicidas de triazina de muestras de alimentos y suelos (208), para la extracción de nicosulfirón de muestras de agua y suelo (209), para la extracción enantioselectiva de L-glutamina (210) o para la extracción de monocrotofós de muestras de suelo (211).

2. Objetivos

Los fenoles volátiles como el 4-etilfenol (4EP) y su precursor el 4-vinilfenol (4VPh) tienen un impacto importante en el aroma del vino. En altas concentraciones están relacionados con aromas indeseables y otros defectos del vino. Además de estos fenoles en el vino también pueden estar presentes otros precursores en su ruta metabólica, el ester etílico del ácido cumárico y el ácido cumárico. Esta ruta metabólica tiene lugar debido a la presencia en el vino de las levaduras del género *Brettanomyces/Dekkera* sp. Evaluando las concentraciones de 4-etilfenol y el resto de los compuestos de su ruta metabólica se puede controlar la actividad de estos microorganismos, antes de llegar a concentraciones de los fenoles volátiles que hagan que el vino no sea apto para su consumo.

En este sentido el objetivo principal de este trabajo engloba el diseño de un método de extracción en fase sólida basado en polímeros MIP para los compuestos pertenecientes a la ruta metabólica del 4-etilfenol y para su posterior separación por cromatografía líquida de forma que sea posible su cuantificación en vino.

Para alcanzar este objetivo principal, es necesario el cumplimiento de los siguientes objetivos metodológicos:

- Síntesis y caracterización de un polímero de huella molecular para el grupo de compuestos que constituyen la ruta metabólica del 4-etilfenol.
- Desarrollo de un método de extracción en fase sólida utilizando como sólido adsorbente el polímero impreso sintetizado (MISPE).
- Síntesis y caracterización de un polímero de huella molecular que pueda ser utilizado como fase estacionaria para la correcta separación por cromatografía de líquidos, de los compuestos pertenecientes a la ruta metabólica del 4-etifenol.
- Desarrollo de un método cromatográfico usando como fase estacionaria el polímero sintetizado, para la cuantificación de los compuestos objetivo en muestras de vino.

3. Material y equipamiento

En este apartado se detallará el material utilizado en la síntesis de los polímeros de huella molecular, así como el equipamiento necesario para su caracterización y aplicación en técnicas de separación cromatográficas y no cromatográficas.

3.1. Reactivos y disolventes

Los patrones 4-etilfenol (4EP) (99.7 %) y 4-etilguaiacol (4EG) (≥98 %) fueron obtenidos de Sigma-Aldrich (Madrid, España), el éster etílico del ácido cumárico (CAEE) (≥90 %) fue adquirido en LGC Standards (Barcelona, España) y el 4-vinilfenol (4VPh) (10 % en etilenglicol) y el ácido cúmarico (CA) (≥ 90%) en Cymit Química (Barcelona, España).

Los monómeros entrecruzadores trimetacrilato de trimetilpropano (TRIM), divinilbenceno (DVB) y dimetacrilato de etileno (EDMA) y el iniciador 1,1'-azobis(ciclohexanocarbonitrilo) y los monómeros funcionales 4-vinilpiridina (4VPy), fosfato de etilenglicol metacrilato (EGMP), acrilamida (AA), ácido metacrílico (MA), ácido itacónico (IA) y estireno (Sty) fueron adquiridos en Sigma-Aldrich. Dado que el monómero 4VPy es facilmente polimerizable, antes de su uso se destilaba para su purificación a

vacío obteniendo un líquido transparente, que era almacenado a –20ºC y en atmósfera inerte de nitrógeno hasta su uso.

Los reactivos formiato amónico (>99 %) y ácido fórmico (≥98%) de grado de espectrometría de masas fueron adquiridos en Sigma-Aldrich. Los disolventes de grado (HPLC) acetonitrilo (ACN), metanol (MeOH), diclorometano (DCM), tolueno (TLN), dimetil sulfóxido (DMSO) y dimetilformamida (DMF) se adquirieron en Scharlab (Barcelona, España).

Todos los medios tamponados fueron preparados con agua previamente desmineralizada mediante ósmosis inversa Elix20 y purificada por un sistema de filtración MilliQ de Millipore (Milford, USA).

3.2. Equipamiento

La síntesis de los polímeros molecularmente impresos se realizó por radiación UV con una lámpara modeloUVAcube 100 UV (100 W) de la casa comercial Dr. Hönle (Gräfelfing, Alemania). Una vez sintetizados, los polímeros en bloque eran molidos con un molino Pulverisette 14 de Fristch (Idar-Oberstein, Alemania).

La evaluación del material impreso y las posteriores medidas analíticas se realizaron mediante un sistema de cromatrografía de líquidos de la serie 1200 de Agilent Technologies (Palo Alto, EE.UU.) provisto con una bomba binaria Agilent 1260,

un desgasificador de vacío y un inyector manual Rheodyne con un *loop* de 20 µL. Este sistema estaba acoplado a un detector de línea de fotodiodos y a un detector de fluorescencia, conectados en serie. Para el control del sistema y el análisis de datos se uso el software Agilent LC ChemStation (Agilent Technologies). Para poder usar los polímeros impresos como fases estacionarias en este sistema cromatográfico, se empaquetaron en columnas vacías de acero inoxidable de 100 y 250 mm de largo y 4.6 mm de diámetro (Phenomenex-Micron Analítica, Madrid, España) mediante el sistema de empaquetado Pack in a Box de Restek (Bellefonte, USA), que está formado por una bomba de pistón dual y un reservorio de 20 mL. Para los ensayos de unión se utilizó un agitador de tubos MovilROB (P. Selecta, Barcelona, España)

En los ensayos de extracción en fase sólida (SPE) se usaron tubos de propileno vacíos de 6 ml con fritas de polietileno (Sigma-Aldrich). El control del proceso de extracción en fase sólida se realizó en un colector a vacío de la casa comercial Varian (Lake Forrest, California) conectado a una bomba de vacío para el control de la presión.

4. Desarrollo y evaluación de polímeros molecularmente impresos específicos para los compuestos que forman parte de la ruta metabólica del 4-etilfenol.

Los fenoles volátiles 4-vinilfenol, 4-vinilguayacol, 4-etilfenol y 4-etilguayacol tienen una gran influencia en las propiedades organolépticas de los vinos (246). Aunque a bajas concentraciones, pueden contribuir a la complejidad aromática del vino, a mayores concentraciones enmascaran su perfil sensorial con olores y sabores desagradables (247). Normalmente, estos compuestos se generan por la actividad de levaduras del género *Dekkera/Brettanomyces.* Cuando un vino posee estas características, se dice que tiene un carácter "brett", que se manifiesta por la presencia de aromas fenólicos, de tinta, de cuero, medicinales y en ocasiones asociados a una sensación de ahumado, sudor de caballo, establo u olor a ratón.

Durante la fermentación del vino los ácidos ferúlico y cumárico se pueden transformar en 4-vinilguayacol y 4-vinilfenol por medio de la enzima hidroxicinamato descarboxilasa (figura 3.5). Esta enzima se puede encontrar en una gran variedad de microorganismos como *Saccharomices cerevisiae*, bacterias del ácido láctico, bacterias del ácido acético y *Brettanomyces/Dekkera* sp. Estos vinilfenoles pueden ser reducidos a sus derivados 4-

etilguayacol y 4-etilfenol, mediante la enzima vinilfenol reductasa (figura 3.5) que es producida por la levadura *Brettanomyces/Dekkera* sp. (247). La producción de 4-vinilfenol y 4-etilfenol partiendo de su precursor, el ácido cumárico, es la reacción predominante en términos de frecuencia y cantidad (248).

En los últimos años se ha descubierto que las levaduras *Brettanomyces/Dekkera* poseen actividad esterasa, pudiendo transformar esteres hidroxicinámicos en los precursores de los fenoles volátiles, los ácidos hidroxicinámicos. El compuesto, etil ester del ácido cumárico puede contribuir al aumento de la concentración de 4-etilfenol presente en un vino madurado en presencia de estas levaduras (249). En conclusión, la mayor producción de 4-etilfenol está definida por la relativa cantidad de ácido cumárico libre presente en la uva o liberado por reacciones enzimáticas durante la maduración y por el etil ester del ácido cumárico producido durante la vinificación y la maduración (249).

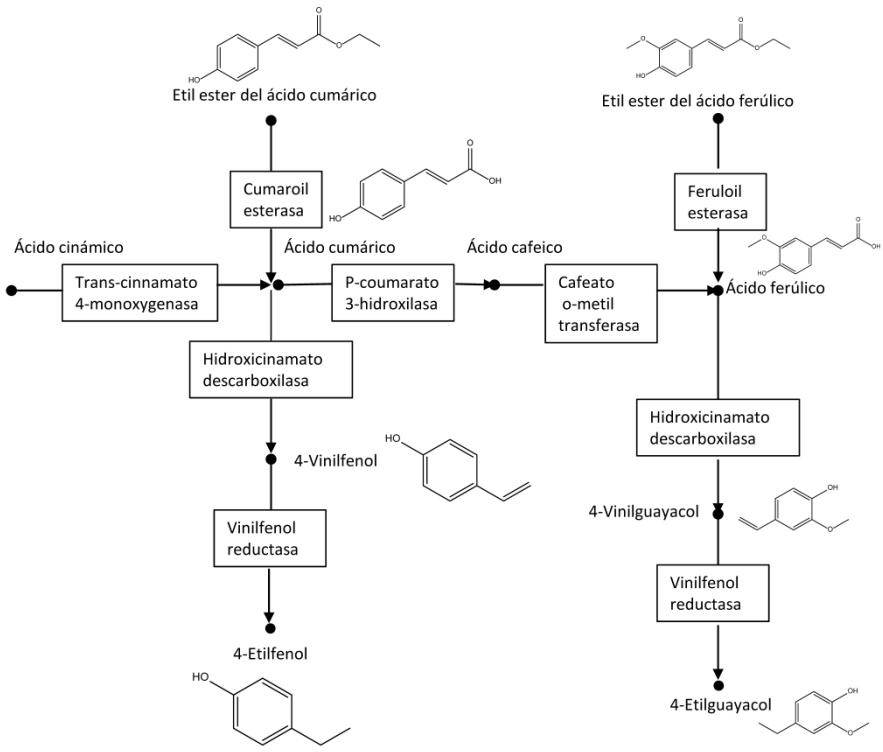

Figura 3. 5. Ruta metabólica del 4-etilfenol y 4-etilguayacol.

La aparición del carácter brett, es el indicador del deterioro organoléptico de un vino. Cualquier herramienta diseñada para la detección de las etapas previas a la aparición de estos compuestos, resultaría de gran utilidad en bodega para establecer medidas correctoras que evitaran la presencia de *Brettanomyces/Dekkera.*

En este trabajo se sintetizaron dos polímeros impresos con el objetivo de desarrollar una metodología analítica, que permitiera la extracción y el análisis cromatográfico de los compuestos fenólicos que pertenecen a la ruta metabólica del 4EP en vinos.

En primer lugar se desarrolló un polímero impreso utilizando como molécula template el compuesto 4EP (MIP_{4EP}). Este material fue utilizado como fase sólida para la extracción del vino, de aquellos fenoles que constituyen la ruta metabólica del 4EP. También se desarrolló un MIP usando el compuesto ácido cumárico como *template* (MIP_{CA}). Este polímero impreso fue posteriormente utilizado como fase estacionaria en la separación cromatográfica de los citados compuestos.

4.1. Desarrollo y evaluación de un polímero molecularmente impreso para el compuesto 4-etil fenol

En el desarrollo de un polímero molecularmente impreso para el compuesto 4-etil fenol (4EP), se probaron diferentes monómeros funcionales y entrecruzadores y diferentes proporciones de éstos respecto al *template* en la composición del polímero. Para la selección del monómero funcional se ensayaron monómeros que pudieran formar enlaces por puentes de hidrógeno y/o enlaces π-π con el 4EP. Como monómeros entrecruzadores se ensayaron los

más habitualmente utilizados, etilen dimetacrilato (EDMA), trimetacrilato de trimetilolpropano (TRIM) y divinil benceno (DVB).

4.1.1. Selección del monómero funcional

La selección del monómero funcional es una etapa clave en la síntesis de materiales impresos MIP, ya que es el componente que principalmente se encuentra involucrado en la formación de enlaces químicos efectivos con la molécula huella. Una buena interacción entre el monómero funcional y el *template* representa la condición preliminar esencial para obtener redes MIP con sitios potenciales de reconocimiento. Inicialmente y con el fin de conocer qué monómero funcional mostraba una mayor afinidad por la molécula de 4EP, se sintetizaron diferentes polímeros no impresos (NIP) utilizando como monómeros funcionales 4-vinilpiridina (4VPy), fosfato de etilenglicol metacrilato (EGMP), acrilamida (AA), ácido metacrílico (MA) o ácido itacónico (IA). Adicionalmente, se sintetizaron otros dos polímeros usando mezclas de acrilamida y estireno por un lado y acrilamida y 4-vinilpiridina por otro.

Para la síntesis de cada polímero se utilizó dimetacrilato de etileno (EDMA) como entrecruzador debido a su carácter polar, acetonitrilo como porógeno al 100% en peso respecto al peso de los monómeros y como iniciador 1,1'-

azobis(ciclohexanocarbonitrilo) (ABCN) al 1 % en peso respecto al peso de los monómeros. En los ensayos realizados con el monómero funcional IA, al presentar baja solubilidad en acetonitrilo se utilizó como disolvente dimetil formamida (DMF).

En todos los casos se seleccionó una relación molar monómero funcional: entrecruzador 1:4 y en el caso de la mezcla, la relación fue FM_1:FM_2: CL 1:1:8. (tabla 3.4).

Tabla 3. 4. Composición de las diferentes mezclas de polimerización ensayadas en la síntesis de cada material no impreso.

Polímero	Monómero Funcional (0.0050 mol)	Entrecruzador (EDMA) (0.0202 mol)	Porógeno	Iniciador (ABCN)
$FM_1$4VPy	4VPy 0.526 g	4 g	4.526 g	0.045 g
FM_2EGMP	EGMP 1.077 g	4 g	5.077 g	0.050 g
FM_3AA	AA 0.363 g	4 g	4.363 g	0.044 g
FM_4MA	MA 0.44 g	4 g	4.440 g	0.044 g
FM_5IA	IA 0.666 g	4 g	4.666 g	0.047 g
FM_6AASty	AA /Sty 0.182 g/ 0.267 g	4g	4.448 g	0.044 g
FM_7AA4VPy	AA /4VPy 0.182 g/ 0.168 g	4 g	4.350 g	0.044 g

Una vez disueltas las cantidades fijadas de los monómeros en el porógeno previamente desoxigenado con nitrógeno durante 30 min, se añadía el iniciador y se desoxigenaba nuevamente durante 1 minuto. Posteriormente se realizaba la síntesis por polimerización radical iniciada fotoquímicamente por radiación ultravioleta durante 120 min, manteniendo la mezcla en un baño de hielo para evitar el aumento de la temperatura durante la polimerización. El polímero resultante se trituraba automáticamente con un molino y el polvo obtenido se tamizaba en húmedo con metanol. Se emplearon para tal fin tamices de 25 y 50 µm de paso de luz. Con el fin de estudiar la afinidad de cada uno de los polímeros no impresos con la molécula del 4EP, estas micropartículas NIP fueron utilizadas como fases estacionarias en cromatografía líquida. Para ello fueron empacadas en columnas cromatográficas de acero inoxidable de 100 mm de longitud y 4.6 mm de diámetro.

El empaquetado se llevó a cabo a flujo constante de 20 mL/min empleando como disolvente acetonitrilo. Este disolvente, accionado por una bomba, moviliza hacia la columna las micropartículas de polímero previamente suspendidas en acetonitrilo y añadidas al reservorio de la estación de empaquetado. La presión alcanzada en el sistema fue de 1000 psi a lo largo de todo el proceso.

Posteriormente estas columnas fueron conectadas al sistema de cromatografía y se realizaron los ensayos de afinidad

utilizando como fase móvil los disolventes acetonitrilo, metanol o diclorometano. Los resultados obtenidos quedan recogidos en la figura 3.6.

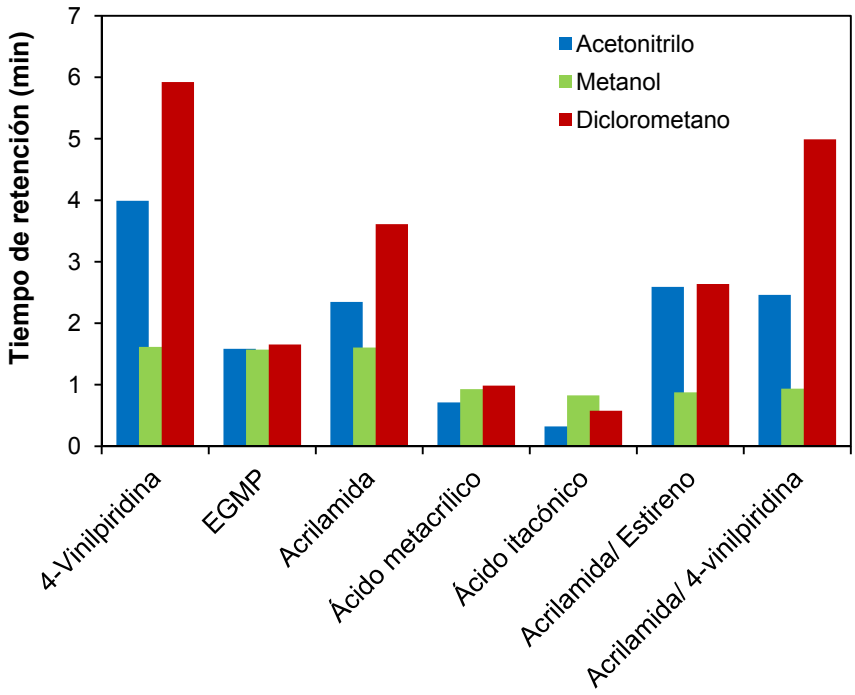

Figura 3. 6. Tiempos de retención para el 4EP utilizando como fases estacionarias materiales no impresos sintetizados con diferentes monómeros funcionales.

Se pudo observar, como el compuesto 4EP mostraba mayores tiempos de retención para el polímero sintetizado utilizando 4-vinilpiridina como monómero funcional ($FM_1$4VPy) y cuando se utilizaban los disolventes acetonitrilo o diclorometano como fases móviles. También se pudo comprobar como para el disolvente metanol no tenía lugar la retención del 4EP en ninguno de los polímeros sintetizados, por lo que se descartó como fase móvil para futuras pruebas. Sin embargo a la vista de estos resultados, este disolvente sí podría ser utilizado en la etapa de lavado de la molécula plantilla en las siguientes pruebas a realizar con los polímeros impresos para la molécula 4EP (MIP_{4EP}). Las mayores retenciones observadas podrían explicarse ya que el monómero 4VPy además de unirse con el 4EP por enlaces por puentes de hidrógeno con el grupo hidroxilo, ambas moléculas aromáticas podrían interactuar también por uniones π-π. Teniendo en cuenta estos resultados y el hecho de que la 4VPy, también había sido utilizada por otros autores para la síntesis de materiales impresos para compuestos fenólicos (250-258), se seleccionó como monómero funcional para los siguientes ensayos.

4.1.2. Selección del porógeno

Para evaluar el efecto de la polaridad del porógeno en la eficacia del material impreso se sintetizaron diferentes MIP_{4EP} en acetonitrilo, diclorometano y tolueno y se evaluaron utilizándose como fases estacionarias en cromatografía líquida.

Estos polímeros se sintetizaron manteniendo las mismas relaciones comentadas anteriormente pero ahora en presencia de la molécula 4EP. Se disolvieron 0.122 g de 4EP (0.0010 mol), 0.421 g de 4VPy (0.0040 mol) y 4 g de EDMA (0.0202 mol) en 4.543 g de porógeno (ACN, DCM o TLN) previamente desoxigenado con nitrógeno. Una vez disueltos los componentes se añadía 0.045 g del iniciador ABCN y se desoxigenaba la mezcla durante 1 minuto. Los polímeros una vez sintetizados, se molieron, tamizaron y empacaron para su utilización como fases estacionarias en cromatografía líquida. Antes de comenzar los ensayos de afinidad y para eliminar la presencia de 4EP del polímero impreso se realizaba un lavado utilizando MeOH como fase móvil a un flujo de 1mL/min durante 60 minutos.

Para cada uno de los polímeros impresos MIP_{4EP} se sintetizó un polímero no impreso NIP, usando las mismas proporciones pero sin añadir a la mezcla 4EP.

Para la evaluación de la afinidad de los polímeros por cromatografía líquida, se compararon los tiempos de retención de la molécula objetivo en las fases estacionarias impresas (MIP) y no

impresas (NIP) empleando como fases móviles acetonitrilo, metanol y diclorometano (figura 3.7). La diferencia entre estos tiempos de retención indicaría la existencia de interacciones específicas entre el *template* y las cavidades impresas. Habitualmente, el grado de este tipo de interacciones, se cuantifica por el factor de impresión (IF), el cual se calcula a partir de los factores de retención de la molécula plantilla en la columna MIP y NIP a partir de la expresión

$$IF = \frac{K_{MIP}}{K_{NIP}} \qquad \textbf{3. 4}$$

El factor de retención (K) para cada caso se calculó utilizando la expresión

$$K = (t_R - t_0)/t_0 \qquad \textbf{3. 5}$$

Donde t_R y t_0 son el tiempo de retención del analito y el tiempo muerto respectivamente.

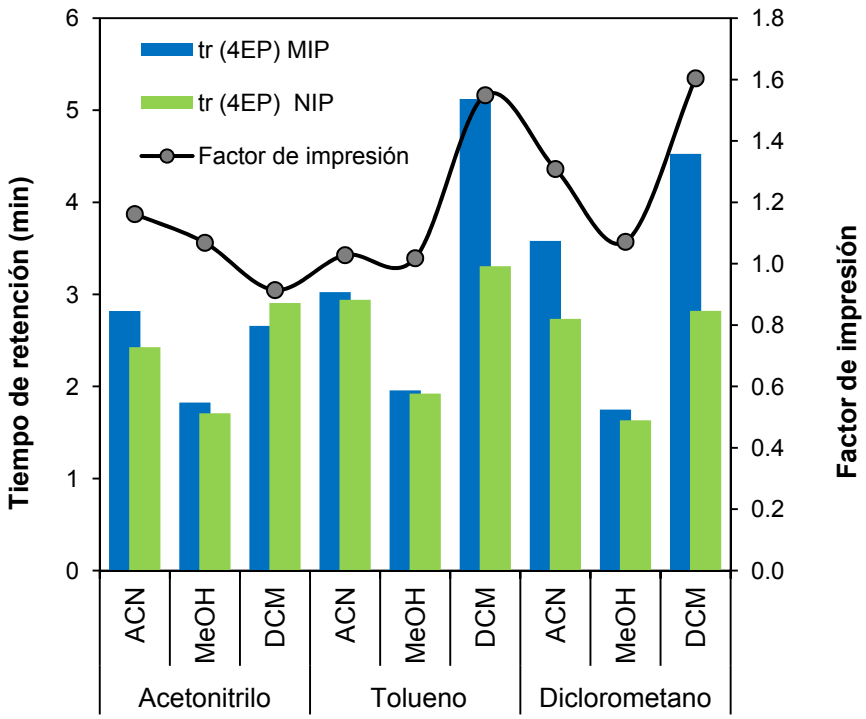

Figura 3. 7. Tiempos de retención y factores de impresión para el 4EP en las fases estacionarias impresas y no impresas sintetizadas en ACN, TLN o DCM y usando como fase móvil ACN, MeOH o DCM.

Los resultados obtenidos con los polímeros sintetizados en TLN y DCM fueron muy similares. Sin embargo en el caso del polímero impreso en DCM, se obtienen los mejores factores de impresión cuando también se utiliza este disolvente como fase móvil. Por otro lado, el MIP_{4EP} sintetizado en ACN, porógeno más polar, fue el que mostró menor afinidad por el 4EP. De acuerdo a los resultados obtenidos, fue el DCM el disolvente que se escogió

como porógeno más adecuado para la síntesis del material impreso MIP_{4EP}.

4.1.3. Optimización de la composición del polímero

Como último paso en el desarrollo del MIP_{4EP} se optimizaron la relación molar *template*: monómero funcional (T:FM), el tipo de entrecruzador y su relación molar respecto al monónero funcional. Para ello se sintetizaron diferentes polímeros impresos MIP_{4EP} y no impresos NIP, utilizando distintas relaciones *template*: monómero funcional: entrecruzador (tabla 3.5).

Tabla 3. 5. Composiciones ensayadas en las mezclas de polimerización para la síntesis de los materiales impresos

Polímero	Relación molar T:FM:CL	4EP	4VPy	Entrecruzador
$MIP_{4EP}EDMA1$	1:2:6	3.37 mmol 0.411 g	6.74 mmol 0.709 g	EDMA 20.2 mmol 4 g
$MIP_{4EP}EDMA2$	1:3:9	2.24 mmol 0.274 g	6.74 mmol 0.709 g	
$MIP_{4EP}EDMA3$	1:4:12	1.68 mmol 0.206 g	6.74 mmol 0.709 g	
$MIP_{4EP}EDMA4$	1:6:18	1.12 mmol 0.137 g	6.74 mmol 0.709 g	EDMA 20.2 mmol 4 g
$MIP_{4EP}EDMA5$	1:2:4	5.05 mmol 0.617 g	10.1 mmol 1.062	
$MIP_{4EP}EDMA6$	1:2:8	2.53 mmol 0.309 g	5.05 mmol 0.530	
$MIP_{4EP}EDMA7$	1:2:12	1.68 mmol 0.206 g	3.37 mmol 0.354 g	

Tabla 3. 5. cont. Composiciones ensayadas en las mezclas de polimerización para la síntesis de los materiales impresos

Polímero	Relación molar T:FM:CL	4EP	4VPy	Entrecruzador
MIP_{4EP}TRIM1	1:2:4	2.96 mmol 0.361 g	5.91 mmol 0.621 g	TRIM 11.82 mmol 4 g
MIP_{4EP}TRIM2	1:2:6	1.97 mmol 0.241 g	3.94 mmol 0.414 g	
MIP_{4EP}TRIM3	1:2:8	1.48 mmol 0.180 g	2.96 mmol 0.311 g	
MIP_{4EP}TRIM4	1:2:12	0.99 mmol 0.120 g	1.97 mmol 0.207 g	
MIP_{4EP}DVB1	1:2:4	7.68 mmol 0.938 g	15.43 mmol 1.614 g	DVB 30.72 mmol 4 g
MIP_{4EP}DVB2	1:2:6	5.12 mmol 0.625 g	10.24 mmol 1.077 g	
MIP_{4EP}DVB3	1:2:8	3.84 mmol 0.469 g	7.68 mmol 0.807 g	
MIP_{4EP}DVB4	1:2:12	2.56 mmol 0.313 g	5.12 mmol 0.538 g	

En todos los casos el porógeno utilizado fue DCM al 100% en peso respecto de la masa de los monómeros y el iniciador 1,1'-azobis(ciclohexanocarbonitrilo) se añadió al 1% en peso respecto de la masa de los monómeros. Después de la síntesis, molido y tamizado de los polímeros, estos fueron evaluados utilizándolos como fases estacionarias en cromatografía líquida.

En primer lugar y para seleccionar la relación molar más adecuada entre el *template* y el monómero funcional, se evaluaron los polímeros sintetizados con el monómero entrecruzador EDMA y que mantenían constante la relación molar monómero funcional:entrecruzador 1:3 (los polímeros MIP_{4EP}EDMA1, MIP_{4EP}EDMA2, MIP_{4EP}EDMA3 y MIP_{4EP}EDMA4). Los mejores resultados para los factores de impresión se obtuvieron cuando se utilizaba como fase estacionaria el material impreso MIP_{4EP}EDMA1, por lo que se fijó la relación molar *template*: monómero funcional 1:2 (figura 3.8).

El monómero entrecruzador (CL) juega un papel muy importante para la habilidad de reconocimiento del MIP y en sus propiedades fisicoquímicas, (259). La polaridad del polímero está relacionada con la naturaleza del entrecruzador (260), siendo también el máximo responsable de las interacciones no específicas e hidrofóbicas habitualmente presentes en los MIP.

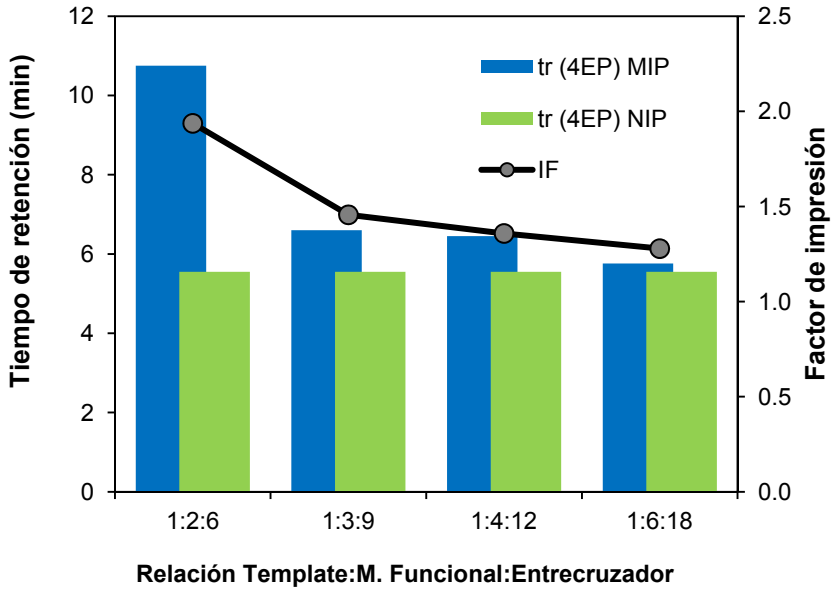

Figura 3. 8. Tiempos de retención y factores de impresión para el 4EP en las fases estacionarias impresas y no impresas variando la relación *template*:monómero funcional.

Para la selección del monómero entrecruzador y su relación molar respecto al monómero funcional, se seleccionaron como entrecruzadores del aducto entre el monómero 4VPy y el *template*, divinil benceno (DVB), trimetacrilato de trimetilolpropano (TRIM) y etilen dimetacrilato (EDMA). Los factores de impresión para los polímeros sintetizados con DVB y EDMA eran mayores que los obtenidos con TRIM, entrecruzador que fue descartado para posteriores experimentos debido a los bajos valores de los factores

de impresión obtenidos para estos materiales (figura 3.9). En cualquier caso los valores obtenidos para los factores de impresión en las mejores condiciones eran muy próximos a 2, valor modesto para un material impreso. Esto podría deberse a la baja funcionalidad del *template* (presencia sólo de un grupo hidroxilo) y a su débil acidez. Sin embargo, un valor de factor de impacto de 2 puede considerarse suficiente para demostrar el efecto de impresión en el polímero y también para conseguir un material capaz de extraer la molécula objetivo de la muestra. Los polímeros entrecruzados tanto con DVB como con EDMA obtuvieron valores de IF similares, sin embargo, los tiempos de retención observados en el polímero sintetizado con EDMA eran mayores, probablemente gracias a la mayor polaridad de este monómero entrecruzador. Por ello, fue el seleccionado, para minimizar las posibles uniones inespecíficas e hidrofóbicas y para conseguir un polímero más compatible con el agua, teniendo en cuenta que la aplicación final seria la extracción de los compuestos en muestras de vino. Teniendo en cuenta los mejores valores para el factor de impresión se seleccionó como óptima para la composición del polímero una relación molar 1:2:6.

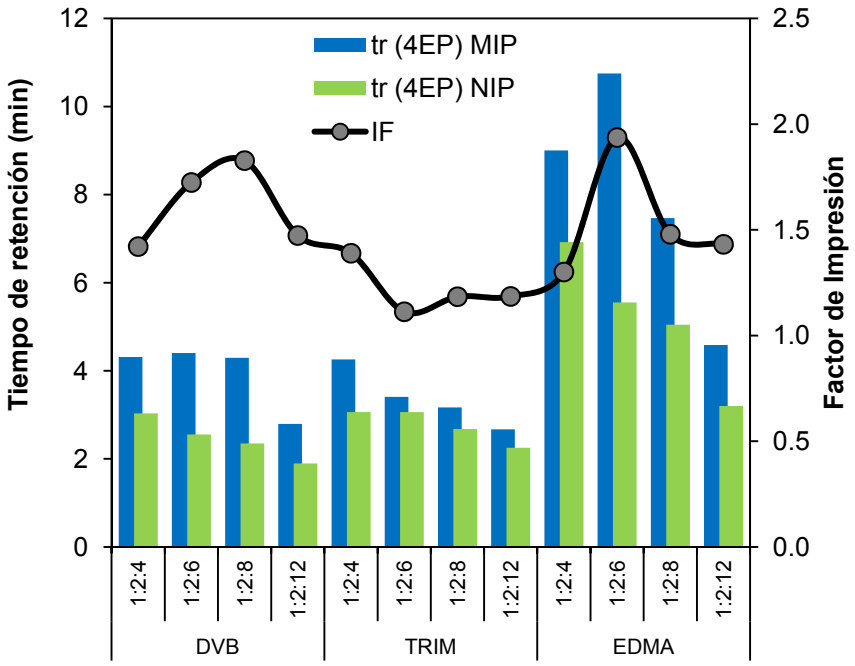

Figura 3. 9. Tiempos de retención y sus correspondientes IF para 4EP registrados con columnas empaquetadas con materiales MIP y NIP sintetizados con diferentes relacioness de template: monómero funcional: monómero entrecruzador.

4.2. Evaluación de la capacidad del polímero molecularmente impreso para el 4-etilfenol.

Una vez optimizada la composición del material impreso MIP_{4EP}, se realizó a partir de los ensayos de unión, la evaluación de la impresión del polímero, lo que permitió conocer las propiedades de los sitios de unión así como su afinidad y selectividad por la molécula *template*. Además y para evaluar la capacidad del polímero para la extracción de los compuestos pertenecientes a la ruta metabólica del 4EP y su selectividad, se realizaron ensayos en estático usando como fase estacionaria el polímero de huella molecular MIP_{4EP}.

4.2.1. Capacidad y selectividad del polímero

Teniendo en cuenta que el objetivo final del polímero desarrollado era su utilización como fase sólida para la extracción del 4EP y los compuestos pertenecientes a su ruta metabólica, inicialmente se evaluó su capacidad para la retención de los compuestos 4EP, 4VPh, CA y CAEE. Para ello se estudió el comportamiento de estos compuestos por cromatografía líquida utilizando como fase estacionaria el polímero impreso MIP_{4EP} y como fase móvil diclorometano. Adicionalmente, se evaluó la selectividad del polímero para el 4EG, compuesto potencialmente interferente, ya

que aunque no pertenece a la ruta del 4EP, presenta una estructura análoga y también puede estar presente en el vino.

En la figura 3.10 se muestra el desarrollo cromatográfico para la separación de cada uno de los compuestos considerados. Para los compuestos pertenencientes a la ruta metabólica, el 4EP era el compuesto menos retenido presentando un tiempo de retención de 11.1 min. Los tiempos de retención para el CAEE y el 4VPh fueron 16.6 y 19.8 minutos respectivamente, permaneciendo totalmente retenido en el polímero el compuesto CA. Cuando el acetonitrilo era utilizado como fase móvil, los compuestos presentaban tiempos de retención menores que para el caso del diclorometano, excepto para el ácido cumárico que también permanecía totalmente retenido con esta fase móvil.

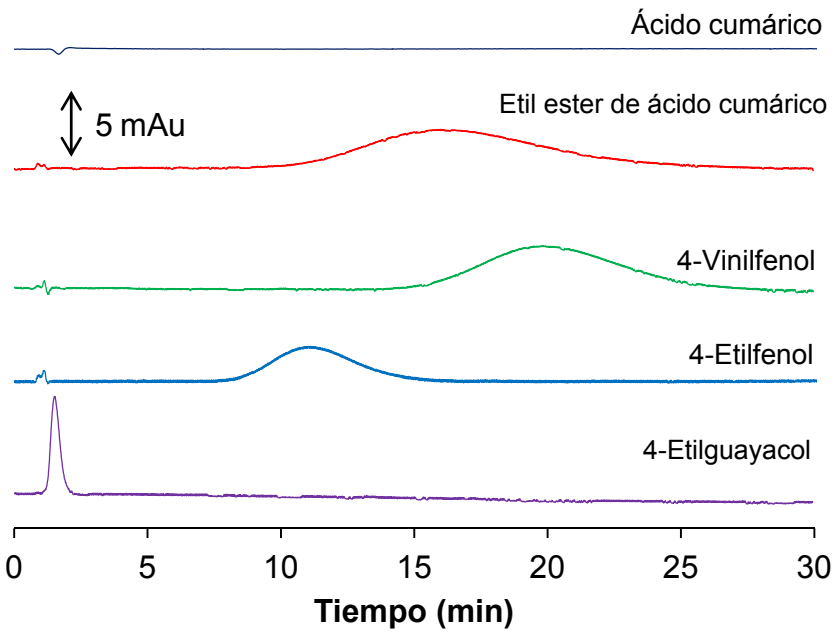

Figura 3. 10. Cromatogramas registrados para una disolución de 10 mg L^{-1} de 4EG, 4EP, 4VPh, CAEE y CA. En todos los casos como fase estacionaria se utilizó el material impreso para el 4EP y como fase móvil diclorometano.

El 4EP en comparación con sus precursores, es un compuesto pequeño y poco funcionalizado, presentando sólo un grupo hidroxilo. En cambio, CA, 4VPh y CAEE disponen de más grupos polares que podrían interactuar no específicamente con el polímero. La razón para la obtención de tiempos de retención ligeramente mayores para 4VPh y CAEE puede radicar en las uniones no específicas que se pueden generar con los monómeros funcionales distribuidos aleatoriamente en el polímero, fuera de

los sitios de unión. Por otro lado, el CA permanece totalmente retenido gracias al grupo carboxílo que puede formar uniones iónicas con el monómero básico 4VPy (*2*). Finalmente, no se observó retención para el 4EG, por lo que se puede concluir que este polímero retiene selectivamente los compuestos de la ruta metabólica del 4EP en comparación con un compuesto estructuralmente análogo.

4.2.2. Ensayos de unión

La capacidad de reconocimiento molecular del MIP se basa en la formación de cavidades creadas por el *template* durante la síntesis polimérica. En el caso de los MIP no covalentes, no se puede hablar de cavidades de reconocimiento idénticas en el polímero formado, sino que se habla de sitios de unión similares entre sí con diferente capacidad de reconocimiento. Mediante los ensayos de unión, se pueden calcular diferentes parámetros descriptivos de los MIP como el número de sitios de unión y su heterogeneidad. Estos datos resultan indispensables para evaluar tanto el efecto de impresión del polímero como la reactividad cruzada del material impreso.

4.2.2.1. Isotermas de unión

Las isotermas de unión son representaciones gráficas del comportamiento en el reconocimiento-concentración dependiente que presenta un sistema. Se representa la relación existente entre la concentración de analito libre en disolución (F) y la del analito unido a la fase estacionaria (B).

Para la obtención de las isotermas de unión se han desarrollado distintos procedimientos, siendo los más comunes los ensayos en estático y por cromatografía frontal. En los ensayos en estático se mantiene una cantidad determinada de polímero en contacto con una disolución de concentración fija de analito hasta alcanzar el equilibrio termodinámico, habitualmente 24h (261,262). Alcanzado este equilibrio, el MIP es eliminado por filtración y se determina la concentración de ligando remanente en la disolución.

En cromatografía frontal, se emplea como fase estacionaria el polímero impreso empacado en una columna cromatográfica. La molécula objetivo, disuelta a una concentración dada (F) en la fase móvil, satura poco a poco los sitios de unión, incrementando la cantidad de elución de la misma, dando lugar a un cromatograma frontal que describe una típica curva sigmoidal conocida como curva de ruptura (figura 3.11). El punto de inflexión de esta curva de ruptura es igual al volumen de retención (V_R), por medio del cual calculamos la capacidad de unión de cada polímero para este

determinado compuesto, en un determinado disolvente. El cálculo de la concentración de *template* unida (µM) por g de polímero (B) se calcula a partir de la ecuación 3.6.

$$B = \frac{V_R F}{m_{polímero}} \qquad \textbf{3. 6}$$

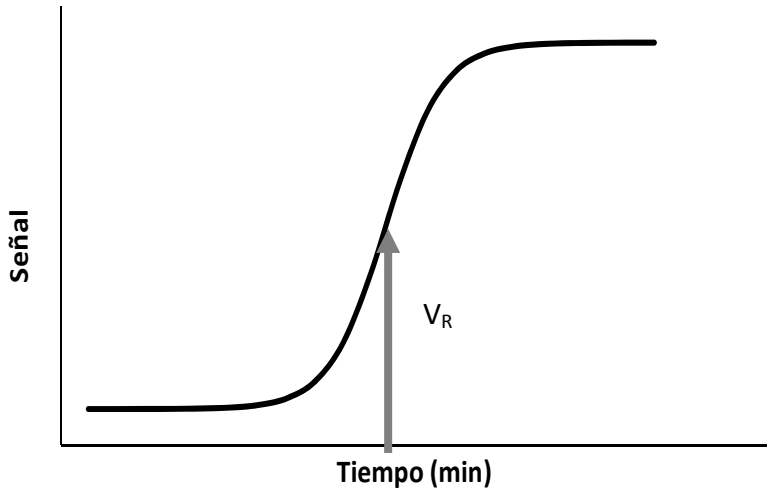

Figura 3. 11. Curva de ruptura obtenida por cromatografía frontal.

Los datos experimentales son ajustados a distintos modelos matemáticos con el fin de estimar el valor de los parámetros que describen el comportamiento del sistema ligando-receptor. La relación matemática de los valores experimentales con cada modelo está basada en presunciones acerca de las propiedades del polímero, especialmente en lo que concierne al número de sitios de unión, así como sus poblaciones relativas (263). Los modelos de unión utilizados con mayor frecuencia para describir el comportamiento de MIP son los siguientes:

Modelo Langmuir

Este modelo asume que todos los sitios de unión son idénticos (N) y que presentan la misma afinidad por el *template*. Estos comportamientos de unión suelen darse en sistemas estructuralmente homogéneos, entre los que se pueden encontrar algunos tipos de MIP (261,263). La ecuación matemática que describe este modelo es la siguiente:

$$B = \frac{NKF}{(1+KF)} \qquad \textbf{3. 7}$$

El cálculo de los parámetros del ajuste del modelo puede realizarse a partir de la ecuación de Scatchard (ecuación 3.11), la cual es una reorganización de la ecuación de Langmuir que permite transformar la isoterma hiperbólica inicial en una recta, pudiéndose calcular de forma sencilla el número de sitios de unión (N) y la constante de afinidad (K) a partir de la pendiente (-K) y la ordenada en el origen (NK), ya que para y=0, se cumple que B=N.

A partir de la ecuación 3.7 de Langmuir se obtiene que,

$$B=\frac{NKF}{(1+KF)}=\frac{NK}{\frac{1}{F}+K} \qquad \textbf{3. 8}$$

Lo que llevaría a,

$$B\left(\frac{1}{F}+K\right)=NK \qquad \textbf{3. 9}$$

O lo que es lo mismo,

$$\frac{B}{F}+KB=NK \qquad \textbf{3. 10}$$

Dando lugar a la ecuación de Scatchard,

$$\frac{B}{F}=NK\text{-}KB \qquad \textbf{3. 11}$$

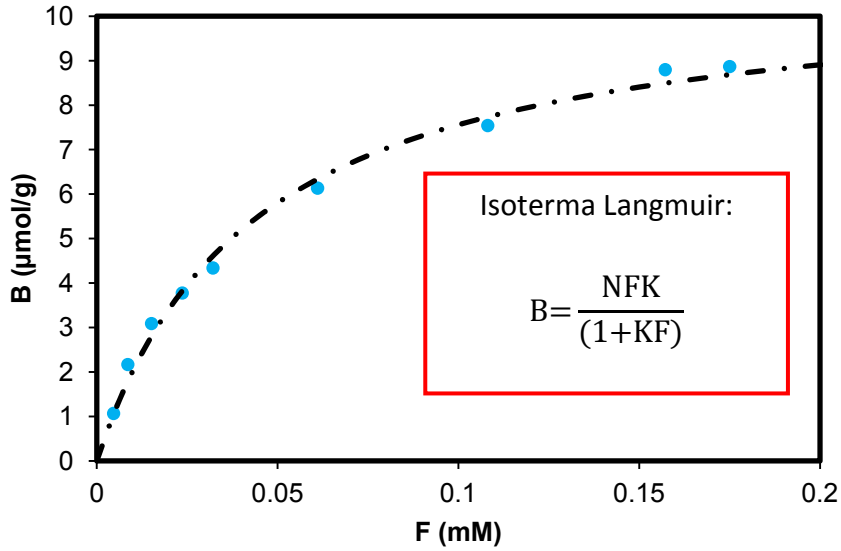

Figura 3. 12. Representación de la isoterma de Langmuir

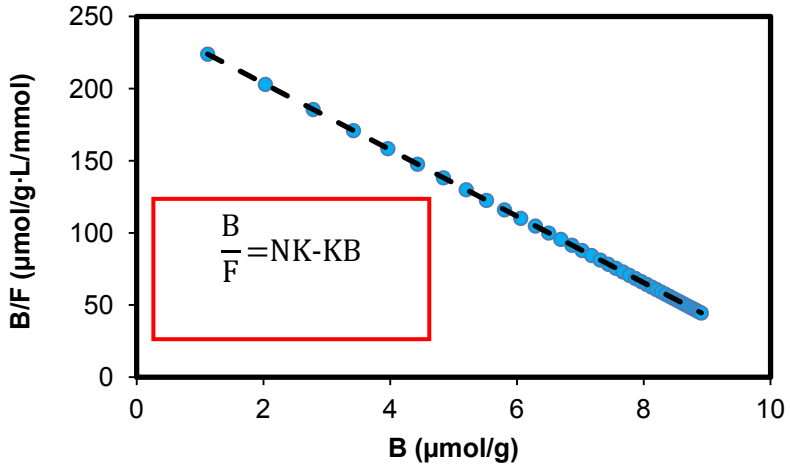

Figura 3. 13. Representación de Scatchard correspondiente a una isoterma de Langmuir.

Modelo Bi-Langmuir:

Como se ha expresado anteriormente, la mayoría de los MIP sintetizados por medio de uniones no-covalentes entre la molécula modelo y el correspondiente monómero funcional, no poseen una distribución homogénea de sitios de unión. Entre los modelos que describen MIP heterogéneos, el modelo Bi-Langmuir es el más simple. Este modelo asume la existencia de dos tipos de cavidades de unión, los de alta afinidad con un número de sitios de unión (N_1) y su constante de afinidad (K_1) y los de baja afinidad con un número de sitios de unión (N_2) y su constante de afinidad (K_2). De esta manera la ecuación de Langmuir se puede extender para la caracterización de estas dos poblaciones de cavidades de unión mediante la ecuación 3.12 :

$$B = \frac{N_1 K_1 F_1}{(1 + K_1 F_1)} + \frac{N_2 K_2 F_2}{(1 + K_2 F_2)} \qquad \textbf{3. 12}$$

Donde debe cumplirse que N2K2 >> N1K1 (264).

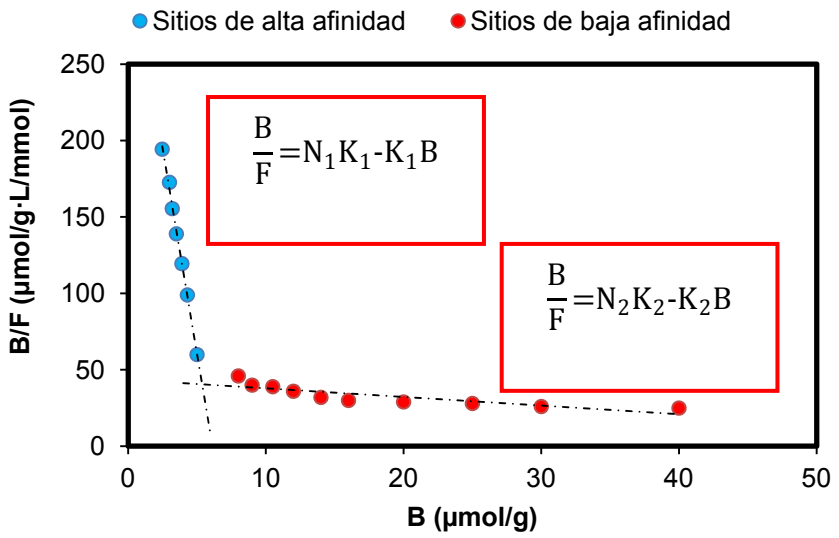

Figura 3. 14. Representación de Scatchard correspondiente a una isoterma de Bi-Langmuir.

De la misma manera que el modelo Bi-Langmuir asume la existencia de dos poblaciones de sitios de unión, existen otros modelos que consideran tres, cuatro e incluso más poblaciones. Estos modelos se describen de acuerdo a las ecuaciones 3.13 y 3.14.

$$B=\frac{N_1K_1F_1}{(1+K_1F_1)}+\frac{N_2K_2F_2}{(1+K_2F_2)}+\frac{N_3K_3F_3}{(1+K_3F_3)} \qquad \textbf{3. 13}$$

$$B=\frac{N_1K_1F_1}{(1+K_1F_1)}+\frac{N_2K_2F_2}{(1+K_2F_2)}+\frac{N_3K_3F_3}{(1+K_3F_3)}+\frac{N_4K_4F_4}{(1+K_4F_4)} \qquad \textbf{3. 14}$$

Modelo Freundlich

Para poder explicar el comportamiento del polímero tanto a altas concentraciones de ligando próximas a la saturación, como a bajas concentraciones, se requiere de un modelo con capacidad de describir el comportamiento del polímero en todo el intervalo de concentraciones del ligando. El modelo de distribución continua de sitios de unión más común, es el modelo Freundlich descrito por la ecuación 3.15: Donde *a* representa una medida de la capacidad (N) y de la afinidad media (K). El parámetro m, representa el factor de heterogeneidad, si este fuera cercano a 1, se podría asumir que existe una distribución homogénea de los sitios de unión. En cambio, si m se encuentra entre 1 y 0 se considerará una distribución más heterogénea (265,266).

$$B = aF^{m} \qquad \textbf{3. 15}$$

La representación en forma logarítmica de las concentraciones libres y unidas permite la obtención de los parámetros a y m a partir de la pendiente y la ordenada en el origen, tal y como se deduce de la ecuación 3.16.

$$\log B = m \log F + \log a \qquad \textbf{3. 16}$$

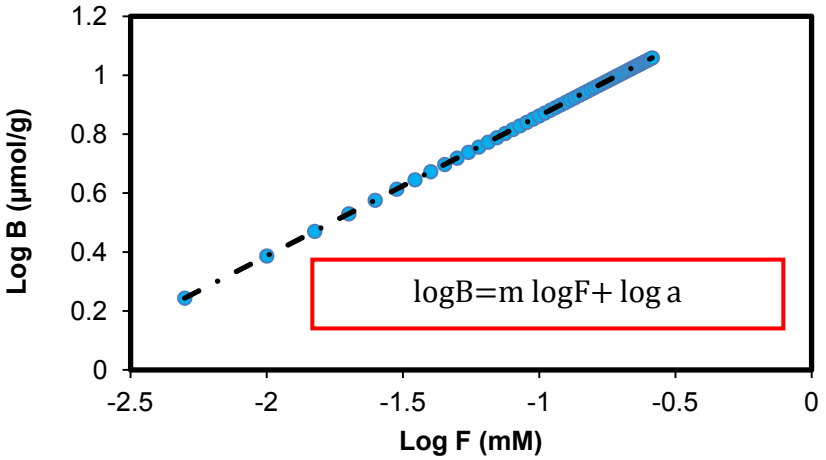

Figura 3. 15. Representación logarítmica de la isoterma de Freundlich.

La ecuación 3.17 es una expresión que permite calcular el número de sitios de unión (N_i) que presentan una misma afinidad K_i. En ella se incluyen los parámetros de ajuste a y m, necesarios para el cálculo de la distribución de afinidades. Conocidos los valores de a y m, podría representarse N en función de K obteniéndose una curva semejante a la que se recoge en la figura 3.16.

$$N_i = 2.3am(1 - m^2)K_i^{-m} \qquad \textbf{3. 17}$$

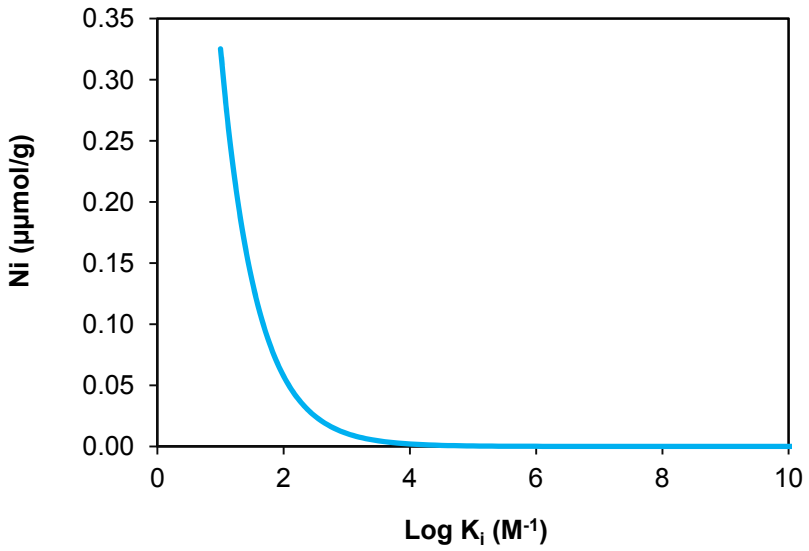

Figura 3. 16. Diagrama de distribución de afinidades basada en el modelo Freundlich.

Aunque la mayoría de las isotermas para MIP se ajusten adecuadamente al modelo Freundlich, en algunos casos, se han observado variaciones en los índices de heterogeneidad en función de las concentraciones de ligando empleadas en los ensayos de unión (266). Para los casos en los que se estudia el comportamiento del MIP tanto a altas concentraciones de ligando, próximas a la saturación del polímero, como a bajas concentraciones, se requiere de un modelo con capacidad de describir el comportamiento del polímero en todo el intervalo de concentraciones del ligando. Dado que el modelo Freundlich no

describe adecuadamente el comportamiento a bajas concentraciones de ligando, se emplea en su lugar el modelo Freundlich-Langmuir.

Modelo Freundlich-Langmuir

La diferencia entre este modelo y el modelo Freundlich es evidente a altas concentraciones de la molécula de estudio. En estas concentraciones el modelo Freundlich-Langmuir puede representar el comportamiento de saturación. A bajas concentraciones, sin embargo, la ecuación Freundlich-Langmuir (3. 18) se reduce a la clásica ecuación Freundlich (3. 15). Por otra parte, a medida que el parámetro *m* se acerca a la unidad, lo que indicaría un adsorbente homogéneo, la ecuación Frendluich-Langmuir se reduce a la clásica Langmuir (ecuación 3.7) (267). Por ello, Umpleby y colaboradores (265), demostraron que este era el modelo que mejor describía las isotermas de unión de un MIP. La ecuación correspondiente a este modelo es la siguiente:

$$B = \frac{N_t a F^m}{1 + a F^m} \qquad \textbf{3. 18}$$

Donde N es el número total de sitios de unión y *m* es el factor de heterogeneidad. Las variables *a* y *m* están relacionadas con la constante de afinidad de unión (K) mediante la siguiente expresión:

$$N_i = N_t a m \left(\frac{1}{K_i}\right)^m \frac{\left(1+2a\left(\frac{1}{K_i}\right)^m + a^2\left(\frac{1}{K_i}\right)^{2m} + 4a\left(\frac{1}{K_i}\right)^m m^2 - a^2\left(\frac{1}{K_i}\right)^{2m} m^2 - m^2\right)}{\left(1+a\left(\frac{1}{K_i}\right)^m\right)^4} \quad \textbf{3. 19}$$

4.2.2.2. Isoterma de unión experimental para el ligando 4EP

Las isotermas de adsorción para el ligando 4EP fueron obtenidas mediante ensayos en estático. Para ello se pesaron 40 mg de polímero impreso o no impreso en viales de vidrio de 5 mL y se le añadieron 2 mL de diferentes disoluciones estándar de 4EP en acetonitrilo comprendidas entre 0.001 mM y 0.75 mM. A continuación, dichos viales fueron agitados a 15 rpm y a temperatura ambiente en un agitador de tubos. Después de 24h, el polímero fue filtrado y el sobrenadante fue analizado mediante cromatografía líquida con detección de fluorescencia.

La representación de la concentración libre de 4EP frente a la unida se muestra en la figura 3.17. Puede apreciarse como la concentración unida del 4EP aumenta a medida que la concentración a la que se expone el polímero es mayor. Este incremento es más pronunciado en el caso del MIP, obteniéndose

para el caso del NIP una curva lineal, típica de los sistemas de unión no específicos. Cuando todos los sitios de unión en el polímero MIP están ocupados, se alcanza la saturación a partir de la cual, el polímero deja de ser específico y se comporta de manera lineal como el NIP.

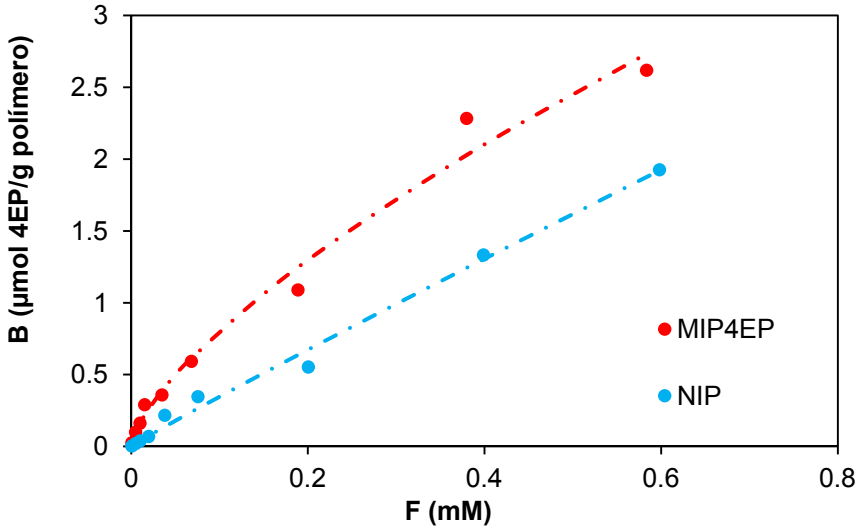

Figura 3. 17. Isotermas de unión experimental para los polímeros impreso con 4EP (MIP_{4EP}) y no impreso (NIP).

La isoterma de unión experimental fue ajustada por regresión no lineal empleando los modelos de unión descritos anteriormente. Para el ajuste, se utilizó el software Graphpad®. Los

parámetros obtenidos para los posibles ajustes se presentan en la tabla 3.6.

Tabla 3. 6. Parámetros de ajuste del MIP_{4EP} y NIP para las isotermas de unión Langmuir, Freundlich, Freundlich-Langmuir.

Modelo Langmuir		MIP	NIP
Constante de afinidad	K_a (mM^{-1})	1.229± 0.492	0.065 ± 0.278
Número de sitios de unión	N_t ($\mu mol\ g^{-1}$)	6.666 ± 1.361	51.190 ± 206.000
Coeficiente de determinación	R^2	0.986	0.989
Suma absoluta de los cuadrados		0.128	0.030
Modelo Freundlich		**MIP**	**NIP**
Afinidad de unión media	a (mM^{-1})	3.975 ± 0.181	3.142 ± 0.227
Factor de heterogenidad	m	0.695 ± 0.056	0.958 ± 0.085
Coeficiente de determinación	R^2	0.988	0.989
Suma absoluta de los cuadrados		0.110	0.029
Modelo Freundlich-Langmuir		**MIP**	**NIP**
Número de sitios de unión	N_t ($\mu mol\ g^{-1}$)	544 ± 47687	712 ± 143164
Afinidad de unión media	a (mM^{-1})	0.007 ± 0.646	0.004 ± 0.946
Factor de heterogenidad	m	0.697 ± 0.212	0.959 ± 0.314
Coeficiente de determinación	R^2	0.988	0.989
Suma absoluta de los cuadrados		0.110	0.029

La simple comparación de los parámetros R^2 y la suma absoluta de los cuadrados, no permite establecer el modelo que mejor describe el comportamiento experimental. Por ello, para una

comparación más precisa, se llevo a cabo un test estadístico a través del software Graphpad®. Este programa realiza una adaptación del análisis de la varianza (ANOVA), conocido como el test de Fischer o test F, el cual está basado en un cociente modificado de la suma de los cuadrados residuales de los dos modelos a comparar. De este modo, calcula el valor de Fischer (F) y su correspondiente valor p para cada estudio comparativo. El valor F se calcula tal y como se muestra en la ecuación 3.20, a partir de la suma de los cuadrados (SS) y los grados de libertad (DF), que son indicativos de la complejidad del modelo. El programa ajusta el modelo más simple como hipótesis nula (h_0), realizando un análisis para elegir entre la hipótesis nula y la hipótesis alternativa (h_1).

$$F = \frac{(SS_{nula} - SS_{alt})/SS_{alt}}{(DF_{nula} - DF_{alt})/DF_{alt}} \qquad \textbf{3. 20}$$

Para rechazar o aceptar la hipótesis alternativa, el programa calcula el parámetro *p* a partir del valor calculado F. Si $p<0.05$ se acepta h_1 como verdadera, en caso contrario el modelo más simple explicaría mejor los datos experimentales.

Tabla 3. 7. Datos obtenidos para las comparaciones entre modelos matemáticos de isotermas de unión.

Comparación	Modelo preferido	Valor de F	Valor de p
Freundlich frente a Langmuir	Freundlich	Mismos grados de libertad	
Freundlich frente a Frendluich-Langmuir	Frendluich	0.008	0.933

En la tabla 3.7 se aprecia que el modelo que mejor describe el comportamiento experimental es el modelo Freundlich (ecuación 3.15). Los ajustes realizados para los modelos Frendluich y Langmuir poseen el mismo número de grados de libertad anulando el divisor en la expresión 3.20, por lo que no es posible calcular el valor de F. Observando los parámetros del ajuste a partir de este modelo, se aprecia como la afinidad de unión media en el MIP (3.975 ± 0.181 mM^{-1}) es ligeramente mayor al del NIP (3.142 ± 0.227 mM^{-1}). Por otro lado, el NIP es más homogéneo (m = 0.958 ± 0.085) que el MIP (m=0.695 ± 0.056), esto es debido a que las uniones entre el NIP y el 4EP son solo las inespecíficas, relacionadas con la composición del polímero.

A partir de los parámetros obtenidos al ajustar los datos a la isoterma Freundlich (tabla 3.6), se obtiene el diagrama de distribución de afinidades de los sitios de unión en base a la ecuación 3.17 (figura 3.18).

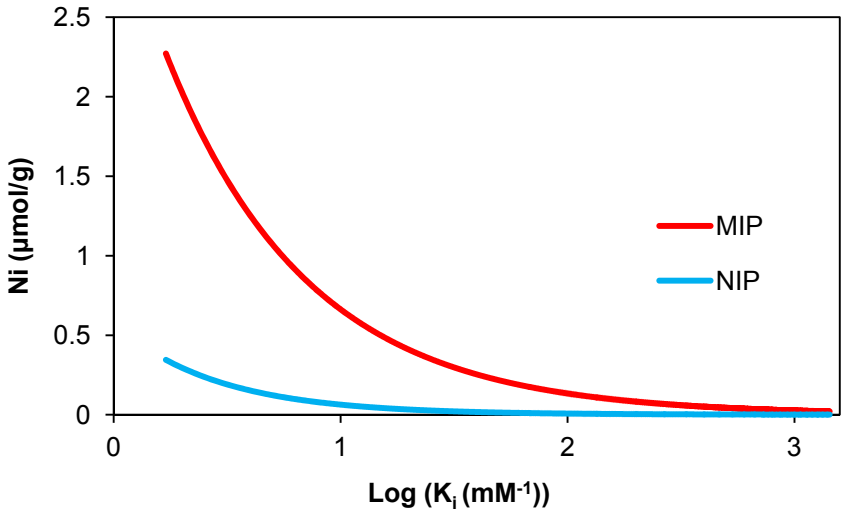

Figura 3. 18. Diagrama de distribución de afinidades para los datos modelizados a partir de las isotermas de unión para el polímero impreso y no impreso.

5. Desarrollo de un polímero molecularmente impreso para el ácido cumárico.

El polímero impreso desarrollado para el 4EP, permitía la extracción de los compuestos pertenecientes a su ruta metabólica, sin embargo cuando el material impreso era utilizado como fase estacionaria no era posible la separación cromatográfica de los compuestos objetivo. En el cromatograma que se presenta en la figura 3.19, podemos ver como el CAEE, el 4VPh y el 4EP, coeluían en un solo pico cromatográfico, quedando el CA totalmente retenido en la fase estacionaria. Esto puede deberse a que el 4EP es una molécula pequeña y poco funcionalizada, y durante la síntesis del polimero impreso, los aductos formados entre el *template* y el monómero no eran muy estables dando lugar a una débil impresión. Por ello, se desarrolló otro material impreso, usando como *template* el ácido cumárico (MIP_{CA}). Este compuesto fue escogido para el desarrollo del nuevo MIP, ya que presenta en su molécula un grupo carboxilo que puede formar aductos más fuertes con el monómero funcional (4VPy). Además, ya se había observado que era el compuesto dentro de la ruta metabólica, que mayor retención presentaba en el polímero sintetizado para el monómero 4VPy utilizando como *template* el compuesto 4EP.

Para sintetizar un polímero impreso con las características adecuadas que permitiera la correcta separación cromatográfica de los compuestos de la ruta metabólica del 4EP, manteniendo como monómero funcional 4VPy y como entrecruzador EDMA, se ajustó el medio y la composición de la mezcla de polimerización.

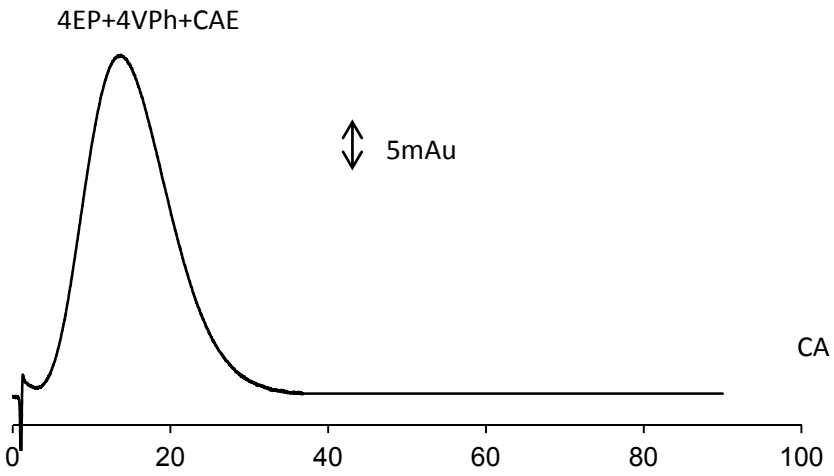

Figura 3. 19. Cromatograma registrado para una disolución estándar de 5 mg L^{-1} de 4EP, 4VPh, CAEE y CA. Como fase estacionaria se utilizó el material impreso MIP_{4EP} y diclorometano como fase móvil.

5.1. Selección del medio de polimerización

El polímero impreso para el compuesto 4EP presentaba una fuerte retención para el compuesto CA utilizando acetonitrilo o diclorometano como fase móvil. Se podía pensar que el monómero funcional 4VPy y el CA podrían formar aductos fuertes en presencia de estos disolventes. Sin embargo, el CA no es muy soluble en estos porógenos, por lo que se probaron como medios de polimerización otros disolventes más polares como metanol y dimetilsulfoxido.

Los materiales impresos para el compuesto CA se sintetizaron disolviendo 0.276 g de CA (0.0017 mol), 0.531 g de 4VPy (0.00505 mol) y 4 g de EDMA (0.0202 mol) en 4.807 g de porógeno (MeOH o DMSO) previamente desoxigenado con nitrógeno. Una vez disueltos los componentes se añadía 0.048 g del iniciador ABCN y se desoxigenaba la mezcla durante 1 minuto. Los polímeros impresos sintetizados para la molécula CA (MIP_{CA}) se molieron, tamizaron y empaquetaron en columnas cromatográficas. Para cada uno de los materiales impresos para el compuesto CA se sintetizó un polímero no impreso. En ambos materiales, el compuesto CA quedaba totalmente retenido utilizando ACN como fase móvil, por ello 15 minutos después de la inyección, para favorecer su elución la fase móvil fue modificada a una composición del 95% de ACN y un 5% de MeOH.

El factor de impresión obtenido para el material impreso MIP_{CA} sintetizado en DMSO era notablemente mayor que el observado para el MIP_{CA} sintetizado en MeOH, 31.05 frente a 6.85. Esto demuestra que la fuerza de unión es considerablemente mayor en el polímero sintetizado en DMSO, sin embargo sólo el polímero impreso sintetizado en MeOH permitía la separación cromatográfica de todos los compuestos objetivo (figura 3.20). Probablemente en presencia de DMSO el aducto template-monómero funcional en la mezcla de prepolimerización es más estable y en consecuencia, la distribución de sitios de unión resultante es más homogénea produciendo un MIP_{CA} más selectivo para la molécula objetivo y menos específico para el resto de compuestos de su ruta metabólica. Se concluyó que el polímero impreso preparado en DMSO era menos específico para la familia de fenoles objetivo, por ello se seleccionó MeOH como medio para la polimerización.

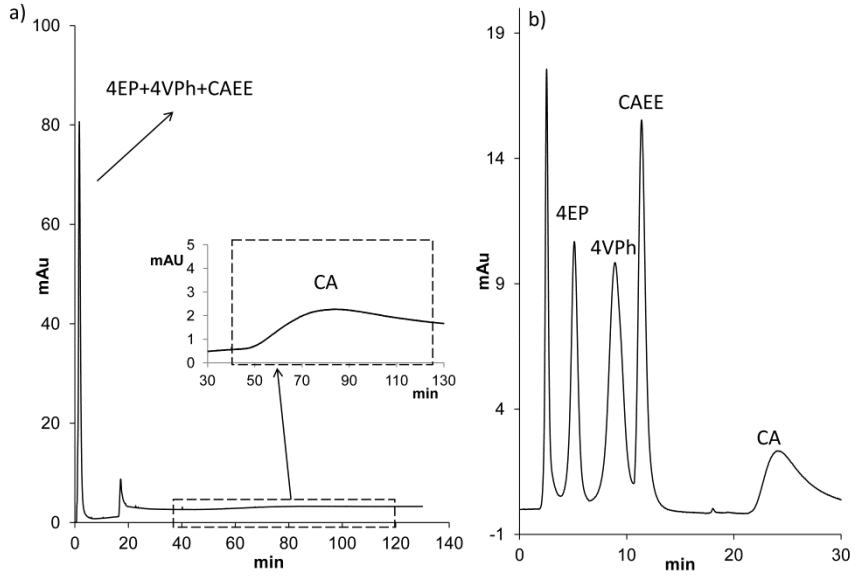

Figura 3. 20. Cromatogramas registrados para una disolución estándar de 5 mg L^{-1} de 4EP, 4VPh, CAEE y CA. Como fase estacionaria se utilizaron materiales impresos para CA en distintos medios a) DMSO y b) MeOH.

5.2. Optimización de la composición del polímero

Para determinar la relación molar *template*: monómero funcional: monómero entrecruzador, se sintetizaron una serie de polímeros impresos MIP_{CA} con 4VPy como monómero funcional y EDMA como monómero entrecruzador. Primero se sintetizaron cuatro polímeros variando la relación molar template: monómero funcional, manteniendo la relación de los monómeros funcional:

entrecruzador en 1:4 (1:2:8, 1:3:12, 1:4:16 y 1:6:24), las cantidades usadas para las mezclas de polimerización se muestran en la tabla 3.8. En todos ellos el porógeno utilizado fue MeOH al 100% en peso respecto de la masa de los monómeros y el iniciador ABCN se añadió al 1% en peso respecto de la masa de los monómeros. Los polímeros impresos y no impresos, una vez sintetizados, se molieron, tamizaron y empacaron en columnas cromatográficas para ser evaluados cromatográficamente.

Tabla 3. 8 Cantidades utilizadas en las mezclas de polimerización para cada MIP_{CA}/NIP en la optimización de los componentes del MIP_{CA}

Polímero	Relación molar T:FM:CL	4EP	4VPy	EDMA
MIP_{CA}EDMA1	1:2:8	5.05 mmol 0.531 g	2.53 mmol 0.415 g	20.2 mmol 4 g
MIP_{CA}EDMA2	1:3:12	5.05 mmol 0.531 g	1.68 mmol 0.276 g	
MIP_{CA}EDMA3	1:4:16	5.05 mmol 0.531 g	1.26 mmol 0.207 g	
MIP_{CA}EDMA4	1:6:24	5.05 mmol 0.531 g	0.84 mmol 0.138 g	

Tabla 3.8. cont. Cantidades utilizadas en las mezclas de polimerización para cada MIP_{CA}/NIP en la optimización de los componentes del $MIP_{CA.}$

Polímero	Relación molar T:FM:CL	4EP	4VPy	EDMA
MIP_{CA}EDMA5	1:3:9	6.73 mmol 0.708 g	2.24 mmol 0.368 g	
MIP_{CA}EDMA6	1:3:15	4.04 mmol 0.425 g	1.35 mmol 0.221 g	

Además de calcular los factores de impresión, se estudió la capacidad de los polímeros para la separación cromatográfica de los compuestos objeto de estudio.

La capacidad de una determinada fase estacionaria para separar dos compuestos A y B se expresa mediante el factor de separación o factor de selectividad, α, el cual se calcula a partir de los factores de retención K (ecuación 3.5) de cada compuesto en dicha fase estacionaria (268):

$$\alpha_{A/B} = \frac{K_B}{K_A} \qquad \textbf{3. 21}$$

El factor de selectividad α describe la separación entre los centros de las bandas cromatográficas, pero no tiene en cuenta las anchuras de pico. Por esto, resulta más adecuado obtener la resolución (R) a partir de la expresión 3.22 (268):

$$R=\frac{2(t_{RB}-t_{RA})}{1.699(w_{1/2A}+w_{1/2B})} \qquad \textbf{3. 22}$$

Si R = 1.5 los dos picos sólo se superponen un 0.3% mientras que si R = 1, la superposición es del orden del 2%, que puede considerarse adecuada para muchos análisis (268).

Comparando los factores de impresión obtenidos para cada uno de los polímeros sintetizados, el polímero sintetizado para una relación molar 1:3 *template*: FM (MIP_{CA}EDMA2) obtuvo los mejores resultados (figura 3.21). Los factores de impresión obtenidos en la mayoría de los polímeros específicos de la molécula CA, son notablemente mayores que los obtenidos para el MIP_{4EP}, gracias a que el CA es un compuesto más funcionalizado. Esta mayor funcionalización, permite formar aductos más fuertes con el 4VPy y por lo tanto es posible sintetizar polímeros más específicos a pesar de no utilizar el porógeno más adecuado para su impresión.

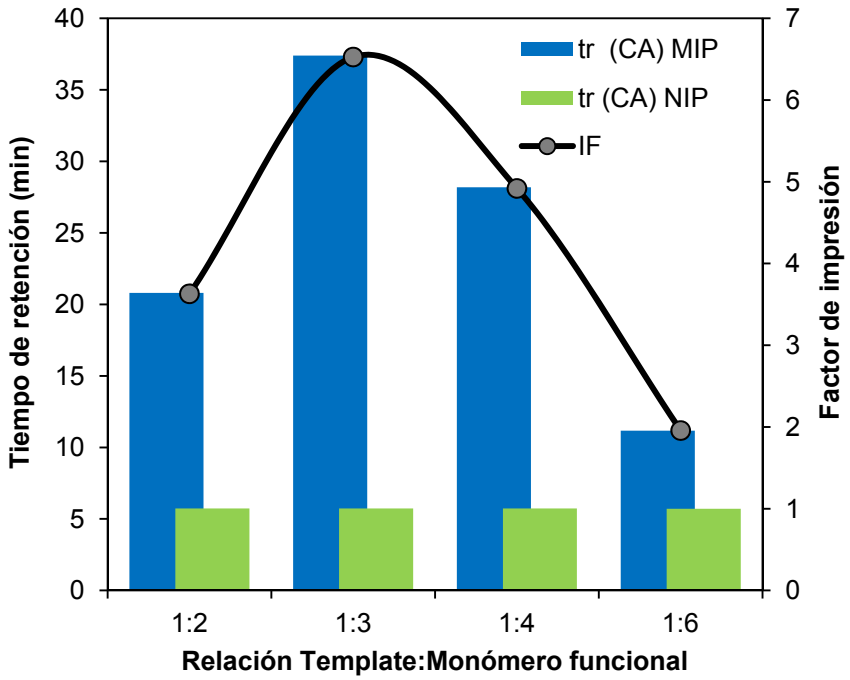

Figura 3. 21. Tiempos de retención y factores de impresión para el CA en las fases estacionarias impresas y no impresas sintetizadas para diferentes relaciones molares de *template*:monómero funcional.

Por otro lado, al comparar los factores de separación (α) y la resolución (R) entre los picos cromatográficos pertenecientes a los diferentes compuestos objetivo (tabla 3.9), se puede observar que el polímero impreso con una relación molar *template*: monómero funcional 1:3, es el único con una resolución entre el pico de 4EP y 4VPh por encima de la unidad, coincidiendo con el mayor valor de $\alpha_{4EP/4VPh}$. Las estructuras moleculares de los compuestos 4EP y 4VPh son muy similares, por lo que parece

lógico que sea más difícil sintetizar un polímero que separe cromatograficamente estos dos compuestos. Por ello, se escogió esta relación 1:3 como la óptima para la correcta resolución cromatográfica de los compuestos pertenecientes a la ruta metabólica del 4EP.

Tabla 3. 9. Factores de separación y resolución (4EP/4VPh) y (4VPh/CAEE) e IF del CA para los diferentes MIP_{CA}, variando la relación molar T:MF.

Relación T:FM	α 4EP/4VPh	α 4VPh/CAEE	R 4EP/4VPh	R 4VPh/CAEE	IF CA
1:2	1.53	2.49	0.28	2.18	3.70
1:3	2.25	1.87	1.99	3.91	6.85
1:4	1.42	3.01	0.40	5.41	6.12
1:6	1.59	1.19	0.12	0.13	0.98

Una vez seleccionada la relación molar *template*: monómero funcional, se sintetizaron materiales impresos para diferentes proporciones de monómero entrecruzador (tabla 3.8). En todos ellos el porógeno utilizado fue MeOH al 100% en peso respecto de la masa de los monómeros y el iniciador ABCN se añadió al 1% en peso respecto de la masa de los monómeros.

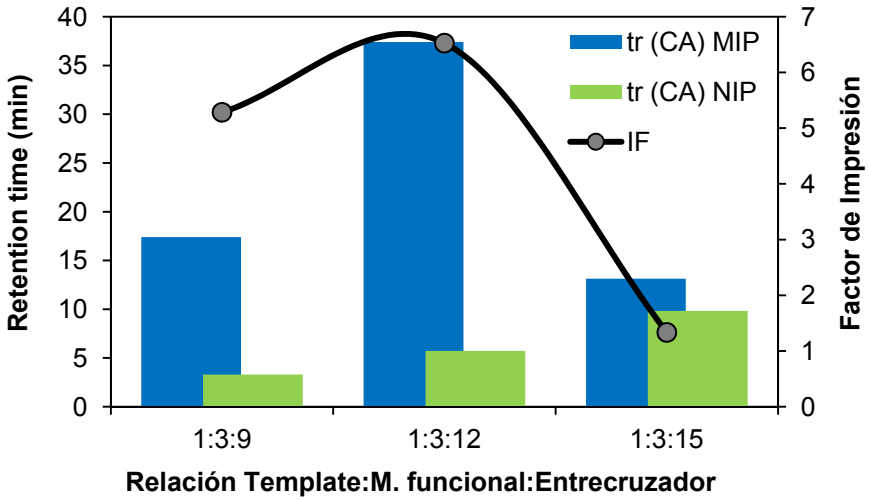

Figura 3. 22. Tiempos de retención y factores de impresión para el CA en las fases estacionarias impresas y no impresas sintetizadas para diferentes relaciones molares de monómero funcional: monómero entrecruzador.

Los polímeros impresos y no impresos fueron evaluados cromatográficamente, observándose que el mayor factor de impresión tenía lugar para un material polimerizado con una relación molar 1:4 para monómero funcional:monómero entrecruzador (figura 3.22). Además, este polímero era el que también obtenía la mejor resolución cromatográfica entre el pico de 4EP y 4VPh (tabla 3.10).

Tabla 3. 10 Factores de separación y resolución (4EP/4VPh) y (4VPh/CAEE) e IF del CA para los diferentes MIP_{CA}, variando el relación molar FM:CL.

Relación FM:CL	α 4EP/4VPh	α 4VPh/CAEE	R 4EP/4VPh	R 4VPh/CAEE	IF CA
1:3	2.22	1.81	1.18	0.77	3.37
1:4	2.25	1.87	1.99	3.91	6.85
1:5	1.17	3.42	0.09	2.45	1.38

El polímero MIP_{CA}EDMA2 (de ahora en adelante referido como MIP_{CA}) fue el elegido como el óptimo para la separación cromatográfica de los compuestos pertenecientes a la ruta metabólica del 4EP. En la figura 3.23 se puede observar como usando como fase estacionaria el material impreso MIP_{CA} se obtiene una resolución cromatográfica adecuada para los compuestos objetivo, en cambio, la fase estacionaria no impresa no permite la separación de los compuestos 4EP, 4VPh y CAEE.

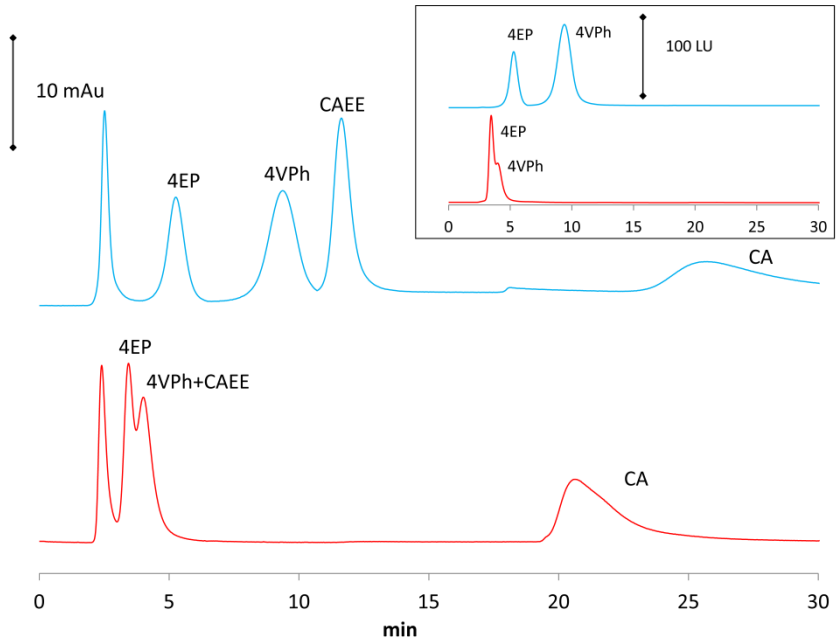

Figura 3. 23. Cromatogramas registrados en el detector de línea de fotodiodos para una disolución de 5 mg L^{-1} de 4EP, 4VPh, CAEE y CA usando como fase estacionaria el material impreso MIP_{CA} (——) y no impreso NIP (——) como fase estacionaria. En el recuadro se muestra la señal en el detector de fluorescencia.

5.3. Evaluación de la capacidad del polímero molecularmente impreso para el ácido cumárico.

Una vez optimizada la composición del material impreso MIP_{CA}, se realizó a partir de los ensayos de unión la evaluación de la impresión, lo que permitió conocer las propiedades de los sitios de unión así como su afinidad para la molécula *template*.

5.3.1. Isotermas de unión

Los datos experimentales para la representación de las isotermas de unión para el material impreso MIP_{CA} y su respectivo polímero no impreso NIP, se obtuvieron mediante ensayos en estático. Para ello se pesaron 40 mg de material polimérico y se puso en contacto con concentraciones de ácido cumárico comprendidas entre 0.004 mM y 0.8 mM. A continuación, dichos viales fueron agitados a 15 rpm y a temperatura ambiente en un agitador de tubos. Después de 24h, el polímero fue filtrado y el sobrenadante fue analizado mediante cromatografía líquida con detección de línea de fotodiodos.

La representación de la concentración de CA libre frente a la unida se muestra en la figura 3.24. Puede apreciarse que a medida que la concentración de CA a la que expone el polímero es mayor la concentración unida. Este incremento es más pronunciado en el caso del MIP que del NIP, hasta que en el

primero se alcanza la saturación, por la ocupación de todos los sitios de unión.

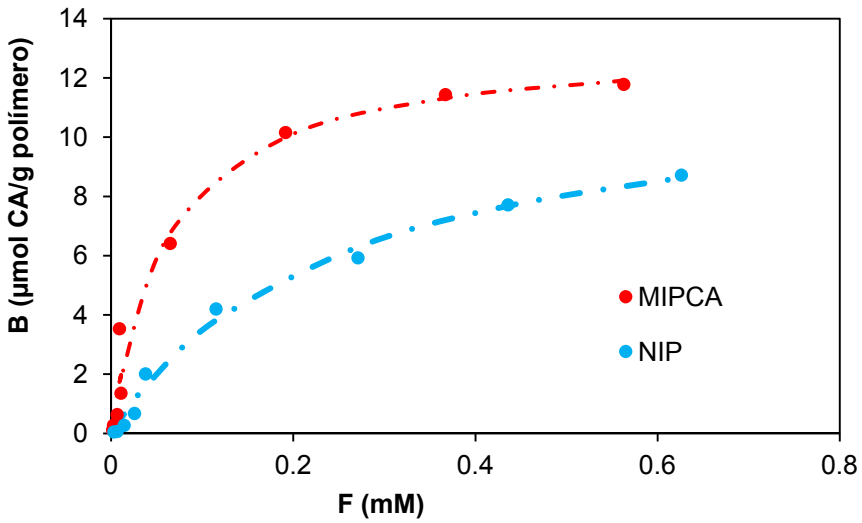

Figura 3. 24. Isotermas de unión para los polímeros impreso con CA (MIP_{CA}) y no impreso (NIP).

Las isotermas de unión experimental se ajustaron a distintos modelos matemáticos de regresión no lineal. En la tabla 3.11, se resumen los distintos parámetros de unión derivados de cada ajuste.

Tabla 3. 11. Parámetros de ajuste del MIP_{CA} para las isotermas de unión Langmuir, Bi-Langmuir, Freundlich y Freundlich-Langmuir.

Modelo Langmuir		**MIP**	**NIP**
Constante de afinidad	K_a (mM^{-1})	16.170 ± 3.861	4.024 ± 0.762
Número de sitios de unión	N_t ($\mu mol\ g^{-1}$)	13.220 ± 0.806	12.060 ± 0.948
Coeficiente de determinación	R^2	0.980	0.991
Suma absoluta de los cuadrados		4.490	0.885
Modelo Bi-Langmuir		**MIP**	**NIP**
Constante de afinidad	K_{a1} (mM^{-1})	12.830 ± 71.670	0.036 ± 1.033
	K_{a2} (mM^{-1})	44.970 ± 931.600	$1{\cdot}10^{-7}$ ± $1.485{\cdot}10^{15}$
Número de sitios de unión	N_{t1} ($\mu mol\ g^{-1}$)	11.460 ± 82.410	462.000 ± 12895.000
	N_{t2} ($\mu mol\ g^{-1}$)	1.983 ± 84.570	0.009 ± 0.999
Coeficiente de determinación	R^2	0.980	0.876
Suma absoluta de los cuadrados		4.451	11.840
Modelo Freundlich		**MIP**	**NIP**
Afinidad de unión media	a (mM^{-1})	16.900 ± 1.728	12.180 ± 0.895
Factor de heterogenidad	m	0.425 ± 0.064	0.593 ± 0.063
Coeficiente de determinación	R^2	0.935	0.973
Suma absoluta de los cuadrados		14.330	2.603
Modelo Freundlich-Langmuir		**MIP**	**NIP**
Número de sitios de unión	N_t ($\mu mol\ g^{-1}$)	13.390 ± 1.618	12.000 ± 2.345
Afinidad de unión media	a (mM^{-1})	14.510 ± 12.610	4.078 ± 2.772
Factor de heterogenidad	m	0.975 ± 0.193	1.000 ± 0.167
Coeficiente de determinación	R^2	0.980	0.991
Suma absoluta de los cuadrados		4.478	0.886

La simple comparación de los parámetros, no permitía establecer el modelo que mejor describía el comportamiento experimental. Por ello se realizó un test de Fischer por medio del software Graphpad® (tabla 3.12).

Tabla 3. 12 Datos obtenidos para las comparaciones entre modelos matemáticos de isotermas de unión.

Comparación	Modelo preferido	Valor de F	Valor de p
Langmuir frente a Freundlich	Langmuir	Mismos grados de libertad	
Langmuir frente a Bi-Langmuir	Langmuir	0.027	0.974
Langmuir frente a Freundlich-Langmuir	Langmuir	0.019	0.894

En la tabla 3.12 se aprecia que el modelo que mejor describe el comportamiento experimental es el modelo Langmuir (ecuación 3.8). Los ajustes realizados para los modelos Frendluich y Langmuir poseen el mismo número de grados de libertad anulando el divisor en la expresión 3.20, por lo que no es posible la comparación entre ambos modelos de ajuste. Observando los parámetros del ajuste a partir de este modelo en la tabla 3.11, la constante de afinidad es mucho mayor en el MIP (16.170 ± 3.861 mM^{-1}) que en el NIP (4.024 ± 0.762 mM^{-1}), como también se observa en la diferencia de las pendientes en la representación Scatchard (figura 3.25). Sin embargo, las diferencias en números de sitios de unión son mínimas (13.220 ± 0.806 para MIP y 12.060 ± 0.948 para NIP). Se puede deducir que la la mayor capacidad de

unión de los sitios de unión es debido a la influencia del *template* en la orientación de los monómeros funcionales durante la síntesis del MIP.

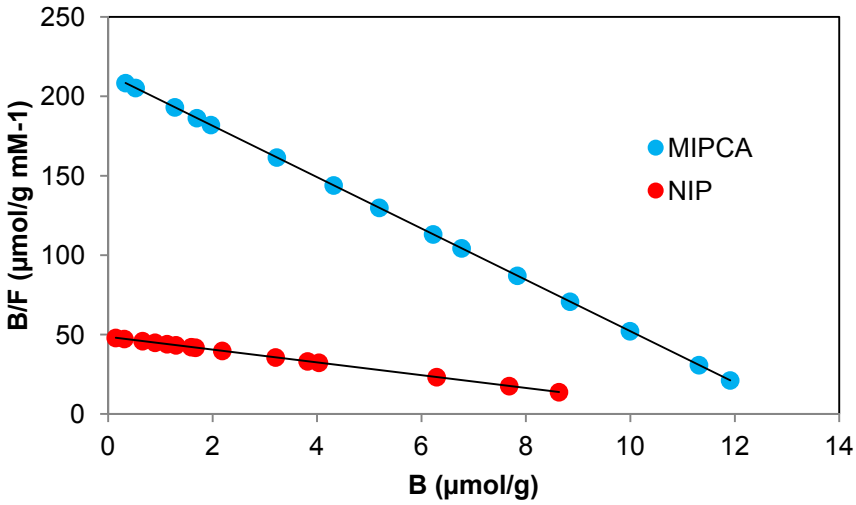

Figura 3. 25. Representación Scatchard para el polímero impreso específico para el ácido cumárico MIP_{CA} y su respectivo polímero no impreso NIP.

6. Desarrollo de un método de extracción en fase sólida basado en un adsorbente MIP

Para la correcta medida de los compuestos de la ruta metabólica del 4EP en vino, resultaría de gran ayuda la eliminación de las interferencias que podrían encontrarse en una matriz tan compleja como es el vino. Con este fin se desarrolló un método de extracción en fase sólida, utilizando como adsorbente un polímero MIP (MISPE).

6.1. Selección del material impreso para su uso como adsorbente en extracción en fase sólida. MISPE

Para la selección del polímero más adecuado para su utilización como adsorbente específico para los compuestos de la ruta metabólica del 4EP, se estudiaron las capacidades de unión para la molécula de 4EP, de cada uno de los polímeros impresos desarrollados MIP_{4EP} y MIP_{CA}. Se seleccionó este compuesto, por resultar el más crítico debido a su baja funcionalidad.

Estas capacidades fueron evaluadas mediante cromatografía frontal, usando como fase estacionaria los polímeros impresos y no impresos y como fase móvil diferentes disolventes conteniendo 5 mg L^{-1} de 4EP.

Los resultados obtenidos para cada polímero ensayado con cada disolvente se muestran en la figura 3.26.

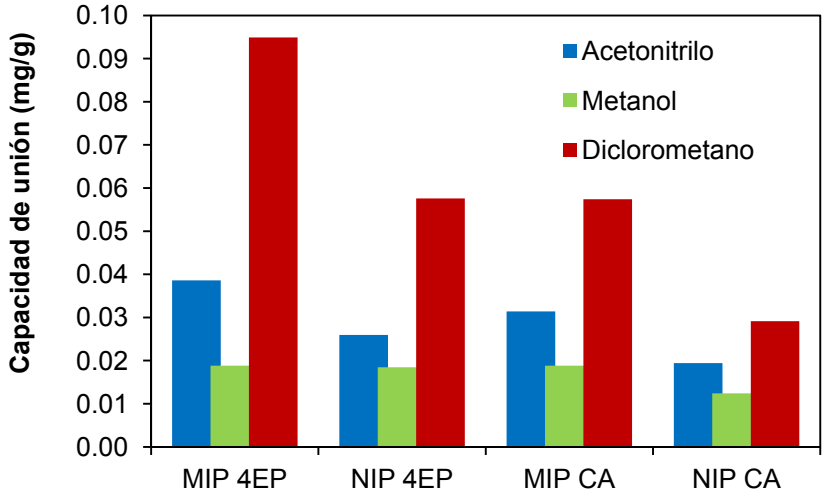

Figura 3. 26. Capacidades de unión de los polímeros impresos MIP_{4EP} y MIP_{CA} y no impresos para la molécula 4EP utilizando como fases móviles ACN, MeOH o DCM.

Los resultados mostraron que la mejor capacidad de unión para la molécula del 4EP era obtenida para la fase estacionaria constituida por el polímero MIP_{4EP} y utilizando diclorometano como fase móvil. Por esta razón el material impreso MIP_{4EP} se utilizó como polímero adsorbente para la etapa de extracción en fase sólida y de acuerdo a los resultados ya comprobados en el apartado anterior, el polímero MIP_{CA} fue el utilizado como fase

estacionaria para la separación cromatográfica de los compuestos correspondientes a la ruta metabólica del 4EP.

6.2. Optimización de la etapa de lavado de interferencias

La extracción en fase sólida (SPE) se basa en la partición diferencial de los compuestos entre una fase sólida (polímero impreso) y una fase líquida (disolvente). En aplicaciones analíticas el proceso SPE consta de 4 pasos (269):

- Acondicionamiento del adsorbente.
- Carga de la muestra.
- Lavado de interferencias.
- Elución de los analitos.

En la optimización del proceso MISPE, una vez elegido el adsorbente más adecuado, se procedió a la optimización de la etapa de lavado de interferencias. De acuerdo a los resultados observados para la capacidad de unión del $MIP4_{EP}$ (figura 3.26), se pudo observar que en MeOH la capacidad del polímero resultaba mínima (18.8 $\mu g\ g^{-1}$), aumentando en ACN hasta 38.6 $\mu g\ g^{-1}$ y hasta 94.9 $\mu g\ g^{-1}$ en DCM. Por ello DCM y ACN fueron los disolventes ensayados para el lavado de interferencias, mientras que para la elución de los compuestos se utilizó MeOH.

Las micropartículas de polímero MIP_{4EP} y sus polímeros no impresos NIP (0.5 g) fueron empacadas manualmente en cartuchos

para SPE vacíos entre discos fritados de polietileno de 20 µm de tamaño de poro. El adsorbente fue acondicionado con 5 mL de metanol y posteriormente se eliminó el exceso del disolvente de solvatación con 5 ml agua con un 12% de etanol con el fin de preparar el sólido para la carga con la matriz vino.

La optimización del proceso comenzó con la etapa de retención de un patrón de 10 mg L^{-1} de 4EP, 4VPh, CAEE y CA en agua con un 12% de etanol. Después del acondicionamiento del polímero se cargaban 5 mL del patrón y a continuación, se lavaba con otros 5 mL de agua (12% etanol). Esta última etapa fue incluída en el proceso de optimización del estándar, para comprobar el comportamiento del sólido en el lavado de compuestos polares o poco adsorbidos en el sólido que pudieran estar presentes en la matriz vino.

Posteriormente se evaluó el disolvente (ACN o DCM) y la cantidad de éste que podía ser utilizado en la etapa de limpieza de interferencias sin pérdida de los analitos. Para ello se repitió el proceso explicado en el párrafo anterior y después del lavado con 5 mL agua (12% etanol) el polímero con los compuestos adsorbidos se secaba a vacío durante 15 minutos. Una vez seca la fase estacionaria, esta se lavó con 1 mL de acetonitrilo y los compuestos fueron eluidos en 5 ml de metanol. Este proceso se repitió para varios volúmenes (1, 2, 3, 4 y 5 mL) y con acetonitrilo o diclorometano como disolventes de lavado (figura 3.27). Con el objetivo de calcular la recuperación de cada uno de los

compuestos, el mismo proceso se realizó omitiendo el paso de limpieza con disolvente orgánico. Los eluatos se midieron por LC-DAD-FD utilizando como fase estacionaria el polímero impreso MIP_{CA}. La separación de los compuestos en gradiente se realizó usando agua ultra-pura como fase acuosa y ACN como fase orgánica. Al comienzo del análisis se empleó 100 % de ACN como fase móvil durante 5 minutos, posteriormente el porcentaje de fase orgánica fue modificado durante 15 minutos hasta un 90 % al final del análisis. En la tabla 3.13 se recogen las longitudes de onda de absorción/excitación y emisión seleccionadas para cada compuesto.

Tabla 3. 13. Condiciones para los detectores en la medida de los compuestos objetivo.

Compuesto	Detector		
	DAD	FD	
	λ absorción	λ excitación	λ emisión
4EP	225 nm	230 nm	320 nm
4VPh	260 nm	260 nm	320 nm
CAEE	310 nm	--------	-------
CA	310 nm	--------	-------

En la figura 3.27 se representa la recuperación de los diferentes compuestos objetivo en el eluato final para cada volumen de disolvente de lavado ensayado.

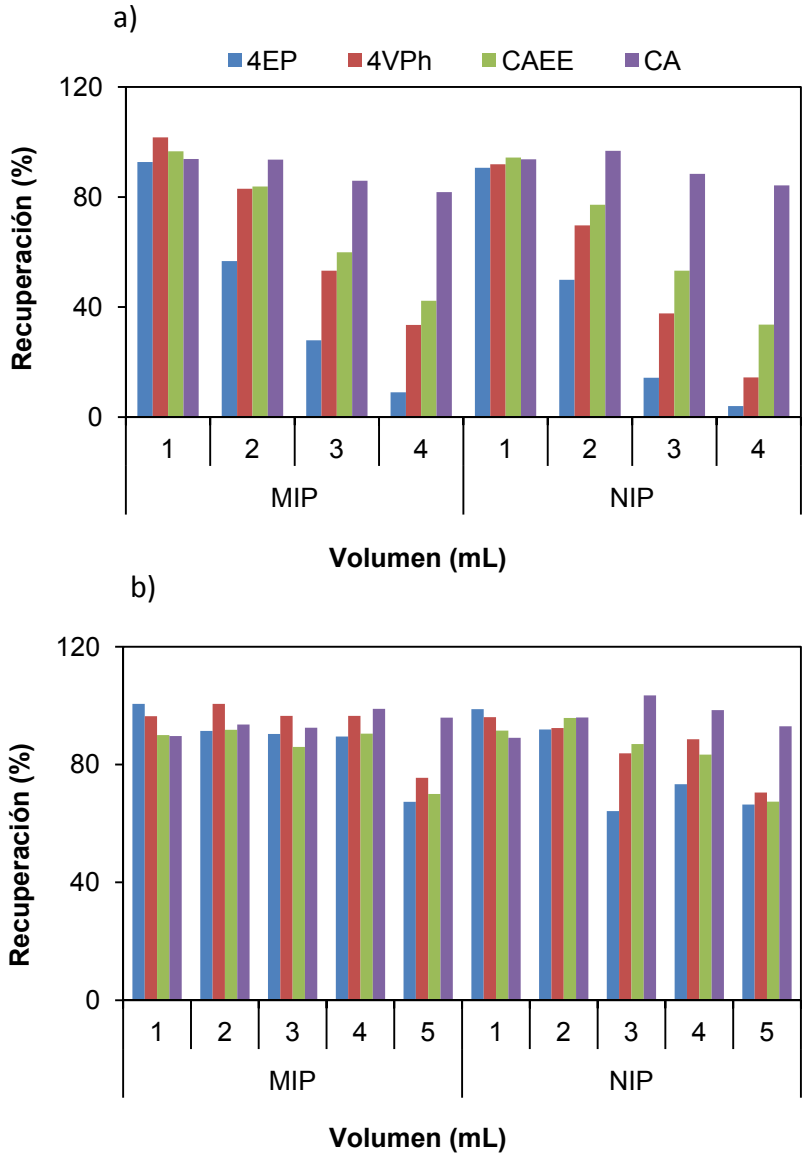

Figura 3. 27. Recuperaciones (%) obtenidas para 4EP, 4VPh, CAEE y CA en el polímero impreso MIP_{4EP} y no impreso utilizando volúmenes crecientes de a) acetonitrilo y b) diclorometano en la etapa de lavado de interferencias.

El acetonitrilo fue descartado como disolvente en la etapa de lavado, ya que 1mL es el volumen máximo permitido para el lavado de interferencias. Para un volumen de 2 mL se perdería más del 40% de la cantidad de 4EP cargado. Sin embargo, el diclorometano, permitía aumentar el volumen de lavado, mostrando para 4 mL recuperaciones en la fase sólida impresa del 89.5 %, 96.5 % y 90.5 % para 4EP, 4VPh y CAEE respectivamente y 58.9 %, 68.8 %y 45.5 % para la no impresa. En la recuperación del CA no había practicamente diferencia entre los materiales impreso y no impreso, ya que como hemos visto en apartados anteriores este compuesto permanece totalmente retenido en el polímero.

6.3. Optimización de la etapa de elución

Una vez establecida la etapa de lavado, se optimizó la etapa de elución de los analitos adsorbidos. En este caso, el compuesto más crítico era el CA ya que permanecía muy retenido por el polímero. El objetivo de la optimización de este paso del método era conseguir eluir todos los compuestos de la ruta metabólica del 4EP, en la menor cantidad de disolvente posible y con la menor presencia de interferentes.

Como posibles disolventes de elución, se ensayaron MeOH y diferentes mezclas ACN:MeOH. Complementariamente se probaron mezclas de estos disolventes con tampón formiato 10

mM a pH 3, medio para el que el ácido cumárico estaría como especie neutra.

Los cartuchos para extracción en fase sólida una vez acondicionados, se cargaron con 5 mL de un patrón de 10 mg L^{-1} de los compuestos objetivo en agua (12% etanol), y se procedió a la limpieza de interferentes con 5 mL de agua (12% etanol) y 4 mL de diclorometano (previo secado del polímero). Finalmente se probaron 5 mL de diferentes disolventes de elución. Los eluatos se midieron por medio de LC-DAD-FD y se compararon las recuperaciones obtenidas (figura 3.28).

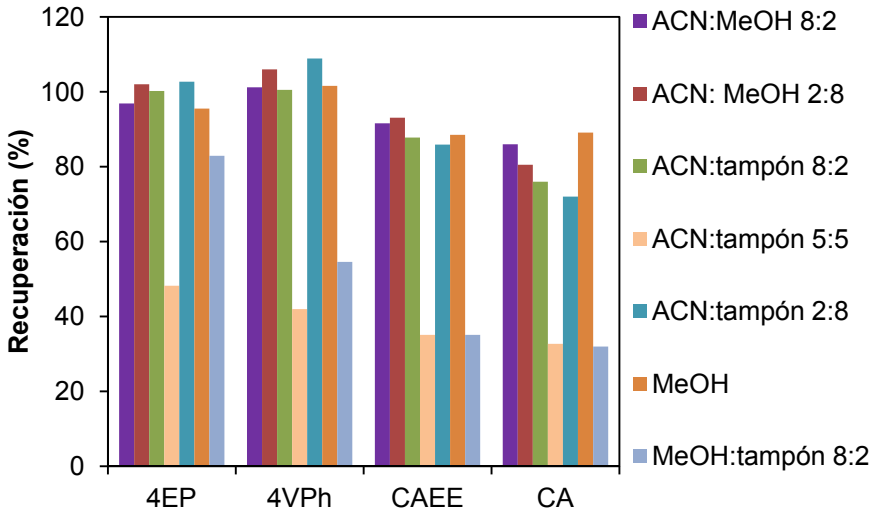

Figura 3. 28. Recuperaciones obtenidas para 4EP, 4VPh, CAEE y CA después de la elución con 5 mL de diferentes disolventes.

A pesar de que los mejores resultados para la elución de todos los compuestos en la disolución estándar fueron obtenidos con MeOH, al aplicar el método a muestras de vino, los eluatos presentaban más color y mayor señal asociada a los interferentes presentes en la matriz. Para evitar este hecho se utilizó la mezcla ACN:MeOH 8:2. Posteriormente, se optimizó el volumen de elución para conseguir la máxima recuperación de los analitos objetivo (figura 3.29). A pesar de que 3 mL era volumen suficiente para eluir el 4EP, 4VPh y CAEE, fue necesario ampliar este volumen hasta 5 mL para poder obtener una recuperación mayor del 80% para el compuesto CA.

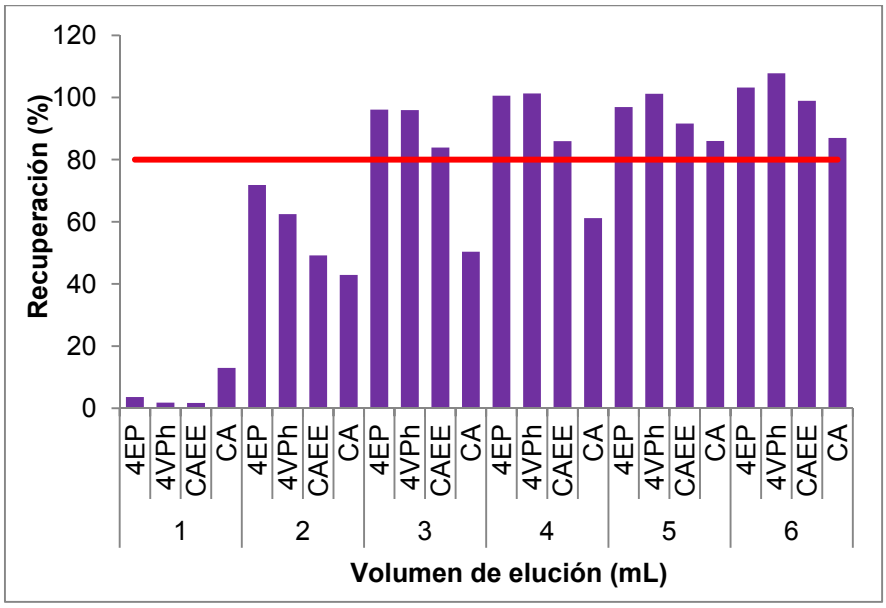

Figura 3. 29. Recuperaciones obtenidas para 4EP, 4VPh, CAEE y CA después de la elución con diferentes volúmenes de ACN: MeOH 8:2.

En la tabla 3.14 se resumen las distintas etapas del proceso de extracción de los compuestos pertenecientes a la ruta metabólica del 4EP, utilizando como fase sólida un polímero impreso MIP_{4EP}.

Tabla 3. 14. Resumen del proceso MISPE.

Etapa	Disolvente	Volumen
Acondicionamiento del adsorbente	Metanol	5 mL
	Agua (12% etanol)	5 mL
Carga	Muestra	5 mL
Lavado de interferencias	Agua (12% etanol)	5 mL
	Diclorometano	4 mL
Elución	Acetonitrilo:Metanol (8:2)	5 mL

7. Aplicación del método analítico a la extracción y cuantificación de los compuestos pertenecientes a la ruta metabólica del 4-etilfenol en vino

Una vez optimizadas las composiciones de los diferentes polímeros impresos MIP, la extracción en fase sólida con adsorbente MIP_{4EP} y la posterior separación cromatográfica utilizando como fase estacionaria el polímero MIP_{CA}, acoplada a un detector DAD y FD, se procedió al análisis de una muestra de vino para la comprobación de la aplicabilidad del método en muestras reales.

Dado que los compuestos objetivo se encuentran en el vino de forma natural, fue necesario utilizar el método de adiciones estándar para su cuantificación. Inicialmente, la información analítica del método fue obtenida a partir del estudio de la dependencia de la señal con la concentración para disoluciones patrón de los compuestos y se calculó el límite de detección (LOD) y de cuantificación (LOQ) instrumental para cada uno de ellos. Finalmente se midió la concentración de los compuestos pertenecientes a la ruta metabólica del 4EP en una muestra de vino y se calculó la exactitud del método.

7.1. Calibración del método, límite de detección y cuantificación

Para la calibración del método se cargaron en la fase impresa MIP_{4EP} disoluciones conjuntas de 4EP, 4VPh, CAEE y CA en agua (12% etanol) con concentraciones comprendidas entre 0.010 y 10 mg L^{-1}. Se llevo a cabo el método de extracción en fase sólida optimizado y los eluatos se midieron por LC-DAD-FD utilizando como fase estacionaria el polímero impreso MIP_{CA}. De la representación del área del pico de cada compuesto frente a la concentración, se obtuvo la curva de calibrado que fue ajustada por el método de mínimos cuadrados. Los resultados obtenidos se presentan en la tabla 3.15. Para el caso del 4EP y el 4VPh la dependencia del área del pico frente a la concentración era lineal en todo el rango de concentraciones estudiadas. Para el CAEE este era algo menor y para el CA el rango lineal se reducía a un intervalo de concentraciones comprendido entre 0.25 y 10 mg L^{-1}.

Los límites de detección y cuantificación instrumental, se calcularon según las siguientes expresiones:

$$C_{LOD} = \frac{3\sigma_B}{S} \qquad \textbf{3. 23}$$

$$C_{LOQ} = \frac{10\sigma_B}{S} \qquad \textbf{3. 24}$$

Donde σ_B es la desviación estándar de las medidas del blanco y S es la sensibilidad, obtenida del valor de la pendiente de la recta de calibración (tabla 3.15). El LOD para todos los compuestos era menor que 7 µg L^{-1} y el LOQ era menor que 23 µg L^{-1}, excepto para el CA. Esto puede ser debido a la mayor anchura de pico obtenida en el desarrollo cromatográfico para este compuesto, como es habitual para la separación del *template* en el material impreso cuando este se utiliza como fase estacionaria. Sin embargo, el límite de cuantificación resulta suficiente ya que los niveles de CA en vino suelen estar comprendidos entre 1 y 10 mg L^{-1} (270).

Tabla 3. 15. Parámetros correspondientes al calibrado, LOD y LOQ.

	Rango lineal (mg L^{-1})	Ordenada en el origen (µg L^{-1})	Pendiente (Au L µg^{-1})	R^2	LOD (µg L^{-1})	LOQ (µg L^{-1})
4EP	0.010 - 10	-58.52±93.8	526.24±32.76	0.992	2.63	8.77
4VPh	0.010 - 10	41.98±132.92	656.12±32.76	0.990	2.82	9.42
CAEE	0.025 - 10	-34.04±5.12	143.02±3.27	0.996	6.81	22.7
CA	0.25 - 10	26.69±26.56	25.22±8.01	0.987	66.1	220

7.2. Aplicación del método a la medida de los compuestos de la ruta del 4EP en vinos

Para la cuantificación de los compuestos pertenecientes a la ruta metabólica del 4EP en vino y en base a la dependencia de la señal frente a la concentración observada en el apartado anterior, se diseñó un método de adiciones estándar.

El método de adiciones estándar, se basa en la medida del aumento de señal que experimenta la muestra a medida que se añaden concentraciones conocidas de un patrón. Este método es especialmente adecuado cuando la composición de la muestra es desconocida o compleja y puede afectar a la señal analítica, siendo necesaria para su utilización una respuesta lineal del analito (271).

De acuerdo al método desarrollado, se analizó un vino tinto y ese mismo vino después de la adición de 5 mg L^{-1} de cada compuesto. En la figura 3.30 se muestran los cromatogramas obtenidos, donde se puede identificar la presencia de CAEE y CA en la muestra de vino. La cuantificación de estos dos analitos, se realizó después de la adición de concentraciones de 1, 2 y 3 mg L^{-1} de CAEE y 10, 20 y 30 mg L^{-1} de CA a 3 alicuotas del mismo vino. Estas muestras fueron analizadas y de acuerdo al método de adiciones estándar se cuantificaron 0.63±0.09 mg L^{-1} de CAEE y 7.07± 0.56 mg L^{-1} de CA en el vino.

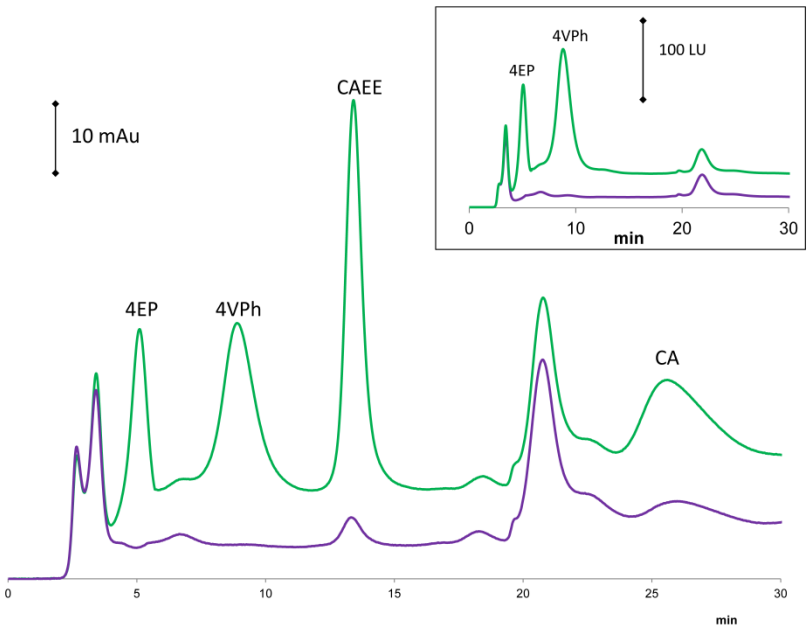

Figura 3. 30. Cromatogramas registrados para una muestra de vino tinto (——) y una muestra de vino tinto después de la adición de 5 mg L^{-1} de 4EP, 4VPh, CAEE y CA (——).

Finalmente, se calculó la exactitud del método, añadiendo a diferentes alicuotas del vino dos concentraciones conocidas de todos los compuestos objetivo 0.1 y 0.5 mg L^{-1} para todos los compuestos excepto para el CA que se añadieron 1 y 5 mg L^{-1} respectivamente. Las concentraciones de estas muestras fueron medidas por el método optimizado y se calcularon las recuperaciones para cada compuesto (tabla 3.16).

Para todos los compuestos y a todas las concentraciones añadidas las recuperaciones fueron superiores al 95 %, e inferiores

al 105% siendo las desviaciones estándar relativas inferiores al 8%. Esto demuestra que el método desarrollado es adecuado para la cuantificación de los compuestos pertenecientes a la ruta metabólica del 4EP en vinos.

Tabla 3. 16. Resumen de los resultados obtenidos en muestras de vino. Los valores medidos se presentan como la media ± DS para n= 3.

Compuesto	Añadido (mg L^{-1})	Medido (mg L^{-1})	Recuperación (%)	RSD (%)
4EP	-	<LOD	-	-
	0.1	0.095±0.005	95.2±5.1	5.3
	0.5	0.52±0.01	104.6±3.6	1.9
4VPh	-	<LOD	-	-
	0.1	0.099±0.007	99.2±7.0	7.1
	0.5	0.51±0.02	102.5±4.1	3.9
CAEE	-	0.63±0.09	-	14.3
	0.1	0.72±0.04	98.0±6.2	5.5
	0.5	1.23±0.05	109.2±8.4	4.1
CA	-	7.07±0.56	-	7.9
	1.0	8.28±0.54	102.6±6.7	6.5
	5.0	12.35±0.45	102.4±5.0	3.6

8. Conclusiones

En base al objetivo principal establecido y conforme a los resultados presentados a lo largo del capítulo, se puede concluir que se ha desarrollado un método para la extracción del 4-etilfenol y los compuestos pertenecientes a su ruta metabólica y su posterior separación cromatográfica y cuantificación en vino.

A su vez, se han alcanzado los objetivos operativos previamente descritos:

- Se ha sintetizado y caracterizado un polímero de huella molecular específico para el grupo de compuestos que constituyen la ruta metabólica del 4-etilfenol, utilizando como *template* este compuesto.
- Se ha desarrollado un método de extracción en fase sólida, utilizando como adsorbente el polímero impreso para la molécula 4EP (MIP_{4EP}).
- Se ha sintetizado y caracterizado un polímero de huella molecular capaz de separar con suficiente resolución cromatográfica, los compuestos pertenecientes a la ruta metabólica del 4-etifenol, usando como *template* el ácido cumárico.
- Se ha desarrollado un método que permite la extracción, separación cromatográfica y

cuantificación de los compuestos que forman parte de la ruta metabólica del 4EP en vinos.

Bibliografía

1. Alexander, C., Andersson, H.S., Andersson, L.I., Ansell, R.J., Kirsch, N., Nicholls, I.A., O'Mahony, J., Whitcombe, M.J. (2006). Molecular imprinting science and technology: A survey of the literature for the years up to and including 2003. *Journal of Molecular Recognition*, **19**, 106-180.
2. Yilmaz, E., Schmidt, R.H., Mosbach, K. (2004). The non-covalent approach. En *Molecularly Imprinted Materials*, Mingdi, Y. and Olof, R. (eds.) CRC Press, New York, págs. 25-57.
3. Haupt, K., Linares, A., Bompart, M., Bui, B. (2012). Molecularly Imprinted Polymers. En *Molecular Imprinting*, Springer Berlin Heidelberg, Vol. 325, págs. 1-28.
4. Wulff, G., Sarhan, A. (1972). Use of polymers with enzyme-analogous structures for the resolution of racemates. *Angewandte Chemie International Edition*, **11**, 341.
5. Arshady, R., Mosbach, K. (1981). Synthesis of substrate-selective polymers by host-guest polymerization. *Macromolecular Chemistry and Physics*, **182**, 687-692.
6. Shea, K.J., Thompson, E. (1978). Template synthesis of macromolecules. Selective functionalization of an organic polymer. *The Journal of Organic Chemistry*, **43**, 4253-4255.
7. Beckett, A.H., Anderson, P. (1957). A method for the determination of the configuration of organic molecules using "stereo-selective adsorbents." *Nature*, **179**, 1074-1075.
8. Mosbach, K. (1983). Novel affinity techniques. En *Affinity Chromatography and Biological Recognition*, Chaiken, I. (ed.) Elsevier Science, Orlando, FL, págs. 209-222.
9. Ramström, O., Andersson, L.I., Mosbach, K. (1993). Recognition sites incorporating both pyridinyl and carboxy functionalities prepared by molecular imprinting. *Journal of Organic Chemistry*, **58**, 7562-7564.
10. Polyakov, M.V. (1931). Adsorption properties and structure of silica gel. *Zhurnal Fizicheskoi Khimii*, **2**, 799-805.

11. Polyakov, M.V., Kuleshina, L.P., Neimark, I.E. (1937). The dependence of the adsorptive properties of silica gel on the character (nature) of its porosity. *Zhurnal Fizicheskoi Khimii*, **10**, 100-112.
12. Polyakov, M.V., Stadnik, P.M., Paritzkii, M.V., Malkin, I.M., Dukhina, F.S. (1933). The question of the structure of silica gel. *Zhurnal Fizicheskoi Khimii*, **4**, 454-456.
13. Pauling, L. (1940). Theory of the structure and process of formation of antibodies. *Journal of American Chemical Society*, **62**, 2643-2657.
14. Dickey, F.H. (1949). Preparation of specific adsorbents. *Proceedings of the National Academy of Sciences*, **35**, 227-229.
15. Pauling, L. (1949). Chemistry and the world of today. *Chemical Engineering News*, **27**, 2775-2778.
16. Dickey, F.H. (1955). Specific adsorption. *The Journal of Physical Chemistry*, **59**, 695-707.
17. Bernhard, S.A. (1953). The preparation of specific adsorbents. *Journal of the American Chemical Society*, **74**, 4946-4947.
18. Haldeman, R.G., Emmett, P.H. (1955). Specific adsorption of alkyl orange dyes on silica gel. *The Journal of Physical Chemistry*, **59**, 1039-1043.
19. Takagishi, T., Klotz, I.M. (1972). Macromolecule-small molecule interactions. Introduction of additional binding sites in polyethylenimine by disulfide crosslinkages. *Biopolymers*, **11**, 483-491.
20. Matthews, B.W., Sigler, P.B., Henderson, R., Blow, D.M. (1967). Three-dimensional structure of tosyl-alpha-chymotrypsin. *Nature*, **214**, 652-656.
21. Sagiv, J. (1980). Organized monolayers by adsorption. 1. Formation and structure of oleophobic mixed monolayers on solid surfaces. *Journal of American Chemical Society*, **102**, 92-98.
22. Sagiv, J. (1980). Organized monolayers by adsorption. III. Irreversible adsorption and memory effects in skeletonized silane monolayers. *Israel Journal of Chemistry*, **18**, 346-353.

23. Cohen, S.R., Naaman, R., Sagiv, J. (1986). Thermally induced disorder in organized organic monolayers on solid substrates. *The Journal of Physical Chemistry*, **90**, 3054-3056.
24. Rubinstein, I., Steinberg, S., Tor, Y., Shanzer, A., Sagiv, J. (1988). Ionic recognition and selective response in self-assembling monolayer membranes on electrodes. *Nature*, **332**, 426-429.
25. Andersson, L.I., Mandenius, C.F., Mosbach, K. (1988). Studies on guest-selective molecular recognition on an octadecylsilylated silicon surface using ellipsometry. *Tetrahedron Letters*, **29**, 5437-5440.
26. Kim, J.H., Cotton, T.M., Uphaus, R.A. (1988). Molecular recognition in monolayers and species detection by surface-enhanced resonance Raman spectroscopy. *Thin Solid Films*, **160**, 389-397.
27. Starodub, N.F., Piletsky, S.A., Lavryk, N.V., El'skaya, A.V. (1993). Template sensors for low weight organic molecules based on silica surfaces. *Sensors and Actuators B: Chemical*, **14**, 708-710.
28. Morita, M., Niwa, O., Horiuchi, T. (1997). Interdigitated array microelectrodes as electrochemical sensors. *Electrochimica Acta*, **42**, 3177-3183.
29. Glad, M., Norrloew, O., Sellergren, B., Siegbahn, N., Mosbach, K. (1985). Use of silane monomers for molecular imprinting and enzyme entrapment in polysiloxane-coated porous silica. *Journal of Chromatography A*, **347**, 11-23.
30. Marty, J.D., Mauzac, M., Fournier, C., Rico-Lattes, I., Lattes, A. (2002). Liquid crystal polysiloxane networks as materials for molecular imprinting technology: memory of the mesomorphic organization. *Liquid Crystals*, **29**, 529-536.
31. Zhang, Z., Dai, S., Hunt, R.D., Wei, Y., Qiu, S. (2001). Ion-imprinted zeolite: a surface functionalization methodology based on the "ship-in-bottle" technique. *Advanced Materials*, **13**, 493-496.

32. Wulff, G. (2013). Fourty years of molecular imprinting in synthetic polymers: origin, features and perspectives. *Microchimica Acta*, **180**, 1359-1370.
33. Wulff, G., Sarhan, A., Zabrocki, K. (1973). Enzyme-analogue built polymers and their use for the resolution of racemates. *Tetrahedron Letters*, **14**, 4329-4332.
34. Wulff, G., Sarhan, A. (1974). Patent DE2242796A1.
35. Damen, J., Neckers, D.C. (1980). Memory of synthesized vinyl polymers for their origins. *The Journal of Organic Chemistry*, **45**, 1382-1387.
36. Nishide, H., Tsuchida, E. (1976). Selective adsorption of metal ions on poly(4-vinylpyridine) resins in which the ligand chain is immobilized by crosslinking. *Die Makromolekulare Chemie*, **177**, 2295-2310.
37. Kabanov, V.A., Efendiev, A.A., Orudzhev, D.D. (1979). Complex-forming polymeric sorbents with macromolecular arrangement favorable for ion sorption. *Journal of Applied Polymer Science*, **24**, 259-267.
38. Yan, H., Row, K.H. (2006). Characteristic and synthetic approach of molecularly imprinted polymer. *International Journal of Molecular Sciences*, **7**, 155-178.
39. Piletska, E.V., Guerreiro, A.R., Whitcombe, M.J., Piletsky, S.A. (2009). Influence of the polymerization conditions on the performance of molecularly imprinted polymers. *Macromolecules*, **42**, 4921-4928.
40. Umpleby, R.J., II, Bode, M., Shimizu, K.D. (2000). Measurement of the continuous distribution of binding sites in molecularly imprinted polymers. *Analyst*, **125**, 1261-1265.
41. Venn, R.F., Goody, R.J. (1999). Synthesis and properties of molecular imprints of darifenacin: the potential of molecular imprinting for bioanalysis. *Chromatographia*, **50**, 407-414.
42. Ye, L., Mosbach, K. (2001). Polymers recognizing biomolecules based on a combination of molecular imprinting and proximity scintillation: A new sensor

concept. *Journal of American Chemical Society*, **123**, 2901-2902.

43. Ye, L., Weiss, R., Mosbach, K. (2000). Synthesis and characterization of molecularly imprinted microspheres. *Macromolecules*, **33**, 8239-8245.
44. Zhang, Z., Cheng, Z., Zhang, C.F., Wang, H., Li, J. (2012). Precipitation polymerization of molecularly imprinted polymers for recognition of melamine molecule. *Journal of Applied Polymer Science*, **123**, 962-967.
45. Perez, N., Whitcombe, M.J., Vulfson, E.N. (2000). Molecularly imprinted nanoparticles prepared by core-shell emulsion polymerization. *Journal of Applied Polymer Science*, **77**, 1851-1859.
46. Perez-Moral, N., Mayes, A.G. (2004). Comparative study of imprinted polymer particles prepared by different polymerisation methods. *Analytica Chimica Acta*, **504**, 15-21.
47. Tan, C.J., Wangrangsimakul, S., Bai, R., Tong, Y.W. (2008). Defining the interactions between proteins and surfactants for nanoparticle surface imprinting through miniemulsion polymerization. *Chemistry of Materials*, **20**, 118-127.
48. Vaihinger, D., Landfester, K., Krauter, I., Brunner, H., Tovar, G.E.M. (2002). Molecularly imprinted polymer nanospheres as synthetic affinity receptors obtained by miniemulsion polymerisation. *Macromolecular Chemistry and Physics*, **203**, 1965-1973.
49. Poma, A., Guerreiro, A., Whitcombe, M.J., Piletska, E.V., Turner, A.P.F., Piletsky, S.A. (2013). Solid-phase synthesis of molecularly imprinted polymer nanoparticles with a reusable template-"plastic antibodies". *Advanced Functional Materials*, **23**, 2821-2827.
50. Whitcombe, M.J. (2016). MIP database. http://www.mipdatabase.com/ **Consulta:** 29/02/2016.
51. Bowen, J.L., Manesiotis, P., Allender, C.J. (2013). Twenty years since 'antibody mimics' by molecular imprinting were first proposed: a critical perspective. *Molecular Imprinting*, **1**, 35-40.

52. Pichon, V., Chapuis-Hugon, F. (2008). Role of molecularly imprinted polymers for selective determination of environmental pollutants-A review. *Analytica Chimica Acta*, **622**, 48-61.
53. Gkementzoglou, C., Kotrotsiou, O., Koronaiou, M., Kiparissides, C. (2016). Development of a sandwich-type filtration unit packed with MIP nanoparticles for removal of atrazine from water sources. *Chemical Engineering Journal*, **287**, 233-240.
54. Ashrafian, S., Ataei, S.A., Jahanshahi, M. (2015). Novel composite membranes embedded with molecularly imprinted porous polymeric nanospheres for targeted phenol. *Polymers for Advanced Technologies*, **DOI: 10.1002/pat.3716**.
55. Tarley, C., de Oliveira, F.M., Segatelli, M.G. (2015). Preparation of a new restricted access molecularly imprinted hybrid adsorbent for the extraction of folic acid from milk powder samples. *Analytical Methods*, Ahead of Print.
56. Song, R., Hu, X., Guan, P., Li, J., Du, C., Qian, L., Wang, C. (2016). Surface modification of imprinted polymer microspheres with ultrathin hydrophilic shells to improve selective recognition of glutathione in aqueous media. *Materials Science and Engineering: C*, **60**, 1-6.
57. Anirudhan, T.S., Alexander, S. (2015). Selective determination of monosodium glutamate (Ajinomoto) in food samples using a potentiometric method with a modified multiwalled carbon nanotube based molecularly imprinted polymer. *RSC Advances*, **5**, 96840-96850.
58. Basozabal, I., Guerreiro, A., Gomez-Caballero, A., Goicolea, M.A., Barrio, R.J. (2014). Direct potentiometric quantification of histamine using solid-phase imprinted nanoparticles as recognition elements. *Biosensors and Bioelectronics*, **58**, 138-144.
59. Sanchez-Gonzalez, J., Jesus Tabernero, M., Maria Bermejo, A., Bermejo-Barrera, P., Moreda-Pineiro, A. (2015). Development of magnetic molecularly imprinted polymers

for solid phase extraction of cocaine and metabolites in urine before high performance liquid chromatography - tandem mass spectrometry. *Talanta*, **147**, 641-649.

60. Duan, H., Li, L., Wang, X., Wang, Y., Li, J., Luo, C. (2015). CdTe quantum dots@luminol for trace-level chemiluminescence sensing of phenacetin based on biological recognition materials. *New Journal of Chemistry*, **40**, 458-463.
61. Gutiérrez-Climente, R., Gómez-Caballero, A., Halhalli, M., Sellergren, B., Goicolea, M.A., Barrio, R.J. (2015). Iniferter-mediated grafting of molecularly imprinted polymers on porous silica beads for the enantiomeric resolution of drugs. *Journal of Molecular Recognition*, n/a-n/a.
62. Li, Y., Song, H., Zhang, L., Zuo, P., Ye, B.-c., Yao, J., Chen, W. (2016). Supportless electrochemical sensor based on molecularly imprinted polymer modified nanoporous microrod for determination of dopamine at trace level. *Biosensors and Bioelectronics*, **78**, 308-314.
63. Zeng, S., She, Y., Jiao, B., Liu, G., Wang, J., Su, X., Ma, X., Jin, M., Jin, F., Wang, S. (2015). Molecularly imprinted polymer for selective extraction and simultaneous determination of four tropane alkaloids from Przewalskia tangutica Maxim. fruit extracts using LC-MS/MS. *RSC Advances*, **5**, 94997-95006.
64. Kryscio, D.R., Peppas, N.A. (2012). Critical review and perspective of macromolecularly imprinted polymers. *Acta Biomaterialia*, **8**, 461-473.
65. Karfa, P., Roy, E., Patra, S., Kumar, D., Madhuri, R., Sharma, P.K. (2015). A fluorescent molecularly-imprinted polymer gate with temperature and pH as inputs for detection of alpha-fetoprotein. *Biosensors and Bioelectronics*, **78**, 454-463.
66. Li, W., Chen, M., Xiong, H., Wen, W., He, H., Zhang, X., Wang, S. (2015). Surface protein imprinted magnetic nanoparticles for specific recognition of bovine hemoglobin. *New Journal of Chemistry*, Ahead of Print.

67. Wulff, G., Biffis, A. (2001). Molecular imprinting with covalent or stoichiometric non-covalent interactions. En *Molecularly Imprinted Polymers Man-made Mimics of Antibodies and their Applications in Analytical Chemistry*, Börje, S. (ed.) Elsevier, Vol. 23, págs. 71-111.
68. Sellergren, B., Lepistoe, M., Mosbach, K. (1988). Highly enantioselective and substrate-selective polymers obtained by molecular imprinting utilizing noncovalent interactions. NMR and chromatographic studies on the nature of recognition. *Journal of American Chemical Society*, **110**, 5853-5860.
69. Mosbach, K., Ramstrom, O. (1996). The emerging technique of molecular imprinting and its future impact on biotechnology. *Nature Biotechnology*, **14**, 163-170.
70. Gupta, S.N., Neckers, D.C. (1982). Template effects in chelating polymers. *Journal of Polymer Science Part A: Polymer Chemistry*, **20**, 1609-1622.
71. Kato, M., Nishide, H., Tsuchida, E., Sasaki, T. (1981). Complexation of metal ion with poly(1-vinylimidazole) resin prepared by radiation-induced polymerization with template metal ion. *Journal of Polymer Science Polymer Chemistry Edition*, **19**, 1803-1809.
72. Wulff, G., Schulze, I., Zabrocki, K., Vesper, W. (1980). Enzyme-analog built polymers. 11. Binding sites in polymers with different numbers of binding groups. *Die Makromolekulare Chemie*, **181**, 531-544.
73. Wulff, G., Stellbrink, H. (1990). On the chemistry of binding sites. VII. Enantioselective binding using chiral boronic acids. *Recueil des Travaux Chimiques des Pays-Bas*, **109**, 216-221.
74. Wulff, G., Vietmeier, J. (1989). Enzyme-analogue built polymers. 25. Synthesis of macroporous copolymers from alpha-amino acid-based vinyl compounds. *Die Makromolekulare Chemie*, **190**, 1717-1726.
75. Kugimiya, A., Matsui, J., Takeuchi, T., Yano, K., Muguruma, H., Elgersma, A.V., Karube, I. (1995). Recognition of sialic

acid using molecularly imprinted polymer. *Analytical Letters*, **28**, 2317-2323.

76. Wulff, G., Vesper, W., Grobe-Einsler, R., Sarhan, A. (1977). Enzyme-analog built polymers, 4. The synthesis of polymers containing chiral cavities and their use for the resolution of racemates. *Die Makromolekulare Chemie*, **178**, 2799-2816.
77. Wulff, G., Poll, H.G. (1987). Enzyme-analog built polymers. 23. Influence of the structure of the binding sites on the selectivity for racemic resolution. *Die Makromolekulare Chemie*, **188**, 741-748.
78. Wulff, G., Haarer, J. (1991). Enzyme-analog built polymers. 29. The preparation of defined chiral cavities for the racemic resolution of free sugars. *Die Makromolekulare Chemie*, **192**, 1329-1338.
79. Wulff, G., Schauhoff, S. (1991). Enzyme-analog-built polymers. 27. Racemic resolution of free sugars with macroporous polymers prepared by molecular imprinting. Selectivity dependence on the arrangement of functional groups versus spatial requirements. *The Journal of Organic Chemistry*, **56**, 395-400.
80. Lin, Z., Wang, J., Tan, X., Sun, L., Yu, R., Yang, H., Chen, G. (2013). Preparation of boronate-functionalized molecularly imprinted monolithic column with polydopamine coating for glycoprotein recognition and enrichment. *Journal of Chromatography A*, **1319**, 141-147.
81. Li, L., Lu, Y., Bie, Z., Chen, H.-Y., Liu, Z. (2013). Photolithographic boronate affinity molecular imprinting: A general and facile approach for glycoprotein imprinting. *Angewandte Chemie International Edition*, **52**, 7451-7454.
82. Huynh, T.-P., Pietrzyk-Le, A., Bikram K. C, C., Noworyta, K.R., Sobczak, J.W., Sharma, P.S., D'Souza, F., Kutner, W. (2013). Electrochemically synthesized molecularly imprinted polymer of thiophene derivatives for flow-injection analysis determination of adenosine-5'-triphosphate (ATP). *Biosensors and Bioelectronics*, **41**, 634-641.

83. Shen, F., Ren, X. (2014). Covalent molecular imprinting made easy: a case study of mannose imprinted polymer. *RSC Advances*, **4**, 13123-13125.
84. Wulff, G., Best, W., Akelah, A. (1984). Enzyme-analog built polymers, 17. Investigations on the racemic resolution of amino acids. *Reactive Polymers, Ion Exchangers, Sorbents*, **2**, 167-174.
85. Wulff, G., Vietmeier, J. (1989). Enzyme-analog built polymers. 26. Enantioselective synthesis of amino acids using polymers possessing chiral cavities obtained by an imprinting procedure with template molecules. *Die Makromolekulare Chemie*, **190**, 1727-1735.
86. Wulff, G., Heide, B., Helfmeier, G. (1986). Enzyme-analog built polymers. 20. Molecular recognition through the exact placement of functional groups on rigid matrixes via a template approach. *Journal of American Chemical Society*, **108**, 1089-1091.
87. Shea, K.J., Stoddard, G.J., Shavelle, D.M., Wakui, F., Choate, R.M. (1990). Synthesis and characterization of highly crosslinked poly(acrylamides) and poly(methacrylamides). A new class of macroporous polyamides. *Macromolecules*, **23**, 4497-4507.
88. Wullf, G. (1982). Selective binding to polymers via covalent bonds. The construction of chiral cavities as specific receptor sites. *Pure and Applied Chemistry*, **54**, 2093-2102.
89. Shea, K.J., Dougherty, T.K. (1986). Molecular recognition on synthetic amorphous surfaces. The influence of functional group positioning on the effectiveness of molecular recognition. *Journal of American Chemical Society*, **108**, 1091-1093.
90. Shea, K.J., Sasaki, D.Y., Stoddard, G.J. (1989). Fluorescence probes for evaluating chain solvation in network polymers. An analysis of the solvatochromic shift of the dansyl probe in macroporous styrene-divinylbenzene and styrene-diisopropenylbenzene copolymers. *Macromolecules*, **22**, 1722-1730.

91. Shea, K.J., Sasaki, D.Y. (1989). On the control of microenvironment shape of functionalized network polymers prepared by template polymerization. *Journal of American Chemical Society*, **111**, 3442-3444.
92. Marty, J.D., Tizra, M., Mauzac, M., Rico-Lattes, I., Lattes, A. (1999). New molecular imprinting materials: liquid crystalline networks. *Macromolecules*, **32**, 8674-8677.
93. Shea, K.J., Thompson, E.A., Pandey, S.D., Beauchamp, P.S. (1980). Template synthesis of macromolecules. Synthesis and chemistry of functionalized macroporous poly(divinylbenzene). *Journal of American Chemical Society*, **102**, 3149-3155.
94. Damen, J., Neckers, D.C. (1980). Stereoselective syntheses via a photochemical template effect. *Journal of the American Chemical Society*, **102**, 3265-3267.
95. Damen, J., Neckers, D.C. (1980). On the memory of synthesized vinyl polymers for their origins. *Tetrahedron Letters*, **21**, 1913-1916.
96. Mosbach, K. (1994). Molecular imprinting. *Trends in Biochemical Sciences*, **19**, 9-14.
97. Sellergren, B., Hall, A.J. (2001). Fundamental aspects on the synthesis and characterisation of imprinted network polymers. En *Molecularly Imprinted Polymers Man-made Mimics of Antibodies and their Applications in Analytical Chemistry*, Börje, S. (ed.) Elsevier, Amsterdam, Vol. Volume 23, págs. 21-57.
98. Ronald, H.S., Klaus, M., Ecevit, Y. (2004). The Noncovalent Approach. En *Molecularly Imprinted Materials*, CRC Press, págs. 25-57.
99. Martins, M.C.G., Maia, P.P., Bergamin Boralli, V., Figueiredo, E.C., Martins, I. (2015). Determination of cotinine in urine by molecularly imprinted polymer solid phase and liquid-liquid extraction coupled with gas chromatography. *Analytical Letters*, **48**, 1245-1256.
100. Lv, Y.-K., Zhang, J.-Q., Guo, Z.-Y., Zhang, W., Sun, H.-W. (2015). Determination of tetracyclines residues in egg, milk, and milk powder by online coupling of a precolumn packed

with molecular imprinted hybrid composite materials to RP-HPLC-UV. *Journal of Liquid Chromatography & Related Technologies*, **38**, 1-7.

101. Wang, P., Liu, X., Su, X., Zhu, R. (2015). Sensitive detection of beta-agonists in pork tissue with novel molecularly imprinted polymer extraction followed liquid chromatography coupled tandem mass spectrometry detection. *Food Chemistry*, **184**, 72-79.
102. Motghare, R.V., Tadi, K.K., Dhawale, P., Deotare, S., Kawadkar, A.K., Chillawar, R., Khan, S. (2015). Voltammetric determination of uric acid based on molecularly imprinted polymer modified carbon paste electrode. *Electroanalysis*, **27**, 825-832.
103. Duan, F., Chen, C., Chen, L., Sun, Y., Wang, Y., Yang, Y., Liu, X., Qin, Y. (2014). Preparation and evaluation of water-compatible surface molecularly imprinted polymers for selective adsorption of bisphenol A from aqueous solution. *Industrial & Engineering Chemistry Research*, **53**, 14291-14300.
104. Lata, K., Sharma, R., Naik, L., Rajput, Y.S., Mann, B. (2015). Synthesis and application of cephalexin imprinted polymer for solid phase extraction in milk. *Food Chemistry*, **184**, 176-182.
105. Krupdam, R.J., Gour, D., Patel, G. (2014). Highly sensitive liquid chromatography-mass spectrometry detection of microcystins with molecularly imprinted polymer extraction from complicated aqueous ecosystems. *Chromatography & Separation Techniques*, **5**, 236-245.
106. Kugimiya, A., Kuwada, Y., Takeuchi, T. (2001). Preparation of sterol-imprinted polymers with the use of 2-(methacryloyloxy)ethyl phosphate. *Journal of Chromatography A*, **938**, 131-135.
107. Piacham, T., Isarankura-Na-Ayudhya, C., Prachayasittikul, V. (2015). Quercetin-imprinted polymer for anthocyanin extraction from mangosteen pericarp. *Materials Science and Engineering: C*, **51**, 127-131.

108. Egli, S.N., Butler, E.D., Bottaro, C.S. (2015). Selective extraction of light polycyclic aromatic hydrocarbons in environmental water samples with pseudo-template thin-film molecularly imprinted polymers. *Analytical Methods*, **7**, 2028-2035.
109. Duan, Z., Yi, J., Fang, G., Fan, L., Wang, S. (2013). A sensitive and selective imprinted solid phase extraction coupled to HPLC for simultaneous detection of trace quinoxaline-2-carboxylic acid and methyl-3-quinoxaline-2-carboxylic acid in animal muscles. *Food Chemistry*, **139**, 274-280.
110. Vishnuvardhan, V., Kalyan, Y., Prathish, K.P., Gangadhar, B., Tharakeswar, Y., Rao, T.P., Naidu, G.R. (2011). Imprinted polymer inclusion membrane based potentiometric sensor for determination and quantification of diethyl chlorophosphate in natural waters. *American Journal of Analytical Chemistry*, **2**, 374-380.
111. De Lima, G.C., Lago, A.C., Chaves, A.A., Fadini, P.S., Luccas, P.O. (2013). Determination of selenium using atomically imprinted polymer (AIP) and hydride generation atomic absorption spectrometry. *Analytica Chimica Acta*, **768**, 35-40.
112. Muhammad, K., Muhammad, T., Turahun, Y., Yakup, B. (2014). Screening the best functional monomer for preparation of molecularly imprinted polymer of 4-nitrophenol and its application on solid phase extraction of water sample. *Yingyong Huaxue*, **31**, 482-488.
113. Gai, Q.-Q., Qu, F., Zhang, T., Zhang, Y.-K. (2011). The preparation of bovine serum albumin surface-imprinted superparamagnetic polymer with the assistance of basic functional monomer and its application for protein separation. *Journal of Chromatography A*, **1218**, 3489-3495.
114. Cela-Perez, M.C., Barbosa-Pereira, L., Vecino, X., Perez-Ameneiro, M., Latorre, A.L., Lopez-Vilarino, J.M., Gonzalez Rodriguez, M.V., Moldes, A.B., Cruz, J.M. (2015). Selective removal of ATP degradation products from food matrices II: Rapid screening of hypoxanthine and inosine by molecularly

imprinted matrix solid-phase dispersion for evaluation of fish freshness. *Talanta*, **135**, 58-66.

115. Iqbal, N., Mustafa, G., Lieberzeit, P.A. (2013). Mass sensitive multi-sensor platform for receptor screening and quantification purposes. *Journal of the Chinese Advanced Materials Society*, **1**, 200-209.
116. Lu, X.-F., Shi, Y.-f., Lv, H.-L., Fu, Y.-Y., Ma, D., Xue, W. (2014). Preparation and characterization of molecularly imprinted poly(hydroxyethyl methacrylate) microspheres for sustained release of gatifloxacin. *Journal of Materials Science:Materials in Medicine*, **25**, 1461-1469.
117. Omranipour, H.M., Sajadi, T.S.A., Kowsari, R., Rad, M.S., Mohajeri, S.A. (2015). Brimonidine imprinted hydrogels and evaluation of their binding and releasing properties as new ocular drug delivery systems. *Current Drug Delivery*, **12**, 717-725.
118. Wulff, G., Schoenfeld, R. (1998). Polymerizable amidines. Adhesion mediators and binding sites for molecular imprinting. *Advanced Materials*, **10**, 957-959.
119. Aherne, A., Alexander, C., Payne, M.J., Perez, N., Vulfson, E.N. (1996). Bacteria-mediated lithography of polymer surfaces. *Journal of the American Chemical Society*, **118**, 8771-8772.
120. Hall, A.J., Manesiotis, P., Emgenbroich, M., Quaglia, M., De Lorenzi, E., Sellergren, B. (2005). Urea host monomers for stoichiometric molecular imprinting of oxyanions. *Journal of Organic Chemistry*, **70**, 1732-1736.
121. Urraca, J.L., Moreno-Bondi, M.C., Hall, A.J., Sellergren, B. (2007). Direct extraction of penicillin G and derivatives from aqueous samples using a stoichiometrically imprinted polymer. *Analytical Chemistry*, **79**, 695-701.
122. Sellergren, B., Andersson, L. (1990). Molecular recognition in macroporous polymers prepared by a substrate analog imprinting strategy. *The Journal of Organic Chemistry*, **55**, 3381-3383.
123. Whitcombe, M.J., Vulfson, E.N. (2001). Covalent imprinting using sacrificial spacers. En *Molecularly Imprinted Polymers*

Man-made Mimics of Antibodies and their Applications in Analytical Chemistry, Börje, S. (ed.) Elsevier, Amsterdam, Vol. Volume 23, págs. 203-212.

124. Fu, J., Chen, L., Li, J., Zhang, Z. (2015). Current status and challenges of ion imprinting. *Journal of Material Chemistry A*, **3**, 13598-13627.
125. Branger, C., Meouche, W., Margaillan, A. (2013). Recent advances on ion-imprinted polymers. *Reactive and Functional Polymers*, **73**, 859-875.
126. Chen, L., Xu, S., Li, J. (2011). Recent advances in molecular imprinting technology: current status, challenges and highlighted applications. *Chemical Society Reviews*, **40**, 2922-2942.
127. Spivak, D.A. (2004). Selectivity in molecularly imprinted matrices. En *Molecularly Imprinted Materials*, Yan, M. and Ramström, O. (eds.) CRC Press, págs. 395-417.
128. Sellergren, B. (1999). Polymer- and template-related factors influencing the efficiency in molecularly imprinted solid-phase extractions. *Trends in Analytical Chemistry*, **18**, 164-174.
129. Komiyama, M., Takeuchi, T., Mukawa, T., Asanuma, H. (2002). Experimental Methods (1) – Procedures of Molecular Imprinting. En *Molecular Imprinting*, Wiley-VCH Verlag GmbH & Co. KGaA, págs. 21-45.
130. Molinelli, A., O'Mahony, J., Nolan, K., Smyth, M.R., Jakusch, M., Mizaikoff, B. (2005). Analyzing the mechanisms of selectivity in biomimetic self-assemblies via IR and NMR spectroscopy of prepolymerization solutions and molecular dynamics simulations. *Analytical Chemistry*, **77**, 5196-5204.
131. Navarro-Villoslada, F., San Vicente, B., Moreno-Bondi, M.C. (2004). Application of multivariate analysis to the screening of molecularly imprinted polymers for bisphenol A. *Analytica Chimica Acta*, **504**, 149-162.
132. Shi, X., Wu, A., Qu, G., Li, R., Zhang, D. (2007). Development and characterization of molecularly imprinted polymers based on methacrylic acid for selective recognition of drugs. *Biomaterials*, **28**, 3741-3749.

133. Kubo, T., Koterasawa, K., Naito, T., Otsuka, K. (2015). Molecularly imprinted polymer with a pseudo-template for thermo-responsive adsorption/desorption based on hydrogen bonding. *Microporous and Mesoporous Materials*, **218**, 112-117.
134. Miura, C., Li, H., Matsunaga, H., Haginaka, J. (2015). Molecularly imprinted polymer for chlorogenic acid by modified precipitation polymerization and its application to extraction of chlorogenic acid from Eucommia ulmodies leaves. *Journal of Pharmaceutical and Biomedical Analysis*, **114**, 139-144.
135. Pschenitza, M., Hackenberg, R., Niessner, R., Knopp, D. (2014). Analysis of benzo[a]pyrene in vegetable oils using molecularly imprinted solid phase extraction (MISPE) coupled with enzyme-linked immunosorbent assay (ELISA). *Sensors*, **14**, 9720-9737.
136. Sun, G.-Y., Zhong, D.-D., Li, X.-J., Luo, Y.-Q., Ba, H., Liu, Z.-S., Aisa, H.A. (2015). Effect of minimizing amount of template by addition of macromolecular crowding agent on preparation of molecularly imprinted monolith. *Analytical and Bioanalytical Chemistry*, **407**, 7401-7412.
137. Rodriguez-Fernandez, R., Pena-Vazquez, E., Bermejo-Barrera, P. (2015). Synthesis of an imprinted polymer for the determination of methylmercury in marine products. *Talanta*, **144**, 636-641.
138. Vallo, L.L., Laxamana, R.T., Paredes, F.U., Arellano, I.H.J., Arco, S.D. (2015). Harnessing non-covalent interactions in molecular traps for probable human carcinogen butylated hydroxyanisole. *Materials Letters*, **159**, 317-320.
139. Sun, X., Zhang, C., Huang, Y.-P., Liu, Z.-S. (2015). Separation of epigallocatechin gallate from natural plant extracts using crowding agents-assisted imprinted polymers. *Chromatographia*, **78**, 995-1003.
140. Ebarvia, B.S., Ubando, I.E., Sevilla, F.B., III (2015). Biomimetic piezoelectric quartz crystal sensor with chloramphenicol-imprinted polymer sensing layer. *Talanta*, **144**, 1260-1265.

141. Zeng, S., She, Y., Jiao, B., Liu, G., Wang, J., Su, X., Ma, X., Jin, M., Jin, F., Wang, S. (2015). Molecularly imprinted polymer for selective extraction and simultaneous determination of four tropane alkaloids from Przewalskia tangutica Maxim. fruit extracts using LC-MS/MS. *RSC Advances*, **5**, 94997-95006.
142. Hajizadeh, S., Xu, C., Kirsebom, H., Ye, L., Mattiasson, B. (2013). Cryogelation of molecularly imprinted nanoparticles: A macroporous structure as affinity chromatography column for removal of beta-blockers from complex samples. *Journal of Chromatography A*, **1274**, 6-12.
143. Arabzadeh, N., Khosravi, A., Mohammadi, A., Mahmoodi, N.M. (2014). Enhanced photodegradation of hazardous tartrazine by composite of nanomolecularly imprinted polymer-nanophotocatalyst with high efficiency. *Desalination and Water Treatment*, **57**, 3142-3151.
144. Huang, C., Shen, X. (2014). Janus molecularly imprinted polymer particles. *Chemical Communications*, **50**, 2646-2649.
145. Eisenberg, A. (1970). Clustering of ions in organic polymers. A theoretical approach. *Macromolecules*, **3**, 147-154.
146. Khokhlov, A.R., Kramarenko, E.Y. (1996). Weakly charged polyelectrolytes: Collapse induced by extra ionization. *Macromolecules*, **29**, 681-685.
147. Piletska, E.V., Guerreiro, A.R., Romero-Guerra, M., Chianella, I., Turner, A.P.F., Piletsky, S.A. (2008). Design of molecular imprinted polymers compatible with aqueous environment. *Analytica Chimica Acta*, **607**, 54-60.
148. Vendamme, R., Eevers, W., Kaneto, M., Minamizaki, Y. (2009). Influence of polymer morphology on the capacity of molecularly imprinted resins to release or to retain their template. *Polymer Journal*, **41**, 1055-1066.
149. Kempe, M., Mosbach, K. (1991). Binding studies on substrate- and enantio-selective molecularly imprinted polymers. *Analytical Letters*, **24**, 1137-1145.

150. Mosbach, K., Ramstroem, O. (1996). The emerging technique of molecular imprinting and its future impact on biotechnology. *Bio/Technology*, **14**, 163-170.
151. Bakas, I., Ben Oujji, N., Istamboulie, G., Piletsky, S., Piletska, E., Ait-Addi, E., Ait-Ichou, I., Noguer, T., Rouillon, R. (2014). Molecularly imprinted polymer cartridges coupled to high performance liquid chromatography (HPLC-UV) for simple and rapid analysis of fenthion in olive oil. *Talanta*, **125**, 313-318.
152. Rosengren, A.M., Karlsson, B.C.G., Nicholls, I.A. (2013). Consequences of morphology on molecularly imprinted polymer-ligand recognition. *International Journal of Molecular Sciences*, **14**, 1207-1217.
153. O'Shannessy, D.J., Ekberg, B., Mosbach, K. (1989). Molecular imprinting of amino acid derivatives at low temperature (0°C) using photolytic homolysis of azobisnitriles. *Analytical Biochemistry*, **177**, 144-149.
154. O'Mahony, J., Moloney, M., McCormack, M., Nicholls, I.A., Mizaikoff, B., Danaher, M. (2013). Design and implementation of an imprinted material for the extraction of the endocrine disruptor bisphenol A from milk. *Journal of Chromatography B*, **931**, 164-169.
155. Torres, J.J., Gsponer, N., Ramirez, C.L., Vera, D.M.A., Montejano, H.A., Chesta, C.A. (2012). Experimental and theoretical studies on the enantioselectivity of molecularly imprinted polymers prepared with a chiral functional monomer. *Journal of Chromatography A*, **1266**, 24-33.
156. Mijangos, I., Navarro-Villoslada, F., Guerreiro, A., Piletska, E., Chianella, I., Karim, K., Turner, A., Piletsky, S. (2006). Influence of initiator and different polymerisation conditions on performance of molecularly imprinted polymers. *Biosensors and Bioelectronics*, **22**, 381-387.
157. Piletsky, S.A., Piletska, E.V., Karim, K., Freebairn, K.W., Legge, C.H., Turner, A.P.F. (2002). Polymer cookery: Influence of polymerization conditions on the performance of molecularly imprinted polymers. *Macromolecules*, **35**, 7499-7504.

158. Carraher, C.E. (2000). Free Radical Chain Polymerization (Addition Polymerization). En *Polymer chemistry*, Lagowski, J.J. (ed.) Marcel Dekker, New York, págs. 326-366.
159. Kyzas, G.Z., Bikiaris, D.N., Lazaridis, N.K. (2009). Selective separation of basic and reactive dyes by molecularly imprinted polymers (MIPs). *Chemical Engineering Journal*, **149**, 263-272.
160. Guo, T.Y., Xia, Y.Q., Hao, G.J., Song, M.D., Zhang, B.H. (2004). Adsorptive separation of hemoglobin by molecularly imprinted chitosan beads. *Biomaterials*, **25**, 5905-5912.
161. Holroyd, S.E., Groves, P., Searle, M.s., Gerhard, U., Williams, D.H. (1993). Rational design and binding of modified cell-wall peptides to vancomycin-group antibiotics: factorizing free energy contributions to binding. *Tetrahedron*, **49**, 9171-9182.
162. Wulff, G. (1995). Molecular imprinting in crosslinked materials with the aid of molecular templates - a way towards artificial antibodies. *Angewandte Chemie International Edition*, **34**, 1812-1832.
163. Yu, C., Mosbach, K. (2000). Influence of mobile phase composition and cross-linking density on the enantiomeric recognition properties of molecularly imprinted polymers. *Journal of Chromatography A*, **888**, 63-72.
164. Sellergren, B., Shea, K.J. (1993). Influence of polymer morphology on the ability of imprinted network polymers to resolve enantiomers. *Journal of Chromatography A*, **635**, 31-49.
165. Bruyneel, C., Zeegers-Huyskens, T. (2000). Infrared spectra of N-tert-butoxycarbonylamino acids at different temperatures. *Journal of Molecular Structure*, **552**, 177-185.
166. Steinke, J.H.G., Dunkin, I.R., Sherrington, D.C. (1999). A simple polymerizable carboxylic acid receptor: 2-acrylamido pyridine. *Trends in Analitycal Chemistry*, **18**, 159-164.
167. Sellergren, B., Dauwe, C., Schneider, T. (1997). Pressure-induced binding sites in molecularly imprinted network polymers. *Macromolecules*, **30**, 2454-2459.

168. Beuermann, S., Buback, M. (2002). Rate coefficients of free-radical polymerization deduced from pulsed laser experiments. *Progress in Polymer Science*, **27**, 191-254.
169. Piletsky, S.A., Guerreiro, A., Piletska, E.V., Chianella, I., Karim, K., Turner, A.P.F. (2004). Polymer cookery. 2. Influence of polymerization pressure and polymer swelling on the performance of molecularly imprinted polymers. *Macromolecules*, **37**, 5018-5022.
170. Piletsky, S.A., Mijangos, I., Guerreiro, A., Piletska, E.V., Chianella, I., Karim, K., Turner, A.P.F. (2005). Polymer cookery: influence of polymerization time and different initiation conditions on performance of molecularly imprinted polymers. *Macromolecules*, **38**, 1410-1414.
171. Harris, D.C. (2007). Introduction to separation sciences. En *Quantitative Chemical Analysis*, W. H. Freeman and Co., New York, USA, págs. 501-522.
172. Vasapollo, G., Del Sole, R., Mergola, L., Lazzoi, M.R., Scardino, A., Scorrano, S., Mele, G. (2011). Molecularly Imprinted Polymers: present and future prospective. *International Journal of Molecular Sciences*, **12**, 5908-5945.
173. Wei, S., Mizaikoff, B. (2007). Recent advances on noncovalent molecular imprints for affinity separations. *Journal of Separation Science*, **30**, 1794-1805.
174. Kadhirvel, P., Azenha, M., Silva, A.F., Sellergren, B. (2015). Chromatographycally efficient microspherical composites of molecularly imprinted xerogels deposited inside mesoporous silica. *Journal of Chromatography A*, **1355**, 158-163.
175. Liu, J., Zhang, L., Le, L.H.S., Liu, Y., Tang, H., Li, Y. (2015). Synthesis of metronidazole-imprinted molecularly imprinted polymers by distillation precipitation polymerization and their use as a solid-phase adsorbent and chromatographic filler. *Journal of Separation Science*, **38**, 1172-1178.
176. Niu, Y., Ma, M., Gong, Y., Wang, Y., Gong, B. (2014). Synthesis of chlorogenic acid imprinted chromatographic packing by surface-initiated atom transfer radical

polymerization and its application. *Chemical Research in Chinese Universities*, **30**, 855-862.

177. Li, P., Wang, T., Lei, F., Tang, P., Tan, X., Liu, Z., Shen, L. (2014). Rosin-based molecularly imprinted polymers as the stationary phase in high-performance liquid chromatography for selective separation of berberine hydrochloride. *Polymer International*, **63**, 1699-1706.
178. Dong, H., Wang, Y., Ou, Y., She, J., Shen, X., Li, J., Zhang, C., Liu, L. (2014). Preparation of molecularly imprinted polymer for chiral recognition of racemic 1,1'-binaphthalene-2,2'-diamine by HPLC. *Acta Chromatographica*, **26**, 683-693.
179. Rodríguez-Reino, M.P., Rodríguez-Fernández, R., Peña-Vázquez, E., Domínguez-González, R., Bermejo-Barrera, P., Moreda-Piñeiro, A. (2015). Mercury speciation in seawater by liquid chromatography-inductively coupled plasma-mass spectrometry following solid phase extraction pre-concentration by using an ionic imprinted polymer based on methyl-mercury-phenobarbital interaction. *Journal of Chromatography A*, **1391**, 9-17.
180. Asir, S., Derazshamshir, A., Yilmaz, F., Denizli, A. (2015). Triazine herbicide imprinted monolithic column for capillary electrochromatography. *Electrophoresis*, **36**, 2888-2895.
181. Wu, Y., Zhang, W., Chen, Y., Chen, Z. (2015). Electroosmotic pump-supported molecularly imprinted monolithic column for capillary chromatographic separation of nitrophenol isomers. *Electrophoresis*, **36**, 2881-2887.
182. Zong, H.-Y., Liu, X., Liu, Z.-S., Huang, Y.-P. (2015). Molecular crowding-based imprinted monolithic column for capillary electrochromatography. *Electrophoresis*, **36**, 818-824.
183. Derazshamshir, A., Yilmaz, F., Denizli, A. (2015). Molecularly imprinted hydrophobic polymers as a tool for separation in capillary electrochromatography. *Analytical Methods*, **7**, 2659-2669.
184. Zhao, M., Ma, X., Zhao, F., Guo, H. (2016). Molecularly imprinted polymer silica monolith for the selective extraction of alpha-cypermethrin from soil samples. *Journal of Materials Science*, **51**, 3440-3447.

185. He, H., Gu, X., Shi, L., Hong, J., Zhang, H., Gao, Y., Du, S., Chen, L. (2015). Molecularly imprinted polymers based on SBA-15 for selective solid-phase extraction of baicalein from plasma samples. *Analytical and Bioanalytical Chemistry*, **407**, 509-519.
186. Fasihi, J., Shamsipur, M., Khanchi, A., Mahani, M., Ashtari, K. (2016). Imprinted polymer grafted from silica particles for on-line trace enrichment and ICP OES determination of uranyl ion. *Microchemical Journal*, **126**, 316-321.
187. Divya, M.P., Rajput, Y.S., Sharma, R., Singh, G. (2015). Molecularly imprinted polymer for separation of lactate. *Journal of Analytical Chemistry*, **70**, 1213-1217.
188. Yuan, K., Wang, J., Zhai, H., Chen, Z., Huang, L., Su, Z. (2015). Sensitive determination of rose bengal in brown sugar by a molecularly imprinted solid-phase extraction monolithic capillary column coupled with capillary electrophoresis. *Analytical Methods*, **7**, 8297-8303.
189. Santos, M.G., Tavares, I.M.C., Boralli, V.B., Figueiredo, E.C. (2015). Direct doping analysis of beta-blocker drugs from urinary samples by on-line molecularly imprinted solid-phase extraction coupled to liquid chromatography/mass spectrometry. *Analyst*, **140**, 2696-2703.
190. Alizadeh, T., Shamkhali, A.N. (2016). Chiral resolution of salbutamol in plasma sample by a new chiral ligand-exchange chromatography method after its extraction with nano-sized imprinted polymer. *Journal of Chromatography B*, **1009-1010**, 96-106.
191. Gao, R., Cui, X., Hao, Y., He, G., Zhang, M., Tang, Y. (2016). Preparation of Cu2+-mediated magnetic imprinted polymers for the selective sorption of bovine hemoglobin. *Talanta*, **150**, 46-53.
192. Wu, S.G., Lai, E.P.C., Mayer, P.M. (2004). Molecularly imprinted solid phase extraction-pulsed elution-mass spectrometry for determination of cephalexin and alpha-aminocephalosporin antibiotics in human serum. *Journal of Pharmaceutical and Biomedical Analysis*, **36**, 483-490.

193. Mullett, W.M., Dirie, M.F., Lai, E.P.C., Guo, H., He, X. (2000). A 2-aminopyridine molecularly imprinted polymer surrogate micro-column for selective solid phase extraction and determination of 4-aminopyridine. *Analytica Chimica Acta*, **414**, 123-131.
194. Mullett, W.M., Lai, E.P. (1999). Rapid determination of theophylline in serum by selective extraction using a heated molecularly imprinted polymer micro-column with differential pulsed elution. *Journal of Pharmaceutical and Biomedical Analysis*, **21**, 835-843.
195. M. Mullett, W., P. C. Lai, E., Sellergren, B. (1999). Determination of nicotine in tobacco by molecularly imprinted solid phase extraction with differential pulsed elution. *Analytical Communications*, **36**, 217-220.
196. Hashemi-Moghaddam, H., Ahmadifard, M. (2016). Novel molecularly-imprinted solid-phase microextraction fiber coupled with gas chromatography for analysis of furan. *Talanta*, **150**, 148-154.
197. Ji, X., Li, D., Li, H. (2015). Preparation and application of a novel molecularly imprinted solid-phase microextraction monolith for selective enrichment of cholecystokinin neuropeptides in human cerebrospinal fluid. *Biomedical Chromatography*, **29**, 1280-1289.
198. Zhang, X., Xu, S., Lim, J.-M., Lee, Y.-I. (2012). Molecularly imprinted solid phase microextraction fiber for trace analysis of catecholamines in urine and serum samples by capillary electrophoresis. *Talanta*, **99**, 270-276.
199. Li, J.-W., Wang, Y.-L., Yan, S., Li, X.-J., Pan, S.-Y. (2016). Molecularly imprinted calixarene fiber for solid-phase microextraction of four organophosphorous pesticides in fruits. *Food Chemistry*, **192**, 260-267.
200. Moein, M.M., Javanbakht, M., Karimi, M., Akbari-adergani, B. (2015). Molecularly imprinted sol-gel nanofibers based solid phase microextraction coupled on-line with high performance liquid chromatography for selective determination of acesulfame. *Talanta*, **134**, 340-347.

201. Zhou, M., Hu, F., He, H., Shu, S., Wang, M. (2015). Determination of phosphorothioate pesticides in environmental water by molecularly imprinted matrix solid-phase dispersion coupled with gas chromatography and a nitrogen phosphorus detector. *Instrumentation Science & Technology*, **43**, 669-680.
202. Chen, X.-H., Zhao, Y.-G., Zhang, Y., Shen, H.-Y., Pan, S.-D., Jin, M.-C. (2015). Ethylenediamine-functionalized superparamagnetic carbon nanotubes for magnetic molecularly imprinted polymer matrix solid-phase dispersion extraction of 12 fluoroquinolones in river water. *Analytical Methods*, **7**, 5838-5846.
203. Wang, Y., Chen, L. (2015). Analysis of Malachite Green in aquatic products by carbon nanotube-based molecularly imprinted - matrix solid phase dispersion. *Journal of Chromatography B*, **1002**, 98-106.
204. Ganan, J., Morante-Zarcero, S., Gallego-Pico, A., Garcinuno, R.M., Fernandez-Hernando, P., Sierra, I. (2014). Evaluation of a molecularly imprinted polymer for determination of steroids in goat milk by matrix solid phase dispersion. *Talanta*, **126**, 157-162.
205. Fan, W., Gao, M., He, M., Chen, B., Hu, B. (2015). Cyromazine imprinted polymers for selective stir bar sorptive extraction of melamine in animal feed and milk samples. *Analyst*, **140**, 4057-4067.
206. Unceta, N., Gomez-Caballero, A., Garcia, D., Diaz, G., Guerreiro, A., Piletsky, S., Goicolea, M.A., Barrio, R.J. (2013). Enantioselective extraction of (+)-(S)-citalopram and its main metabolites using a tailor-made stir bar chiral imprinted polymer for their LC-ESI-MS/MS quantitation in urine samples. *Talanta*, **116**, 448-453.
207. Wang, S., Wei, J., Hao, T.T., Guo, Z.Y. (2012). Determination of ractopamine in pork by using electrochemiluminescence inhibition method combined with molecularly imprinted stir bar sorptive extraction. *Journal of Electroanalytical Chemistry*, **664**, 146-151.

208. Hu, Y., Li, J., Hu, Y., Li, G. (2010). Development of selective and chemically stable coating for stir bar sorptive extraction by molecularly imprinted technique. *Talanta*, **82**, 464-470.
209. Yang, L., Zhao, X., Zhou, J. (2010). Selective enrichment and determination of nicosulfuron in water and soil by a stir bar based on molecularly imprinted polymer coatings. *Analytica Chimica Acta*, **670**, 72-77.
210. Zhu, X., Zhu, Q. (2008). Molecular imprinted nylon-6 stir bar as a novel extraction technique for enantioseparation of amino acids. *Journal of Applied Polymer Science*, **109**, 2665-2670.
211. Zhu, X., Cai, J., Yang, J., Su, Q., Gao, Y. (2006). Films coated with molecular imprinted polymers for the selective stir bar sorption extraction of monocrotophos. *Journal of Chromatography A*, **1131**, 37-44.
212. Sellergren, B., Ekberg, B., Mosbach, K. (1985). Molecular imprinting of amino acid derivatives in macroporous polymers. Demonstration of substrate- and enantio-selectivity by chromatographic resolution of racemic mixtures of amino acid derivatives. *Journal of Chromatography*, **347**, 1-10.
213. Song, X., Xu, S., Chen, L., Wei, Y., Xiong, H. (2014). Recent advances in molecularly imprinted polymers in food analysis. *Journal of Applied Polymer Science*, **131**, 40766.
214. Lee, W.-C., Cheng, C.-H., Pan, H.-H., Chung, T.-H., Hwang, C.-C. (2008). Chromatographic characterization of molecularly imprinted polymers. *Analytical and Bioanalytical Chemistry*, **390**, 1101-1109.
215. Cheong, W.J., Yang, S.H., Ali, F. (2013). Molecular imprinted polymers for separation science: A review of reviews. *Journal of Separation Science*, **36**, 609-628.
216. Harris, D.C. (2007). Chromatographic methods and capillary electrophoresis. En *Quantitative Chemical Analysis.* , W. H. Freeman and Co., New York, USA, págs. 588-620.
217. Turiel, E., Martín-Esteban, A. (2010). Molecularly imprinted polymers for sample preparation: A review. *Analytica Chimica Acta*, **668**, 87-99.

218. Smith, R.M. (2003). Before the injection - modern methods of sample preparation for separation techniques. *Journal of Chromatography A*, **1000**, 3-27.
219. Pichon, V., Bouzige, M., Miege, C., Hennion, M.-C. (1999). Immunosorbents: natural molecular recognition materials for sample preparation of complex environmental matrixes. *Trends in Analytical Chemistry*, **18**, 219-235.
220. Nelson, M.A., Moser, A., Hage, D.S. (2010). Biointeraction analysis by high-performance affinity chromatography: Kinetic studies of immobilized antibodies. *Journal of Chromatography B*, **878**, 165-171.
221. Luo, P., Chen, X., Liang, C., Kuang, H., Lu, L., Jiang, Z., Wang, Z., Li, C., Zhang, S., Shen, J. (2010). Simultaneous determination of thiamphenicol, florfenicol and florfenicol amine in swine muscle by liquid chromatography-tandem mass spectrometry with immunoaffinity chromatography clean-up. *Journal of Chromatography B*, **878**, 207-212.
222. Klinglmayr, C., Noebauer, K., Razzazi-Fazeli, E., Cichna-Markl, M. (2010). Determination of deoxynivalenol in organic and conventional food and feed by sol-gel immunoaffinity chromatography and HPLC-UV detection. *Journal of Chromatography B*, **878**, 187-193.
223. Caro, E., Marce, R.M., Borrull, F., Cormack, P.A.G., Sherrington, D.C. (2006). Application of molecularly imprinted polymers to solid-phase extraction of compounds from environmental and biological samples. *Trends in Analytical Chemistry*, **25**, 143-154.
224. Pichon, V., Haupt, K. (2006). Affinity separations on molecularly imprinted polymers with special emphasis on solid-phase extraction. *Journal of Liquid Chromatography & Related Technologies*, **29**, 989-1023.
225. Tamayo, F.G., Turiel, E., Martin-Esteban, A. (2007). Molecularly imprinted polymers for solid-phase extraction and solid-phase microextraction: Recent developments and future trends. *Journal of Chromatography A*, **1152**, 32-40.

226. Lasakova, M., Jandera, P. (2009). Molecularly imprinted polymers and their application in solid phase extraction. *Journal of Separation Science*, **32**, 799-812.
227. Martin-Esteban, A. (2013). Molecularly-imprinted polymers as a versatile, highly selective tool in sample preparation. *Trends in Analytical Chemistry*, **45**, 169-181.
228. D'Orazio, G., Hernandez-Borges, J., Asensio-Ramos, M., Rodriguez-Delgado, M.A., Fanali, S. (2016). Capillary electrochromatography and nano-liquid chromatography coupled to nano-electrospray ionization interface for the separation and identification of estrogenic compounds. *Electrophoresis*, **37**, 356-362.
229. Kim, J.-Y., Chae, Y.-S., Moon, J.-A., Baek, S.-H. (2014). Establishment of a method for analyzing the zilpaterol residue in beef using tandem mass spectrometry. *Food Science and Technology Research*, **20**, 1165-1171.
230. Sellergren, B. (1994). Direct drug determination by selective sample enrichment on an imprinted polymer. *Analytical Chemistry*, **66**, 1578-1582.
231. Haginaka, J. (2009). Molecularly imprinted polymers as affinity-based separation media for sample preparation. *Journal of Separation Science*, **32**, 1548-1565.
232. Zhu, Q.-Z., Degelmann, P., Niessner, R., Knopp, D. (2002). Selective trace analysis of sulfonylurea herbicides in water and soil samples based on solid-phase extraction using a molecularly imprinted polymer. *Environmental Science & Technology*, **36**, 5411-5420.
233. Mullett, W.M., Lai, E.P. (1998). Determination of theophylline in serum by molecularly imprinted solid-phase extraction with pulsed elution. *Analytical Chemistry*, **70**, 3636-3641.
234. Qiao, F., Sun, H., Yan, H., Row, K.H. (2006). Molecularly imprinted polymers for solid phase extraction. *Chromatographia*, **64**, 625-634.
235. Andersson, L.I., Paprica, A., Arvidsson, T. (1997). A highly selective solid-phase extraction sorbent for

preconcentration of sameridine made by molecular imprinting. *Chromatographia*, **46**, 57-62.

236. Zhang, Y., Liu, R., Hu, Y., Li, G. (2009). Microwave heating in preparation of magnetic molecularly imprinted polymer beads for trace triazines analysis in complicated samples. *Analytical Chemistry*, **81**, 967-976.
237. Chen, L., Liu, J., Zeng, Q., Wang, H., Yu, A., Zhang, H., Ding, L. (2009). Preparation of magnetic molecularly imprinted polymer for the separation of tetracycline antibiotics from egg and tissue samples. *Journal of Chromatography A*, **1216**, 3710-3719.
238. Ji, Y., Yin, J., Xu, Z., Zhao, C., Huang, H., Zhang, H., Wang, C. (2009). Preparation of magnetic molecularly imprinted polymer for rapid determination of bisphenol A in environmental water and milk samples. *Analytical and Bioanalytical Chemistry*, **395**, 1125-1133.
239. Kong, J., Wang, Y., Nie, C., Ran, D., Jia, X. (2012). Preparation of magnetic mixed-templates molecularly imprinted polymer for the separation of tetracycline antibiotics from egg and honey samples. *Analytical Methods*, **4**, 1005-1011.
240. Lee, T.P., Saad, B., Khayoon, W.S., Salleh, B. (2012). Molecularly imprinted polymer as sorbent in micro-solid phase extraction of ochratoxin A in coffee, grape juice and urine. *Talanta*, **88**, 129-135.
241. Lord, H.L. (2007). Strategies for interfacing solid-phase microextraction with liquid chromatography. *Journal of Chromatography A*, **1152**, 2-13.
242. Koster, E.H., Crescenzi, C., Hoedt den, W., Ensing, K., Jong de, G.J. (2001). Fibers coated with molecularly imprinted polymers for solid-phase microextraction. *Analytical Chemistry*, **73**, 3140-3145.
243. Turiel, E., Tadeo, J.L., Martin-Esteban, A. (2007). Molecularly imprinted polymeric fibers for solid-phase microextraction. *Analytical Chemistry*, **79**, 3099-3104.
244. Mullett, W.M., Martin, P., Pawliszyn, J. (2001). In-tube molecularly imprinted polymer solid-phase microextraction

for the selective determination of propranolol. *Analytical Chemistry*, **73**, 2383-2389.

245. Yu, J.C.C., Krushkova, S., Lai, E.P.C., Dabek-Zlotorzynska, E. (2005). Molecularly-imprinted polypyrrole-modified stainless steel frits for selective solid phase preconcentration of ochratoxin A. *Analytical and Bioanalytical Chemistry*, **382**, 1534-1540.
246. Chatonnet, P., Dubourdieu, D., Boidron, J.N., Pons, M. (1992). The origin of ethylphenols in wines. *Journal of the Science of Food and Agriculture*, **60**, 165-178.
247. Zhou, Q., Qian, Y., Qian, M.C. (2015). Analysis of volatile phenols in alcoholic beverage by ethylene glycol-polydimethylsiloxane based stir bar sorptive extraction and gas chromatography-mass spectrometry. *Journal of Chromatography A*, **1390**, 22-27.
248. Kheir, J., Salameh, D., Strehaiano, P., Brandam, C., Lteif, R. (2013). Impact of volatile phenols and their precursors on wine quality and control measures of Brettanomyces/Dekkera yeasts. *European Food Research and Technology*, **237**, 655-671.
249. Hixson, J.L., Sleep, N.R., Capone, D.L., Elsey, G.M., Curtin, C.D., Sefton, M.A., Taylor, D.K. (2012). Hydroxycinnamic acid ethyl esters as precursors to ethylphenols in wine. *Journal of Agricultural and Food Chemistry*, **60**, 2293-2298.
250. Baggiani, C., Anfossi, L., Giovannoli, C. (2007). Solid phase extraction of food contaminants using molecular imprinted polymers. *Analytica Chimica Acta*, **591**, 29-39.
251. Caro, E., Marce, R.M., Cormack, P.A.G., Sherrington, D.C., Borrull, F. (2003). On-line solid-phase extraction with molecularly imprinted polymers to selectively extract substituted 4-chlorophenols and 4-nitrophenol from water. *Journal of Chromatography A*, **995**, 233-238.
252. Garde-Cerdán, T., Zalacain, A., Lorenzo, C., Alonso, J.L., Salinas, M.R. (2008). Molecularly imprinted polymer-assisted simple clean-up of 2,4,6-trichloroanisole and ethylphenols from aged red wines. *American Journal of Enology and Viticulture*, **59**, 396-400.

253. Herrero-Hernandez, E., Carabias-Martinez, R., Rodriguez-Gonzalo, E. (2009). Use of a bisphenol-A imprinted polymer as a selective sorbent for the determination of phenols and phenoxyacids in honey by liquid chromatography with diode array and tandem mass spectrometric detection. *Analytica Chimica Acta*, **650**, 195-201.
254. Maier, N.M., Buttinger, G., Welhartizki, S., Gavioli, E., Lindner, W. (2004). Molecularly imprinted polymer-assisted sample clean-up of ochratoxin A from red wine: merits and limitations. *Journal of Chromatography B*, **804**, 103-111.
255. Masque, N., Marce, R.M., Borrull, F., Cormack, P.A.G., Sherrington, D.C. (2000). Synthesis and evaluation of a molecularly imprinted polymer for selective on-line solid-phase extraction of 4-nitrophenol from environmental water. *Analytical Chemistry*, **72**, 4122-4126.
256. Vicente, B., Navarro Villoslada, F., Moreno-Bondi, M.C. (2004). Continuous solid-phase extraction and preconcentration of bisphenol A in aqueous samples using molecularly imprinted columns. *Analytical and Bioanalytical Chemistry*, **380**, 115-122.
257. Sanbe, H., Hoshina, K., Moaddel, R., Wainer, I.W., Haginaka, J. (2006). Uniformly-sized, molecularly imprinted polymers for nicotine by precipitation polymerization. *Journal of Chromatography A*, **1134**, 88-94.
258. Schwarz, L.J., Danylec, B., Harris, S.J., Boysen, R.I., Hearn, M.T.W. (2011). Preparation of molecularly imprinted polymers for selective recognition of bioactive polyphenol, (E)-resveratrol. *Journal of Chromatography A*, **1218**, 2189-2195.
259. Muhammad, T., Nur, Z., Piletska, E.V., Yimit, O., Piletsky, S.A. (2012). Rational design of molecularly imprinted polymer: the choice of cross-linker. *Analyst*, **137**, 2623-2628.
260. Horemans, F., Weustenraed, A., Spivak, D., Cleij, T.J. (2012). Towards water compatible MIPs for sensing in aqueous media. *Journal of Molecular Recognition*, **25**, 344-351.

261. Diñeiro, Y., Menendez, M.I., Blanco-Lopez, M.C., Lobo-Castañón, M.J., Miranda-Ordieres, A.J., Tuñón-Blanco, P. (2006). Computational predictions and experimental affinity distributions for a homovanillic acid molecularly imprinted polymer. *Biosensors and Bioelectronics*, **22**, 364-371.
262. Ng, S.M., Narayanaswamy, R. (2011). Molecularly imprinted polymers as optical sensing receptors: Correlation between analytical signals and binding isotherms. *Anal. Chim. Acta*, **703**, 226-233.
263. Shimizu, K.D. (2005). Binding isotherms. En *Molecularly imprinted materials science and technology*, Yan, M. and Ramström, O. (eds.) Marcel Dekker, New York.
264. Spivak, D., Campbell, J. (2001). Systhematic study of steric and spatial contributions to molecular recognition by non-covalent imprinted polymers. *Analyst*, **126**, 793-797.
265. Umpleby , R.J., Baxter, S.C., Rampey, A.M., Rushton, G.T., Chen, Y., Shimizu, K.D. (2004). Characterization of the heterogeneous binding site affinity distributions in molecularly imprinted polymers. *Journal of Chromatography B*, **804**, 141-149.
266. Rushton, G., Karns, C., Shimizu, K. (2005). A critical examination of the use of the Freundlich isotherm in characterizing molecularly imprinted polymers (MIPs). *Analytica Chimica Acta*, **528**, 1123-1133.
267. García-Calzón, J.A., Díaz-García, M.E. (2007). Characterization of binding sites in molecularly imprinted polymers. *Sensors and Actuators B: Chemical*, **123**, 1180-1194.
268. Hernández Hernández, L., González Pérez, C. (2002). Introducción a los métodos cromatográficos. En *Introducción al análisis instrumental*, Ciencia, A. (ed.), Barcelona, Spain, págs. 331-356.
269. Ye, L. (2005). Solid phase extraction and by-product removal. En *Molecularly imprinted materials. Science and Technology*, Yan, M. and Ramstrom, O. (eds.) Marcel Dekker, New York ,USA, págs. 603-618.

270. Rothwell, J., Pérez-Jiménez , J., Neveu, V., Medina-Ramon, A., M'Hiri, N., Garcia Lobato, C., Manach, P., Knox, K., Eisner, R., Wishart, D., Scalbert, A. (2013). Phenol-Explorer 3.0. http://phenol-explorer.eu/ **Consulta:** 21/10/2015.

271. Harris, D.C. (2007). Quality assurance and calibration methods. En *Quantitative Chemical Analysis*, W. H. Freeman and Co., New York, USA, págs. 78-95.

Chapter 4

DEVELOPMENT OF VOLTAMMETRIC SENSORS WITH MOLECULARLY IMPRINTED POLYMERS AS RECOGNITION ELEMENTS FOR 4-ETHYLPHENOL SENSING

Contents

1. Introduction

1.1. Molecularly imprinted electrochemical sensors

Electrochemical sensors consist of a recognition element that binds selectively the target compound and a transducer that transforms the chemical event (selective binding) into a quantifiable output signal (figure 4.1). Commonly, biological receptors such as antibodies (1), enzymes (2), DNA probes (3), aptamers (4) and cells (5) have been employed as recognition elements. However, their main drawbacks, mostly related with their low availability, their high cost and their low stability under non-physiological conditions, make these biological receptors be far from ideal. Alternatively, synthetic receptors such as MIP can be used instead for sensor development. As opposed to natural receptors, these polymers are robust, stable under extreme conditions, cost-effective and they can be synthesised for almost any target molecule (6).

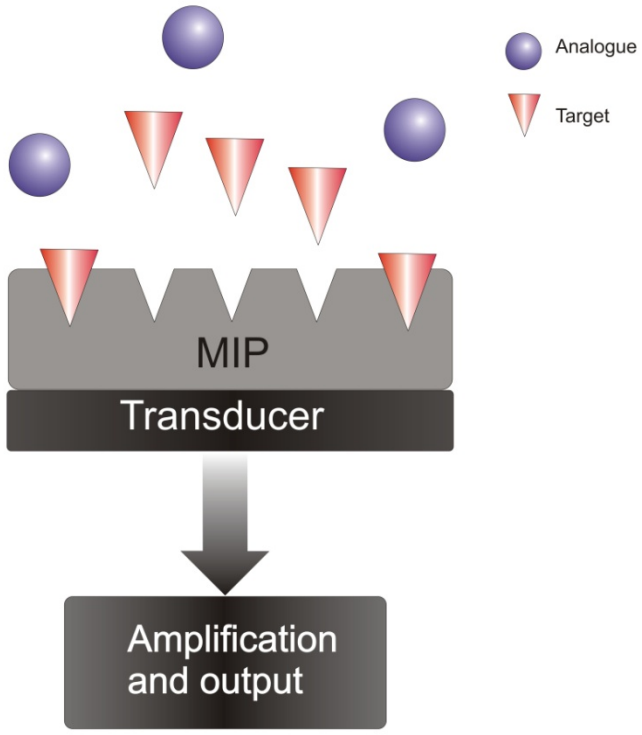

Figure 4. 1. Schematic representation of a MIP sensor.

On the other hand, the inherent specificity of molecularly imprinted materials and their ability to adapt to different formats, have provided many opportunities for their integration into sensing applications. The development of highly sensitive transducers capable of monitoring the binding process, the development of polymers capable of interacting with the template and the integration of MIP with the transducer, are the critical issues in the design of electrochemical sensors based on MIP (7).

In most cases, the MIP has to be brought into contact with the transducer surface. Otherwise, the signal output of the MIP sensor will be greatly affected, resulting a low sensing efficiency. The common way to solve this problem is that either the polymer can be synthesized on the transducer surface or the surface can be coated with a preformed polymer.

According to the electrical magnitude used for transduction, electrochemical sensors can be classified, in transducers measuring signals arising from a change in the properties of a system as a result of analyte binding with the MIP - potentiometric, conductometric and capacitive transduction- or as that measure signals coming from analytes undergoing electron transfer reaction –amperometry and voltammetry- (8).

Table 4. 1. Examples of MIP electrochemical sensors.

Transducer	Target analyte	MIP implementation	Reference	Year
Potentiometric	Atrazine	PVC membrane	Prasad *et al.* (9)	2007
	Uranium	PVC membrane	Metilda *et al.* (10)	2007
	Levamisole hydrochloride	PVC membrane	Sadhegi *et al.* (11)	2007
	Melamine	PVC membrane	Liang *et al.* (12)	2009
	Chlorpyrifos	PVC membrane	Liang *et al.* (13)	2010
	Prometazine	PVC membrane	Alizadeh *et al.* (14)	2010
	Oxytetracline	PVC membrane	Moreira *et al.* (15)	2010
	Diethyl chlorophosphate	PVC membrane	Vishnuvardhan *et al.* (16)	2011
	Histamine	PVC membrane	Basozabal *et al.* (17)	2014
	Imidocarb dipropionate	PVC membrane	Rizk *et al.* (18)	2014

Table 4.1. cont. Examples of MIP electrochemical sensors.

Transducer	Target analyte	MIP implementation	Reference	Year
Potentiometric	As^{3+}	PVC membrane	Alizadeh *et al.* (19)	2014
	Cu(II)	PVC membrane	Abu-Dalo *et al* (20)	2015
	Dextrometharphan	PVC membrane	El-Naby *et al.* (21)	2015
	Monosodium glutamate	Phisically+ Agarose	Anirudhan *et al.* (22)	2015
	Toluene	PVC membrane	Liang *et al.* (23)	2015
	S-citalopram	PVC membrane	Gutierrez-Climente *et al.* (24)	2016
	Taurine	Electropolymerisation	Kupis-Rozmyslowicz *et al.* (25)	2016
	Neopterin	Electropolymerisation	Sharma *et al.* (26)	2016
	Cyanide	Carbon paste	Alizadeh et al. (27)	2016
Conductometric	Atrazine	Phisically	Piletsky *et al.* (28)	1995
	Benzyltriphenyl phosphonium ions	Phisically	Kriz *et al.*(29)	1996
	L-phenylalanine 6-amino-1-propyluracil Atrazine	Phisically	Piletsky *et al.* (30)	1998
	Atrazine	Phisically	Sergeyeva et al. (31,32)	1999
	Haloacetic acids	PVC membrane	Suedee *et al.* (33)	2004
	Haloacetic acids	Phisically	Suedee *et al.* (34)	2006
	Chloroacetic acids	Phisically	Najafi *et al.* (35)	2011
	Phosphates	Thiourea membrane	Warwick *et al.* (36)	2014
Capacitive	Phenylalanine	Electropolymerisation	Panasyuk *et al.* (37)	1999
	Desmetryn	Grafting from	Panasyuk-Delaney *et al.* (38)	2001
	Glucose	Electropolymerisation	Cheng *et al.* (39)	2001
	Creatinine	Grafting from	Panasyuk-Delaney *et al.* (40)	2002
	Fenvalerate	Electropolymerisation	Gong *et al.* (41)	2004
	Glutathione	Electropolymerisation	Yang *et al.* (42)	2005
	Nicotine	Electropolymerisation	Liu *et al.* (43)	2006
	Creatinine	Grafting from	Delaney *et al.* (44)	2007
	Glutamic acid	Electropolymerisation	Ouyang *et al.* (45)	2007
	Theophylline	Electropolymerisation	Wang et al. (46)	2007

Table 4.1. cont. Examples of MIP electrochemical sensors

Transducer	Target analyte	MIP implementation	Reference	Year
Capacitive	Pazufloxacin mesilate	Grafting to	Zhou *et al.* (47)	2007
	Tiopenthal	Electropolymerisation	Najafi et al. (48)	2012
	α-pinene γ-terpinene terpinolene	Phisically	Hawari *et al.* (49)	2013
	Creatinine	Carbon paste	Reddy *et al.*(50)	2013
	Metergoline	Grafting to	Lenain *et al.* (51)	2015
	Ascorbic acid	Electropolymerisation	Pandey *et al.* (52)	2016
Amperometric	Morphine	Electropolymerisation	Weng *et al.* (53)	2007
	Hydroquinone	Grafting thorugh	Wang *et al.* (54)	2011
	Dopamine	Grafting through/ electropolymerisation	Xue *et al.* (55)	2013
	Norfloxacin	Grafting through	Wang *et al.* (56)	2013
	3-hydroxyanthronilic acid	Phisically	Huang *et al.* (57)	2015
Voltammetric	β-estradiol	Grafting from	Des Azevedo *et al.* (58)	2013
	Trinitrotoluene	Grafting through/ electropolymerisation	Guo *et al.* (59)	2015
	Diuron	Carbon paste	Wong et al. (60)	2015
	Ascorbic acid	Electropolymerisation	Pandey *et al.* (61)	2015
	Vanillin	Electropolymerisation	Wang *et al.* (62)	2015
	Tulathromycin	Grafting through/ electropolymerisation	Sun *et al.* (63)	2015
	Carbofuran	Electropolymerisation	Li *et al.* (64)	2016
	Bovine serum albumin	Electropolymerisation	Xia *et al.* (65)	2016
	Glutathione species	Electropolymerisation	Zhang *et al.* (66)	2016
	Carcinogenic embryonic antigen	Electropolymerisation	Moreira *et al.* (67)	2016
	Vancomycin	Grafting to	Mazzota et al. (68)	2016

1.1.1. Pontentiometric sensors based on MIP

Potentiometric sensors consist of electrodes having membranes permselective for a particular ion. Thanks to this membrane, the cell potential is measured when the sensor is put in contact with a solution containing the ionised analyte. Target ions interact with the membrane leading to a potential change, under zero-current conditions (8), that depends on analyte activity in solution. This kind of electrodes are known as ion selective electrodes (ISE) and have been widely used as chemical sensors.

There are two main strategies for MIP incorporation as recognition element in potentiometric sensors. The classical design involves the synthesis of a MIP membrane that will separate two compartments with solutions of different analyte activity. These solutions are the internal reference solution and the sample itself. The interaction of the target ion with the membrane will occur as a consequence of the molecular interaction between the MIP and the analyte at both sides of the surface. This arrangement for the construction of potentiometric electrodes is known as symmetric (8), since a solution of the analyte is in contact with the membrane in the inner and the outer side, what results in a stable potential on both sides. MIP particles incorporated in ISE sensors via PVC membranes constitute one example of the symmetric arrangement (17,20,23,24).

Symmetric MIP potentiometric sensors have widely been used to determine chemicals in environmental samples, for instance, Prasad *et al.* developed a potentiometric sensor for the direct, rapid and highly selective detection of atrazine in groundwaters (9). The sensor showed stability, reusability and dynamic response time comparable to conventional chemical sensors. Vishnuvardan *et al.* optimised the effect of membrane composition and the amount of the imprinted material for the development of a potentiometric sensor for diethyl chlorophosphate (16). The sensor was succesfully used to quantify diethyl chlorophosphate in natural waters by the standard addition method. Metilda *et al.* reported a potentiometric sensor imprinted with uranyl to monitorise uranium levels in environmental samples (10). The sensor showed low detection limit ($2 \cdot 10^{-8}$ M) and high selectivity for the target versus alkali, alkaline earth, transition and heavy metal cations. In the same way, Abu-Dalo *et al.* used an ion imprinted polymer for copper as recognition element for potentiometric sensing (20). It showed high selectivity and good recoveries (94% - 100%) in wastewater samples. On the other hand, Alizadeh *et al.* developed a potentiometric sensor for arsenic but this time using an arsenic methacrylate imprinted polymer (19). The developed sensor was used to determine arsenic in water, urine and pharmaceutical samples.

MIP based potentiometric sensors have also been employed in fields other than environmental analysis. In this

regard, potentiometry has also widely been used for drug determination in pharmaceuticals and biological samples. Sadhegi *et al.* developed a potentiometric sensor for levamisole (11) that showed short response time and reusability for 4 months, moreover, it was demonstrated to be highly selective when sensor response for the target was compared with its response to structural analogues. Alizadeh *et al.* compared the performance of promethazine imprinted materials synthesised with methacrylic acid and vinylbenzene as functional materials (14). The vinylbenzene MIP showed better results when it was implemented in a potentiometric sensor, and it was succesfully applied for promethazine detection in syrup and biological fluids. Oxytetracycline MIP particles were implemented in potentiometric devices by Moreira *et al.* (15). The sensor was highly selective, pH independent and showed good reproducibility, fast response and good sensitivity. It was applied to the detection of the drug in pharmaceutical and urine samples. El-Naby *et al.* implemented dextrometorphan imprinted polymer particles in a potentiometric sensor (21). They developed an accurate, sensible and precise method for dexthrometorphan detection in pharmaceutical products using the potentiometric sensor. Rizk *et al.* developed a potentiometric MIP sensor for the veterinary drug imidocarb (18). The sensor showed low detection limit ($2\cdot 10^{-6}$ M) and was applied to potentiometric determination of imidocarb in different pharmaceutical formulations. Gutierrez-Climente *et al.* synthesised

chiral MIP nanoparticles by precipitation polymerisation to be used as recognition elements in potentiometric sensing (24).The developed sensor was selective to the S enantiomer of citalopram and was applied to determine this target in urine.

Potentiometric MIP sensors have also been applied to food analysis. Liang *et al.* fabricated a melamine specific sensor for its determination in milk samples (12). High concentrations of interfering ions in milk samples (pH 6.7) were eliminated by the on-line use of anion- and cation-exchanger tandem columns. Basozabal *et al.* used high affinity MIP nanoparticles as synthetic receptors for histamine (17). The sensor showed high selectivity being able to quantify histamine in fish and wine samples in the presence of other biogenic amines.

On the other hand, asymmetric arrangements have also been used for the construction of potentiometric sensors. Here, the inner side of the MIP membrane is in contact with a solid-phase (a conductor, a semi conductor or an insulator) whereas the outer is in contact with the target ions in the test solution (8). Using this arrangement, thin MIP films have been electopolymerised on different conducting surfaces (25,26), and also MIP particles have directly been assembled on electrodes with agarose (22) or via carbon composites in carbon paste electrodes (27).

The main drawback of these sensors is the need of a target analyte capable of being ionised in solution or even a gas that

dissociates giving charged species in a liquid or solid electrolyte (69). However, sensing of neutral species can be performed using an ionisable analogue as indicator. For example, Liang *et al*. used 3,5,6-trichloro-2-pyridyxolacetic acid as indicator for chlorpyrifos sensing (13) or benzoic acid for toluene sensing in gas phase (23).

1.1.2. Conductometric MIP sensors

The configuration of conductometric MIP sensors consists of two platinum electrodes separated by a MIP membrane as sensing material (8). An increase in analyte concentration bound to the MIP will alter membrane conductivity (6), what could be attributed to conformational changes in the polymer upon analyte binding, which together with the presence of charged ions in the polymer matrix leads to an increase in membrane conductivity. However, in some instances membrane conductivity decreases due to template interaction with functional monomers such as esterification of sialic acid and the monomer boronic acid (30) and ion pairing conducted by haloacetic acids with vinylpyridine groups (33).

Piletsky *et al.* synthesised atrazine imprinted polymer membranes to be implemented in conductometric sensors (28). The same technique was used for the development of conductometric sensors for other target analytes such as L-phenylalanine, 6-amino-1-propyluracil and sialic acid (30). Sensor

response time and the detection limit were improved adding oligourethane acrylate to the monomer mixture, what resulted in thin, flexible and mechanically stable membranes (31,32). Kriz *et al.* implemented MIP particles on the surface of a polished bar to construct a conductometric sensor for benzyltriphenyl phosphonium ions (29). Suedee *et al.* used MIP particles on PVC membranes for the development of a conductometric sensor for haloacetic acid (33), subsequently, they extended this work to the construction of a lab-on-chip device (34). Najafi *et al.* used an electropolymerised MIP film to measure chloroacetic acid (35). Recently, Warwick *et al.*, used a MIP as a class selective receptor membrane for conductometric sensing of soluble phosphates in wastewaters (36). Despite MIP implementation has been more or less widely described in the literature so far, conductometric MIP sensors are not very popular due to their poor selectivity especially when high ionic strength buffers are used for measurements, as membrane conductivity can be altered by the buffer solution (8).

1.1.3. Capacitive sensors

These sensors are based on the concept of the electric double layer at the electrode-electrolyte solution interface. Capacitance is the amount of charge stored by a capacitor at a given electric potential. The measurement of the capacitance involves an

insulating film between two parallel plate conductors, with definite thickness. In capacitive MIP sensors, MIP films will be separating the electrode surface and the electrolyte forming a capacitor. Capacitance measured by these sensors can be described as,

$$C = \frac{\varepsilon \varepsilon_0}{d} \qquad \textbf{4. 1}$$

Where ε ($F \cdot m^{-1}$) and ε_0 ($F \cdot m^{-1}$) are the electric permittivity of the insulator and the free space, respectively, A (m^2) is the surface area of the capacitor and d (m) is the distance between plates. The only parameters that are not constant in the equation are ε and d, in consequence, capacitance changes will occur with changes on the electric permittivity or thickness of the MIP insulating layer. Selective binding between MIP and the target ligand will disturb the dielectric characteristics of the interface, which is noticeable by capacitance changes (7). As capacitance is part of the impedance of a conducting layer, Electrochemical Impedance Spectroscopy (EIS) can be used to measure impedance and relate it to capacitance.

Different works report measured capacitance related to analyte concentration. Panasyuk *et al.* developed the first capacitive MIP sensor by electropolymerising phenol on a gold electrode in the presence of phenylalanine as template (37). The same group also developed capacitive sensors coating gold electrodes with MIP films for desmetryn (38) and creatinine (40).

These sensors measure capacitive change due to the effective thickness of the insulating layers. On the other hand, Panasyuk *et al.* developed a capacitive sensor coating an electrode with a thin polymer layer. Due to the use of a thin layer, measured capacitance change upon template binding (creatinine) happened as a result of the modification of the polymer dielectric constant (44).

Cheng *et al.* developed a capacitive sensor for glucose (39) which showed high selectivity versus fructose and ascorbic acid. Gong *et al.* developed a capacitive sensor for the pesticide fenvalerate, based on MIP electropolymerised on a gold electrode (41). The sensor did not show any significant signal for other pyrethroid insecticides achieving a detection limit of 0.36 μg mL^{-1}. Yang *et al.* used the same technique to develop a capacitive sensor for glutathione (42), obtaining good selectivity and a detection limit of 1.25 μM. The sensor was applied to the direct measurement of glutathione in real samples. Liu *et al*. developed a MIP capacitive sensor for nicotine (43), showing good reproducibility, which proved to be applicable to the analysis of real samples. Ouyang *et al.* developed enantioselective MIP sensors using both L- and D-glutamic acid as templates (45). These sensors showed chiral selectivity, good reproducibility, stability and repeatability. Wang *et al.* constructed a capacitive sensor for theophylline electropolymerising phenol on gold electrodes (46). Zhou *et al.* coated an electrode with MIP *via* electropolymerisation

(47). The developed sensor was used for capacitive sensing of pazufloxacin, showing good sensibility, selectivity and stability.

On the other hand, Najafi *et al.* electropolymerised a MIP on an electrode for capacitive measurement of thiopental on human serum (48). Hawari *et al.* determined mango ripeness measuring volatiles such as α-pinene, γ-terpinene and terpinolene through capacitive sensing with a MIP modified electrode (49). Lenain *et al.* measured capacitance change after metergoline binding to a MIP coated electrode to measure this target in water samples (51).

Other authors related the charge transfer resistance measured by EIS to the concentration of the analyte. Pandey *et al.* developed a chiral impedimetric sensor for the discrimination of L-ascorbic acid from D-ascorbic acid (52) and Chen *et al.* measured creatinine in urine and serum samples by the same approach (50).

1.1.4. Amperometic and voltammetric sensors

If the analyte is electroactive, electroanalytical techniques based on Faradaic processes such as amperometry and voltammetry can be employed. The analyte is identified by the current change registered as a result of redox reactions of analytes at a certain potential.

The principal drawback of these techniques is that molecules with similar functional groups present very close oxidation/reduction potentials. A way to overcome this, is to modify the working electrode using MIP materials. The analyte will diffuse selectively through the MIP films towards the electrode surface (7), improving sensor selectivity and sensibility thanks to analyte preconcentration on electrode surface.

Sensors based on this type of transduction mechanism can be subdivided into different categories based on the way the potential is applied. For instance, in amperometric sensors, a constant potential is applied and current intensity is registered as a function of time. MIP amperometric sensors have been developed for several targets such as dopamine (55), hydroquinone (54) or norfloxacin (56) among others. One of the main advantage of this type of transduction is the possibility of coupling it with flow injection analysis (53,57).

In voltammetric sensors, the current is registered while a potential scan is being applied. In Linear Sweep Voltammetry (LSV) (59), and Cyclic Voltammetry (CV) (58) the potential changes linearly with time, whereas in Square Wave Voltammetry (SWV), the potential changes with square wave oscillations (60). In Differential Pulse Voltammetry (DPV) the potential changes linearly with a few mV superimposed rectangular pulses; this is the most popular transduction method for MIP sensor development. DPV MIP sensors have been constructed for Ascorbic acid (61),

carbofuran (64) or vanillin (62). Among voltammetric techniques, DPV and SWV provide the lower signal-to-noise ratio due to their programmed current recording (7), as an effective discrimination of charging current and faradaic current is achieved (70).

In principle, these sensors are only applicable to electroactive compounds, however, indirect approaches have also been developed to measure non-electroactive species. The usual approach for voltammetric sensing of non-electroactive analytes is the use of an electrochemical probe, that is, an electroactive compound different from the analyte such as the ferrocyanide/ferricyanide redox couple (63,65,66) or Ru(III) (67). Usually, as a consequence of analyte binding to the sensor, the peak current of the redox probe decreases, what can be related to analyte concentration. Recently, Mazzotta *et al.* developed a voltammetric MIP sensor for poorly electroactive vancomycin without the need of any electroactive probe. In this work, they synthesised MIP nanoparticles (MIN) adding electroactive vinylferrocene and ferrocenylmethyl methacrylate monomers which act as electroactive probe. The anodic and cathodic peak currents obtained thanks to the electrochemical activity of ferrocene monomers decrease upon template binding with nanoparticles (68).

Due to the non-conductive nature of highly crosslinked MIP, for proper analyte detection, an important concentration of well-connected recognition sites through a network of pores, of

appropriate size and density, close enough to the electrode surface is highly desirable. Therefore, the porosity and the thickness of the polymer must be controlled to avoid strong diffusion impediments (71).

1.2. Molecularly imprinted nanoparticles as recognition elements for sensing

MIP have traditionally been prepared in bulk format, and obtained bulk monoliths were ground and sieved through 25-125 μm pore size sieves obtaining irregular fine particles. MIP particles prepared this way, have successfully been employed as recognition elements for sensor fabrication, however, typical intrinsic drawbacks of these materials has made research focus on other MIP formats for sensor construction. Irregular fine particles coming from bulky materials are usually associated with slow mass transfer kinetics, what results in slow analyte diffusion towards binding sites. This may not be desirable for sensor applications since it may lengthen sensor response. Moreover, a relatively high number of binding sites, most of them located in the inside part of the particle, are inaccessible for the target compound, and the template may be permanently trapped in the binding site since the polymerisation step (72).

For these reasons, in the last years, research has focused on regularly shaped imprinted polymers, especially in the nanometer scale (73). The main advantage of MIP nanoparticles (MIN) is their high surface-volume ratio in comparison with irregular polymer microparticles, leading to more accessible binding cavities and faster association-dissociation kinetics (74,75). To date, MIN synthesis for sensor development has almost been exclusively carried out by precipitation polymerisation, mini and micro-emulsion polymerisation, core-shell approaches and solid-phase synthesis.

1.2.1. Precipitation polymerisation

Precipitation polymerisation is a procedure that takes place under high porogen volumes, usually 50-100 times higher than in bulk polymerisation (76). In the begining of the process, primary radicals are formed due to thermal or photochemical decomposition of the initiator. These radicals interact with the vinyl groups of the monomers in solution leading to polymeric structures, which continue growing giving rise to polymeric chain cores (figure 4.2a). If the employed solvent is not adequate for the gelification of the growing polymer chains (figure 4.2c), the formed cores will precipitate after reaching a certain mass and then, their growth stops (figure 4.2b).

This straightforward technique provides good yields (77) and favours the production of spherical particles with higher binding capacity and more homogeneous binding site distribution than through bulk polymerisation (78).

This approach was first applied in 1999, the synthesised MIP particles showed better selectivity and load capacity compared to the bulk monoliths (79). Throughout the years, MIN production by precipitation polymerisation has been widely studied, improving polymer binding characteristics, thereby reducing the level of non-specific interactions (80). Nanoparticles with low polydispersity indexes are usually obtained by this strategy (81-84), however, temperature, monomer concentration and/or the initiator amount can affect nanoparticle characteristics. Increasing monomer concentration leads to larger and more uniform particles. In the same way, particle size increases not only with the polymerisation temperature, but also with the amount of initiator (85). Instead, very high reaction temperatures can negatively affect particle uniformity.

Different modifications of this MIP particle synthesis technique have been reported in the literature. Sunbrahmanyam *et al.* proposed a "post-dilution" method where after starting polymerisation of a concentrated monomer solution, polymer growth was stopped to avoid macrogelation. Then, the oligomer mixture was further diluted employing porogens such as acetonitrile (86). In any case, the idea of "post-dilution

polymerisation" was first reported by Wulff *et al.* aiming to increase selectivity and economise template (87). With the aim of avoiding the use of organic solvents Hoshino *et al.* performed precipitation polymerisation in water in the presence of a surfactant at very low concentration (88). In order to improve precipitation polymerisation yields, Renkecz *et al.* used high molar volume solvents (such as paraffin oil or chloroform). These solvents avoid the formation of monoliths during precipitation, achieving MIP particles with yields up to 100%. This technique was successfully applied to microparticle synthesis, however, further research is required to produce MIP nanoparticles by this approach (89,90).

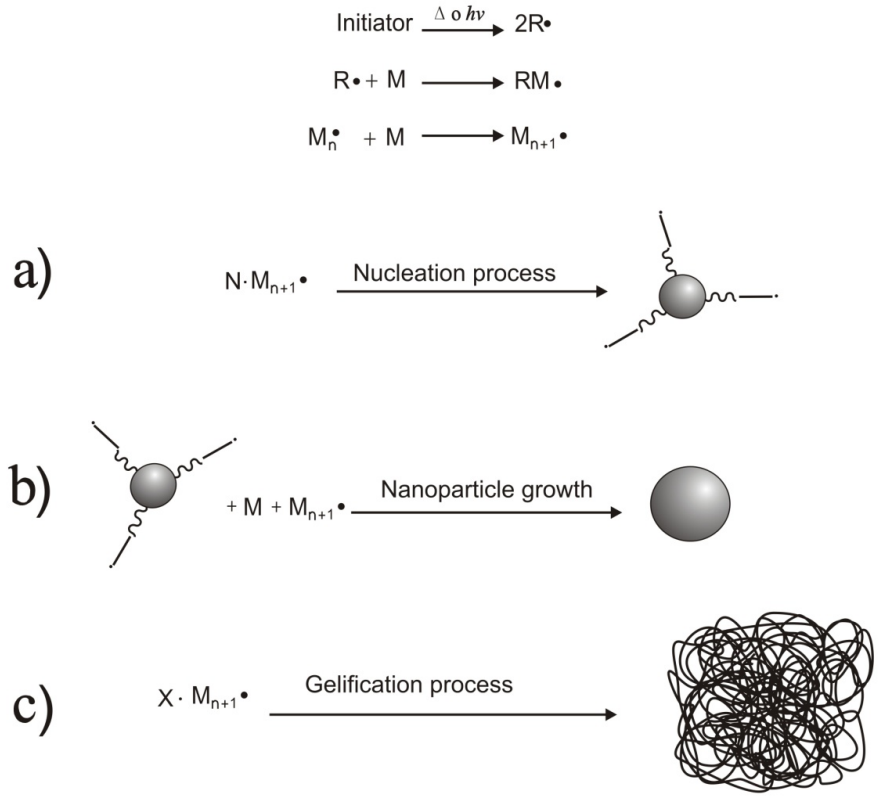

Figure 4.2. Precipitation polymerisation steps (76).
M: monomer, $\mathbf{M_{n+1}}$: polymer chain, **n:** number of monomers in the polymeric chain, **N:** number of polymeric chains.

This technique can also be used to synthesise microgels/nanogels with sizes comprised between 10 and 300 nm in diameter. The main characteristic of these materials is that they lead to low-viscosity colloidal solutions after preparation in a

suitable porogen that never precipitate. The nature of these gels make them suitable materials for their use as receptors in enzyme like assays (91).

1.2.2. Mini and micro-emulsion polymerisation

In emulsion polymerisation, the crosslinker, the functional monomer(s) and the template are emulsified in an aqueous phase containing a surfactant. When a co-stabiliser is added to avoid diffusion processes to the continuous phase it is called mini-emulsion polymerisation, achieving stable emulsions with homogeneous droplet size (92). The droplet size will depend on the stirring speed and the co-stabiliser used and the morphology of the synthesised particles will be determined by monomer and polymer solubility on the droplets (93).

The main drawback of this approach is the influence of water on the interactions between the functional monomer and the template. In this polymerisation strategy, water is used as continuous phase and it displaces monomer-template interactions in the prepolymerisation mixture, what leads to polymers with higher binding site heterogeneity and lower binding capacity. These interactions can be further affected by the surfactant, obtaining molecular imprints with weaker binding strength (94). In order to overcome these drawbacks, micro-emulsion

polymerisation has been performed in non-aqueous media and with a non ionic emulsifier (94). It takes places in a dispersion made of water, oil and surfactants (95).

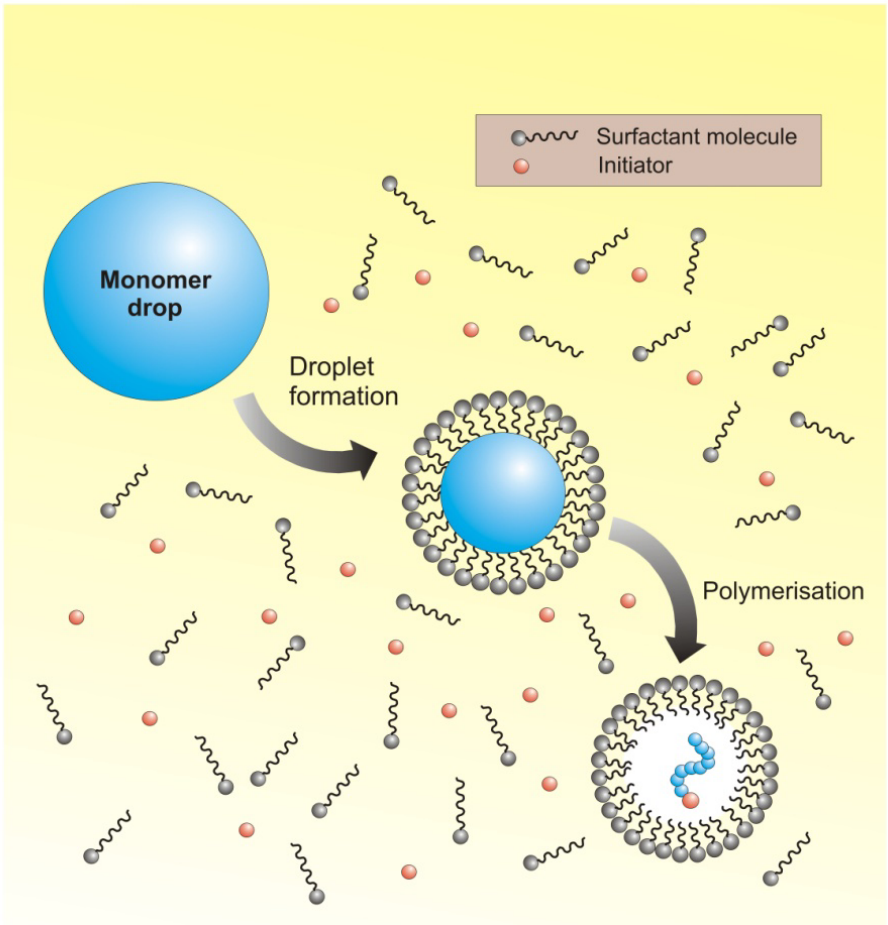

Figure 4.3. Emulsion polymerisation process.

These procedures are proper methods to obtain monodisperse nanoparticles with sizes down to a few nanometers. However, one of the major disadvantages of this method is the need of surfactants that stabilise the monomer droplets. These chemicals have to be later removed and the purification steps may be long and tedious. Moreover, the chemicals may interfere in the imprinting process, broadening the distribution of affinity sites (77).

1.2.3. Solid-phase synthesis

Nanoparticles synthesised under conventional methods, such as precipitation or emulsion polymerisation, still present several disadvantages like binding site heterogeneity, low number of binding sites, and template leakage after MIN synthesis (96,97). To overcome these major drawbacks, recently a new synthesis approach for MIN has emerged, the solid-phase synthesis (98).

In solid-phase synthesis the template is covalently immobilised on a solid support (glass beads) prior to polymerisation. Thereafter, it is mixed with the polymerisation mixture, including the functional monomer and the crosslinker, and the polymerisation initiates thanks to the chemical or photochemical decomposition of an iniferter (initiator) (figure 4.4). Polymerisation conditions must be carefully optimised in order to

favour nanoparticle formation. These conditions include short polymerisation time or high dilution in order to avoid macrogel or monolith formation.

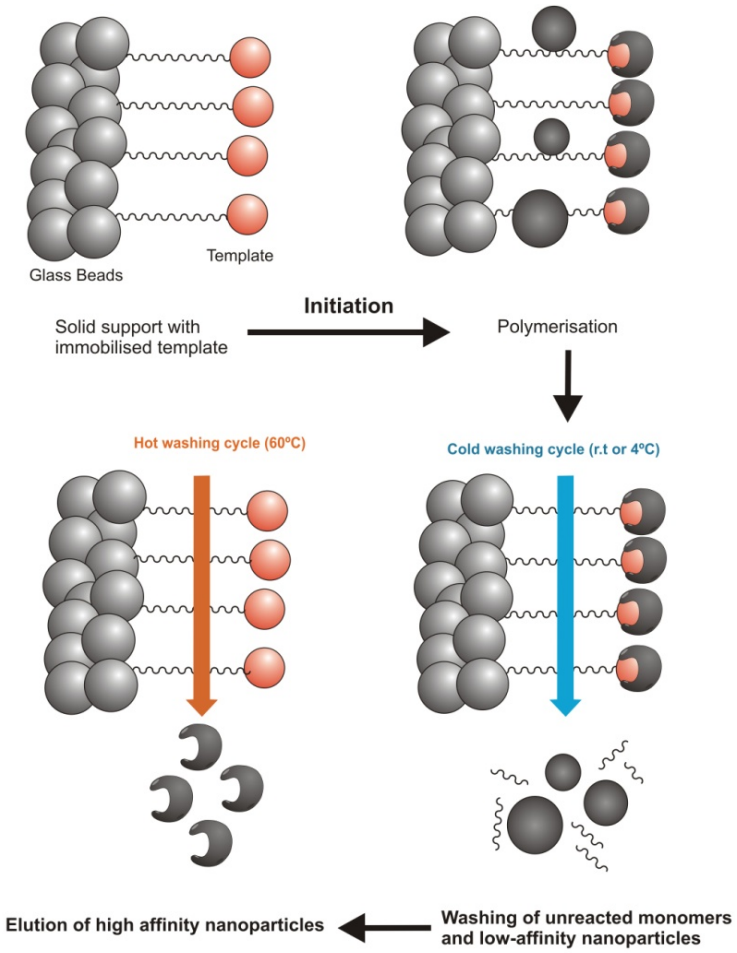

Figure 4. 4. Schematic representation of the solid-phase synthesis and affinity-purification of imprinted nanoparticles.

After the polymerisation step, nanoparticles of a few nanometers will be formed around the template, immobilised on the solid glass beads (figure 4.4). These nanoparticles remain bound to the glass beads until affinity-based purification of the imprinted particles is performed. This purification step favours removing the remaining unreacted monomers, oligomers and low-affinity nanoparticles (98). Thanks to this, the number of nanoparticles having high-affinity binding sites is maximised in the final product removing nanoparticles with low or no affinity.

For the affinity-based purification of nanoparticles the glass beads are transferred to empty solid-phase extraction cartridges. Then, they are washed with an aprotic solvent like ACN at room temperature to remove unreacted remaining compounds and low affinity nanoparticles. Subsequently, high affinity nanoparticles are collected after percolating the solvent at 60 ºC through the cartridge (99).

Imprinted nanoparticles obtained by this approach show high affinity for the template and present homogeneous binding site distribution. They usually fit to the Langmuir isotherm binding model, which describes a unique type of binding site with a single binding affinity (97). Additionally, unlike in conventional imprinted nanoparticles, binding sites in nanoparticles synthesised by solid-phase imprinting are located at the surface of the nanoparticles. This has the potential to minimise diffusion effects and therefore allows for faster association-dissociation kinetics in the rebinding

step what may contribute to faster sensor response (97). Moreover, the synthesised and purified nanoparticles will be template free, avoiding tedious protocols for template removal (required by the classical synthesis approaches) and template leakage (98).

Solid-phase synthesis of MIN can be used for the polymerisation of MIN in different media. Small molecules (MW < 500 Da) have successfully been imprinted by this approach using organic solvents (17,96,100), whereas proteins (97,101) or viruses (102), due to protein incompatibility with organic solvents, have been imprinted in water.

The solid-phase synthesis approach was first reported by Poma *et al.*, combining this synthesis approach with an automatic chemical reactor for the synthesis of melamine, vancomycin and a model peptide imprinted nanoparticles (96). This reactor has also been proved to be useful on the synthesis of MIP nanoparticles in water for templates such as pepsin A, trypsin and α-amilase (103).

Since the solid-phase imprinting approach was first reported, nanoparticles developed through this strategy have been used for different applications. Chianella *et al.* implemented nanoparticles in developed by solid-phase imprinting microplate wells for measuring vancomycin. These microplates were used for assays similar to enzyme-linked immunosorbent assays (ELISA) (104). Moreover, Caceres *et al.* compared this work with other ELISA-like nanoparticle approaches, in order to know how template

size affects the performance of MIP nanoparticles. They synthesised horse radish peroxidase, cytochrome C, biotin and melamine imprinted nanoparticles by the solid-phase approach, concluding that the size of the template has little effect on the sensitivity of pseudo-ELISA tests based on MIP nanoparticles (105).

As regards sensor development, Korposh *et al.* applied nanoparticles in an optical fibre long-period grating sensor for vancomycin detection (106). Basozabal *et al.*, used histamine imprinted nanoparticles implemented in a PVC membrane for the potentiometric determination of histamine in fish and wine samples (17). Other sensor applications of this nanoparticles include their implementation in Surface Plasmon Resonance (SPR) optical sensors for diclofenac (107) or their use as sensing elements in a voltammetric sensor for vancomycin (68).

Nanoparticles synthesised *via* the solid-phase approach, have the potential benefit for being used in biological applications. Guerreiro *et al.* examined the effect of trypsin imprinted nanoparticles on the activity of the enzyme, concluding that the binding of nanoparticles could inhibit or stabilize the enzyme depending on the orientation of the immobilised template during imprinting (108). Solid-phase nanoparticle synthesis has also been combined with other biological receptors. In this regard, the template immobilised on the glass beads is added to a solution containing the complementary biological receptor fraction -an oligonucleotide (109), aptamer (110) or nucleotide (111)-

functionalised with polymerisable groups. Once the template binds the complementary fraction, the solid-phase synthesis is performed. The resulting nanoparticles, show very high binding affinity and selectivity together with intrinsic polymer stability in comparison with biological receptors (figure 4.5).

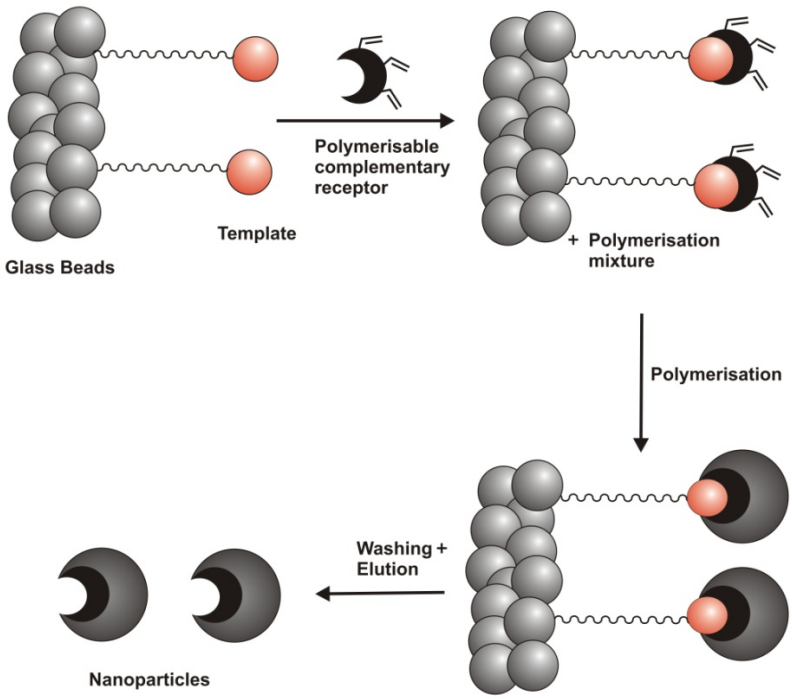

Figure 4.5. Schematic representation of the solid-phase synthesis combined with biological receptors.

One of the principal drawbacks of this strategy is the need of immobilising the template on a solid support. For certain compounds, especially for those having very low molecular weight (MW < 300 Da), immobilising the template on the solid support would mean sacrificing one of the functional groups available for imprinting. This may lead to nanoparticles with lower binding affinity than other synthesised through conventional techniques. This problem could be overcome employing a suitable template analogue with an additional functional group dedicated to the immobilisation (98). This procedure usually results in lower polymer yield in comparison with conventional procedures, due to the purification step, which allows obtaining only high affinity nanoparticles, discriminating the low affinity ones (98).

1.2.4. Core-shell approaches

Core-shell nanoparticles are composite materials consisting of a solid core coated with a MIP shell (72). MIN with complex architectures and controlled sizes are achieved by this method. The core particles can be made of different organic or inorganic materials depending on the application (112). The shell formed around the core usually is thin to get faster binding kinetics (113).

With the objective of introducing different characteristics to MIN, different cores have been developed such as sol-gel derived

xerogels (114), lanthanide ion complexes (115), metals (116,117), silica (118,119), quantum dots (120-123) or carbon based nanoparticles (124-128). Among the last ones, multi-walled carbon nanotube (MWCNT) cores are the most popular ones for electrochemical sensing due to their larger specific surface area and their electrocatalyst nature (22,62,129). Magnetic MIPs (Fe_3O_4 cores with MIP shell) have also been used for electrochemical sensing *via* their implementation on the electrodes (130-132) or attracting them to the electrode by a magnet for the electrochemical measurement after extraction (133). Gold nanoparticles present conductivity and catalytic properties, for this reason, they can enhance sensitivity of electrochemical sensors by amplifying sensor surface, enhancing electron transfer and catalyzing electrochemical reactions (134). Gold nanoparticles for electrochemical sensing have been used for the construction of core-shell nanoparticles (135) and also as part of the grafted MIP on electrodes (62,136) .

Moczko *et al.* developed a method for combining core-shell and solid phase nanoparticle synthesis (Figure 4.6). In this case, the core was the MIP nanoparticle and the shell different polymers grafted on the nanoparticles for the introduction of surface characteristics, such as high polarity (polyethylene glycol), electroactivity (vinylferrocene), fluorescence (eosin acrylate) or thiol groups (pentaerythritol tetrakis (3-mercaptopopionate), without affecting MIP affinity and selectivity. The synthesis of the

grafted shell was accomplished after the low temperature purification step while the nanoparticles remain attached to the solid support via their interaction with the template (figure 4.6) (100). This method has also been applied for the introduction of amine groups in nanoparticles for its assembly on Surface Plasmon Resonance based optical sensors for metropolol (137) and *E. Coli* endotoxins (138).

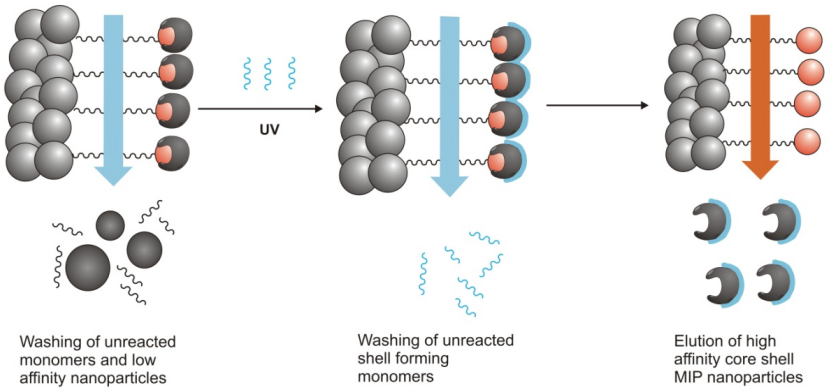

Figure 4. 6. Schematic representation of the combination of the solid-phase synthesis approach with core–shell synthesis.

On the other hand, Shutov *et al.*, developed solid-phase synthesis of core-shell nanoparticles through the addition of Fe_3O_4 cores with peroxidase activity (modified with 3-(trimethoxysilyl)propyl methacrylate) to the monomer mixture. Thereafter, they applied the imprinted nanoparticles as enzyme substitute in ELISA tests (139).

1.3. Integration of imprinted nanoparticles in electrochemical transduction systems

For the construction of molecularly imprinted electrochemical sensors, different methods have been reported to date such as the use of membranes (17,20,140,141), carbon composites (50,60,84,142) or self-assembled monolayers (68,143).

One of the most employed strategies is the combination of nanoparticles with carbon composites to fabricate carbon paste electrodes (CPE). MIN are homogenised with graphite powder and oily solvents such as n-eicosane (50,142) or mineral oil (60), to form the paste. Recently, Bagheri *et al.* have compared the use of paraffin oil and the ionic liquid 1-butyl-methyl-pyrrolidinium bis(trifluoromethylsulfonyl)imide to fabricate a nanographene-MIN composite (84).

Polyvinyl chloride (PVC) membranes have also been widely used to assemble MIN with electrochemical transducers. Usually

MIN are mixed with PVC and other plasticisers in a volatile solvent; after solvent drying a membrane is formed having MIN immobilised. This approach has mainly been used for MIN integration in potentiometric sensors (17,20,140). However, they have also been assembled with other transduction elements such as capacitive sensors (141).

Other immobilisation approaches include the use of self-assembled monolayers (SAM) on electrode surfaces. In SAM formation, suitably functionalised molecules are spontaneously assembled on surfaces to form a densely packed monolayer convalently anchored to the surface. As SAM are very stable, physisorbed or unreacted molecules can be washed without affecting the formed monolayer. For polymer immobilisation with SAM there are three main approaches, the "grafting to", the "grafting through" and the "grafting from" approaches (figure 4.7) (144). For MIN immobilisation the grafting to approach must be used, since grafting from and grafting through approaches are mainly used to surface syntheses of polymer films.

In the SAM grafting to approach (Figure 4.7a), a preformed polymer (MIN in this case) is grafted to the exposed functional group of the preformed SAM (144). Zia *et al.* formed an aminopropyltrietoxysilane SAM on a semi conducting single crystal silicon wafer for the immobilisation of MIP particles and used it as impedometric sensor (143). On the other hand, Mazzotta *et al.*

immobilised MIN on a glassy carbon electrode using a nafion SAM for the development of a voltammetric sensor for vancomycin (68).

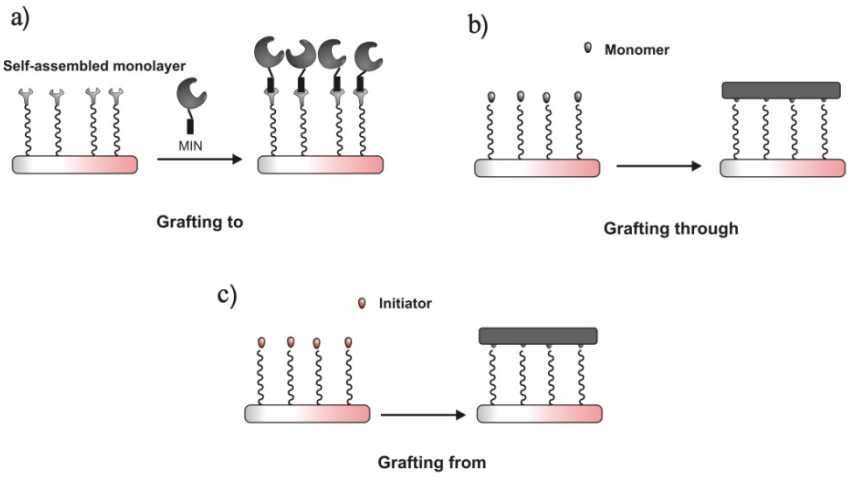

Figure 4. 7. Schematic representation of the MIP grafting approaches via SAM formation.

1.4. Molecularly imprinted thin films as recognition elements for electrochemical sensing

Other formats than nanoparticles have also been described in the literature to develop synthetic recognition elements for sensing. In this regard, MIP have directly been synthesised on electrode surfaces, leading to MIP films. Electropolymerisation, has been by far, the most widely employed technique for this approach (6,145), however, other techniques such as SAM formation for grafting

from (56,58,146) or grafting through (59,64,65) approaches have also been reported.

Through electropolymerisation, polymers can be synthesised electrochemically on the surface of the conductive substrate without any processing requirement. Electrodes are placed in the polymerisation mixture containing the monomers, the template and the porogen; thereafter a fixed potential or certain potential scans are applied for polymer synthesis. Monomers used for electropolymerisation on the development of electrochemical MIP sensors include thiophene (25,26), aniline (35,52,61,136), dithioaniline (147,148), pyrrole (62,67,149), o-phenylenediamine (66,150-152), Ni(II)-phthalocyane (153), tetra (o-aminophenyl) porphyrin (154), thiopental (48), 2-mercaptobenzothiazole (155,156) or phenol (157). Other authors use mixtures of different monomers such as aniline and o-phenylaniline (158-160), phenylenediamine, galic acid and p-aminobenzoic acid (161,162) or terthiophene and carbazole (163).

The major advantage of electrochemically polymerised MIP films is that the thickness of the polymer can be controlled by the current density and voltage applied, obtaining as a result, uniform surface coatings. Moreover, this approach allows the deposition of the polymer at a precise spot of the detector surface (6).

SAM can also be used for the formation of MIP films on electrochemical transducers by grafting through and grafting from approaches (figure 4.7b and c). The grafting through approach is an

intermediate approach between the grafting to and the grafting from approach. It lies in forming a SAM on the electrode surface with functional groups that will react under polymerisation conditions, such as vinyl groups (figure 4.7b). Concerning this, some reported works describe the immobilisation of the template on the electrode surface using SAM prior to radical polymerisation (164) or electropolymerisation (64,65). Other authors have reported the formation of SAMs with vinyl end groups on the electrode surface to graft MIP films (54). SAMs formed with electropolymerisable functional monomers such as p-aminobenzene thiol can be easily formed on gold substrates, polymer grafting will then occur by electropolymerisation in the presence of the monomer and the template (55,59,63).

The grafting from (figure 4.7c) approach consists in the growth of a polymer layer from the SAM having an exposed functional group capable of initiating polymerisation (144). Lakshmi *et al.* synthesised an acrylic layer by electropolymerisation of N-phenylethylenediamine methacrylamide and next, they assembled the iniferter N-N'-dithiocarbamic acid benzyl ester on it through SAM formation. Polymerisation was subsequently initiated from the electrode surface by UV light (58,146). Another special grafting from approach for electrochemical sensor development was used by Wang *et al.* forming a mercaptohexane SAM on a gold electrode and physisorbing a radical initiator for the subsequent photopolymerisation of the MIP film (56). To achieve MIP films

with controlled thickness, the combination of grafting from approach with reversible deactivation radical polymerisation is a promising approach for electrochemical MIP sensor development as it has been reported for other types of sensors (126,165).

1.5. Reversible deactivation radical polymerisation

Reversible deactivation radical polymerisation (RDRP) is a type of chain polymerisation propagated by radicals that are deactivated reversibly, bringing them into active and dormant equilibria (166).

MIP have been mainly synthesised by free radical polymerisation, due to its simplicity and the fact that is a straightforward technique for large-scale preparation of polymers involving vinylic or acrylic monomers (167). This chain polymerisation consists of three main steps, initiation, propagation and termination (figure 4.8). During initiation, a small amount of an initiating compound is required, this compound will be thermally or photochemically fragmented leading to free radicals. Free radicals will react with double bonds of vinylic or acrylic monomers giving rise to intermediate radical species, which will propagate by further reaction with single monomers. Finally, termination will occur mainly by recombination of two radical species, the reaction of an active chain with a free radical initiator, the transfer of the active centre or the interaction of an active chain with impurities

such as oxygen or other inhibitors (168). The major drawbacks on free radical polymerisation arise from the lack of control over the initiation, propagation, termination and chain transfer reaction steps during polymerisation (167,169). In order to have a better control on the synthesised MIP reversible deactivation radical polymerisation (RDRP) emerged (170).

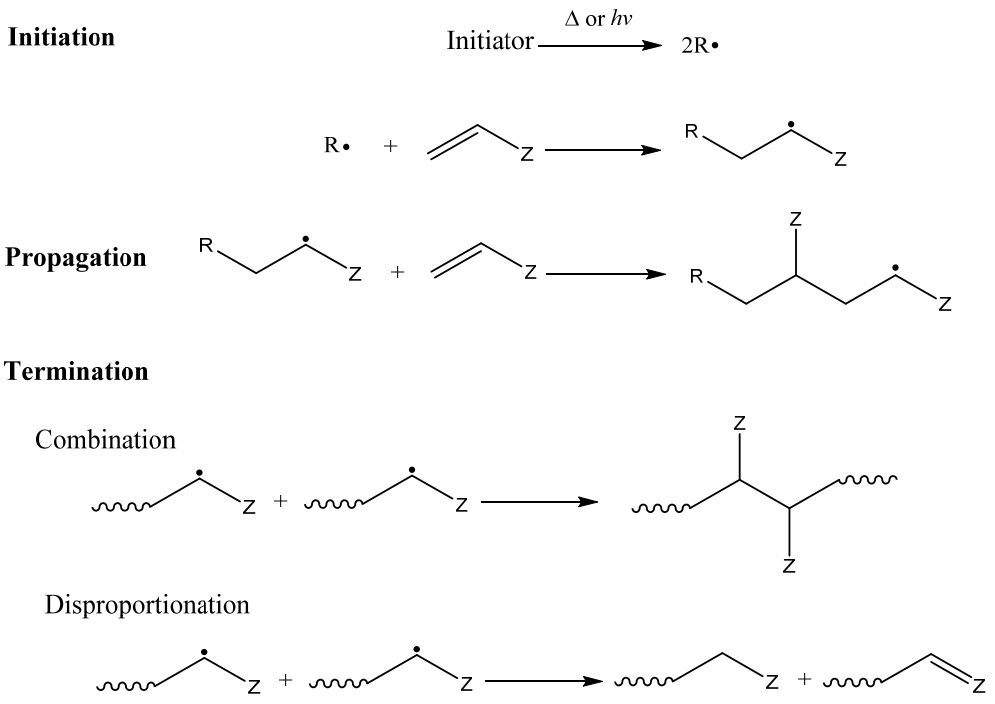

Figure 4. 8. Mechanism of free radical polymerisation.

RDRP can be used with a large number of monomers with different functionalities (171). The most popular RDRP methods include iniferter polymerisation (172), nitroxide-mediated radical polymerization (NMP) (173), atom transfer radical polymerization (ATRP) (174,175), and reversible addition-fragmentation chain transfer (RAFT) polymerization (176). RDRP mechanisms provide polymers of controlled composition, architecture and molecular weight distribution (169,177). The use of this type of initiation can potentially improve MIP performance, since it may favour the generation of polymers with narrower molecular distribution and more homogeneous binding site distribution, in comparison with conventional radical polymerisation (171). The most versatile RDRP methods for MIP development have found to be iniferter polymerisation and RAFT polymerisation, since they are compatible with most of the functional monomers used for molecular imprinting (178).

1.5.1. Iniferter-induced radical polymerisation

The iniferter concept was defined by its developers, Otsu *et al.* (179), as a compound that can act as initiator, transfer agent, and terminator in a radical polymerisation process. Iniferters are normally dithiocarbamates that can be separated into two species, the dormant and the active species. The controllability of this

polymerisation resides on the dynamic equilibrium between the dormant and the active species (172). The growing radical chain is reversibly deactivated by the dormant species that suppresses the propagation reaction, this way the polymerisation occurs under more favorable thermodynamic conditions (figure 4.9).

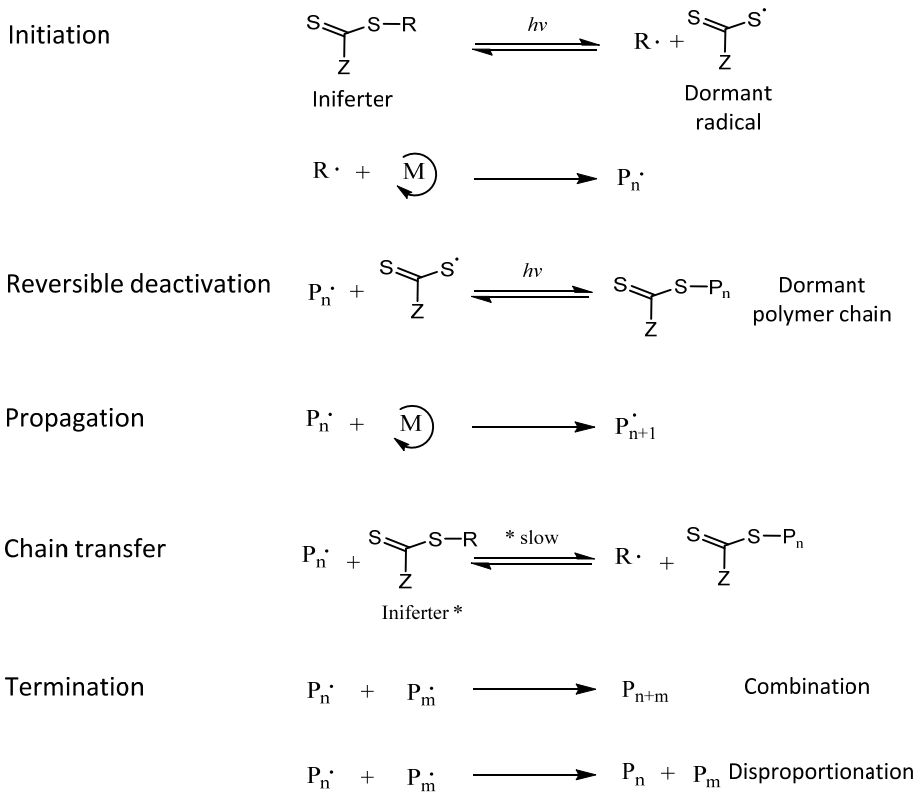

Figure 4. 9. Mechanism of iniferter-induced radical polymerisation.

This approach has been applied to the synthesis of monodisperse, highly crosslinked imprinted particles for diclofenac (137), histamine (17), vancomycin (139), 2,4 dichlorophenoxy acetic acid (180), cocaine (86), gluthanione (181) and dimethoate (182) among others. Using dithiocarbamate (86,180,181) and N-diethyldithiocarbamic acid benzyl ester (17,137,139) as iniferters.

On the other hand, MIP have been grafted from different surfaces such as silica beads (183,184), polystyrene particles (185), gold nanorods (186), MWCNT (187), carbon microspheres (188) or ceramic carbon electrode (189) by iniferter polymerisation. For this approach two main strategies can be followed, on one hand the desired surface can be functionalised with a compound that will subsequently react with an iniferter salt, such as sodium N,N-diethyldithiocarbamate (184,185,187-189). On the other hand, tailor made iniferters can be synthesised with specific end-groups capable of being immobilised on the proposed surface, such as N,N-diethylaminothiocarbamoyl propyl(trimethoxy)silane for silica (183) or 2-(phenoxy)- ethyldiethylcarbamadithionate diazonium chloride for gold surface (186).

1.5.2. Reversible addition-fragmentation chain transfer polymerisation

Reversible addition-fragmentation chain transfer (RAFT) polymerisation has become very popular due to its good control over the polymer structures, its applicability to a wide range of monomers and its tolerance to a wide range of reaction conditions (176,190,191).

Although the term RAFT is also used in a more general sense, it is usually associated to the reactions involving thiocarbonylthio compounds such as dithioesters, dithiocarbamates or trithiocarbamates (169).

RAFT polymerisation starts like free radical polymerisation, where a radical initiator leads to two reactive radicals. The radicals react with monomers leading to a propagating polymeric radical (PPR) which reacts with the C=S bond of the RAFT agent, creating a carbon centered intermediate. When this intermediate is fragmented, it leads to a PPR or a RAFT polymer and a new radical which can reinitiate polymerisation and create a new PPR. Finally, equilibrium is reached between the different PPRs and the RAFT compound, at this point the probability to grow is the same for all chains (figure 4.10) (171).

The R groups on RAFT agents refer to the living radical groups which are able to reinitiate the polymerisation. On the other hand, Z groups refer to groups used for the modification of

the activity of the agent. Transfer constants and in consequence polymerisation activity are affected by these R and Z groups, becoming the sequence of addition-fragmentation equilibria in a key feature on RAFT polymerisation (192).

It is important that Z groups activate the C=S bond towards radical addition in order to have a high transfer constant. For this, suitable Z groups can be aryl and alkyl. The main conditions for an efficient RAFT polymerisation are that initial and polymeric chain transfer agents should have a reactive C=S bond, the intermediate radicals should fragment quickly and finally, the radicals formed in the process should efficiently reinitiate polymerisation (169).

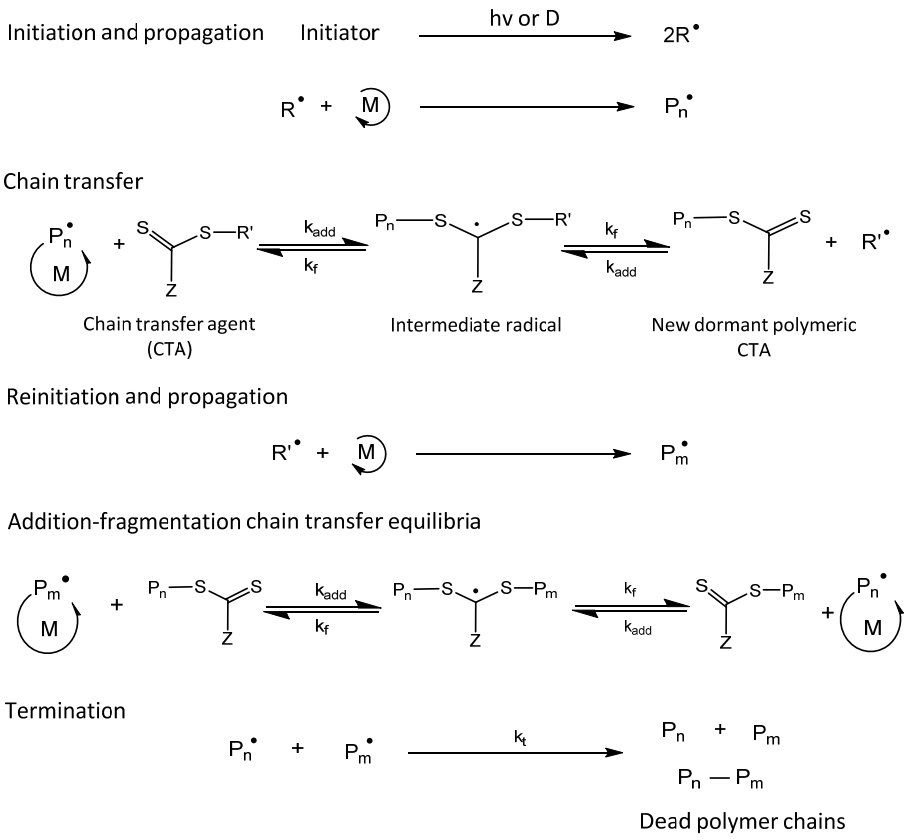

Figure 4. 10. Mechanism of RAFT polymerisation.

RAFT has been used for several MIP synthesis of nanoparticles (193-195) or obtaining uniform and controlled polymer films on different surfaces such as Fe_3O_4 nanoparticles (196-198), graphene oxide (126), silica (118,199) or polymer (200).

2. Objectives

The intrinsic properties of Reversible Deactivation Radical Polymerisation have been exploited in the last years for the development of Molecularly Imprinted Polymers with controlled polymer architectures. In this regard, it was hypothesised if MIP developed through controlled polymerisation strategies could serve as sensing platforms for small organic targets, with enhanced selectivity over traditional MIP. It was therefore established as the principal objective of the present work: **the development of MIP-based synthetic receptors on gold substrates, through different Reversible Deactivation Radical Polymerisation strategies, and the use thereof as sensing elements for voltammetric measurements**. To accomplish this general objective, the following operational goals are to be fulfilled:

- Fabrication of gold microelectrodes and surface activation.
- Functionalisation of gold substrates through self-assembled monolayer formation.
- Synthesis of the MIP-based sensing elements through different strategies:
    - Grafting polymer thin layers from the surface of gold electrodes previously functionalised with a thiol iniferter.

  - Grafting preformed imprinted nanoparticles, developed through the solid phase imprinting approach, to the surface of gold electrodes.

- Verification of the surface step-by-step coating process by Cyclic Voltammetry (CV) an Electrochemical Impedance Spectroscopy (EIS).

- Confirmation of the surface coating homogeneity by Scanning Electron Microscopy (SEM).

- Optimisation of the polymerisation conditions to get sensors with best electrochemical behaviour.

- Application of the developed sensors to 4-ethylphenol sensing by Differential Pulse Voltammetry (DPV). Sensor selectivity assessment employing structural analogues to 4-ethylphenol.

- Analytical evaluation of the developed electrochemical methods.

3. Materials and equipment

3.1. Materials and reagents

4-ethylphenol (4EP) (99.7 %), tyramine (≥98.5%), 4-ethylguaiacol (4EG) (≥98%) and paracetamol analytical standards were obtained from Sigma-Aldrich (Madrid, Spain). Coumaric acid ethyl ester (CAEE) (≥90%) was purchased from LGC Standards (Barcelona, Spain) and 4-vinylphenol (4VPh) (10% in ethylene glycol) from Cymit Química (Barcelona, Spain).

The monomers trimethylolpropane trimethacrylate (TRIM), ethylene dimethacrylate (EDMA), 4-vinylpyridine (4VP) and ferrocenylmethyl methacrylate (FER) were purchased from Sigma-Aldrich whereas the amine monomer N-(3-aminopropyl) methacrylamide hydrochloride (APMA) was acquired from Polysciences Europe GmbH, (Eppelheim,, Germany). Prior to use, 4VP was purified by distillation under vacuum obtaining a colorless liquid which was stored below -20ºC and under nitrogen atmosphere.

N-[3-(trimethoxysilyl)propyl] ethylenediamine, glutaraldehyde (50% in water), lipoic acid (LA), mercaptoundecanoic acid (MUA) and ethanolamine (EA) were also acquired from Sigma-Aldrich. 1-ethyl-3-[dimethylaminopropyl]carbodiimide (EDC) and N-

hydroxysuccinimide (NHS) were purchased from Thermo Fischer Scientific (Waltham, MA USA).

The iniferter N,N,-diethyldithiocarbamic acid benzyl ester (DABE) was obtained from TCI Europe (Belgium) and the chain transfer agent pentaerythritol tetrakis (3-mercaptopropionate) (95%) were acquired from Sigma-Aldrich. 3-chloro-propanethiol (98%) and sodium diethyldithiocarbamate trihydrate, employed for the synthesis of the thiol group containing iniferter, were also acquired from Sigma-Aldrich.

Acetonitrile (ACN), tetrahydrofuran and isopropanol were HPLC grade and they were acquired from Scharlab (Barcelona, Spain). Dry toluene and acetone were purchased from Panreac (Barcelona, Spain).

Sodium dihydrogen phosphate monohydrate (99%), di-sodium hydrogen phosphate (≥99%), hydrochloric acid (37%), phosphoric acid (85%), boric acid (99.8%), acetic acid (96%) and potassiun hydroxide (≥85%) were purchased from Merck (Darmstadt, Alemania). Sodium chloride (99.5%), hydrogen peroxide (33%), sodium hydroxide (99%), potassium hexacyanoferrate (III) (99%) and potassium hexacyanoferrate (II) trihydrate (98%) were purchased from Panreac (Barcelona, Spain).

Every buffer solution was prepared with ultra-pure water obtained from Elix20 reverse osmosis and Milli-Q water purification systems. All other reagents were analytical grade and they were used as received.

Glass beads (Spheriglass®2429, 53 μm < diameter < 106 μm) were from Blagden Chemicals (UK).

3.2. Equipment

Surface polymerisation on gold microelectrodes was performed with a Bluepoint 2 UV lamp acquired from Hönle UV Technology (Gräfelfing, Alemania), provided with an optic fiberglass wire of 1.5 m in length and 8 mm in diameter. On the other hand, polymerisation of imprinted nanoparticles was performed using a Philips UV device, model HB/171/A, fitted with 4x15 W lamps.

For the temperature based affinity separation of imprinted nanoparticles, SPE cartridges fitted with polyethylene frits (20 μm porosity) were acquired from Sigma-Aldrich.

For size analysis of nanoparticles, a Zetasizer Nano (Nano-S) apparatus from Malvern Instruments Ltd. (UK) was employed.

Gold (2 mm diameter) and glassy carbon electrodes (3 mm diameter) were acquired from Metrohm (Utrecht, The Netherlands). For gold microelectrode fabrication, a gold wire (99.99%) of 0.025 mm in diameter was used which was purchased from Goodfellow (Huntingdon, UK). The length of the microelectrode was cut to 4 mm using an Olympus S7 30 binocular (Barcelona, Spain).

All electrochemical measurements were conducted using a classical three-electrode system, where a Ag/AgCl (KCl 3M) was used as the reference electrode and a platinum-wire as the counter electrode, both acquired from Metrohm (Utrecht, The Netherlands). All electrochemical measurements were conducted at room temperature using a PGSTAT12 potentiostat/galvanostat controlled by the NOVA 1.8.17 (Metrohm Autolab B.V, Utrecht, The Netherlands) and GPES 4.9 (Ecochemie B.V. Utrecth, The Netherlands) softwares.

Fourier Transform Infrared Spectroscopy analysis of the synthesised iniferter was performed using a FTIR spectrometer, model 6300 type A, from Jasco (Madrid, Spain). Morphological studies of modified electrodes were carried out by scanning electron microscopy (SEM) using a Schottky-type field emission scanning electron microscope JEOL JSM-7000F (JEOL Ltd., Tokyo, Japan), with an accelerating voltage set to 20 kV. FTIR and SEM analysis were performed by the Advanced Research Facilities (SGIker) of the University of Basque Country.

4. Development of a voltammetric sensor for 4-ethylphenol based on molecularly imprinted films grafted on gold microelectrodes

4-ethylphenol is a volatile phenol that, at high concentrations, has been related with undesirable aroma and deffects in wine and other alcoholic beverages. It is produced by the spoilage yeasts of the genus *Brettanomyces/Dekkera* sp. and its measurement can help on the control of the yeast acitvity. In this regard, a sensor capable of continous monitoring the levels of this compound in a fast, straightforward way would be highly desirable for the wine industry.

4-ethylphenol is an electroactive compound which can be measured using a voltammetric transducer. But due to the well-known complexity of wine matrices, a recognition element that may bind selectively this target is undoubtedly necessary in order to displace electrochemical signals that may arise from redox reactions of potentially interfering compounds. Molecularly imprinted polymers, as synthetic recognition elements could help achieving this goal. Moreover, as opposed to natural receptors, MIP are stable under non-physiological conditions, what constitutes a real advantage to face adverse conditions in direct

sample measurement, mainly related with pH and saline concentration in wine matrices.

The development of the MIP sensor has been planned employing two different strategies. On the one hand, MIP thin films have been photochemically polymerised on the surface of a gold electrode by the grafting from approach. For this purpose, a suitable dual-function thiol iniferter has been synthesised for the first time, which has proved to be capable of self-assembling to gold surface and also to start controlled polymerisation through UV light activation.

Alternatively, MIP nanoparticles have been grafted to gold electrodes as a second strategy for the construction of the 4EP sensor. Here, MIP nanoparticles were synthesised first by the solid-phase imprinting approach and then, they were immobilised on the surface of the gold surface through carbodiimide coupling chemistry.

The sensors obtained by each of these strategies will be subject to electroanaytical evaluation in order to know whether any of them presents better electrochemical performance in terms of sensitivity, selectivity and repeatability/reusability.

In the first instance, the methodology based on the development of MIP thin films on gold substrates will be described.

4.1. Fabrication of gold microelectrodes

Gold microelectrodes were fabricated using a hard tempered gold wire (>99.99% purity) of 25 µm in diameter, following a method reported elsewhere (154,158-160). As supporting material, a 10-100 µL pipette tip was used and as sensing material, a 10 µm diameter gold wire. A small filament of the wire was cut and inserted, at least 1 cm, into the sharpest end of the polyethylene pipette tip, which was used as supporting body. Subsequently, the tip end was thermally sealed to fix the filament inside the tip. Finally, the gold filament was cut to 40 mm long using a microscope provided with a ruler reticle in the eyepiece. In order to allow electric contact between the gold microelectrode and the potentiostat, a copper wire was introduced through the wide end of the tip, until it made contact with the gold wire located inside the tip.

Once microelectrodes were fabricated, the gold surface was cleaned combining chemical and electrochemical cleaning processes. First of all, the electrode was kept in a H_2O_2 (25% v/v) solution prepared in KOH (50 mM) for 15 min. Then, 3 successive reductive scans were applied by linear sweep voltammetry from -0.2 V to -1.2 V using 50 mM KOH as supporting electrolyte. Fischer *et al.* compared the most widely used methods for gold electrode surface cleaning, concluding that the combination of these two processes was the most effective option (201).

4.2. Electrochemical oxidation of 4-ethylphenol on gold microelectrodes

In the first instance, the electrochemical response of the fabricated microelectrodes to 4EP was assessed and the conditions at which they provided best performance were selected. Electrochemical oxidation of 4EP was conducted by Differential Pulse Voltammetry (DPV) and the anodic peak current was monitored. To avoid gold anodisation, the working potential range was set between 0 V and 0.6 V. Higher potentials were found to be courterproductive since they led to gold passivation arising from the electrochemical oxidation of the metallic surface.

The effect of parameters related with the electrochemical technique, namely, modulation time, interval time, step potential and pulse amplitude, on 4EP current signal were evaluated first. Electrochemical measurements performed in this study were conducted at room temperature, using Britton-Robinson 0.04 M buffer at pH 10 as supporting electrolyte. The values of tested parameters that led to highest peak current signal are summarised in table 4.2.

Table 4.2. Optimised parameters for electrochemical oxidation of 10^{-4} M 4EP by DPV.

Differential PulseVoltammetry	
Modulation time	0.01 s
Interval time	0.1 s
Start potential	0 V
End potential	0.6 V
Step potential	0.005 V
Pulse amplitude	0.05 V

The influence of pH and ionic strength on the recorded signal was evaluated next. For this purpose, the anodic current registered for a 10^{-4} M solution of 4EP was monitored using Britton-Robinson 0.04 M buffer as measurement medium, at pH values comprised between 1.8 and 11. Voltammograms recorded at each pH value are registered in figure 4.11. No peak was observed at pH below 7 because the oxidation potential displaces to values over 0.6 V, which is out of the selected working potential range for gold microelectrodes.

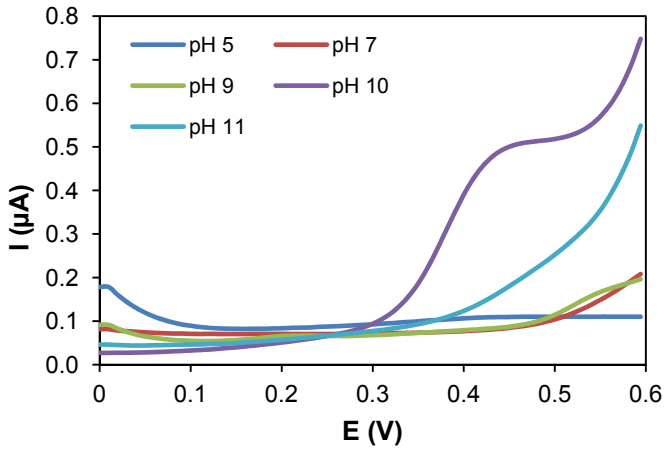

Figure 4.11. DPV voltammograms recorded in 10^{-4} M 4EP solutions in 0.04 M B-R buffer at different pH.

In order to assess the effect of the ionic strength on peak current signal, $NaClO_4$ was added to the electrochemical cell, up to 0.2 M. Obtained voltammograms are depicted in figure 4.12. It was concluded that the peak current signal did not significantly increase even though the ionic strength of the medium was higher (figure 4.12).

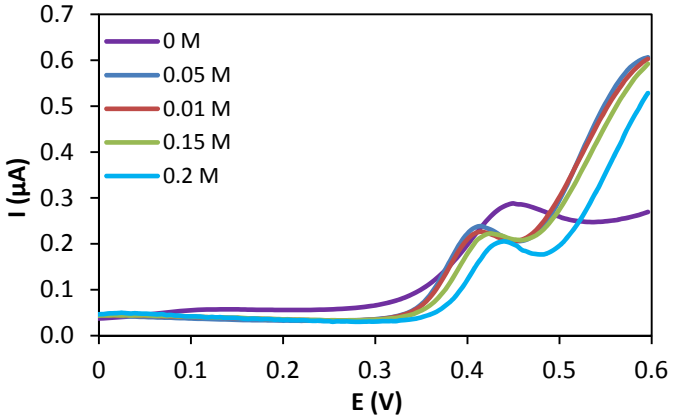

Figure 4. 12. DPV voltammograms recorded in 10^{-4} M 4EP solutions in BR 0.04 M buffer containing increasing concentrations of $NaClO_4$ (pH:10).

4.3. Synthesis and characterisation of the thiol iniferter

SAM of organosulfur compounds such as thiols, disulfides or sulfides assemble to metallic substrates spontaneously. SAM formed on gold, silver, palladium or mercury are most frequently formed by compounds with a thiol end-group. The thiol reaction with gold occurs in two steps: physisorption and chemisorption (202). First a coordinate bond is formed between the thiol group and gold, subsequently deprotonation of the thiol group takes place giving rise to a thiyl radical that will form a gold-thiolate covalent bond at the gold-sulfur interface (figure 4.13) (203).

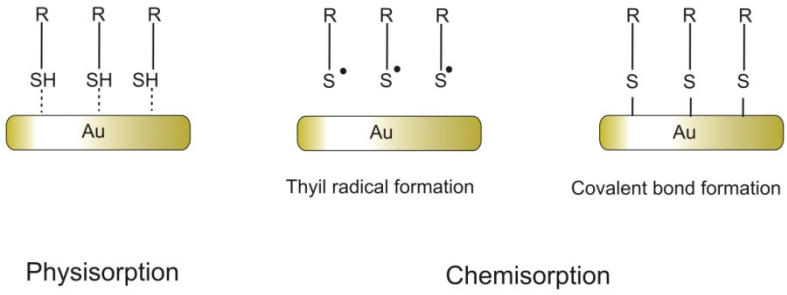

Figure 4.13. Schematic representation of SAM formation employing a thiol-group containing reagent.

In order to be capable of polymerising MIP thin films starting from the surface of gold microelectrodes, the iniferter (3-mercaptopropyl) diethylcarbamadithioate was synthesised due to its dual character, since it can self-assemble to gold surfaces through the thiol end-group and, on the other hand, it can initiate polymerisation by a reversible deactivation mechanism from the surface itself (*grafting from*).

The iniferter synthesis procedure was adapted from a previous work concerning the synthesis of N, N'-diethylaminodithiocarbamoylpropyl (trimethoxysilane), described by Bossi *et al.* (204) (figure 4.14a). In the reported work, the silane reagent 3-chloropropyl (trimethoxysilane) was allowed to react

with a dithiocarbamate salt, obtaining a silane iniferter capable of being attached to a silica surface having activated silanol groups. In this work, the silane compound has been substituted with a thiol compound (3-chloro-1-propanethiol) in order to form an iniferter capable of assembling to Au surfaces. The synthesis procedure of the iniferter is schematically depicted in figure 4.14b.

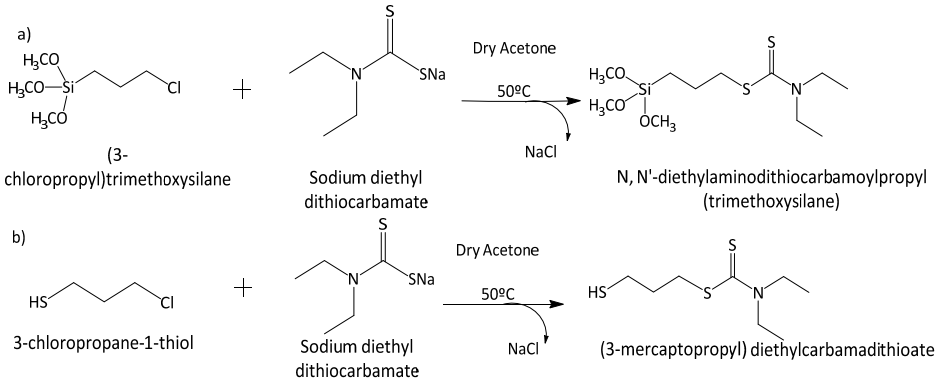

Figure 4. 14. Synthesis of a) the silane iniferter from ref. [75] and b) the thiol iniferter.

The iniferter was synthesised as follows: sodium diethyl dithiocarbamate trihydrate (1.5×10^{-2} mol) was ground obtaining a fine powder. This powder was dissolved in 50 mL of dry acetone in a 100 mL round bottom flask, fitted with a stirrer and a condenser. After dissolving the salt, 3-chloro-1-propanethiol (1.8×10^{-2} mol)

was added dropwise and the mixture was kept stirring for 15 h at 50 ºC. The ratio propanothiol: dithiocarbamate was 1.2:1 mol:mol. After reaction, insoluble salts were removed by filtration and the solvent evaporated, firstly by a rotary evaporator and secondly by a high purity nitrogen stream, obtaining a yellowish oily product. The product was stored in the dark, below 4ºC and under nitrogen atmosphere.

The synthesised compound was characterised by Fourier transform infrared spectroscopy (FT-IR). Figure 4.15 depicts IR spectra of the iniferter and the reagents used for its synthesis. In the sodium diethyl dithiocarbamate trihydrate spectrum (figure 4.15a), a characteristic band at 3345.89 cm^{-1} can be appreciated which may be attributed to the presence of hydration water in the salt. The band observed at 1201.43 cm^{-1} can be assigned to the C-N bond, which may also be appreciated in the iniferter spectrum at 1205.29 cm^{-1} (figure 4.15c). Other characteristic bands observed in the spectra of both compounds at 1475.27 cm^{-1}, 1258.32 cm^{-1} and 985.44 cm^{-1} (Figure 4.15a and c) were attributed to stretching vibrations of the N-C=S group. The band at 1670.05 cm^{-1} was attributed to the C-S bond. Concerning the spectrum of the thiol reagent (figure 4.15b), an intense band can be distinguished at 649.89 cm^{-1}, which probably corresponds to the C-Cl bond of the molecule. It is clear that this band is not present in the iniferter spectrum, what may confirm the loss of chlorine in the synthesis procedure.

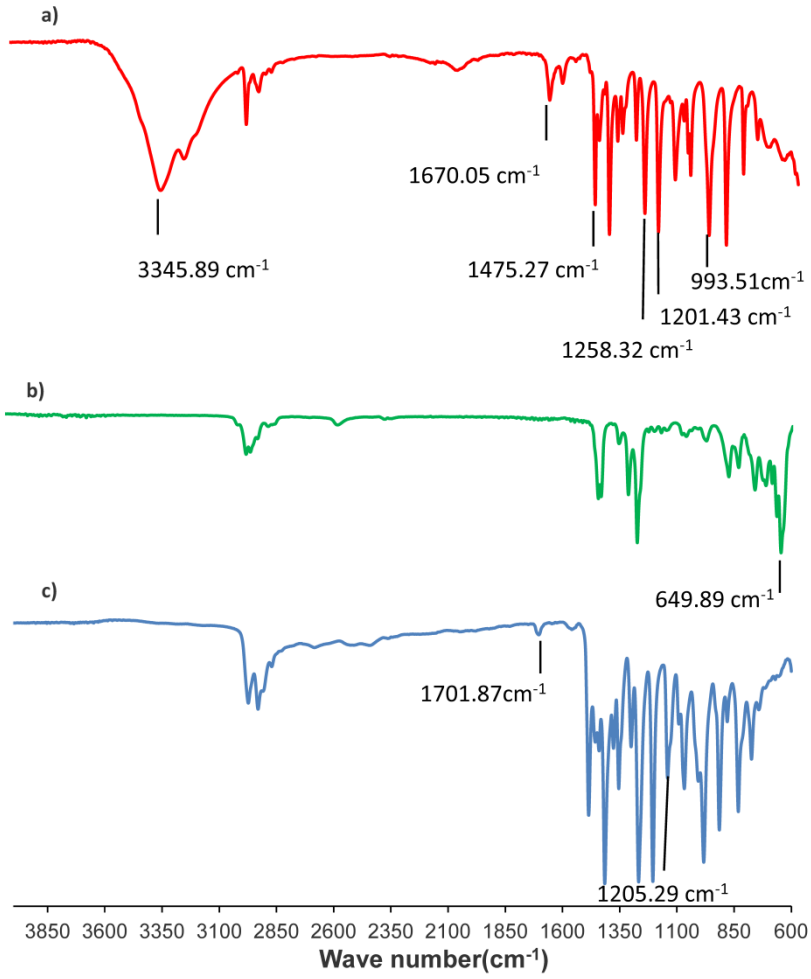

Figure 4.15. FT-IR spectra of a) sodium diethyl dithiocarbamate trihydrate, b) 3-chloro-1-propanethiol and c) the synthesised iniferter

It can be appreciated that the spectra of the iniferter and the dithiocarbamate salt present almost the same bands, what denotes a very similar functionality of both compounds. The most remarkable difference between them is the lack of bands relative to hydration water in the iniferter spectrum, what may be expectable, as water is not present in the reaction product. This fact together with the loss of the band corresponding to the C-Cl bond of the thiol reagent, would confirm the correct synthesis of the thiol iniferter.

4.4. Development of MIP thin layers on the gold surface of the microelectrode

4.4.1. Self-assembly of the thiol iniferter on gold surface

For SAM formation on the surface of gold microelectrodes, they were immersed in a deoxygenated ethanol solution containing 10 mg mL^{-1} of the iniferter for 24 h. This way thiol groups of the iniferter assemble to gold surface through Au-S bonds, leading to an iniferter monolayer (figure 4.16). Finally, microelectrodes were immersed in fresh ethanol for 15 min, under stirring, in order to clean physisorbed molecules.

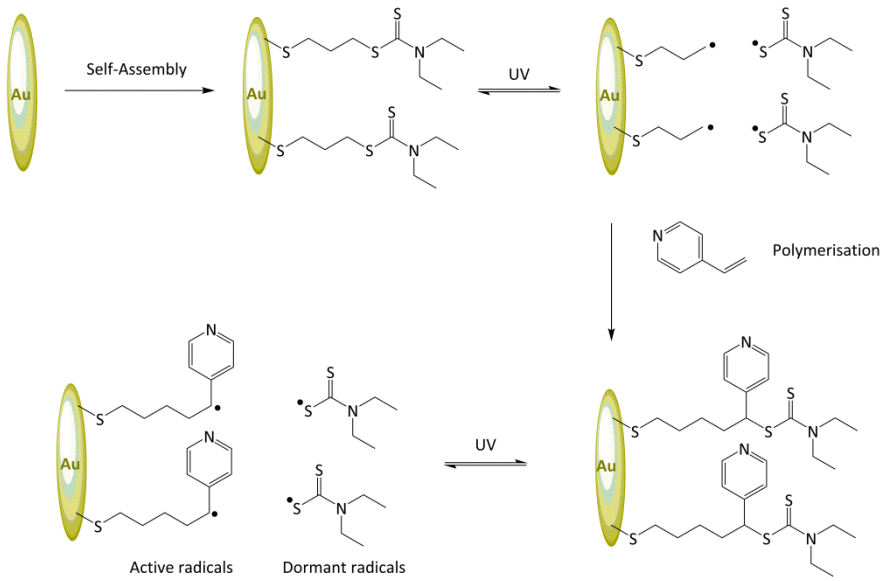

Figure 4. 16. Thiol immobilisation and polimerisation mechanism by iniferter induced polymerisation.

4.4.2. Synthesis of MIP thin layers

Polymer grafting on the gold microelectrode surface was carried out by photo-initiated reversible deactivation radical polymerisation (RDRP). To this end, the "grafting from" approach was selected, so that the polymer grows from the electrode surface allowing for a better control of the thickness.

Based on the results obtained previously (chapter 3), 4-vinylpyrindine (4VP) was chosen as the functional monomer and ethylene dimethacrylate (EDMA) as the crosslinker. Both monomers were added in excess and the thickness of the

polymeric film was controlled through the polymerisation time, since by RDRP the polymer continues growing until UV light is interrupted or until total monomer consumption, the latter not being expected to happen here.

1.1 g of 4VP, 6.1 g of EDMA and 0.6 g of 4EP were dissolved in 7.15 g of ACN in a 20 mL vial and, thereafter, the mixture was deoxygenated with high purity N_2 for 15 min. Thereafter, the gold microelectrode coated with the iniferter SAM monolayer was introduced through a previously perforated silicone septum. Finally, the mixture was further deoxygenated for 5 min using a syringe tip to ensure having an inert atmosphere inside the vial (figure 4.17).

The polymerisation was initiated by UV radiation focused on the gold wire using a fiber optic cable. The non imprinted (NIP) control electrodes were fabricated following the same procedure but without adding the template (4EP) to the polymerisation mixture.

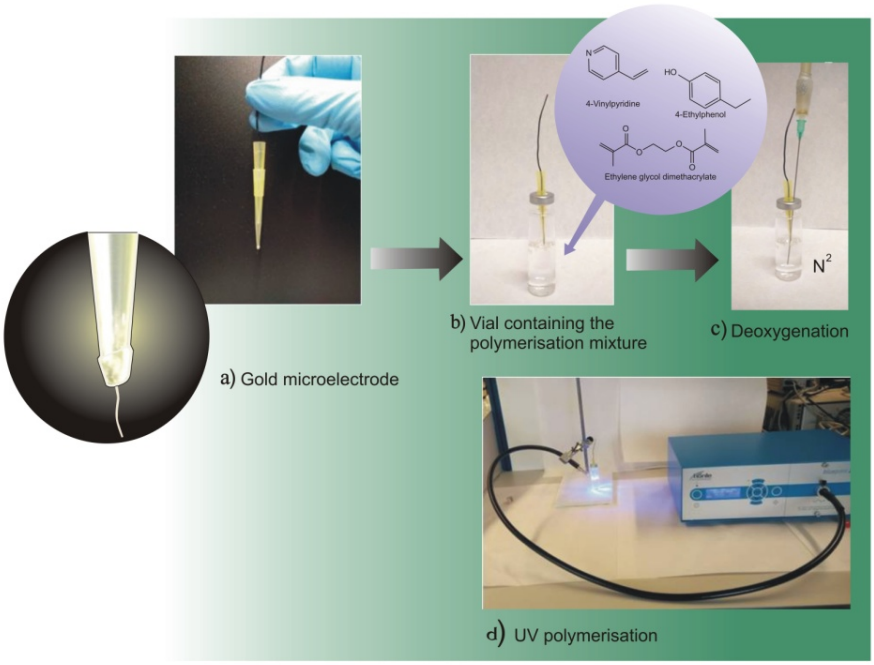

Figure 4. 17. Schematic representation of the MIP polymerisation process on gold microelectrodes.

4.5. Characterisation of the polymer coating

The iniferter assembly and the polymer synthesis on the microelectrodes was confirmed by Cyclic Voltammetry (CV) and Electrochemical Impedance Spectroscopy (EIS). To this end, modified electrodes were immersed in a 50 mL electrochemical cell containing 10 mL of an equimolar mixture of $[Fe(CN)_6^{4-}]/[Fe(CN)_6^{3-}]$ (2 mM) in KCl 0.1 M, which was used as supporting electrolyte.

4.5.1. Cyclic Voltammetry

Cyclic Voltammetry is an electrochemical technique where the potential is swept from an initial potential E_i to a potential E_λ, at this point, the direction of the potential scan is reversed, usually stopping at the initial potential (E_i) (205). The peak current on typical reversible systems in Cyclic Voltammetry is given by the Randles-Sevcik equation (206):

$$i_p = (2.69 \times 10^5) n^{3/2} A C D^{1/2} \nu^{1/2} \qquad \textbf{4. 2}$$

Where n is the number of changed electrons, A is the electrode area (cm^2), C is the concentration (mol L^{-1}), D is the diffusion coefficient ($cm^2\ s^{-1}$) and v is the scan rate ($V\ s^{-1}$). Peak intensity for the anodic and cathodic peaks should be the same for

a reversible system (I_a/I_c=1). Finally, the peak potentials (E_p) will be related with the formal potential (E_0) following the subsequent expression (206) :

$$E^0 = \frac{E_{p,a} + E_{p,c}}{2} \qquad \textbf{4. 3}$$

On the other hand, when irreversible processes occur, the current intensity of the peak is reduced in size and will be a bigger potential difference between the anodic and cathodic peak. The peak potential in irreversible systems is given by (206):

$$E_p = E_0 - \frac{RT}{\alpha n_a F}\left[0.78 + \ln\left(\frac{D^{1/2}}{k^0}\right) + \ln\left(\frac{\alpha n_a F v}{RT}\right)^{1/2}\right] \qquad \textbf{4. 4}$$

Where α is the transfer coefficient, n_a is the number of electrons involved in the electrodic process speed determining step and k^0 is the charge-transfer rate constant. So, E_p occurs at potentials higher than E^0, with the overpotential related to k^0 and α. Typical irreversible systems peak current will be defined as (206):

$$i_p = \left(2.69 \times 10^5\right) n (\alpha n_a)^{1/2} A C D^{1/2} v^{1/2} \qquad \textbf{4. 5}$$

The shape of the voltammogram will depend on $k^0/(\pi aD)^{-1/2}$ (where a=nFv/RT). As the charge transfer processes are more dominant $k^0/(\pi aD)^{-1/2}$ increases and the process will be more similar to a reversible case. On the other hand, when mass transfer processes are predominant, $k^0/(\pi aD)^{-1/2}$ will exhibit low values and the system will show an irreversible behavior (206).

The study of the Cyclic Voltammetry behavior of a redox couple (such as $[Fe(CN)_6^{4-}]/[Fe(CN)_6^{3-}]$) can provide information about the electrochemical process involved using differently treated electrodes.

The iniferter assembly and the polymer synthesis on the microelectrodes were confirmed by Cyclic Voltammetry (CV). To this end, modified electrodes were immersed in a 50 mL electrochemical cell containing 10 mL of an equimolar mixture of $[Fe(CN)_6^{4-}]/[Fe(CN)_6^{3-}]$ (2 mM) in KCl 0.1 M, which was used as supporting electrolyte.

All CV measurements were carried out from -200 mV to 600 mV at a step potential of 10 mV and a scan rate of 100 mV s^{-1}. Figure 4.18 depicts cyclic voltammograms registered with a bare gold microelectrode and an iniferter coated one.

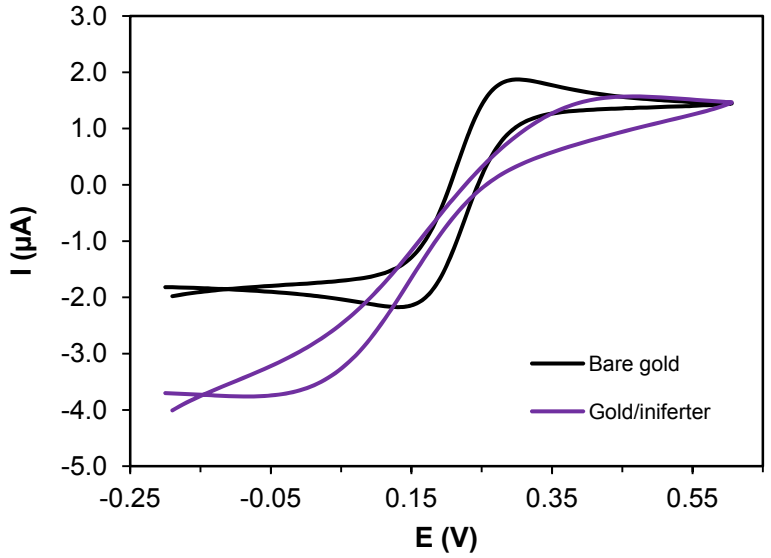

Figure 4.18. Cyclic voltammograms recorded with a bare gold microelectrode and a microelectrode coated with the iniferter.

As it is shown in figure 4.18, anodic and cathodic potentials and peak current intensities of the $[Fe(CN)_6^{4-}]/[Fe(CN)_6^{3-}]$ redox couple in the bare gold electrode suggest a reversible electrochemical reaction . However, when the electrode surface is coated with the iniferter, these peaks tend to disappear, what could be attributed to surface insulation of the microelectrode, showing current controlled by both charge-transfer and mass transfer. In addition, when the electrode surface is coated, the potential difference between the cathodic peak and the anodic peak increases, what may be indicative of an irreversible electrochemical process as a result of electrode modification.

After polymerisation, CV was further employed as a tool to monitor polymer formation on gold microelectrodes. For this study, a series of microelectrodes were coated with polymer films under different polymerisation times in order to know the effect of the resulting polymer thickness on the current values of the ferro/ferricyanide redox pair. Obtained cyclic voltammograms are depicted in figure 4.19.

As it can be deduced from the figure, longer polymerisation times led to lower current values in the ferro/ferricyanide redox pair. This may arise as a result of the formation a thicker polymer film and consequently, higher surface coverage on the electrode.

However, CV provides just partial information, insufficient to completely characterise the electrode modification electrochemically. Only peak currents and potentials are measured and these parameters contain very little information about the whole electron-transfer process. In this regard, surface characterisation was complemented by Electrochemical Impedance Spectroscopy (EIS).

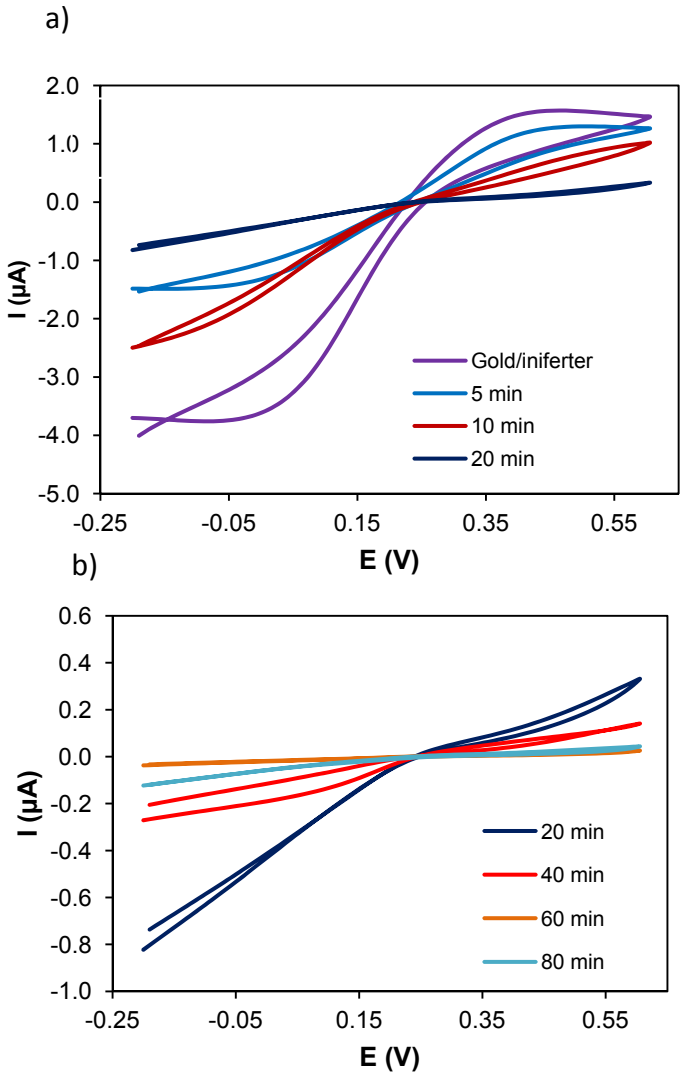

Figure 4.19. Cyclic voltammograms recorded with microelectrodes modified with a) iniferter and with polymer films synthesised for 5, 10 and 20 minutes and b) 20, 40, 60 and 80 minutes.

4.5.2. Electrochemical Impedance Spectroscopy

Electrochemical Impedance Spectroscopy (EIS) is a non-invasive simple technique for the characterisation of solid or liquid materials connected to an electrochemical transducer. Any material or process that could affect the conductivity of an electrode can be studied by EIS (207). The study of the electron transfer between the electrolyte solution and the electrode (or modified electrode) provides information of the integrity of the formed grafted material, including defects and distribution of the material (208). EIS has been successfully applied for the design and development of sensors (208-211), since it allows for the control and monitorisation of all electrode modification stages (207).

Impedance, as resistance, describes the ability of a circuit to resist the electrical current flow, but it is not limited to ideal resistors. Electrochemical Impedance can be measured applying an AC potential and measuring the current through the circuit (212). In electrochemical systems, EIS measures the impedance of a system as a function of the frequency of an applied AC voltage of small amplitude (207).

Resistance can be defined as the ability of an electrochemical element to resist the electrical current flow and it is defined by Ohm's Law. It relates current passing through resistance *i* (A), with voltage *E* (V), and resistance *R* (Ω) as the voltage:

$$R(\Omega)=\frac{E(V)}{I(A)} \qquad \textbf{4. 6}$$

However, this term is limited to systems with direct current (DC). On the other hand, on alternating current systems (AC) the applied potential has a sinusoidal form, the following would be its expression as a function of time:

$$E_t=E_0 \sin(\omega t) \qquad \textbf{4. 7}$$

Where E_t is the potential at time t, E_0 is the amplitude of the wave and ω is the radial frequency (ω = 2 π f(Hz)) . In this type of systems, the output current will be shifted in phase (ϕ) and would have different amplitude (I_0) compared to the input potential:

$$I_t=I_0 \sin(\omega t+\phi) \qquad \textbf{4. 8}$$

To calculate the impedance, an expression similar to Ohm's Law is used:

$$Z=\frac{E_t}{I_t}=\frac{E_0 \sin(\omega t)}{I_0 \sin(\omega t+\phi)}=Z_0 \frac{\sin(\omega t)}{\sin(\omega t+\phi)} \qquad \textbf{4. 9}$$

$$e^{(jx)} = \cos(x) + j\sin(x) \quad \textbf{4. 10}$$

Using Eulers relationship (4.10), potential and current intensity can be expressed as complex number functions:

$$E_t = E_0 e^{(j\omega t)} \quad \textbf{4. 11}$$

$$I_t = I_0 e^{(j\omega t - \phi)} \quad \textbf{4. 12}$$

where E_t and I_t are the potential and current intensity at time t, E_0 and I_0 are their respective wave amplitudes, ω is the radial frequency, ϕ is the phase shift and j the imaginary number ($j=\sqrt{-1}$). From these expressions impedance can be also expressed as a complex number function:

$$Z = \frac{E_t}{I_t} = Z_0 e^{(j\omega t)} = Z_0(\cos\phi + j\sin\phi) \quad \textbf{4. 13}$$

As it can be observed in equation (4.13) impedance can be described by an amplitude (Z_0) and a phase shift (ϕ). If the real part of the impedance expression is plotted on the x-axis ($Z'=Z_0 \cos\phi$) and the imaginary part on the y-axis ($Z''=Z_0\, j \sin\phi$) a plot is obtained which is commonly known as Nyquist plot and is widely used for EIS data interpretation (figure 4.20). Each point of the plot represents the impedance for a certain frequency value (212).

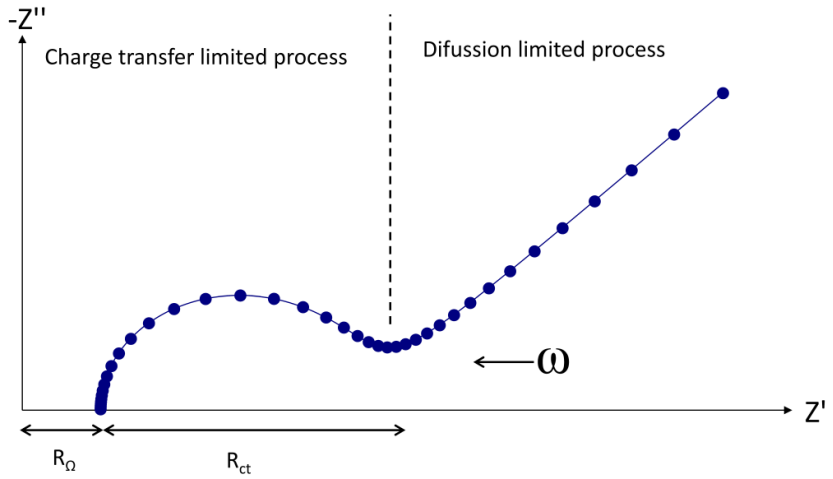

Figure 4. 20. Nyquist plot describing impedance values of a simple electrochemical cell at different frequencies. ref. (207).
R_Ω: solution resistance, **R_{ct}:** Charge transfer resistance, **ω:** frequency.

The Nyquist plot does not show the applied frequency value at each measurement point. Instead, Bode plots can be used (figure 4.21) where the absolute value of the impedance (Z) and the phase shift (ϕ) are plotted as a function of frequency in two different plots (212).

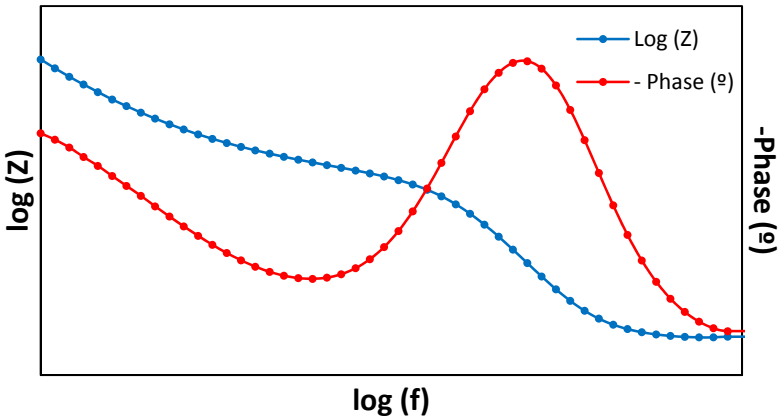

Figure 4. 21. Bode plot describing impedance values of a simple electrochemical cell. **Z:** absolute impedance, **º:** current intensity wave phase(ϕ), **f:** frequency (f=2πω).

Usually EIS data are fitted to an equivalent circuit model where the principal elements are resistors (R), capacitors (C) and inductors (L). These elements can be in series or in parallel on the circuit and their individual impedance value (table 4.3) will contribute to the absolute impedance of the circuit (figure 4.22). The impedance of a resistor is independent of the frequency and has no imaginary component. On the other hand, the impedance of an inductor increases with frequency and only has an imaginary component. Capacitors behave oppositely to inductors with a single imaginary component (table 4.3) (212).

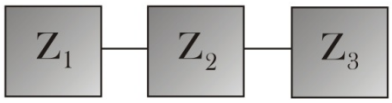

$$Z = Z_1 + Z_2 + Z_3$$

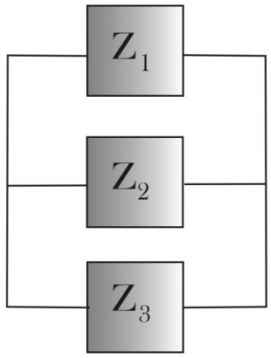

$$\frac{1}{Z} = \frac{1}{Z_1} + \frac{1}{Z_2} + \frac{1}{Z_3}$$

Figure 4. 22. Impedance contribution of each elements in an equivalent circuit in series or in parallel.

Table 4. 3.Impedances for each element on the equivalent circuit.

Element	Impedance
Resistor (R)	$Z = R$
Capacitor (C)	$Z = \frac{1}{j\omega C}$
Constant phase element (CPE)	$Z = \frac{1}{C(j\omega)^{\alpha}}$
Inductor (L)	$Z = j\omega L$
Warburg (W)	$Z = \frac{1}{Y_0\sqrt{j\omega}}$

Resistors on equivalent circuits are modelling resistances produced by the physical electrochemistry of the system. **The electrolyte resistance (R_Ω)** is an important element on the impedance of an electrochemical cell. It describes the solution resistance between the working and the reference electrodes and is independent of the working electrode surface coating, thus, it is an ohmic resistance as it not depends on the applied voltage. This resistance depends on the type of ions and their concentration, temperature and the geometry of the area were the current is flowing. It can be described as (213):

$$R = \frac{l}{\kappa A} \qquad \textbf{4. 14}$$

Where A is the area and l the length of the bounded area where the current is flowing and κ the conductivity of the solution.

The **charge transfer resistance (R_{ct})** is related to the exchange current (I_0), and can be described as (214):

$$R_{ct} = \frac{RT}{nFI_0} \qquad \textbf{4. 15}$$

where n is the number of electrons involved, F Faraday's constant, R gas constant, T temperature and I_0 the exchange

current. This description comes from the Butler-Volmer equation (214):

$$I=I_0\left(e^{\left((1-\alpha)\frac{nF}{RT}\eta\right)}-e^{\left(-\alpha\frac{nF}{RT}\eta\right)}\right) \quad \textbf{4. 16}$$

Where α is the simmetry factor and η the overpotential due to the potential applied on the system. When the overpotential is very low this expression can be simplified using Taylor series to (214):

$$I=I_0\frac{nF\eta}{RT}=\frac{\eta}{R_{ct}} \quad \textbf{4. 17}$$

The Butler-Volmer equation (4.16) can be simplified if one of the exponential terms is small enough. In the anodic process where the overpotential (η) has positive values, the second term becomes negligible (4.18). On the other hand, when the process is cathodic and the overpotential negative, the second part will be negligible (4.19) (214).

$$I=I_0\left(e^{\left((1-\alpha)\frac{nF}{RT}\eta_a\right)}\right) \quad \textbf{4. 18}$$

$$I=I_0\left(e^{\left(-\alpha\frac{nF}{RT}\eta_c\right)}\right) \quad \textbf{4. 19}$$

Where η_a and η_c are the anodic and cathodic overpotentials, n is the number of electrons involved, F Faraday's

constant, R gas constant, T temperature and I_0 the exchange current. From these expressions, the dependence of the overpotential (η) can be related to the current intensity (I) in semi-logarithmic form:

$$\eta_a = \frac{2.303RT}{n(1-\alpha)F}\log I_0 - \frac{2.303RT}{n(1-\alpha)F}\log I \qquad \textbf{4. 20}$$

$$\eta_c = \frac{2.303RT}{n\alpha F}\log I_0 - \frac{2.303RT}{n\alpha F}\log I \qquad \textbf{4. 21}$$

These expressions correspond to the Tafel equations with slope β_a and β_c:

$$\beta_a = \frac{2.303RT}{n(1-\alpha)F} \qquad \textbf{4. 22}$$

$$\beta_c = \frac{2.303RT}{n\alpha F} \qquad \textbf{4. 23}$$

The Tafel equations are very useful for the study of metal corrosion, in this sense, Stern and Geary developed an equation where the corrosion current (I_{corr}) is related with the **polarisation resistance (R_p):**

$$I_{corr} = \frac{\beta_a\beta_c}{\beta_a+\beta_c}\left(\frac{1}{R_p}\right) \qquad \textbf{4. 24}$$

Where I_{corr} is the corrosion current, it is the analogue of the exchange current (I_0) at the potential where metal corrosion occurs. β_a and β_c are the anodic and cathodic Tafel slopes respectively and R_p is the polarization resistance behaving as a resistor (214).

When two conducting plates are separated by a dielectric (a non-conducting media) a capacitor will be formed. Between the working electrode and the surrounding electrolyte exists an electrical double layer, which is formed by ions in solution. In consequence, the charged electrode is separated from the charged ions. This separation forms a capacitor represented by the **double layer capacitance (C_{dl})**, and it depends on many variables as electrode potential, temperature, electrolyte or electrode roughness (212). It is usually expressed as differential capacity (215):

$$C_{dl} = \frac{dQ}{dE} \qquad \textbf{4. 25}$$

Where Q is the excess charge stored and E the potential. The **coating capacitance (C_c)**, on the other hand, occurs when a polymer is coating the substrate and is described by:

$$C_c = \frac{\varepsilon \varepsilon_0 A}{d} \qquad \textbf{4. 26}$$

Where ε is the dielectric constant of the coating, ε_0 is the dielectric constant of vacuum, A is the area of the coating and d is the thickness of the coating. The coating capacitance can increase when water penetrates the coating because it increases the dielectric constant (216).

The above described capacitance concepts are modelling ideal capacitors assuming surface homogeneity, nevertheless, the studied surfaces usually are not strictly homogeneous and the **constant phase element (CPE)** is used for modelling these elements:

$$Z_{CPE} = \frac{1}{(j\omega)^{\alpha} C} \qquad \textbf{4. 27}$$

Where C is the capacitance, ω is the radial frequency, j the imaginary number ($j=\sqrt{-1}$) and α is an empirical constant ranging from 0 to 1, when α is equal to 1 the CPE will act as a pure capacitor (216).

The impedance of **an inductor (L)** can be described as:

$$Z_L = j\omega L \qquad \textbf{4. 28}$$

Inductive behaviour can be due to adsorption of reactants on the surface of the electrode or due to non-uniform current distribution (216).

The **Warburg Impedance (Z_W)** is related to the mass transport of the electroactive species (207). At high frequencies diffusing reactants do not move fast, in consequence, Warburg impedance is small. On the other hand at low frequencies Warburg impedance increases as reactants have to diffuse faster. There are several expressions for the description of this impedance, assuming a semi-infinite diffusion layer, the impedance would be as follows (217):

$$Z_W = \left[\frac{RT}{(nF^2)}\right]\left[(D_{ox}(c_{ox}^0)^2)^{-1/2} + (D_{red}(c_{red}^0)^2)^{-1/2}\right](j\omega)^{-1/2} \quad \textbf{4. 29}$$

where ω is the radial frequency, D_{ox} and D_{red} are the diffusion coefficients for the oxidant and the reductant and c^0_{ox} and c^0_{red} their bulk concentration present in the electrolyte, j is the imaginary number, n the number of electrons involved, F Faraday's constant, R gas constant and T temperature.

Sometimes this equation is presented in terms of a diffusion admittance:

$$Y_0 = \frac{1}{\left[\frac{RT}{(nF^2)}\right]\left[(D_{ox}(c_{ox}^0)^2)^{-1/2} + (D_{red}(c_{red}^0)^2)^{-1/2}\right]} \quad \textbf{4. 30}$$

For the modeling of an electrode impedance behavior, equivalent circuits are used, these circuits are composed by the abovementioned elements which are modeling the different electrochemistry processes occurring in the cell when a perturbing potential is applied. When a single step Faradaic process occurs in the possible presence of diffusion, the simplest equivalent circuit to describe this system is the Randles circuit (201,207,209) (figure 4.23). It is widely used to describe polymer coated electrodes. It consists of an electrolyte resistance (R_Ω), a constant phase element modelling a capacitor (CPE) and a Faradaic impedance due to charge transfer processes (Z_f).This impedance is divided into charge-transfer resistance (R_{ct}) and Warburg impedance (Z_w). The Warburg impedance will be dominant in diffusion controlled processes and when the process is controlled by charge-transfer and no diffusion occurs the Faradaic impedance will be equal to the charge-transfer resistance (207) (figure 4.23).

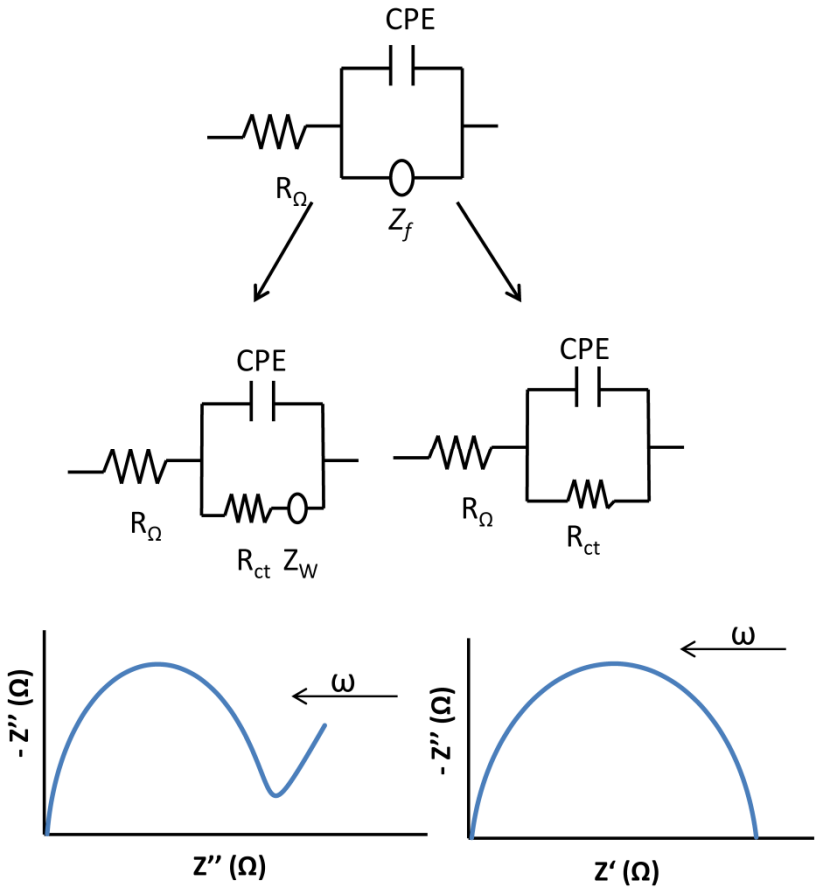

Figure 4. 23. Randles equivalent circuit with the corresponding Nyquist plot.

The elements in the equivalent circuit can be observed on the Nyquist plot shape. For instance, the semicircle that appears at high frequencies is relative to charge-transfer limited processes, while the straight line at low frequencies is describing diffusion limited processes (figure 4.23). When the coating of an electrode is thick enough, diffusion will be hindered on the electrode surface, decreasing the Warburg impedance. The measured impedances are fitted to an appropiate equivalent circuit obtaining a fitting error, described by the χ^2, that can be defined as (218):

$$\chi^2 = \sum_{i=1}^{N} \left\{ \left[\frac{Z_i' - Z_{i,calc}'}{\sigma_i'} \right] + \left[\frac{Z_i'' - Z_{i,calc}''}{\sigma_i'} \right] \right\} \qquad \textbf{4. 31}$$

Where Z_i' (Ω) and Z_i'' (Ω) and $Z_{i,calc}'$ (Ω) and $Z_{i,calc}''$ (Ω) are the experimental and calculated impedances and σ_i' and σ_i'' the standard deviation at each frequency, i.

Based on the valuable information that EIS provides, it was employed in this work to assess the layer-by-layer surface coating of gold microelectrodes. In this regard, impedance spectra were acquired after each electrode coating step in order to determine whether the coating was performed successfully or not.

Acquisition of impedance spectra was carried out applying a potential of 200 mV, at frequencies ranging from 0.1 Hz to 1MHz and an amplitude of 10 mV. Measurements were carried out using an equimolar mixture of $Fe(CN)_6^{4-}$ and $Fe(CN)_6^{3-}$ (2 mM) in a KCl 0.1 M solution. Obtained results were fitted to the Randles equivalent circuits detailed in figure 4.23 by the software (NOVA) and the one with the minimum fitting error (minimum χ^2) was chosen as equivalent circuit.

First of all, impedance spectra of the bare gold electrode and the iniferter coated one were acquired using 10 mL of an equimolar solution of $Fe(CN)_6^{4-}$ and $Fe(CN)_6^{3-}$ (2 mM each) in KCl 0.1 M. Obtained values represented as Nyquist plots are depicted in figure 4.24. As it is shown, it can be noticed that the semicircle of the plot related with the iniferter coated microelectrode is bigger. As the semicircle in Nyquist plots is proportional to the charge-transfer resistance, it can be deduced that the iniferter coated microelectrode presents higher resistance, due to the higher surface covering, which confirms the proper immobilisation of the iniferter on the electrode surface.

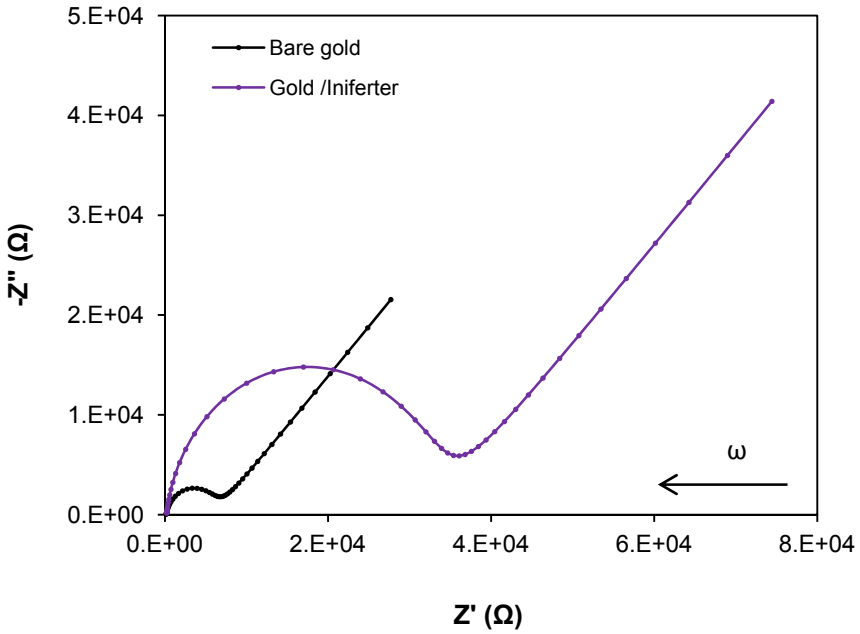

Figure 4. 24. Nyquist plots for a bare gold microelectrode and a microelectrode coated with the iniferter.

After polymerisation, the coverage of the electrode surface increases and it further does as polymerisation time is longer. The Nyquist plots corresponding to these sensors clearly show semicircles that increase with polymerisation time. Moreover, the final straight line at low frequencies, related with diffusion-limited processes, tends to disappear (figure 4.25).

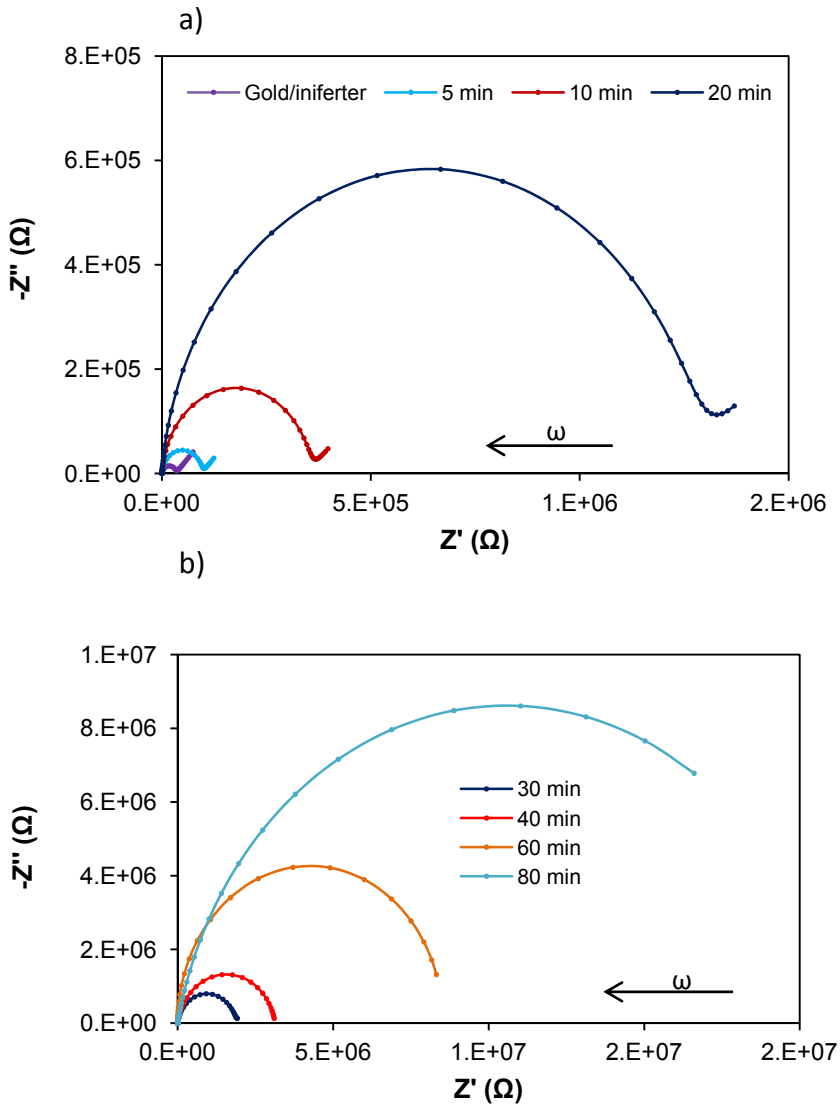

Figure 4. 25. Nyquist plots registered with a) the iniferter coated microelectrode and after 5, 10 min of polymerisation and b) 30, 40, 60 and 80 min of polymerisation.

Obtained impedance data were fitted next to the Randless equivalent circuit (table 4.4). As it can be observed, the Warburg impedance decreases with the polymerisation time, disappearing after 30 minutes. If charge-transfer resistances are compared in MIP electrodes synthesised under different polymerisation times, it can be noticed that resistance change is not remarkable for polymerisation times under 10 minutes. In contrast, from 60 min onwards, the measured resistances are considerably higher.

Observing the α parameter from the constant phase element on the different electrodes it can be stated that, in most of the electrodes, the parameter value is close to 1, what means that the constant phase element is modelling a nearly ideal capacitor and suggests that the electrode surfaces are quite smooth. However, this parameter is lower on the electrodes with high polymerisation times, suggesting that these electrodes surfaces are rougher.

Table 4. 4. Electrochemical impedance spectroscopy data for all the fabricated sensors.

Electrode	R_Ω (Ω)	CPE (nS s^α)	α	R_{ct} (KΩ)	Z_W (µS $s^{1/2}$)	χ^2
Bare gold	142.5	142.8	0.87	6.12	41.40	1.08
Gold + Iniferter	177.5	33.1	0.91	33.05	21.57	0.42
MIP 5 min	129.2	31.6	0.96	95.19	30.48	0.07
MIP 10 min	143.1	19.0	0.95	352.16	19.52	0.05
MIP 20 min	127.3	16.3	0.94	1264.70	8.09	0.03
MIP 30 min	127.2	23.8	0.90	1862.40	12.29	0.03
MIP 40 min	142.7	20.4	0.89	3131.01		0.06
MIP 50 min	131.9	20.4	0.86	4904.10		0.08
MIP 60 min	231.6	57.7	0.87	13047.00		0.09
MIP 70 min	144.9	28.0	0.83	13665.00		0.61
MIP 80 min	179.3	32.2	0.83	21160.00		0.04
MIP 90 min	175.2	29.9	0.86	29365.00		0.03

R_Ω: electrolyte resistance, **CPE:** constant phase element with **α** constant, **R_{ct}:** charge transfer resistance, **Z_W:** Warburg impedance, **χ^2:** fitting error.

Based on presented results, it was concluded that, iniferter was successfully immobilised on the gold electrode and, on the other hand, the increasing time of polymerisation makes the coverage of the electrode surface higher due to the formation of a thicker polymer surface grafted from the gold surface.

4.5.3. Scanning Electron Microscopy

Scanning Electron Microscopy (SEM) is a widely used technique for polymeric material characterisation due to its high resolution and capability for analysing structural and morphological properties. It is based on the same principle as optic microscopy, where the radiation is substituted by an accelerated electron beam. The scanning electron microscope, transforms the secondary electrons generated as a result of the interaction between the electronic beam with a thin superficial layer of the sample in a screening process to images. The fact that the observation is done point by point allows the use of samples of any size, and a high depth of field is achieved, obtaining images with a three-dimensional appearance. The spatial resolution of a SEM image is given by the area of the reflecting sample and depends on the degree of interaction between the sample and the electron beam. This interaction will produce reflected electrons that will be attracted by a detector to produce the topographic images.

For SEM analysis, the uncoated and polymer coated gold microelectrodes were placed on a carbon tape and measured directly, without sputtering any metal on the surface.

The SEM images obtained for the modified and unmodified gold wires are depicted in figure 4.26. Morphological differences observed on the SEM images for the modified microelectrodes confirm the results obtained by EIS and CV. It can be observed that

the coverage of the gold microelectrode is higher with polymerisation time. Complete and more uniform coverage of the gold surface is observed for microelectrodes modified with polymerisation times higher than 60 min (figure 4.26d, e and f).

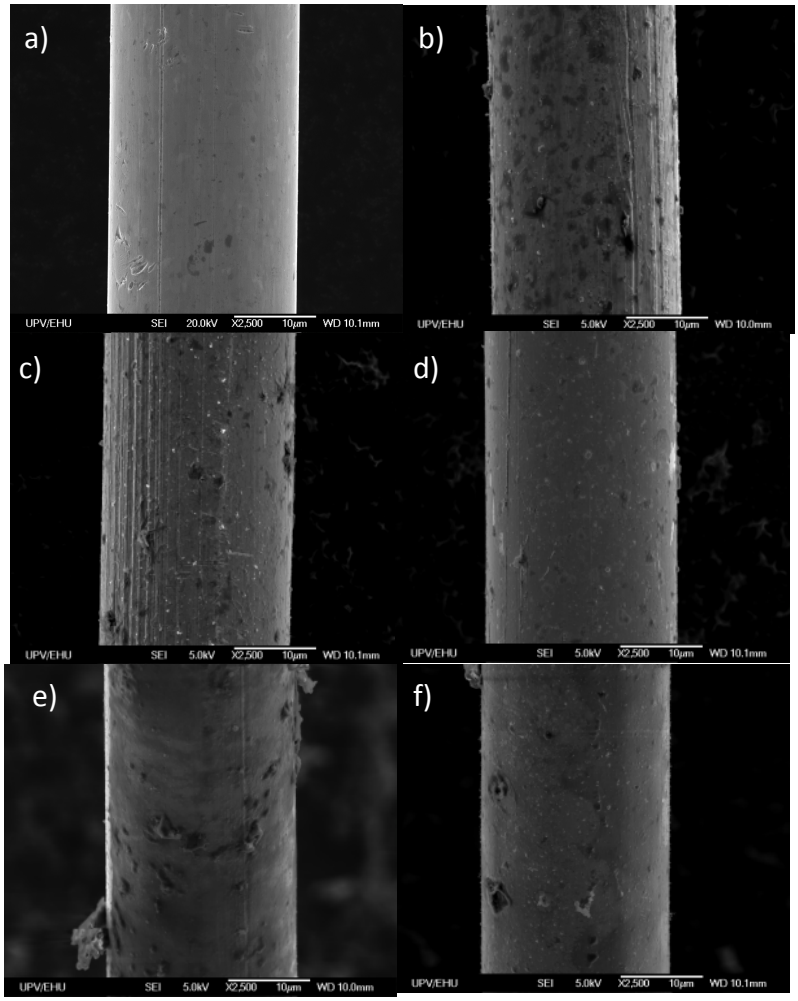

Figure 4. 26. SEM micrographs at 2500 magnification of a) bare gold microelectrode and microelectrodes modified with b) 20 minutes c) 40 minutes d) 60 minutes e) 70 minutes and f) 80 minutes polymerisation time.

4.6. Electrochemical determination of 4-ethylphenol using gold microelectrodes coated with MIP thin films

In section 4.4, surface modification of gold microelectrodes with MIP layers has been described. These sensors were developed employing different polymerisation times, what, as corroborated by CV, EIS and SEM, gave rise to sensors with different polymer thicknesses. Developed sensors were tested next for electrochemical measurement of 4-ethylphenol in order to determine the polymerisation time that allowed obtaining the device with best electrochemical response.

To this end, 4EP was measured by Differential Pulse Voltammetry (DPV) using MIP sensors that had been polymerised from 5 min to 90 min as working electrodes. An electrochemical cell containing 10 mL of a 5 x 10^{-5} M 4EP solution in B-R buffer (pH 10) was used for this purpose. Additionally, electrochemical measurements were also conducted using NIP sensors as working electrodes in order to compare signals of imprinted and non imprinted devices. Obtained anodic peak current values for 4EP are summarised in figure 4.27.

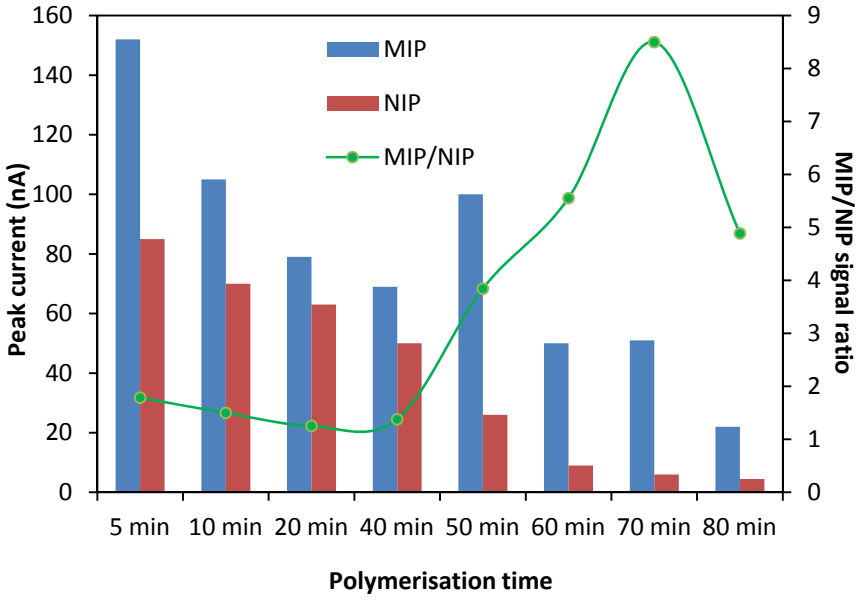

Figure 4.27. Peak current signals and MIP/NIP signal ratios recorded with MIP and NIP sensors at different polymerisation times.

As it is shown in figure 4.27, peak current signals corresponding to NIP sensors decrease as polymerisation time is longer. As the polymer is being synthesised on the surface, an insulating layer coats the microelectrode which hinders proper electron-transfer, since the polymer is non-conducting. Short polymerisation times may lead to incomplete surface coating and consequently, NIP sensors, undesirably, could still oxidise the target compound. In order to ensure the complete coating of the gold microelectrodes, longer polymerisation times were required. As it can be deduced from the figure, polymerisation times over 60

min allow for obtaining NIP sensors that practically do not respond to 4EP, what may be indicative of the complete sensor insulation. Moreover, sensors synthesised for 90 min or longer polymerisation times did not show any electrochemical signal, what may corroborate complete surface insulation. However, the polymer layer at this point was probably too thick, what may later contribute negatively to analyte diffusion in MIP sensors.

Comparatively, MIP sensors polymerised for 60, 70 and 80 min still showed a remarkably higher oxidation current than NIP ones, which are almost insulated. This fact indicates that thanks to the template employed during the synthesis, active sites in MIP polymers must have been created, which allow for electron transfer towards the gold surface. This phenomenon was also observed by EIS, what is deducible from figure 4.28. Impedance values registered with NIP sensors were higher than impedance values of MIP sensor, what denotes lower surface insulation in MIP devices attributable to the presence of binding sites. These active sites may act as selective “pores” or “channels” that can bind the analyte, allowing for its contact with the surface of the transducer, thereby registering the corresponding peak current signal (figure 4.29).

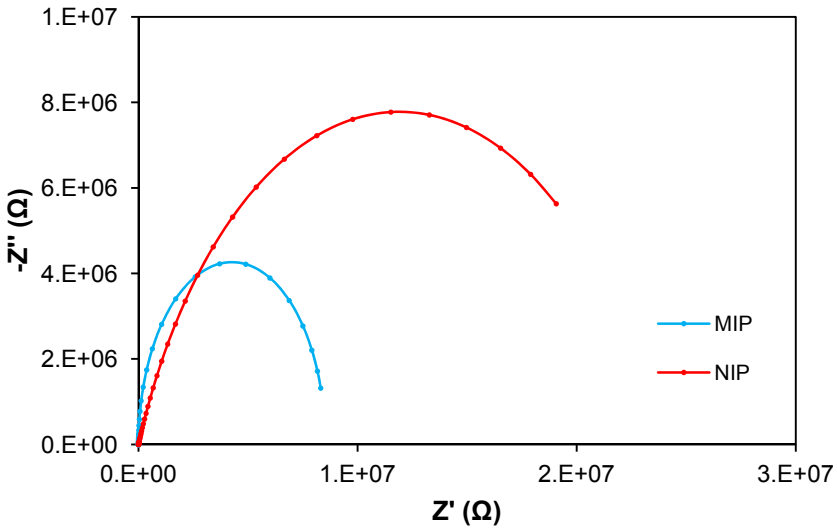

Figure 4. 28. Nyquist plots registered with the 60 min polymerisation time electrodes (MIP and NIP).

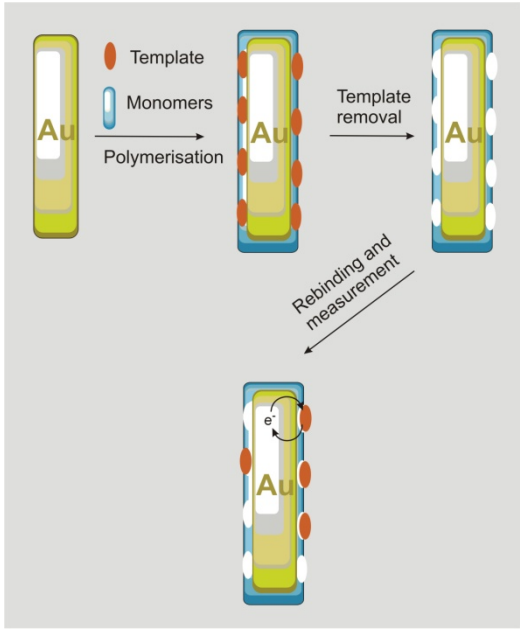

Figure 4. 29. Schematic representation of binding site formation and electron-transfer in subsequent electrochemical measurements.

In order to select proper polymerisation time, the electrochemical MIP/NIP signal ratio registered for 4EP (figure 4.27) was found to be not enough. Apparently, polymerisations carried out for 60, 70 or 80 min could lead to sensors having 4EP imprinted sites created. But it was hypothesised that, if the sensor was not well enough insulated, compounds other than 4EP could also be recognised through the non-coated parts/pores that may still be present on the surface. Accordingly, the response of MIP sensors, synthesised under different polymerisation times, to structural analogues of 4EP was measured. After quantifying peak current signals for each compound, they were compared with the oxidation signal of 4EP. In principle, the MIP sensor showing highest 4EP signal ratio in comparison with each analogue should be the one having a more homogenously coated surface. Since this selective response would indicate that binding was happening preferably through imprinted sites and not through other uncoated parts on the surface.

As structural analogues, volatile phenolic compounds that belong to the 4EP metabolic pathway in wines were selected (4-vinylphenol, coumaric acid and coumaric acid ethyl ester). Not only because of their structural similarity, but also because they may be present in the same matrix together with the target compound, thereby constituting its major interfering compounds. Additionally, another phenolic compound, not belonging to the 4EP metabolic pathway but which may also be present in wines, such as 4-

ethylguaiacol was selected. Other non-volatile phenolic compounds, that are not found in wines but which still are structurally similar to the target, were also chosen for this experiment, namely dopamine and paracetamol (figure 4.30).

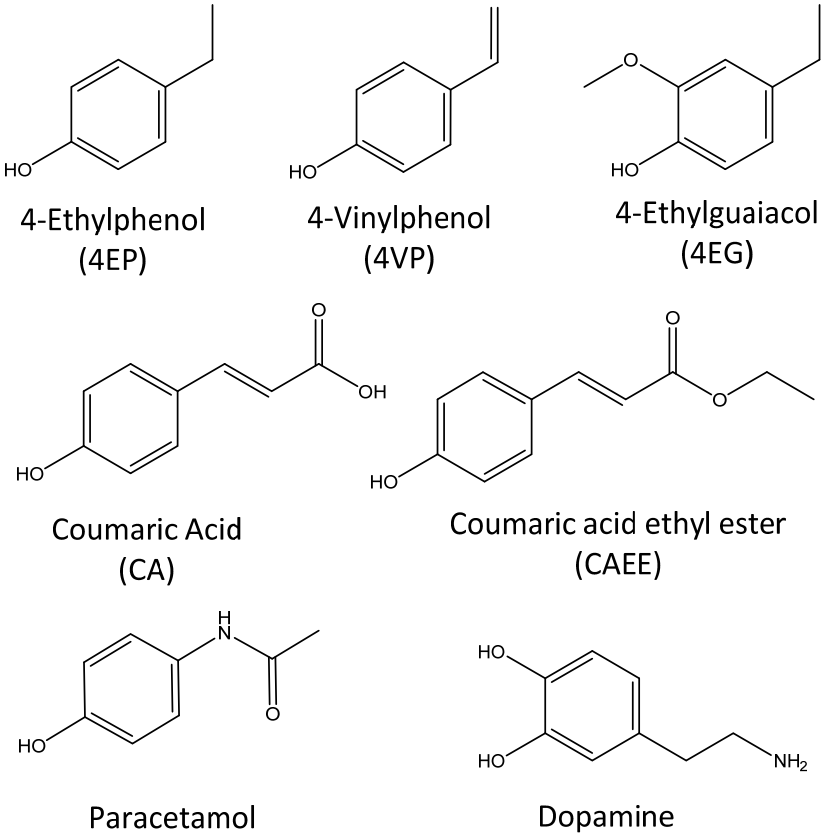

Figure 4. 30. Molecular structures of 4EP and its analogues.

In the first instance, all compounds depicted in figure 4.30 were measured individually employing a bare gold microelectrode in order to know whether they could be electrochemically oxidised at the experimental conditions selected for 4EP measurement (section 4.2). Obtained Differential Pulse voltammograms are depicted in figure 4.31.

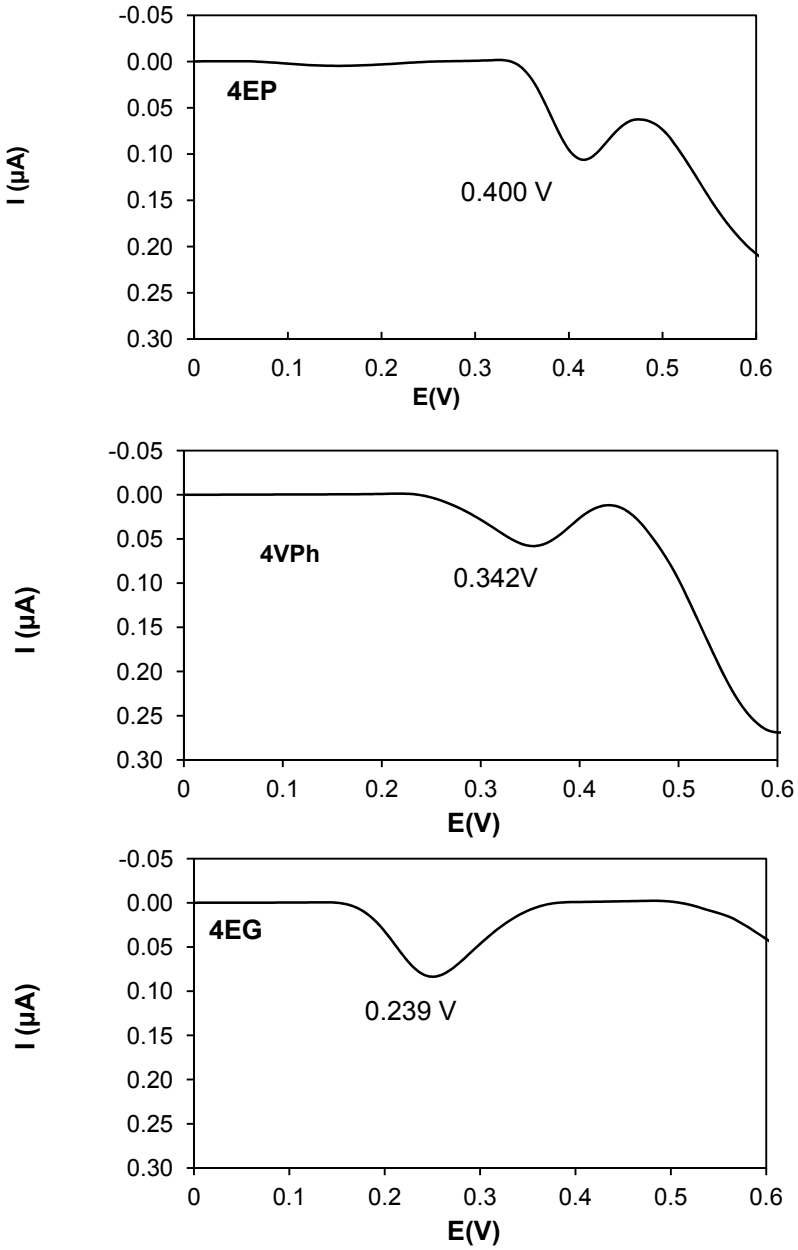

Figure 4. 31. DPV voltammograms registered employing solutions of 5 x 10^{-5} M of 4EP and each of its structural analogues. Supporting electrolyte: BR 0.04 M buffer (pH:10).

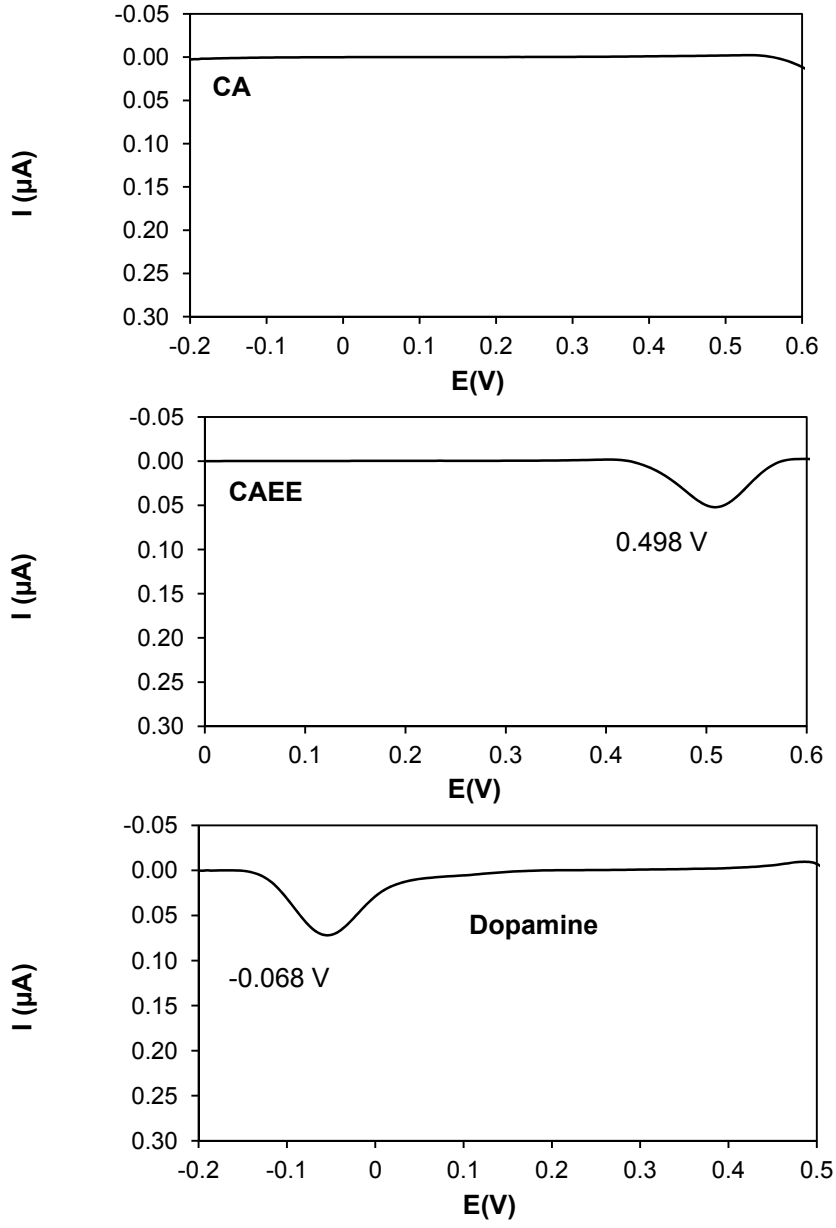

Figure 4.31 cont. DPV voltammograms registered employing solutions of 5 x 10^{-5} M of 4EP and each of its structural analogues. Supporting electrolyte: BR 0.04 M buffer (pH:10).

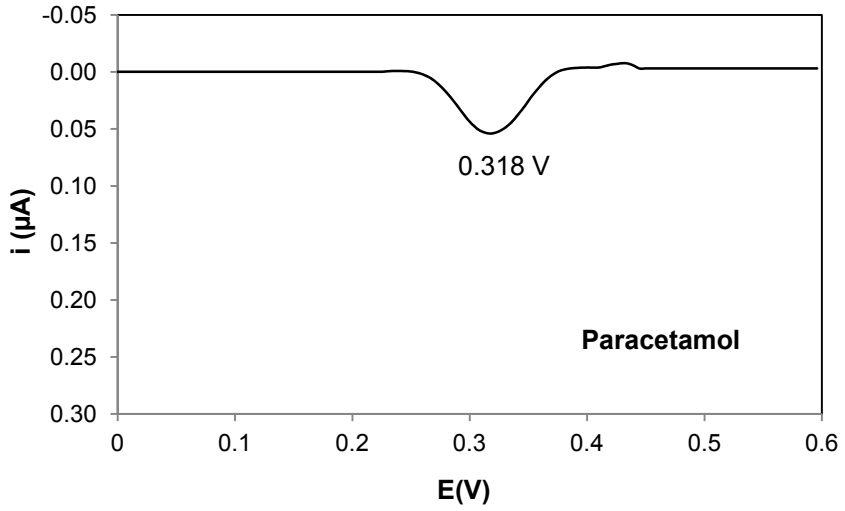

Figure 4.31 cont. DPV voltammograms registered employing solutions of 5 x 10^{-5} M of 4EP and each of its structural analogues. Supporting electrolyte: BR 0.04 M buffer (pH:10).

All selected compounds, except for coumaric acid (CA), present anodic peaks in the working potential range under optimised experimental conditions (section 4.2), as it can be corroborated in figure 4.31, as it was found to be non-electroactive, CA was discarded for further experiments. Next, all these compounds were measured employing MIP sensors synthesised for 50, 60, 70 min and 80 min (figure 4.32). According to characterisation results by CV, EIS and SEM, polymerisation times lower than 60 min were found to be not enough to get completely coated surfaces, consequently, they were discarded for further research. Peak current signals registered with these sensors

for 4EP were compared with signals of each of the structural analogues. Results are depicted in figure 4.32. The figure shows peak current ratios calculated from anodic currents of each of the analogues and the anodic current of the target compound. This ratio, would, in principle, provide information concerning sensor selectivity at each tested polymerisation time. However, due to peak current differences of tested compounds on bare gold microelectrodes, this ratio must be normalised in order to make the signals on MIP sensors comparable. Signal normalisation was performed using the following expression:

$$Ratio = \frac{Signal(4EP)_{MIP}}{Signal(analogue)_{MIP}} \cdot \frac{Signal(analogue)_{Bare\ gold}}{Signal(4EP)_{Bare\ gold}} \quad \textbf{4. 32}$$

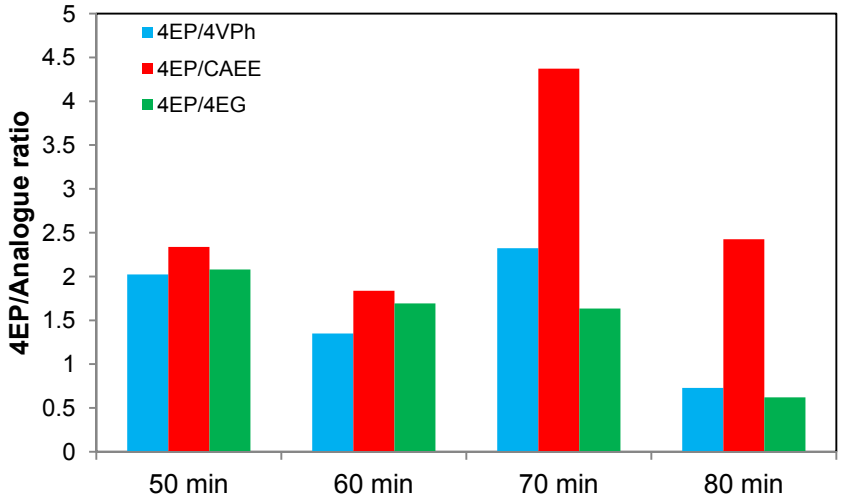

Figure 4.32. Normalised 4EP/analogue signal ratios recorded with MIP sensors synthesised at different polymerisation times.

Figure 4.32 does not include signal ratios for dopamine and paracetamol since the MIP sensor, as opposed to the bare gold microelectrodes, did not respond to these compounds.

It can be deduced from figure 4.32 that the sensor synthesised for 70 min was the one showing highest selectivity. It showed a 4EP/CAEE signal ratio close to 4.5, and ratios close to 2.5 and 2 respectively for 4VP and 4EG. The lower selectivity observed for 4VP and 4EG could be expected, based on the structural similarities of these targets. Presented results corroborate that the sensor shows a remarkable preference for the target compound in

comparison with the analogues that belong to the same metabolic pathway.

On the other hand, sensor selectivity was found to be maximum when other phenolic compounds were tested, such as paracetamol or dopamine, which did not present any electrochemical response using the MIP sensor (figure 4.33).

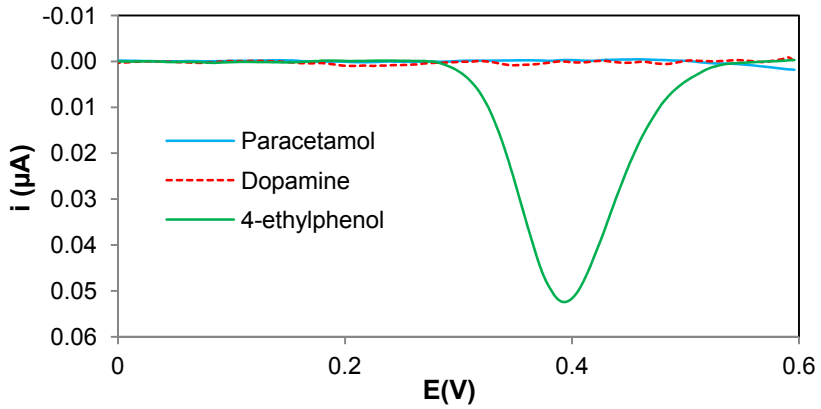

Figure 4. 33. DPV voltammograms registered employing solutions of 5 x 10^{-5} M of 4EP, Paracetamol and Dopamine with the 70 min microelectrode. Supporting electrolyte: BR 0.04 M buffer (pH:10).

These results, in combination with the previously described in figure 4.27 point towards 70 min as the polymerisation time that allows obtaining MIP sensors with most suitable polymer coverage for 4EP sensing. Since, on the one hand, the NIP sensor has proved

to be completely coated using this polymerisation time (see figure 4.27) and, on the other hand, sensor selectivity was found to be maximum at this point, thereby diminishing cross-reactivity arising from the diffusion of analogue compounds through the polymer backbone. On figure 4.34 the voltamograms recorded with the gold microelectrode (figure 4.34a) and the 70 min polymerisation sensor (figure 4.34b) for 4EP, 4VPh and CAEE are depicted. All the compounds were measured on a $5x10^{-5}$ M concentration. It can be observed that despite the fact that all peak currents decrease when using the MIP sensor, the decrease is remarkably higher for the analogues (4VPh and CAEE) comparing to 4EP.

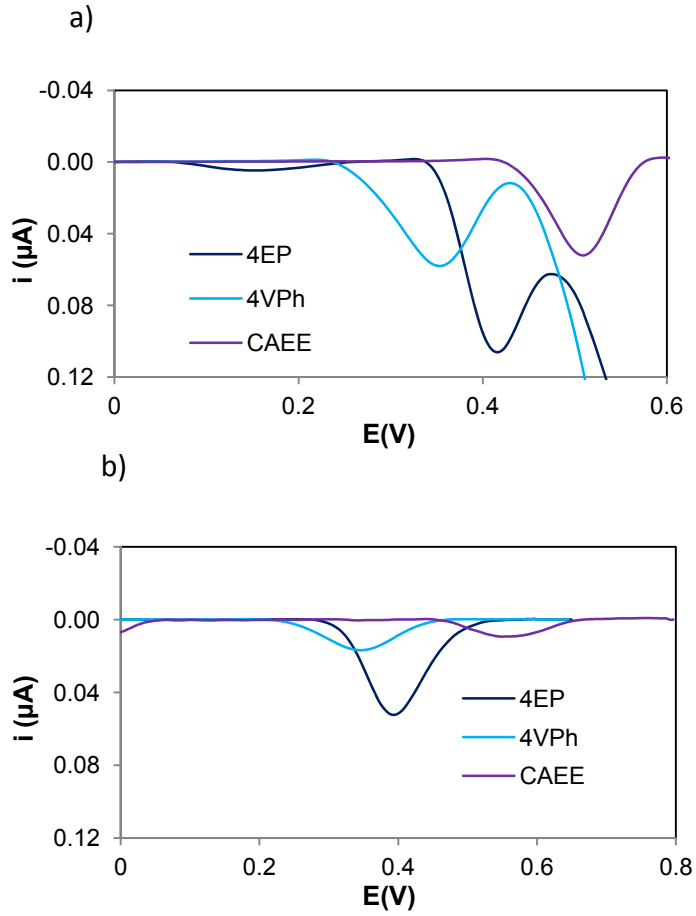

Figure 4. 34. DPV voltammograms registered employing a) bare gold microelectrode and b) sensor synthesised for 70 min and solutions of $5x10^{-5}$ M of 4EP, 4VPh and CAEE employing BR 0.04 M buffer (pH:10). Scan rate: 0.0495 V/s, Modulation amplitude: 0.04995 V.

4.7. Analytical evaluation of the sensor

Once the steps to coat gold microelectrodes with MIP thin layers were established and the conditions for the electrochemical sensing of 4EP were optimised, it was proceed to the analytical evaluation of the developed device. In the first instance, signal dependence on concentration was assessed through sensor calibration, from which the linear range and the instrumental detection (LOD) and quantification (LOQ) limits were determined. Finally measurement repeatability and intermediate precision was assessed.

4.7.1. Sensor calibration

For sensor calibration a series of standard solutions of 4EP were measured by DPV, as detailed in section 4.2. The linear range was found to be comprised between 1 µM and 100 µM and the resulting calibration curve, adjusted by the least squares method, gave rise to the following expression:

$$I_{4EP}=(1.02\pm0.02)C+(0.76\pm0.92) \qquad \textbf{4. 33}$$

where I_{4EP} is the anodic peak current of 4EP expressed in nA and C is the concentration expressed in μM. The coefficient of determination (R^2) was found to be 0.9980 which confirms an adequate linear correlation of the analytical signal versus 4EP concentration.

In order to confirm the goodness of fit of the proposed regression, a statistical analysis of the distribution of the residuals was carried out. The residual (r_i) is the difference between the experimental value of the dependent variable and (y_{exp}) and the predicted value (y_{calc}) which is calculated from the expression from the calibration curve (4.33). This value for each data point is calculated based on the following expression:

$$r_i = y_{calc} - y_{exp} \qquad \textbf{4. 34}$$

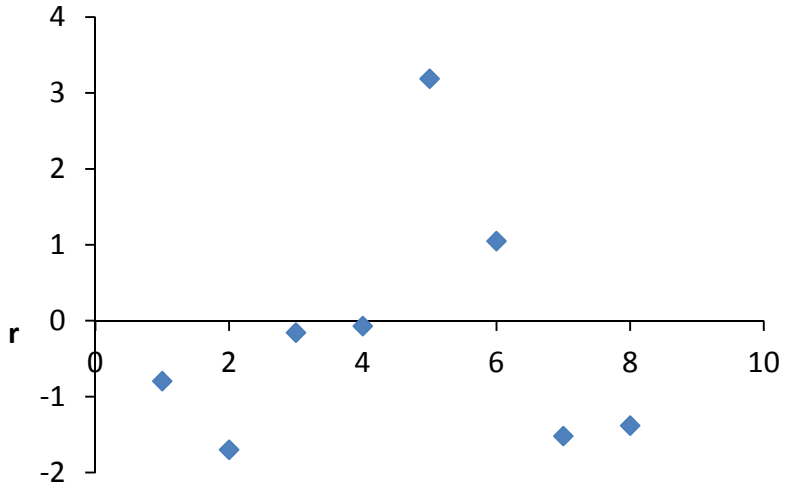

Figure 4. 35. Distribution diagram of the calibration residuals.

In figure 4.35, a random distribution of the residuals can be appreciated, what indicates that the proposed regression fits adequately the experimental data. Additionally, this randomness was confirmed through different parameters associated with the normal distribution of the residuals, such as:

The arithmetic median of the residuals

$$\bar{r}=\frac{\sum(y_{calc}-y_{exp})}{N_P} \qquad \textbf{4. 35}$$

Where N_P is the number of the calibration points. A normal distribution of the residuals would result in a value of $\bar{r}$=0.

The standard deviation of the residuals

$$\sigma(r)=\sqrt{\left(\frac{\sum r_i^2}{N_P}\right)-\left(\frac{\sum r_i}{N_P}\right)} \qquad \textbf{4. 36}$$

This result must be less or equal to the total standard deviation σ_{TOT} for the distribution of residuals to be Gaussian.

The average residual

$$\overline{|r|}=\frac{\sum|y_{calc}-y_{exp}|}{N_P}=\frac{\sum|r_i|}{N_P} \qquad \textbf{4. 37}$$

To ensure that the distribution of the residuals is Gaussian, the resulting residual average value must be less or equal to the standard deviation of the residuals.

The asymmetry coefficient

$$C_s=\frac{\sum(r_i-\overline{r})^3}{N_P\,\sigma(r)^3} \qquad \textbf{4. 38}$$

It indicates the degree of symmetry of the Gaussian curve. This parameter should be zero when the distribution of the residuals is symmetrical, and therefore Gaussian.

The Kurtosis coefficient

$$C_{ku}=\frac{\sum(r_i-\bar{r})^4}{N_P\ \sigma(r)^4} \qquad \textbf{4. 39}$$

The coefficient of kurtosis is a measure for the degree of peakedness/flatness in the variable distribution. A normal distribution of the residuals has a value of 3.

Global standard deviation

$$\sigma_{TOT}=\sqrt{\frac{\sum_{i=1}^{N_P}\left(y_{calc}-y_{exp}\right)^2}{N_p-2}} \qquad \textbf{4. 40}$$

The values calculated for each of these parameters are summarised in table 4.5, as illustrated, most of these values approach theoretical values indicating a Gaussian distribution of the residuals.

Table 4.5. Parameters, experimental and theoretical values of the statistical analysis of the residuals.

Parameter	Experimental Value	Theoretical value
Arithmetic median of the residuals	-3.17×10^{-17}	$\bar{r} \approx 0$
Global standard deviation	1.85	
Standard deviation of the residuals	1.56	$\sigma(r) \leq \sigma(tot)$
Average residual	0.96	$\lvert\bar{r}\rvert \leq \sigma(r)$
Asymmetry coefficient	0.92	$C_s \cong 0$
Kurtosis coefficient	2.83	$C_{Ku} \cong 3$

4.7.2. Detection and Quantification limits

The detection and quantification limits were calculated using the sensitivity value (S) obtained from the slope of the calibration curve (expression 4.36) and the standard deviation of the signals recorded from the blank measurements (σ_B).

$$C_{LOD} = \frac{K\sigma_B}{S} = \frac{3\sigma_B}{S} \quad \textbf{4. 41}$$

$$C_{LOQ} = \frac{K\sigma_B}{S} = \frac{10\sigma_B}{S} \quad \textbf{4. 42}$$

The obtained detection limit (LOD) was 0.3 µM and 1 µM the cuantification limit (LOQ).

4.7.3. Measurement repeatability

In order to know the method repeatability, the sensor response was evaluated through consecutive measurements of 4EP at different concentration levels (50 µM and 100 µM) (n=5). Between measurements, it was necessary to clean the sensor to avoid saturation of the polymer and signal decay. This treatment consisted in immersing the sensor in isopropanol for 10 minutes under stirring. The cleaning step improved sensor repeatability

between measurements, obtaining standard deviations below 4% in all cases (table 4.6).

Additionally, measurement repeatability between different sensors was also assessed. To this end, 4EP was determined at two concentration levels (50 µM and 100 µM) with 5 different sensors. The standard deviation was below 17 % in all cases (table 4.6), what could be assumed as adequate, especially if it is taken into consideration that the sensor modification step is influenced by many factors that contribute to final signal variability.

Table 4. 6. Values obtained for the average peak current and relative standard deviation for the developed sensor (n=5).

	4EP concentration (µM)	Peak current (nA)	RSD (%)
Measurement repeatability using the same sensor	50	73.25 ± 2.50	3.41
	100	104.75 ± 2.01	1.92
Measurement repeatability using different sensors (n=5)	50	98.50 ± 9.87	10.02
	100	125.80 ± 21.35	16.97

5. Development of a voltammetric sensor for 4-ethylphenol based on MIP nanoparticles grafted to gold electrodes

Grafting MIP thin layers from gold microelectrodes has proved to be a useful strategy to fabricate sensors with enhanced selectivity for 4-ethylphenol sensing. However, one of the major drawbacks of this approach is that a part of the gold surface is insulated in the polymerisation process, being imprinted sites in the polymer, the only part through which electron-transfer happens. Moreover, many of the binding sites present in the inner polymer layers, the ones closer to the gold surface, may be inaccessible for the target if the polymer is thick enough. As a result, the anodic peak current of 4-ethylphenol decreases in comparison with the bare gold microelectrode, and so does the sensitivity of the sensor. Consequently, in order to overcome the major disadvantages found with MIP grafted thin layers, alternatively, another approach was followed to develop voltammetric 4-ethylphenol sensors.

Here, MIP nanoparticles synthesised by the solid-phase imprinting approach were used as recognition elements for sensor construction. In this approach, templates remain immobilised on solid supports avoiding the disadvantages of template translation and rotation for being free in solution, which are the main reasons for binding site heterogeneity, one of the principal factors that

contributes to cross-reactivity of imprinted materials. Besides, in the solid-phase imprinting approach, binding sites are created on the surface of imprinted nanoparticles leading to materials with practically no inaccessible binding sites (96) and due to the larger volume to surface ratio of nanoparticles, binding kinetics are improved, what could give rise to faster sensor response. It was therefore hypothesised that if this type of nanoparticles were used as recognition elements, they may help improving sensor sensitivity and selectivity.

5.1. Development of 4-ethylphenol imprinted nanoparticles by the solid phase imprinting approach

5.1.1. Template immobilisation on glass beads

Prior to polymerisation of imprinted nanoparticles, the template had to be immobilised on a solid support. To this end, glass beads of 53-106 µm in diameter were employed.

Initially, 500 g of these glass beads were shaken together with ceramic beads for 5 h on 45 µm sieves using an AS-200-basic vibratory sieve shaker from Retsch (Hope Valley, UK), in order to abrade the surface coating and expose fresh surface. Then, glass beads were activated by boiling in 1 M NaOH for 10 min and, afterwards, rinsed with deionised water, then with acetone and

finally they were dried in an oven at 80ºC. Once the surface of the glass beads was activated, they were functionalised in order to provide them with primary amino groups for template immobilisation. To this end, dry glass beads were incubated overnight in a 2 % v/v solution of N-[3-(trimethoxysilyl)propyl] ethylenediamine (EDPTMS) in dry toluene (figure 4.36) . Next, they were rinsed with acetone and dried under vacuum.

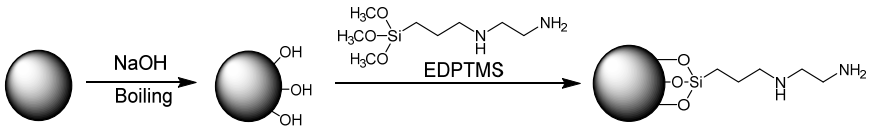

Figure 4.36. Schematic representation of the activation and functionalisation of glass beads.

The compound selected as the template (4EP) has a single polar hydroxyl group for imprinting, and does not have any additional functional group through which immobilisation on glass beads may happen. Alternatively, the structural analogue tyramine was selected as pseudotemplate for immobilisation. This compound is structurally similar to 4EP, but instead of the ethyl

group has an ethylamine group, which may be used for immobilisation, leaving free the hydroxyl group for imprinting (figure 4.37).

Prior to tyramine immobilisation on glass beads, the amine end-group on functionalised glass beads was transformed to aldehyde termination through chemical coupling with glutaraldehyde, employed as linker. To this end, dried functionalised glass beads (figure 4.36) were incubated in a 5 % glutaraldehyde solution in phosphate buffer (pH 7.4) for 2 hours. Then the glass beads were rinsed with deionised water and placed in a 0.5 mg mL^{-1} tyramine solution overnight (figure 4.37).

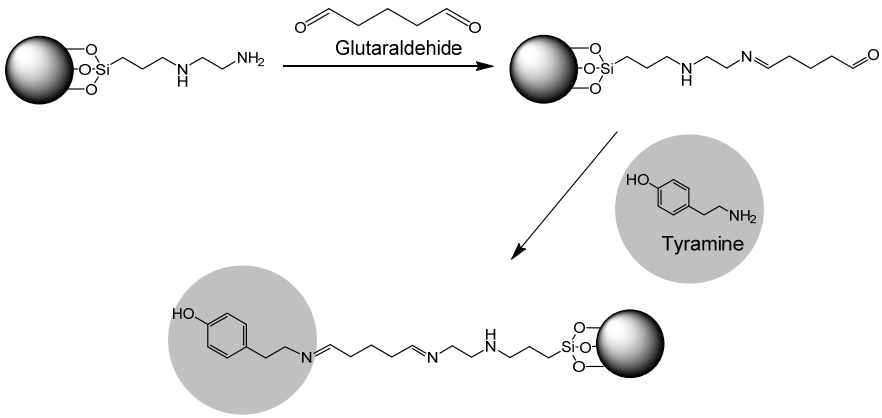

Figure 4. 37. Schematic representation of tyramine immobilisation on glass beads.

Once tyramine was immobilised, 12 µL of ethanolamine was added to the glassbeads/tyramine solution for 15 min to cap any unreacted group on glass beads and prevent nonspecific binding. Moreover, 1 mg mL^{-1} of sodium cyanoborohydride was also added to this solution to reduce the Schiff's base formed between tyramine and glutaraldehyde to a more stable amine (figure 4.38). Finally, glass beads were rinsed with deionised water under vacuum and stored at 4ºC.

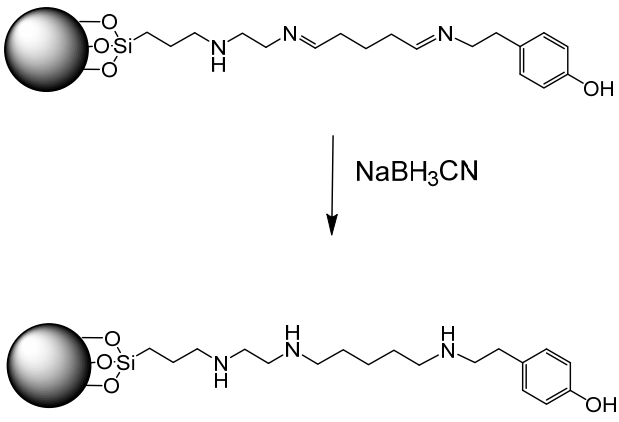

Figure 4. 38. Schiff's base reduction.

5.1.2. Synthesis of imprinted nanoparticles

To synthesise imprinted nanoparticles, the glass beads were placed in a solution containing the polymerisation mixture including the functional monomer, the cross-linkers, the chain-transfer agent and the iniferter. The composition of the prepolymerisation mixture was adapted from other works (17,99).

In this work, three different types of nanoparticles were synthesised employing different functional monomers. One of them were developed using 4-vinylpyridine (4VPy) as functional monomer, other ones using ferrocenylmethyl methacrylate (FER) and the last ones using both functional monomers. 4VPy was chosen because it was found to be the monomer that provided best imprinting performance in previous works concerning MIP for 4EP (Chapter 3). On the other hand, FER was chosen due to its higher electrical conductivity, (219) what could enhance electrode response after being grafted to the gold surface (figure 4.39). All nanoparticle types were synthesised using EDMA and TRIM as cross-linkers, since they are the ones providing the right balance of flexibility/rigidity which is crucial for molecular recognition (99). Additionally, an amine containing monomer was also added to the polymerisation mixture, N-(3-aminopropyl) methacrylamide hydrochloride (APMA), in order to provide all developed nanoparticles with amine groups, necessary to later graft them to gold surfaces (figure 4.39).

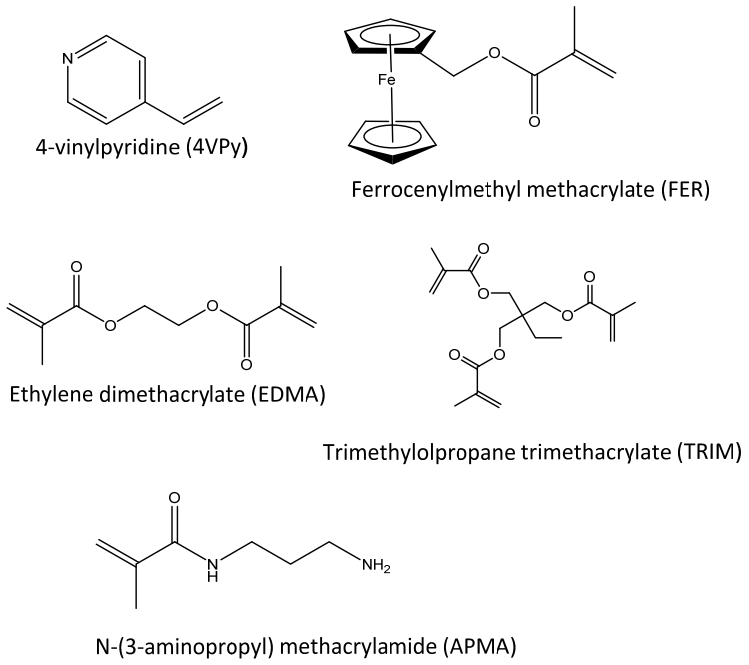

Figure 4. 39. Molecular structures of the monomers used in nanoparticle synthesis.

Nanoparticles made with 4VPy as functional monomer (MIN1) were prepared as follows: 1.759 g of 4VPy (16.7 mmol) was dissolved in 5.26 g of acetonitrile, then 1.62 g of EDMA, 1.62 g of TRIM and 2.98 mg of APMA were added to the solution. Finally, 0.37 g of the iniferter N,N,-diethyldithiocarbamic acid benzyl ester (DABE) and 0.09 g of the chain transfer agent pentaerythritol tetrakis (3-mercaptopropionate) (PTEMP) were also added to the polymersiation mixture.

When FER was used as functional monomer for nanoparticle synthesis (MIN 2), due to solubility limitations, 5% of the molarity used for 4VPy was added to the polymerisation reaction, that is 0.237 g of FER (0.835 mmol), and tetrahydrofuran (5.26 g) was employed as porogen instead of ACN. Other polymerisation components and amounts were the same as the ones employed for MIN1 nanoparticles.

MIN 3 nanoparticles were synthesised using a mixture of the previous two monomers, that is, 1.67 g of 4VPy (15.9 mM) and 0.237 g of FER (0.835 mM). Tetrahydrofuran (5.26 g) was also used this time as porogen. The rest of the polymerisation components were identical to other nanoparticles.

The polymerisation mixture was placed in a glass vial and purged with N_2 for 10 minutes to remove dissolved oxygen. Simultaneously, 30 g of tyramine-derivatised glass beads were placed in a 200 mL flat-bottomed glass beaker, which was covered with a flat glass slide, and vacuum degassed for 5 minutes in a vacuum dessiccator. Afterwards, inert atmosphere was established inside the beaker using N_2. The whole deoxygenating process was repeated three times in order to ensure complete removal of the oxygen. Finally, the polymerisation mixture was poured onto the derivatised glass beads and the mixture was placed between two UV light sources for 2.5 minutes.

After polymerisation, the beads were packed into solid phase extraction empty cartridges fitted with 20 µm pore size

polyethylene frits in order to perform affinity-based washing and elution cycles. First, non reacted monomers and low affinity nanoparticles were eluted percolating 20 mL of ACN (room temperature) through the cartridge, this procedure was repeated 8 times. Then, high affinity nanoparticles were collected washing the cartridges with 20 mL of ACN at 60 ºC. This procedure was repeated 5 times to maximise the amount of eluted nanoparticles (figure 4.40).

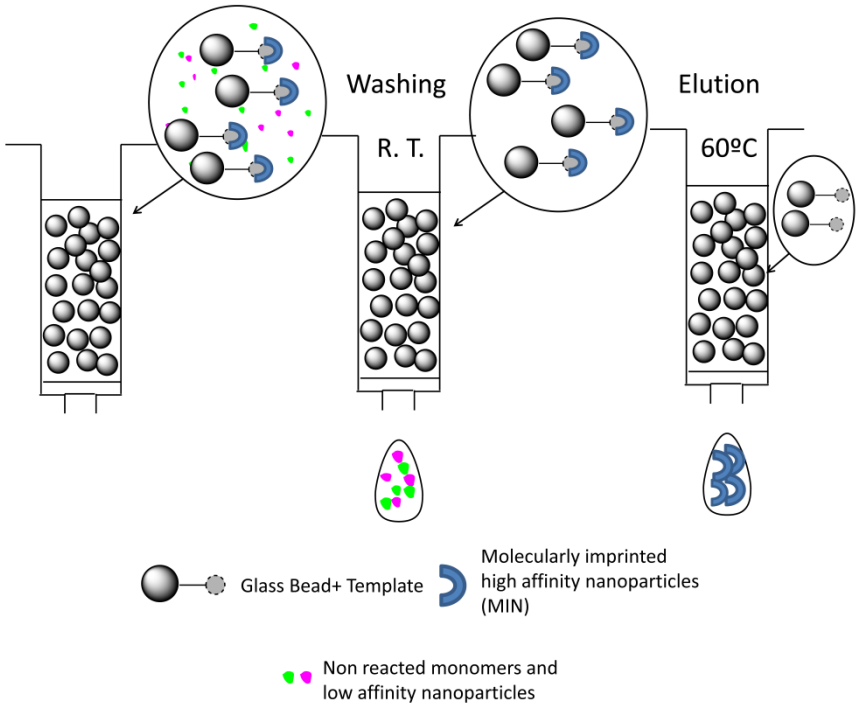

Figure 4. 40. Schematic representation of the nanoparticle washing and elution steps. R.T.: room temperature**.**

5.1.3. Size characterisation of nanoparticles by Dynamic Light Scattering

Particle size distribution of synthesised nanoparticles was performed by Dynamic Light Scattering (DLS). In DLS, the light from a laser scattered by a colloidal suspension is measured. It is based on the measurement of the modulation of the scattered light intensity as a function of time. Analysing the fluctuations of such scattered light, the Brownian motion (random movement) of particles can be determined and this can be related to the particle size.

For DLS measurements, nanoparticle suspensions in ACN, collected from the washing cycles (figure 4.40), were sonicated for 5 minutes and then analysed at room temperature in a 3 cm^3 glass cuvette. Obtained results are ilustrated in table 4.7, including average values of 3 measurements and their standard deviation. The nano-size of the particles was confirmed by DLS analysis, as the size ranged between 128 and 163 nm, being the smallest the nanoparticles synthesised with 4VPy as functional monomer (MIN1). With regard to the polydispersity index (PDI), the lower the PDI the more uniform, monodisperse, the sample; values close to 0 indicating a monodisperse suspension. All PDI values were around 0.3, indicating a quite monodisperse nanoparticle population.

Table 4. 7. Average and standard deviation of the diameter and PDI obtained by DLS for each type of nanoparticle (n=3).

Type	Particle size (nm)	PDI
MIN1	128.58 ± 4.97	0.23 ± 0.01
MIN2	160.71 ± 11.60	0.36 ± 0.02
MIN3	163.18 ± 8.22	0.31 ± 0.03

5.2. Grafting of 4-ethylphenol imprinted nanoparticles on the surface of gold electrodes

5.2.1. Functionalisation of the gold surface through a self-assembled monolayer

Developed nanoparticles were implemented next on gold electrodes to develop voltammetric sensors for 4EP. The first step of the grafting approach lay in the self-assembly of an organosulfur compound-based monolayer on the surface of a gold electrode. Two different organosulfur compounds were tested for the so called self-assembled monolayer (SAM) formation, lipoic acid (LA) and mercaptoundecanoic acid (MUA) (figure 4.41). Both these compounds present sulfur-containing substituents such as a disulfide group for LA and a thiol group for MUA and they spontaneously self-assemble to gold or even to other metallic surfaces through these substituents. On the other hand, they also

present terminal carboxylic groups which will serve for nanoparticle grafting through carbodiimide chemistry, as will be detailed later. Both these compounds were selected to be tested for sensor construction, mainly based on their substantial chain length difference, what could lead to sensors with different electrochemical behaviour. It was believed that MUA, being a compound with a longer chain than LA, would be able to better insulate the electrode surface, hindering electron-transfer and thereby increasing sensor selectivity. However, the SAM formed by MUA would be thicker than the one formed by LA; consequently, sensor sensitivity may be worsened.

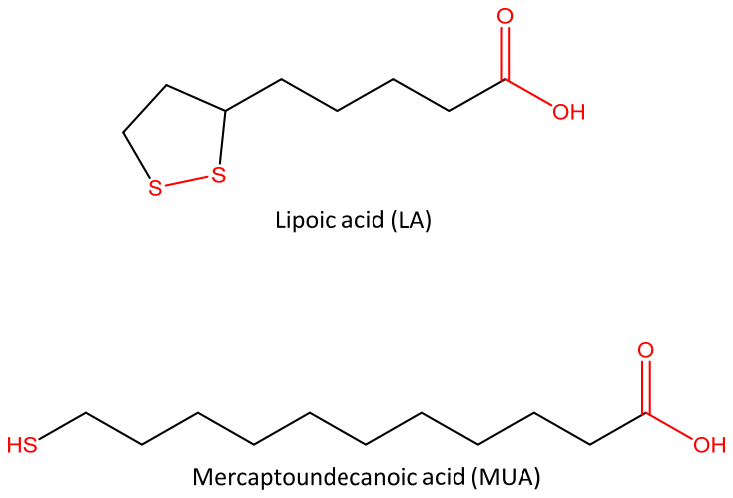

Figure 4. 41. Molecular structures of lipoic acid and mercaptoundecanoic acid.

Prior to SAM formation, gold electrodes were cleaned as detailed in section 4.1. Then, they were rinsed with ethanol and immersed in a 0.5 mgL^{-1} solution of LA or MUA in ethanol for 24 h. Finally, the electrodes were rinsed once again in ethanol to remove physisorbed or weakly adsorbed compounds and they were left to dry at room temperature.

5.2.2. EDC-NHS coupling

After SAM formation, 1-ethyl-3-[3-dimethylaminopropyl] carbodiimide (EDC) and N-hydroxysuccinimide (NHS) were coupled to the carboxylic end-group of the self assembled monolayer (figure 4.42).

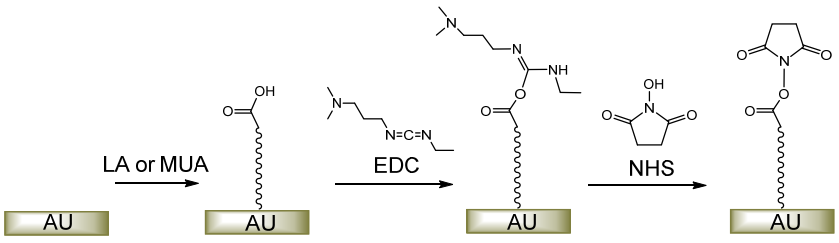

Figure 4. 42. SAM formation and EDC-NHS coupling on the gold electrode.

This coupling is based on the modification of carboxyl-terminated SAMs via carbodiimide chemistry (220). First, the carboxylic group reacts with EDC to form an o-acylisourea intermediate, and further reaction with NHS gives rise to an amine-reactive semi-stable ester (figure 4.43).

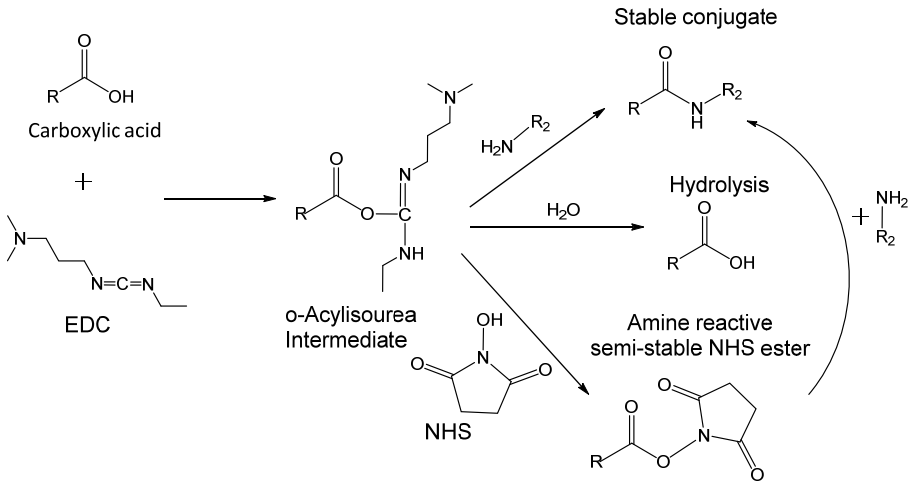

Figure 4. 43. EDC/NHS coupling procedure.

For EDC-NHS coupling, electrodes were immersed in a 200 mM EDC and 50 mM NHS mixture in phosphate buffer (adjusted to pH 6 with HCl) for 1 h. Thereafter, the electrodes were cleaned with phosphate buffer at pH 7.4.

5.2.3. Nanoparticle grafting

Nanoparticles were grafted on the gold surface allowing them to react with the NHS semi-stable amine reactive ester. For this purpose, functionalised electrodes were immersed in 1 mL of a stirring MIN suspension in phosphate buffer (pH 7.4) for 24 h and rinsed next with fresh buffer to remove any physisorbed particle. Some of the fabricated sensors were finally immersed in an ethanolamine (1 mM) solution for 30 min, in order to cap possible unreacted carboxylic groups that may later contribute to non-specific binding in electrochemical sensing. In table 4.8 the different components employed for sensor construction are summarised.

Table 4. 8. Components employed for developing sensors by surface modification of gold electrodes.

Sensor	SAM	Nanoparticles		Ethanolamine capping
		Type	Functional monomer	
MUA1N	MUA	MIN1	4VP	No
MUA1Y	MUA	MIN1	4VP	Yes
LA1N	LA	MIN1	4VP	No
LA1Y	LA	MIN1	4VP	Yes
MUA2N	MUA	MIN2	FER	No
MUA2Y	MUA	MIN2	FER	Yes
LA2N	LA	MIN2	FER	No
LA2Y	LA	MIN2	FER	Yes
MUA3N	MUA	MIN3	4VP/FER	No
MUA3Y	MUA	MIN3	4VP/FER	Yes
LA3N	LA	MIN3	4VP/FER	No
LA3Y	LA	MIN3	4VP/FER	Yes

MUA: Mercaptoundecanoic acid, **LA:** Lipoic acid, **4VP:** 4-Vinylpyridine, **FER:** Ferrocenylmethyl methacrylate.

5.3. Characterisation of the sensors

Every step concerning gold electrode modification was followed by Cyclic Voltammetry (CV) and Electrochemical Impedance Spectroscopy (EIS). For this purpose, as working electrodes, the sensors detailed in table 4.8 were employed and, as supporting electrolyte, 10 mL of an equimolar mixture of $[Fe(CN)_6^{4-}]/[Fe(CN)_6^{3-}]$ (2 mM) in a KCl 0.1 M solution was used.

5.3.1. Cyclic Voltammetry

CV measurements were carried out from -200 mV to 600 mV at a step potential of 10 mV and a scan rate of 100 mV s^{-1}. Obtained voltammograms are depicted in figure 4.44. In this figure, redox peak currents corresponding to the electrochemical oxidation-reduction of the ferro/ferricyanide probe are depicted after each of the electrode modification step, that is, LA or MUA SAM formation, EDC/NHS coupling, nanoparticle grafting and ethanolamine capping. Only results related with MIN1 nanoparticles have been included here as illustrative of the grafting process. Results obtained with sensors fabricated with MIN2 and MIN3 nanoparticles were very similar to the ones presented here and they have not been included here since they provide no significative contribution (see annex I for further information concerning these voltammograms).

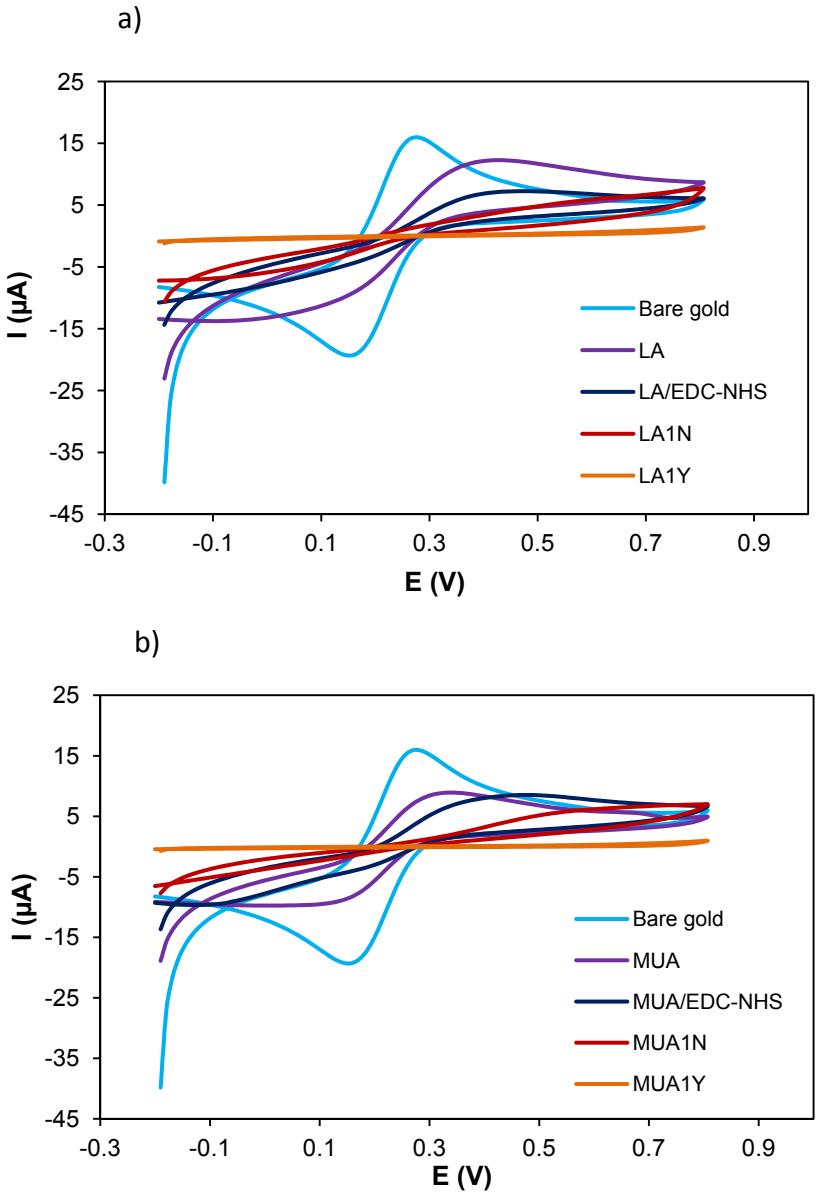

Figure 4.44. Cyclic voltammograms for each step on the fabrication of a) LA1N and LA1Y sensors and b) MUA1N and MUA1Y sensors.

After each sensor modification step, electrode surface coverage increases, consequently, electrode insulation is higher. This may be deduced from the peak current decrease of the ferro/ferricyanide redox pair after each surface modification step (figure 4.44a and b). As previously stated, chain length of MUA is longer than LA, what could contribute to higher surface insulation. This premise was corroborated electrochemically (figures 4.44a and b) and it was observed that anodic and cathodic peak currents of the ferro/ferricyanide redox probe were higher in the LA coated sensor than in the MUA sensor, thereby confirming that insulation in the MUA sensor was higher.

Concerning peak potential, the difference between anodic and cathodic peaks increased with surface coverage, what would mean that the electrochemical reaction tends to irreversibility as the electrode is coated with different components. The electrodes having nanoparticles grafted (LA1N, LA2N, LA3N, MUA1N, MUA2N and MUA3N), showed a fully irreversible redox reaction and the electrodes with ethanolamine capping (LA1Y, LA2Y, LA3Y, MUA1Y, MUA2Y and MUA3Y) did not show any redox peak in the voltammograms, suggesting a too high electrode coverage and hindered electron-transfer on the sensor surface.

5.3.2. Electrochemical Impedance Spectroscopy

Similarly to what it is described for CV experiments, all electrode modification steps were followed by Electrochemical Impedance Spectroscopy (EIS). EIS measurements were carried out applying an AC potential of 200 mV, with an amplitude of 10 mV and measuring the impedance at frequencies ranging from 0.1 Hz to 1MHz. Obtained Nyquist plots were fitted to the Randles circuits described previously (figure 4.23) by the NOVA software and the one with minimum fitting errors (minimum χ^2) was chosen as equivalent circuit (equation 4.16).

Figure 4.45a and b depict Nyquist plots obtained after each electrode modification step, employing sensors with SAM of LA and MUA respectively. Only data concerning sensors fabricated with MIN1 nanoparticles are included in these plots. For the rest of the sensors, a similar impedance tendency was observed after each electrode modification step (annex I can be consulted for further information) and they have not been included here since they did not provide any additional information.

As illustrated in figures 4.45a and b, when the electrode surface is coated with a SAM, LA or MUA respectively, higher charge transfer resistances (observed in the increasing size of the semi circle) are obtained in comparison with bare gold electrodes. Subsequent EDC-NHS coupling, further covers the electrode surface increasing even more the charge transfer resistance. The

same happens when MIN1 nanoparticles are grafted. Charge transfer increases again as a result of higher electrode insulation, due to the non-conducting nature of the polymers employed.

If Nyquist plots depicted here (figures 4.45a and b) are compared with the ones recorded for MIP thin layers developed by the grafting from strategy (section 4.4.3) it can be observed that the impedance values registered with imprinted nanoparticles are much lower than the ones registered previously with MIP thin films. This may lead to think that MIP thin films do insulate the gold surface much more than what MIN do. Consequently, it could preliminarily be observed that sensors developed with grafted nanoparticles could give rise to sensors with higher electrochemical response, since electrode impedance values are lower, thereby sensitivity being higher.

The effect of final ethanolamine capping can be observed in figure 4.46, where the differences of impedance values between EA capped and non-capped sensors may be observed. As it can be deduced from the figure, charge transfer resistance increases remarkably when EA capping is applied. It can be stated that, in these sensors, diffusion processes are not happening, as the Warburg impedance (proportional to the straight line on Nyquist plots) completely disappears.

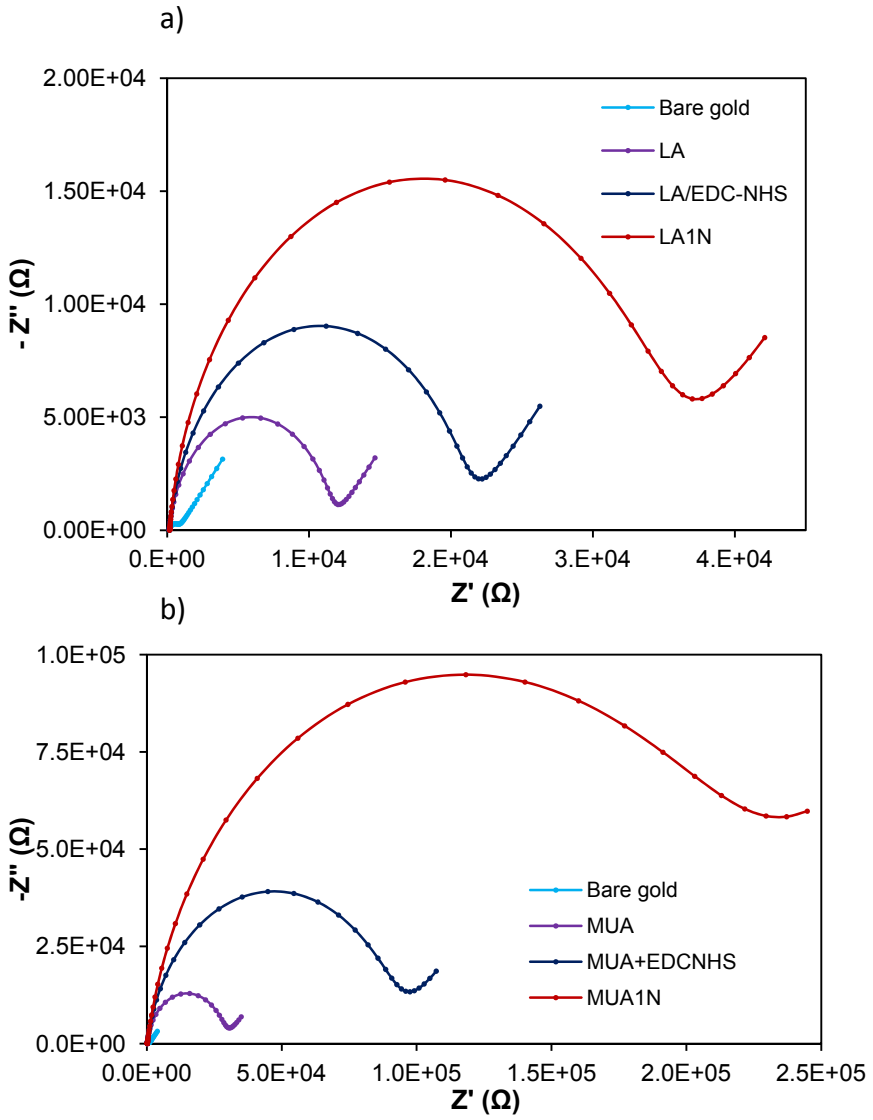

Figure 4. 45. Nyquist plots registered with a) the bare gold electrode and LA based electrodes after each modification step and b) the bare gold electrode and MUA based electrodes after each modification step.

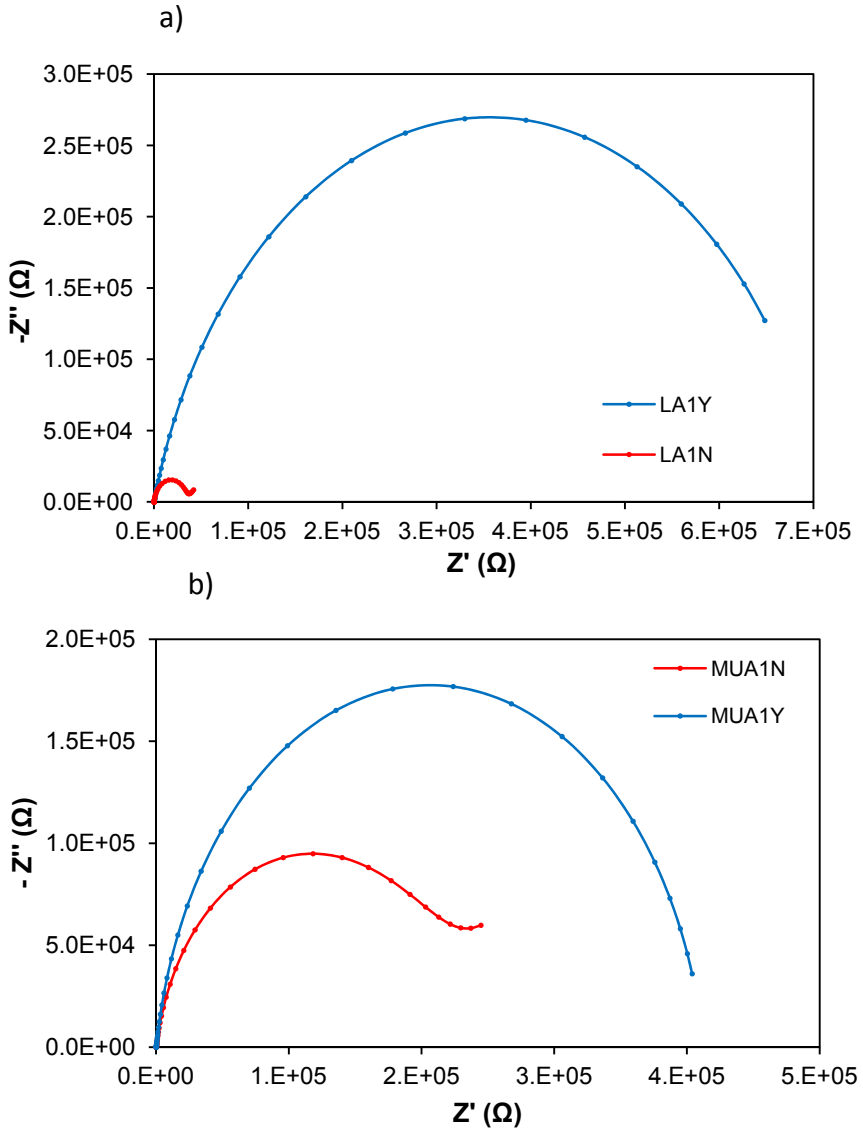

Figure 4. 46. Nyquist plots of electrodes modified with a) LA1N and LA1Y and b) MUA1N and MUA1Y.

Data obtained from fitting the Nyquist plots to the Randles equivalent circuits are illustrated in table 4.9.

Table 4. 9. Electrochemical impedance data for all the fabricated sensors.

Electrode	R_Ω (Ω)	CPE ($nS\ s^\alpha$)	α	R_{ct} (KΩ)	$Z_{W.}$ ($\mu S\ s^{1/2}$)	χ2
Bare gold	164.0	2458.60	0.86	0.63	283.32	0.0073
LA	146.9	307.74	0.91	11.35	281.67	0.0643
LA+EDC-NHS	145.5	248.50	0.90	20.79	165.51	0.0757
MUA	172.4	429.96	0.93	28.43	135.76	0.0109
MUA+EDC-NHS	170.5	480.12	0.91	31.08		0.2421
MUA1N	159.8	253.37	0.88	98.70		0.0612
MUA1Y	160.7	336.98	0.90	412.53		0.0951
LA1N	171.3	594.25	0.92	34.38	112.86	0.0621
LA1Y	149.3	444.39	0.82	712.78		0.0948
MUA2N	168.2	534.61	0.88	241.34		0.1516
MUA2Y	84.0	236.42	0.88	4976.80		0.1215
LA2N	134.2	1121.00	0.88	67.74	18.31	0.2603
LA2Y	163.9	401.91	0.88	1755.30		0.1067
MUA3N	162.2	254.16	0.91	257.51		0.0739
MUA3Y	136.5	329.45	0.89	1923.50		0.1185
LA3N	174.3	259.31	0.90	96.47	140.90	0.0103
LA3Y	133.5	451.31	0.87	1002.90		0.5397

In order to ease the comparison, the charge-transfer resistance values are represented graphically on figure 4.47. Regarding sensor development steps (figure 4.47a), it can be noted

that each step on the modification, increases the charge-transfer resistance of the electrode, what confirms that the modification was successful. If the comparison is made between the different sensors (figure 4.47b), it is clear that electrodes with MUA show higher charge-transfer resistances compared to LA sensors. Due to the larger molecular chain of MUA, it is very likely that it has formed very well ordered defect-free monolayers, typical of long chain alkanethiols, forming a barrier for the electron-transfer process (208). In addition, MUA sensors present almost no diffusion process, as Warburg impedance is low and no Warburg component appears in the subsequent Nyquist plots corresponding to sensor fabrication steps (figure 4.45b). All electrodes with EA capping show very high charge-transfer resistances, regardless of the components used for its fabrication (table 4.9).

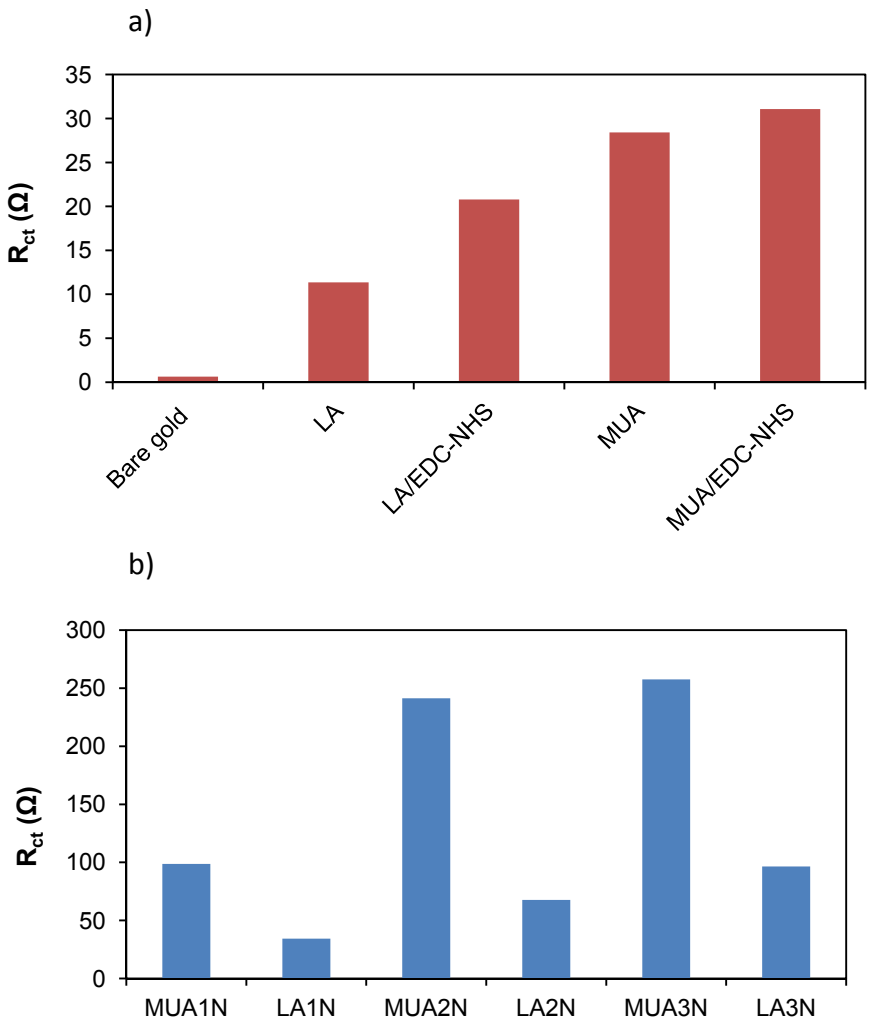

Figure 4. 47. Comparison of charge-transfer resistances a) after each sensor fabrication steps and b) in sensors with no ethanolamine capping.

5.3.3. Scanning Electron Microscopy

SEM images were used to confirm the results obtained by EIS and CV. Due to the morphology of the measurement chamber, it was not possible to take any images of the gold electrodes. For this reason, gold wires of 25 µm in diameter were used as solid supports, instead of gold disk electrodes (2 mm in diameter).

Figure 4.48 depicts obtained SEM images after each electrode modification step. As expected, no significative difference was observed between the bare gold and the lipoic acid coated wire, as changes happen in the molecular range, obviously not appreciable by SEM. On the other hand, in images corresponding to nanoparticles grafted on gold wires (figure 4.48c), the presence of nanoparticles linked to the gold surface is very clear, what can be observed at different magnifications.

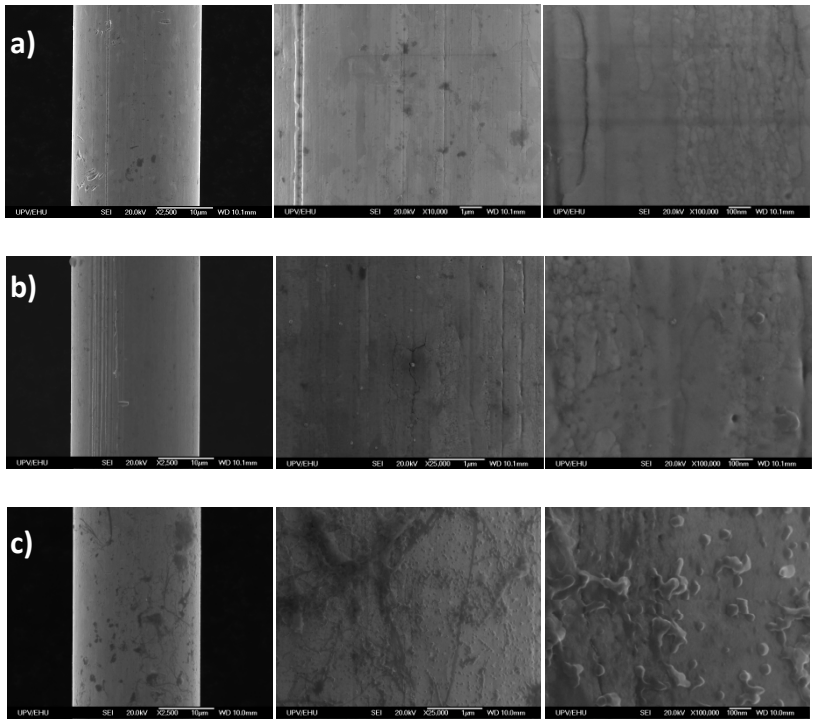

Figure 4. 48. SEM micrographs at 2500, 25000 and 100000 magnifications of a) the bare gold wire, b) the lipoic acid coated wire and c) the gold wire having nanoparticles grafted (*via* lipoic acid).

5.4. Electrochemical determination of 4-ethylphenol using sensor developed with MIP nanoparticles grafted on gold electrodes

5.4.1. Selection of modified sensors providing highest response for 4-ethylphenol

In order to compare the electrochemical behaviour of the developed MIN sensors (detailed in table 4.8), 4EP was measured with each of them by Differential Pulse Voltammetry (DPV). Measurement parameters related with the electrochemical technique employed for this study, are summarised in table 4.10.

Table 4. 10. Optimised parameters for 4EP sensing by DPV.

Diferential Pulse Voltammetry	
Modulation time	0.01 s
Interval time	1 s
Start potential	0 V
End potential	0.6 V
Potential step	0.01 V
Pulse amplitude	0.1 V

Peak current signals recorded with each sensor, corresponding to 4EP oxidation at different concentration levels, 8 µM and 40 µM, are depicted in figure 4.49.

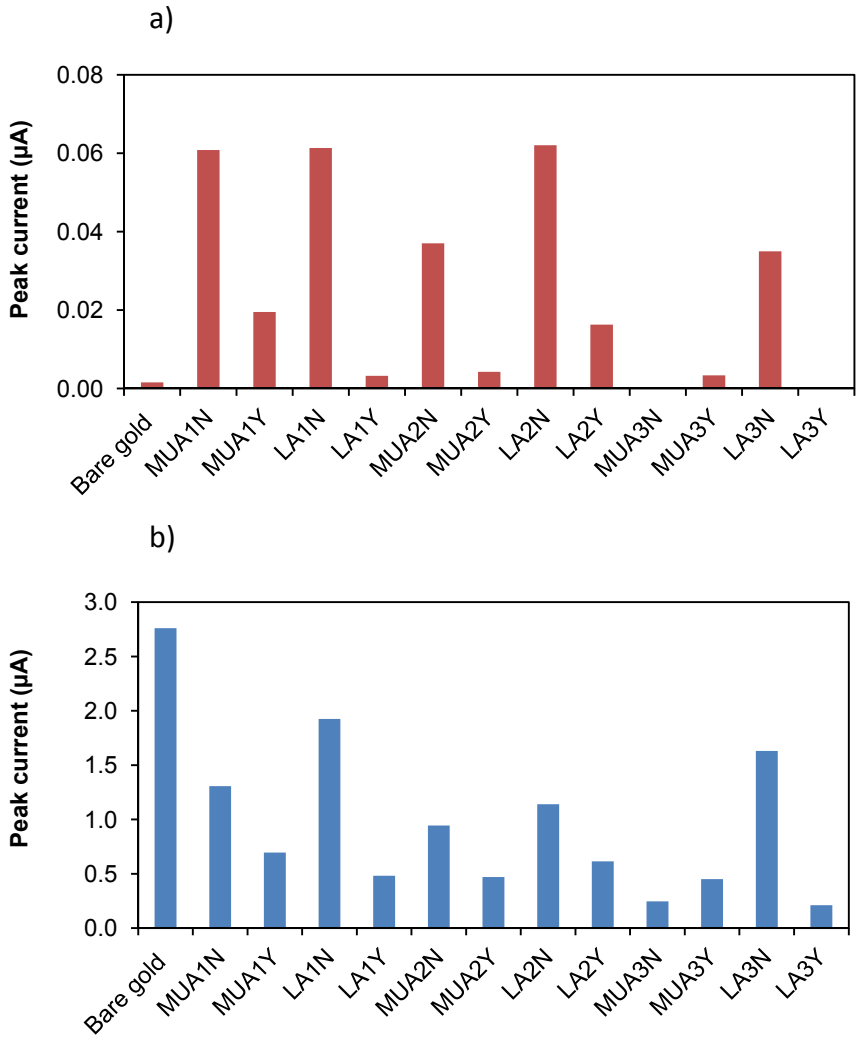

Figure 4. 49. Peak current signals measured by DPV with the developed sensors in a) 8 µM and b) 40 µM 4EP solutions in B-R 0.04 M buffer (pH: 10)

If results provided by MIN sensors are compared with the responses provided by the bare gold electrode, the higher performance of the MIP coating can be clearly distinguished. In almost all cases, developed sensors provided higher peak current signals than the bare gold electrode at 8 µM (figure 4.49a). In this sense, MUA1N, LA1N, LA2N and LA3N modified sensors display highest sensitivity. Ethanolamine capped sensors provided much lower current responses than the non capped ones, moreover, some of them (LA1Y and LA3Y) did not practically present any anodic peak at 8 µM of 4EP. This fact is in agreement with previous results obtained by EIS where ethanolamine capped sensors showed much higher charge-transfer resistance and no Warburg impedance.

Comparing sensors developed using different SAM for nanoparticle immobilisation, MUA electrodes present lower peak current signals. Once again, these results are in agreement with previous results registered by EIS, where the electrodes with MUA showed higher charge-transfer resistance in all cases. Sensors that provided highest charge transfer resistances by EIS gave rise to lowest peak current signals, however, despite the bare gold electrode showed the lowest charge-transfer resistance (figures 4.45a and b), its response to 4EP was remarkably lower than the signal provided by modified electrodes. This fact undoubtedly demonstrates that peak current signal of 4EP is enhanced after the implementation of imprinted nanoparticles on gold substrates.

Even if sensors with nanoparticles have higher surface coverage, which results in higher impedance values, they show better performance for 4EP sensing.

Based on presented results, the sensors developed using a LA monolayer and without ethanolamine capping were chosen for further experiments, since they provided highest peak current signals related to their lower charge-transfer resistance.

5.4.2. Selection of the best nanoparticles for the selective determination of 4-ethylphenol

Developed LA1N, LA2N and LA3N were tested next to determine which provided highest selectivity towards the target compound, 4EP. In the previous section, MUA based electrodes and ethanolamine capped ones were discarded for further experimental, based on their poor electrochemical response. However, all LA based sensors, that is, LA1N, LA2N and LA3N, provided similar peak current intensities for 4EP electrooxidation, what did not help in selecting the most proper nanoparticles for 4EP sensing. In this regard, with each of these sensors, the peak current signal of the target compound was compared with the signals provided by structural analogues, similarly to what previously detailed in section 4.5.

4-ethylguaiacol (4EG), 4-vinylphenol (4VPh) and coumaric acid ethyl ester (CAEE) were selected as potential interfering compounds. As all these compounds present different peak current signals on bare gold electrodes, in order to properly determine the selectivity ratio, the 4EP:analogue peak current ratio was normalised employing peak current signals of these compounds registered with a bare gold electrode, as detailed in equation 4.43. Obtained results are depicted in figure 4.50.

$$\text{Ratio} = \frac{\text{Signal}(4\text{EP})_{\text{MIP}}}{\text{Signal (analogue)}_{\text{MIP}}} \cdot \frac{\text{Signal}(\text{analogue})_{\text{Bare gold}}}{\text{Signal (4EP)}_{\text{Bare gold}}} \qquad \textbf{4. 43}$$

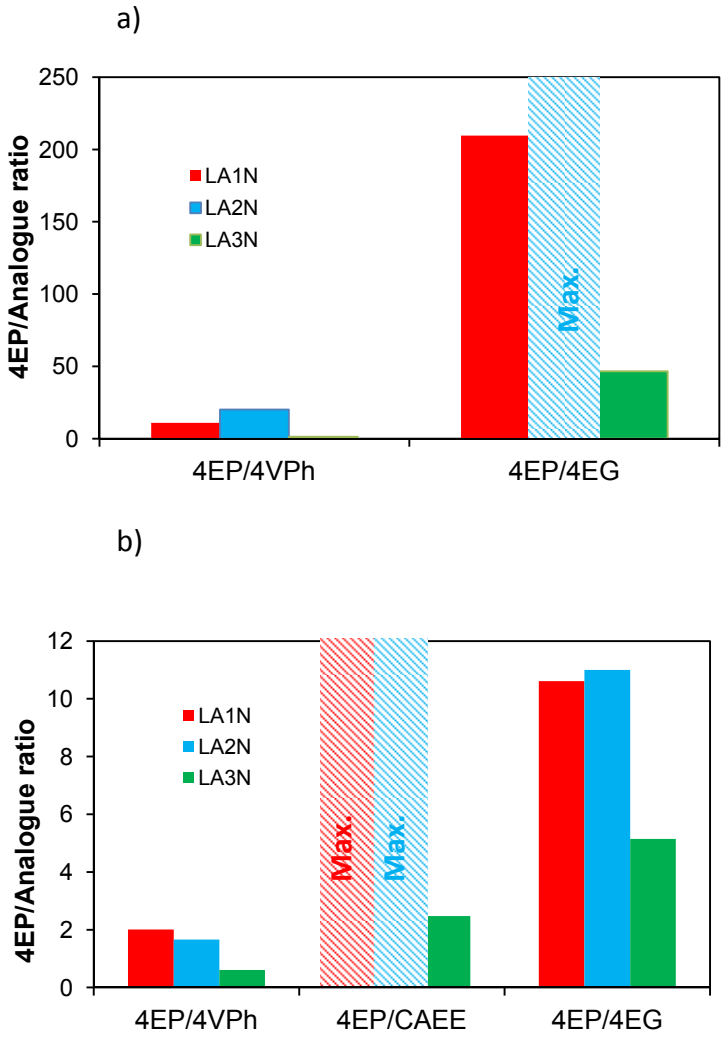

Figure 4. 50. Normalised 4EP:Analogue signal ratios for MIN sensors measured at a) 8 µM and b) 40 µM concentration levels of each compound. B-R 0.04 M buffer (pH: 10) was used as supporting electrolyte.

Sensors fabricated with LA2N particles did not respond to 4EG at 8 µM (figure 4.50a), that is why no signal ratio could be calculated, being sensor selectivity for 4EP maximum (blue lined bar) compared to 4EG. LA1N 4EP/4EG signal ratio was close to 200 whereas the selectivity of the LA3N sensor was considerably lower, being the signal ratio close to 50.

Concerning CAEE, none of the sensors presented any response to this target at 8 µM, whereas at 40 µM, LA3N sensor was the only one that could recognise this compound (green bar in figure 4.50b). It could therefore be asserted selectivity for 4EP in comparison with CAEE was maximum using LA1N and LA2N sensors.

It can be observed in figure 4.50 that the selectivity for 4EP shown by all sensors is really high compared to CAEE and 4EG analogues. However, sensor selectivity decreases considerably if 4EP current is compared versus the signal provided by 4VPh. As it could be expected, due to the structural similarity of 4EP and 4VPh (figure 4.30), which are almost identical, the sensors were unable to differentiate between both these targets in the same extent as they did for the rest of the analogues. In any case, LA1N and LA2N sensors provided in all cases higher signals for 4EP than for 4VPh, what undoubtedly demonstrated that despite their structural similarity, the sensor responded always preferably to 4EP. Moreover, considering the poor functional groups available for

imprinting on the target compound, it may be considered that registered sensor selectivity is really promising.

As regards the differences between LA1N and LA2N sensors, LA1N sensor was the one that provided highest peak current signals for 4EP (figure 4.49), on the other hand, similar selectivity to 4EP was obtained with these sensors. For this reason, LA1N sensor, prepared with MIN1 nanoparticles was selected as the most suitable one for 4EP determination.

In figure 4.51, the voltamograms recorded with the LA1N sensor not only for 4EP, but also for all selected structural analogues, are depicted. All tested compounds were measured at a concentration of 8 µM except for CAEE. As this compound did not show any oxidation peak at low concentration levels in the bare gold electrode, it was measured at 40 µM (figure 4.51).

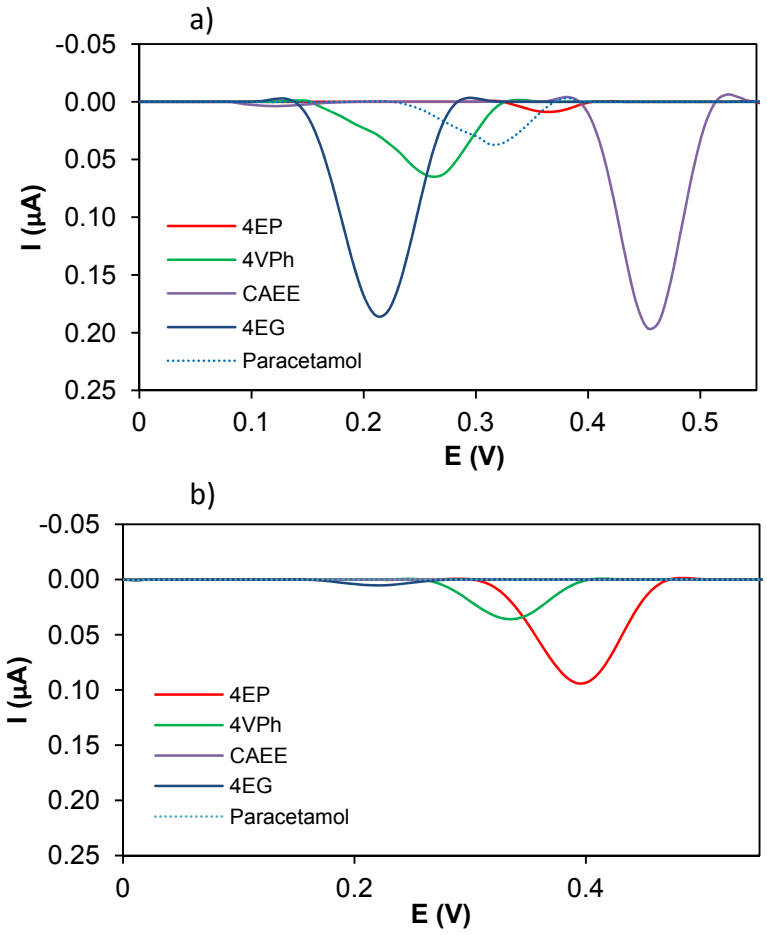

Figure 4. 51. Differential pulse voltammograms for 4EP (8 µM) and the structural analogues 4VPh (8 µM), CAEE (40 µM), 4EG (8 µM) and paracetamol (8 µM) using (a) a bare gold electrode and (b) the developed LA1N sensor.

As it can be observed, when the bare gold electrode was used, 4EP provides the lowest peak current signal among all measured compounds. Oppositely, when the LA1N sensor was used, 4EP provides the highest current, what demonstrates the effect of nanoparticles as recognition elements on the sensor surface. Furthermore, the signal provided by the bare gold electrode for CAEE and paracetamol completely dissapears when the LA1N sensor is employed, thereby demonstrating that sensor selectivity was enhanced by MIN1 nanoparticles. Most of the compounds that were capable of being oxidised on the bare gold electrode, did not present any oxidation peak when using the LA1N sensor, except for 4-vinylphenol and 4-ethylguaiacol. Although, oxidation peaks for these compounds are much lower when using LA1N sensor, they still present a weak peak current, probably due to their similarity with the target compound, which indicates that they are capable of binding, in some extent, to imprinted sites. However, when comparing the signals of 4EG in the bare gold electrode and in the MIN1 sensor, a remarkable current decrease can be appreciated, what reinforces the assumption concerning the selectivity increment.

On the other hand, it is not surprising that 4VPh shows the highest signal among analogues, as 4EP and 4VPh are very similar compounds only differing on the vinyl group of the latter. In conclusion, it can definitely be asserted that the selectivity

improvement achieved by grafting MIN1 nanoparticles to the gold electrode is beyond doubt.

5.5. Analytical evaluation of the LA1N sensor

In the final instance, the analytical evaluation of the LA1N sensor was carried out. For this purpose, peak current dependence to the concentration level was established though a calibration curve and based on this, the working linear range as well as the instrumental detection (LOD) and quantification (LOQ) limits were calculated. Additionally, the measurements repeatability was determined employing a single sensor and different sensors.

5.5.1. Calibration

To construct the calibration curve, a series of standard solutions of 4EP were measured, finding that the working linear range was comprised between 2 µM and 40 µM. The correlation between anodic peak current intensities and the concentration peak was obtained by the least squares method, giving rise to the following expression:

$$I_{4EP}=(13.61\pm0.21)C-(13.23\pm4.66) \quad \textbf{4. 44}$$

Where I_{4EP} is the peak current of 4EP expressed in nA and C is the concentration expressed in μM. The coefficient of determination (R^2: 0.999) confirmed an adequate linear correlation of the analytical signal versus 4EP concentration.

In order to confirm the goodness of fit of the proposed regression, a statistical analysis of the distribution of the residuals was carried out. The residual (r_i) is the difference between the experimental value of the dependent variable and (y_{exp}) and the predicted value (y_{calc}) which is calculated from the expression from the calibration curve (4.44). This value for each data point is calculated based on the following expression:

$$r_i = y_{calc} - y_{exp} \qquad \textbf{4. 45}$$

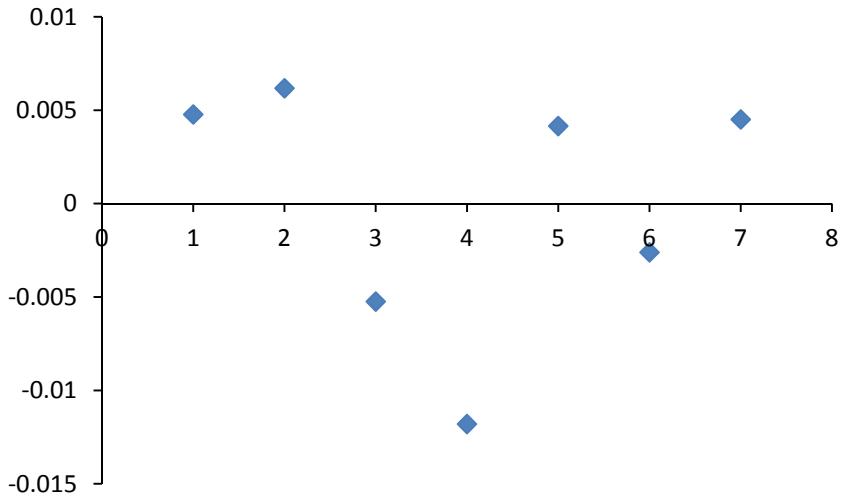

Figure 4. 52. Distribution diagram of the calibration residuals.

In figure 4.52 a random distribution of the residuals can be appreciated, what denotes that the proposed regression fits adequately experimental data. Nevertheless, different statistical parameters that may confirm the normal distribution of the residuals were calculated. The description of the parameters and their values are summarised in table 4.11 most of these values approach theoretical values indicating a Gaussian distribution of the residuals.

Table 4. 11. Parameters, their expression and the obtained and theoretical values of the statistical analysis of the residuals. (Np: number of calibration points).

Parameter	Expression	Value	Theoretical value
Arithmetic median of the residuals	$\bar{r} = \frac{\sum(y_{calc} - y_{exp})}{N_P}$	4.821×10^{-14}	$\bar{r} \approx 0$
Global standard deviation	$\sigma_{TOT} = \sqrt{\frac{\sum_{i=1}^{N_P}(y_{calc} - y_{exp})^2}{N_p - 2}}$	7.375	
Standard deviation of the residuals	$\boldsymbol{\sigma(r)} = \sqrt{\left(\frac{\sum r_i^2}{N_P}\right) - \left(\frac{\sum r_i}{N_P}\right)}$	6.233	$\sigma(r) \leq \sigma(tot)$
Average residual	$\overline{\lvert r \rvert} = \frac{\sum \lvert y_{calc} - y_{exp} \rvert}{N_P} = \frac{\sum \lvert r_i \rvert}{N_P}$	5.609	$\lvert \bar{r} \rvert \leq \sigma(r)$
Asymmetry coefficient	$C_s = \frac{\sum(r_i - \bar{r})^3}{N_P\, \sigma(r)^3}$	-0.762	$C_s \cong 0$
Kurtois coefficient	$C_{ku} = \frac{\sum(r_i - \bar{r})^4}{N_P\, \sigma(r)^4}$	2.160	$C_{Ku} \cong 3$

5.5.2. Detection and quantification limits

The detection and quantification limits were calculated using the sensitivity value (S) obtained from the slope of the calibration curve and the standard deviation of the signals recorded from blank measurements (σ_B).

$$C_{LOD} = \frac{K\sigma_B}{S} = \frac{3\sigma_B}{S} \quad \textbf{4. 46}$$

$$C_{LOQ} = \frac{K\sigma_B}{S} = \frac{10\sigma_B}{S} \quad \textbf{4. 47}$$

The obtained values were 0.5 µM and 1.86 µM for the detection and quantification limits respectively.

5.5.3. Measurement repeatability

Measurement repeatability was evaluated through consecutive measurements of 4EP at different concentration levels (8 µM and 40 µM) (n=5). Between measurements it was necessary to clean the sensor with isopropanol to avoid saturation of the polymer and signal decay. The cleaning step improved measurement

repeatability employing the same sensor. Obtained standard deviations were below 8 % in all cases (table 4.12).

Additionally, measurement repeatability was also assessed employing different sensors (n=5) and measuring 4EP at two concentration levels (8 µM and 40 µM). Results are presented in table 4.12. Calculated relative standard deviation values were always below 18%.

Table 4. 12. Peak current and RSD values for 4EP measured with the developed LA1N sensor.

	4EP concentration (µM)	Peak current (nA)	SD (nA)	RSD (%)
Repeatability between measurements	8	59.594	3.954	6.63
	40	397.73	25.185	7.76
Repeatability between sensors	8	69.994	7.805	11.15
	40	516.913	89.735	17.36

5.6. Comparison between 4-ethylphenol sensors developed under different strategies

The developed sensor for 4-ethylphenol, constructed by grafting MIP nanoparticles synthesised by solid-phase imprinting to the surface of gold electrodes (MIN1 sensor), showed higher sensitivity and lower detection limit compared to the sensor constructed by grafting MIP films on gold microelectrodes (section 4). Although the difference between both sensors sensitivity appears to be remarkably high (1.02 nA/µM for MIP film coated electrode and 13.61 nA/µM for MIN immobilised sensor), it may be related with the type of electrodes employed in each approach, a gold wire microelectrode of 25 µm in diameter in the former and a gold disk electrode of 2 mm in diameter in the latter.

The bare gold microelectrode presented a sensitivity of 1.36 nA/µM for 4EP and the bare gold electrode 10.58 nA/µM. However, MIN1 nanoparticles implemented on the gold disk electrode were capable of improving electrode sensitivity, while the coating of thin MIP layers on gold microelectrodes made sensor sensitivity rather decrease. In this regard, it can be asserted that for sensitivity improvement, immobilising high affinity MIP nanoparticles to the gold surface seems to be a better approach than coating the gold surface with MIP thin layers.

Concerning sensor selectivity, 4EP:analogue signal ratios of sensors developed by the two described approaches are compared

in figure 4.53, with 4VPh and 4EG as analogues. It can be observed that obtained signal ratios are very similar for 4EP:4VPh, what may indicate that both strategies lead to sensors with similar selectivity for 4EP over 4VPh. On the other hand, the differences in 4EP:4EG ratios are quite more remarkable, indicating that the sensor developed by the MIN grafting approach enhances sensor selectivity more than what the MIP thin film approach does.

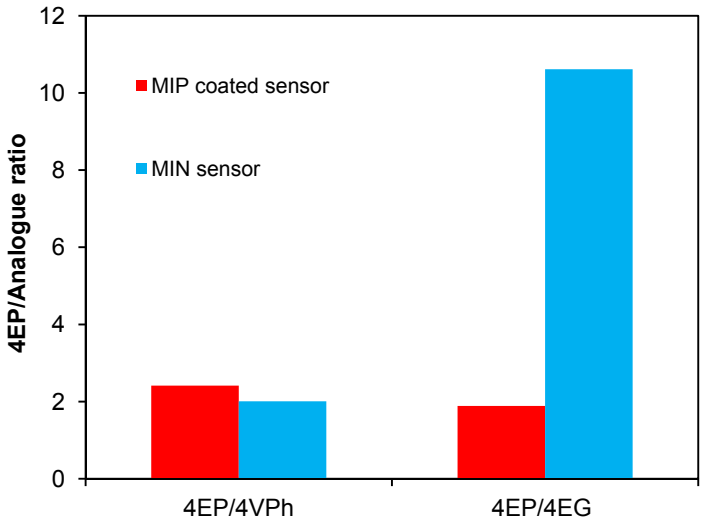

Figure 4. 53. Comparison of the signal ratios obtained for 4EP vs. analogues between the developed sensors (MIP layer coated sensor and MIP nanoparticles immobilised sensor).

6. Conclusions

Based on the previously established objectives, it can be concluded that new MIP based synthetic receptors have successfully been implemented on gold substrates to be employed as sensing elements for voltammetric sensing of 4EP. The methodologies presented along this chapter could be extrapolated to the development of new selective devices for voltammetric sensing of other electrochemically active compounds.

The previously stated operational objectives have been fully accomplished, what allows for concluding that:

- Gold wire microelectrodes and gold disk electrodes have been fabricated and layer-by-layer modified successfully. Surface activation of these electrodes has been performed by chemical and electrochemical treatments, obtaining reduced gold surfaces capable of being assembled with monolayers of organosulfur compounds.

- Both gold substrates have been functionalised with self-assembled monolayers and later MIP materials have been implemented on their surfaces through different strategies:

    - On the one hand, gold microelectrodes have been coated with an iniferter possessing a dual character. Being capable of self-assembling to the gold surface through the thiol end-group, and also initiating

controlled UV polymerisation through a reversible-deactivation mechanism. This iniferter served to graft MIP thin layers on the surface of gold microelectrodes.

  - On the other hand, gold disk electrodes have been coated with a lipoic acid self-assembled monolayer which has been employed to graft MIP nanoparticles, synthesised by the solid-phase imprinting approach, via carbodiimide chemistry.

- The surface modification step of gold substrates has been monitored electrochemically by Cyclic Voltammetry and Electrochemical Impedance Spectroscopy.

- Gold surface modification by thin MIP layers or by imprinted nanoparticle grafting was confirmed by Scanning Electron Microscopy.

- The polymerisation and grafting conditions have been optimised in order to obtain best electrochemical behaviour of the sensors.

- The sensors have been applied to 4-ethylphenol sensing by Differential Pulse Voltammetry. Concluding that the sensitivity obtained by the bare gold electrode was enhanced when MIP nanoparticles were implemented. MIP

thin films tended to isolate the electrode surface and consequently sensor response decreased.

- Both sensor development strategies have increased sensors selectivity, in comparison with the signals obtained with bare gold electrodes.

- Analytical evaluation of the sensors has also been performed, concluding that both sensor fabrication strategies are capable of providing devices that could determine 4EP in real samples.

References

1. Li, D.-Y., He, X.-W., Chen, Y., Li, W.-Y., Zhang, Y.-K. (2013). Novel hybrid structure silica/CdTe/molecularly imprinted polymer: Synthesis, specific recognition, and quantitative fluorescence detection of bovine hemoglobin. *ACS Applied Materials & Interfaces*, **5**, 12609-12616.
2. Ibupoto, Z.H., Usman Ali, S.M., Khun, K., Chey, C.O., Nur, O., Willander, M. (2011). ZnO nanorods based enzymatic biosensor for selective determination of penicillin. *Biosensors*, **1**, 153-163.
3. Gao, W., Dong, H., Lei, J., Ji, H., Ju, H. (2011). Signal amplification of streptavidin-horseradish peroxidase functionalized carbon nanotubes for amperometric detection of attomolar DNA. *Chemical Communications*, **47**, 5220-5222.
4. Li, L., Zhao, H., Chen, Z., Mu, X., Guo, L. (2011). Aptamer biosensor for label-free square-wave voltammetry detection of angiogenin. *Biosensors Bioelectronics*, **30**, 261-266.
5. Hnaien, M., Lagarde, F., Bausells, J., Errachid, A., Jaffrezic-Renault, N. (2011). A new bacterial biosensor for trichloroethylene detection based on a three-dimensional carbon nanotubes bioarchitecture. *Analytical and Bioanalytical Chemistry*, **400**, 1083-1092.
6. Suryanarayanan, V., Wu, C.-T., Ho, K.-C. (2010). Molecularly imprinted electrochemical sensors. *Electroanalysis*, **22**, 1795-1811.
7. Suriyanarayanan, S., Cywinski, P.J., Moro, A.J., Mohr, G.J., Kutner, W. (2010). Chemosensors based on molecularly imprinted polymers. Electrochemical sensors. In *Molecular Imprinting*, Haupt, K. (ed.) Springer, Berlin, pp. 230-260.
8. Antuña-Jiménez, D., Díaz-Díaz, G., Blanco-López, M.C., Lobo-Castañón, M.J., Miranda-Ordieres, A.J., Tuñón-Blanco, P. (2012). Molecularly imprinted electrochemical sensors: past, present and future. In *Molecularly imprinted sensors:*

overview and applications, Li, S., Ge, Y., Piletsky, S. and Lunec, J. (eds.) Elsevier Amsterdam, pp. 2-31.

9. Prasad, K., Prathish, K.P., Gladis, J.M., Naidu, G.R.K., Rao, T.P. (2007). Molecularly imprinted polymer (biomimetic) based potentiometric sensor for atrazine. *Sensors and Actuators B: Chemical*, **123**, 65-70.
10. Metilda, P., Prasad, K., Kala, R., Gladis, J.M., Rao, T.P., Naidu, G.R.K. (2007). Ion imprinted polymer based sensor for monitoring toxic uranium in environmental samples. *Analytica Chimica Acta*, **582**, 147-153.
11. Sadeghi, S., Fathi, F., Abbasifar, J. (2007). Potentiometric sensing of levamisole hydrochloride based on molecularly imprinted polymer. *Sensors and Actuators B: Chemical*, **122**, 158-164.
12. Liang, R., Zhang, R., Qin, W. (2009). Potentiometric sensor based on molecularly imprinted polymer for determination of melamine in milk. *Sensors and Actuators B: Chemical*, **141**, 544-550.
13. Liang, R.-N., Song, D.-A., Zhang, R.-M., Qin, W. (2010). Potentiometric sensing of neutral species based on a uniform-sized molecularly imprinted polymer as a receptor. *Angewandte Chemie, International Edition*, **49**, 2556-2559.
14. Alizadeh, T., Akhoundian, M. (2010). A novel potentiometric sensor for promethazine based on a molecularly imprinted polymer (MIP): The role of MIP structure on the sensor performance. *Electrochimica Acta*, **55**, 3477-3485.
15. Moreira, F.T.C., Kamel, A.H., Guerreiro, J.R.L., Sales, M.G.F. (2010). Man-tailored biomimetic sensor of molecularly imprinted materials for the potentiometric measurement of oxytetracycline. *Biosensors and Bioelectronics*, **26**, 566-574.
16. Vishnuvardhan, V., Kalyan, Y., Prathish, K.P., Gangadhar, B., Tharakeswar, Y., Rao, T.P., Naidu, G.R. (2011). Imprinted polymer inclusion membrane based potentiometric sensor for determination and quantification of diethyl chlorophosphate in natural waters. *American Journal of Analytical Chemistry*, **2**, 374-380.

17. Basozabal, I., Guerreiro, A., Gomez-Caballero, A., Goicolea, M.A., Barrio, R.J. (2014). Direct potentiometric quantification of histamine using solid-phase imprinted nanoparticles as recognition elements. *Biosensors and Bioelectronics*, **58**, 138-144.
18. Rizk, M., Toubar, S.S., El-Din Sayour, H.E., Mohamed, D., Touny, R.M. (2014). A new potentiometric sensor based on molecularly imprinted polymer for analysis of a veterinary drug imidocarb dipropionate. *European Journal of Chemistry*, **5**, 18-23.
19. Alizadeh, T., Rashedi, M. (2014). Synthesis of nano-sized arsenic-imprinted polymer and its use as As^{3+} selective ionophore in a potentiometric membrane electrode: Part 1. *Analytica Chimica Acta*, **843**, 7-17.
20. Abu-Dalo, M.A., Salam, A.A., Nassory, N.S. (2015). Ion imprinted polymer based electrochemical sensor for environmental monitoring of copper(II). *International Journal of Electrochemical Science*, **10**, 6780-6793.
21. El-Naby, E.H., Kamel, A.H. (2015). Potential transducers based man-tailored biomimetic sensors for selective recognition of dextromethorphan as an antitussive drug. *Materials Science and Engineering: C*, **54**, 217-224.
22. Anirudhan, T.S., Alexander, S. (2015). Selective determination of monosodium glutamate (Ajinomoto) in food samples using a potentiometric method with a modified multiwalled carbon nanotube based molecularly imprinted polymer. *RSC Advances*, **5**, 96840-96850.
23. Liang, R., Chen, L., Qin, W. (2015). Potentiometric detection of chemical vapors using molecularly imprinted polymers as receptors. *Sciencetific Reports*, **5**, 12462.
24. Gutierrez-Climente, R., Gomez-Caballero, A., Unceta, N., Goicolea, M.A., Barrio, R.J. (2016). A new potentiometric sensor based on chiral imprinted nanoparticles for the discrimination of the enantiomers of the antidepressant citalopram. *Electrochimica Acta*, **196**, 496-504.
25. Kupis-Rozmyslowicz, J., Wagner, M., Bobacka, J., Lewenstam, A., Migdalski, J. (2016). Biomimetic membranes

based on molecularly imprinted conducting polymers as a sensing element for determination of taurine. *Electrochimica Acta*, **188**, 537-544.

26. Sharma, P.S., Wojnarowicz, A., Sosnowska, M., Benincori, T., Noworyta, K., D'Souza, F., Kutner, W. (2016). Potentiometric chemosensor for neopterin, a cancer biomarker, using an electrochemically synthesized molecularly imprinted polymer as the recognition unit. *Biosensors and Bioelectronics*, **77**, 565-572.
27. Alizadeh, T., Sabzi, R.E., Alizadeh, H. (2016). Synthesis of nano-sized cyanide ion-imprinted polymer via non-covalent approach and its use for the fabrication of a CN--selective carbon nanotube impregnated carbon paste electrode. *Talanta*, **147**, 90-97.
28. Piletsky, S.A., Piletskaya, E.V., Elgersma, A.V., Yano, K., Karube, I., Parhometz, Y.P., El'skaya, A.V. (1995). Atrazine sensing by molecularly imprinted membranes. *Biosensors and Bioelectronics*, **10**, 959-964.
29. Kriz, D., Kempe, M., Mosbach, K. (1996). Introduction of molecularly imprinted polymers as recognition elements in conductometric chemical sensors. *Sensors and Actuators B: Chemical*, **33**, 178-181.
30. Piletsky, S.A., Piletskaya, E.V., Panasyuk, T.L., El'skaya, A.V., Levi, R., Karube, I., Wulff, G. (1998). Imprinted membranes for sensor technology: Opposite behavior of covalently and noncovalently imprinted membranes. *Macromolecules*, **31**, 2137-2140.
31. Sergeyeva, T.A., Piletsky, S.A., Brovko, A.A., Slinchenko, E.A., Sergeeva, L.M., El'skaya, A.V. (1999). Selective recognition of atrazine by molecularly imprinted polymer membranes. Development of conductometric sensor for herbicides detection. *Analytica Chimica Acta*, **392**, 105-111.
32. Sergeyeva, T.A., Piletsky, S.A., Panasyuk, T.L., El'skaya, A.V., Brovko, A.A., Slinchenko, E.A., Sergeeva, L.M. (1999). Conductimetric sensor for atrazine detection based on molecularly imprinted polymer membranes. *Analyst*, **124**, 331-334.

33. Suedee, R., Srichana, T., Sangpagai, C., Tunthana, C., Vanichapichat, P. (2004). Development of trichloroacetic acid sensor based on molecularly imprinted polymer membrane for the screening of complex mixture of haloacetic acids in drinking water. *Analytica Chimica Acta*, **504**, 89-100.
34. Suedee, R., Intakong, W., Dickert, F.L. (2006). Molecularly imprinted polymer-modified electrode for on-line conductometric monitoring of haloacetic acids in chlorinated water. *Analytica Chimica Acta*, **569**, 66-75.
35. Najafi, M., Mollazadeh, M. (2011). Selective recognition of chloroacetic acids by imprinted polyaniline film. *Journal of Applied Polymer Science*, **121**, 292-298.
36. Warwick, C., Guerreiro, A., Gomez-Caballero, A., Wood, E., Kitson, J., Robinson, J., Soares, A. (2014). Conductance based sensing and analysis of soluble phosphates in wastewater. *Biosensors and Bioelectronics*, **52**, 173-179.
37. Panasyuk, T.L., Mirsky, V.M., Piletsky, S.A., Wolfbeis, O.S. (1999). Electropolymerized molecularly imprinted polymers as receptor layers in capacitive chemical sensors. *Analytical Chemistry*, **71**, 4609-4613.
38. Panasyuk-Delaney, T., Mirsky, V.M., Ulbricht, M., Wolfbeis, O.S. (2001). Impedometric herbicide chemosensors based on molecularly imprinted polymers. *Analytica Chimica Acta*, **435**, 157-162.
39. Cheng, Z., Wang, E., Yang, X. (2001). Capacitive detection of glucose using molecularly imprinted polymers. *Biosensors and Bioelectronics*, **16**, 179-185.
40. Panasyuk-Delaney, T., Mirsky, V.M., Wolfbeis, O.S. (2002). Capacitive creatinine sensor based on a photografted molecularly imprinted polymer. *Electroanalysis*, **14**, 221-224.
41. Gong, J.-L., Gong, F.-C., Kuang, Y., Zeng, G.-M., Shen, G.-L., Yu, R.-Q. (2004). Capacitive chemical sensor for fenvalerate assay based on electropolymerized molecularly imprinted polymer as the sensitive layer. *Analytical and Bioanalytical Chemistry*, **379**, 302-307.

42. Yang, L., Wei, W., Xia, J., Tao, H., Yang, P. (2005). Capacitive biosensor for glutathione detection based on electropolymerized molecularly imprinted polymer and kinetic investigation of the recognition process. *Electroanalysis*, **17**, 969-977.
43. Liu, K., Wei, W.-Z., Zeng, J.-X., Liu, X.-Y., Gao, Y.-P. (2006). Application of a novel electrosynthesized polydopamine-imprinted film to the capacitive sensing of nicotine. *Analytical and Bioanalytical Chemistry*, **385**, 724-729.
44. Delaney, T.L., Zimin, D., Rahm, M., Weiss, D., Wolfbeis, O.S., Mirsky, V.M. (2007). Capacitive detection in ultrathin chemosensors prepared by molecularly imprinted grafting photopolymerization. *Analytical Chemistry*, **79**, 3220-3225.
45. Ouyang, R., Lei, J., Ju, H., Xue, Y. (2007). A molecularly imprinted copolymer designed for enantioselective recognition of glutamic acid. *Advanced Functional Materials*, **17**, 3223-3230.
46. Wang, Z., Kang, J., Liu, X., Ma, Y. (2007). Capacitive detection of theophylline based on electropolymerized molecularly imprinted polymer. *International Journal of Polymer Analysis and Characterization*, **12**, 131-142.
47. Zhou, L., Ye, G., Yuan, R., Chai, Y., Chen, S. (2007). A capacitive sensor based on molecularly imprinted polymers and poly(p-aminobenzene sulfonic acid) film for detection of pazufloxacin mesilate. *Science in China Series B: Chemistry*, **50**, 547-553.
48. Najafi, M., Baghbanan, A.A. (2012). Capacitive chemical sensor for thiopental assay based on electropolymerized molecularly imprinted polymer. *Electroanalysis*, **24**, 1236-1242.
49. Hawari, H.F., Samsudin, N.M., Shakaff, A.Y.M., Wahab, Y., Hashim, U., Zakaria, A., Ghani, S.A., Ahmad, M.N. (2013). Highly selective molecular imprinted polymer (MIP) based sensor array using interdigitated electrode (IDE) platform for detection of mango ripeness. *Sensors and Actuators B: Chemical*, **187**, 434-444.

50. Reddy, K.K., Gobi, K.V. (2013). Artificial molecular recognition material based biosensor for creatinine by electrochemical impedance analysis. *Sensors and Actuators B: Chemical*, **183**, 356-363.
51. Lenain, P., De Saeger, S., Mattiasson, B., Hedstrom, M. (2015). Affinity sensor based on immobilized molecular imprinted synthetic recognition elements. *Biosensors and Bioelectronics*, **69**, 34-39.
52. Pandey, I., Kant, R. (2016). Electrochemical impedance based chiral analysis of anti-ascorbutic drug: L-Ascorbic acid and D-ascorbic acid using C-dots decorated conductive polymer nano-composite electrode. *Biosensors and Bioelectronics*, **77**, 715-724.
53. Weng, C.-H., Yeh, W.-M., Ho, K.-C., Lee, G.-B. (2007). A microfluidic system utilizing molecularly imprinted polymer films for amperometric detection of morphine. *Sensors and Actuators B: Chemical*, **121**, 576-582.
54. Wang, T., Shannon, C. (2011). Electrochemical sensors based on molecularly imprinted polymers grafted onto gold electrodes using click chemistry. *Analytica Chimica Acta*, **708**, 37-43.
55. Xue, C., Han, Q., Wang, Y., Wu, J., Wen, T., Wang, R., Hong, J., Zhou, X., Jiang, H. (2013). Amperometric detection of dopamine in human serum by electrochemical sensor based on gold nanoparticles doped molecularly imprinted polymers. *Biosensors and Bioelectronics*, **49**, 199-203.
56. Wang, Z., Li, J., Liu, X., Yang, J., Lu, X. (2013). Preparation of an amperometric sensor for norfloxacin based on molecularly imprinted grafting photopolymerization. *Analytical and Bioanalytical Chemistry*, **405**, 2525-2533.
57. Huang, C.-Y., O'Hare, D., Chao, I.J., Wei, H.-W., Liang, Y.-F., Liu, B.-D., Lee, M.-H., Lin, H.-Y. (2015). Integrated potentiostat for electrochemical sensing of urinary 3-hydroxyanthranilic acid with molecularly imprinted poly(ethylene-co-vinyl alcohol). *Biosensors and Bioelectronics*, **67**, 208-213.

58. Des Azevedo, S., Lakshmi, D., Chianella, I., Whitcombe, M.J., Karim, K., Ivanova-Mitseva, P.K., Subrahmanyam, S., Piletsky, S.A. (2013). Molecularly imprinted polymer-hybrid electrochemical sensor for the detection of beta-estradiol. *Industrial and Engeneering Chemistry Research*, **52**, 13917-13923.
59. Guo, Z., Florea, A., Cristea, C., Bessueille, F., Vocanson, F., Goutaland, F., Zhang, A., Sandulescu, R., Lagarde, F., Jaffrezic-Renault, N. (2015). 1,3,5-Trinitrotoluene detection by a molecularly imprinted polymer sensor based on electropolymerization of a microporous-metal-organic framework. *Sensors and Actuators B: Chemical*, **207**, 960-966.
60. Wong, A., Foguel, M.V., Khan, S., Midori de Oliveira, F., Tarley, C.R.T., Sotomayor, M.D.P.T. (2015). Development of an electrochemical sensor modified with MWCNT-COOH and MIP for detection of diuron. *Electrochimica Acta*, **182**, 122-130.
61. Pandey, I., Jha, S.S. (2015). Molecularly imprinted polyaniline-ferrocene-sulfonic acid-Carbon dots modified pencil graphite electrodes for chiral selective sensing of D-Ascorbic acid and L-Ascorbic acid: A clinical biomarker for preeclampsia. *Electrochimica Acta*, **182**, 917-928.
62. Wang, X., Luo, C., Li, L., Duan, H. (2015). An ultrasensitive molecularly imprinted electrochemical sensor based on graphene oxide/carboxylated multiwalled carbon nanotube/ionic liquid/gold nanoparticle composites for vanillin analysis. *RSC Advances*, **5**, 92932-92939.
63. Sun, J., Ji, J., Wang, Y., Zhao, Y., Zhang, Y., Sun, X. (2015). Electrochemical sensor for determination of tulathromycin built with molecularly imprinted polymer film. *Analytical and Bioanalytical Chemistry*, **407**, 1951-1959.
64. Li, S., Yin, G., Wu, X., Liu, C., Luo, J. (2016). Supramolecular imprinted sensor for carbofuran detection based on a functionalized multiwalled carbon nanotube-supported Pd-Ir composite and methylene blue as catalyst. *Electrochimica Acta*, **188**, 294-300.

65. Xia, J., Cao, X., Wang, Z., Yang, M., Zhang, F., Lu, B., Li, F., Xia, L., Li, Y., Xia, Y. (2016). Molecularly imprinted electrochemical biosensor based on chitosan/ionic liquid-graphene composites modified electrode for determination of bovine serum albumin. *Sensors and Actuators B: Chemical*, **225**, 305-311.
66. Zhang, B., Liu, J., Ma, X., Zuo, P., Ye, B.-c., Li, Y. (2016). Ultrasensitive and selective assay of glutathione species in arsenic trioxide-treated leukemia HL-60 cell line by molecularly imprinted polymer decorated electrochemical sensors. *Biosensors and Bioelectronics*, **80**, 491-496.
67. Moreira, F.T.C., Ferreira, M.J.M.S., Puga, J.R.T., Sales, M.G.F. (2016). Screen-printed electrode produced by printed-circuit board technology. Application to cancer biomarker detection by means of plastic antibody as sensing material. *Sensors and Actuators B: Chemical*, **227**, 927-935.
68. Mazzotta, E., Turco, A., Chianella, I., Guerreiro, A., Piletsky, S.A., Malitesta, C. (2016). Solid-phase synthesis of electroactive nanoparticles of molecularly imprinted polymers. A novel platform for indirect electrochemical sensing applications. *Sensors and Actuators B: Chemical*, **229**, 174-180.
69. Kriz, D., Ansell, R.J. (2001). Biomimetic electrochemical sensors based on molecularly imprinted polymers. In *Molecularly Imprinted Polymers. Man made mimics of antibodies and their applications in analytical chemistry*, Sellergren, B. (ed.) Elsevier Science B.V., Amsterdam, pp. 417-436.
70. Wang, J. (2000). Controlled potential techniques. Pulse voltammetry. In *Analytical electrochemistry*, Wang, J. (ed.) Wiley-VCH, New York, pp. 67.
71. Chillawar, R., Tadi, K., Motghare, R. (2015). Voltammetric techniques at chemically modified electrodes. *Journal of Analytical Chemistry*, **70**, 399-418.
72. Wackerlig, J., Schirhagl, R. (2016). Applications of Molecularly Imprinted Polymer Nanoparticles and Their

Advances toward Industrial Use: A Review. *Analytical Chemistry*, **88**, 250-261.

73. Ye, L., Mosbach, K. (2002). Molecularly imprinted materials: towards the next generation. *Materials Research Society Symposium Proceedings*, **723**, 51-59.
74. Tokonami, S., Shiigi, H., Nagaoka, T. (2009). Review: Micro- and nanosized molecularly imprinted polymers for high-throughput analytical applications. *Analytica Chimica Acta*, **641**, 7-13.
75. Gao, D., Zhang, Z., Wu, M., Xie, C., Guan, G., Wang, D. (2007). A surface functional monomer-directing strategy for highly dense imprinting of TNT at surface of silica nanoparticles. *Journal of American Chemical Society*, **129**, 7859-7866.
76. Medina-Castillo, A.L., Fernández-Sanchez, J.F., Segura-Carretero, A., Fernández-Gutierrez, A. (2010). Micrometer and submicrometer particles prepared by precipitation polymerisation: thermodynamic model and experimental evidence of the relation between Flory's parameter and particle size. *Macromolecules*, **43**, 5804-5813.
77. Poma, A., Turner, A.P.F., Piletsky, S.A. (2010). Advances in the manufacture of MIP nanoparticles. *Trends in Biotechnology*, **28**, 629-637.
78. Yoshimatsu, K., Reimhult, K., Krozer, A., Mosbach, K., Sode, K., Ye, L. (2007). Uniform molecularly imprinted microspheres and nanoparticles prepared by precipitation polymerization: The control of particle size suitable for different analytical applications. *Analytica Chimica Acta*, **584**, 112-121.
79. Ye, L., Cormack, P.A.G., Mosbach, K. (1999). Molecularly imprinted monodisperse microspheres for competitive radioassay. *Analytical Communications*, **36**, 35-38.
80. Ye, L., Weiss, R., Mosbach, K. (2000). Synthesis and characterization of molecularly imprinted microspheres. *Macromolecules*, **33**, 8239-8245.
81. Khan, S., Bhatia, T., Trivedi, P., Satyanarayana, G.N.V., Mandrah, K., Saxena, P.N., Mudiam, M.K.R., Roy, S.K.

(2016). Selective solid-phase extraction using molecularly imprinted polymer as a sorbent for the analysis of fenarimol in food samples. *Food Chemistry*, **199**, 870-875.

82. Sheybani, S., Hosseinifar, T., Abdouss, M., Mazinani, S. (2015). Mesoporous molecularly imprinted polymer nanoparticles as a sustained release system of azithromycin. *RSC Advances*, **5**, 98880-98891.
83. Ashrafian, S., Ataei, S.A., Jahanshahi, M. (2015). Novel composite membranes embedded with molecularly imprinted porous polymeric nanospheres for targeted phenol. *Polymers for Advanced Technologies*, **DOI: 10.1002/pat.3716**.
84. Bagheri, H., Shirzadmehr, A., Rezaei, M. (2015). Designing and fabrication of new molecularly imprinted polymer-based potentiometric nano-graphene/ionic liquid/carbon paste electrode for the determination of losartan. *Journal of Molecular Liquids*, **212**, 96-102.
85. Li, P., Rong, F., Yuan, C. (2003). Morphologies and binding characteristics of molecularly imprinted polymers prepared by precipitation polymerization. *Polymer International*, **52**, 1799-1806.
86. Subrahmanyam, S., Guerreiro, A., Poma, A., Moczko, E., Piletska, E., Piletsky, S. (2013). Optimisation of experimental conditions for synthesis of high affinity MIP nanoparticles. *European Polymer Journal*, **49**, 100-105.
87. Wulff, G., Chong, B.-O., Kolb, U. (2006). Soluble single-molecule nanogels of controlled structure as a matrix for efficient artificial enzymes. *Angewandte Chemie International Edition*, **45**, 2955-2958.
88. Hoshino, Y., Kodama, T., Okahata, Y., Shea, K.J. (2008). Peptide imprinted polymer nanoparticles: A plastic antibody. *Journal of American Chemical Society*, **130**, 15242-15243.
89. Renkecz, T., Laszlo, K., Horvath, V. (2012). In situ synthesis of molecularly imprinted nanoparticles in porous support membranes using high-viscosity polymerization solvents. *Journal of Molecular Recognition*, **25**, 320-329.

90. Renkecz, T., Laszlo, K., Horvath, V. (2014). Molecularly imprinted microspheres prepared by precipitation polymerization at high monomer concentrations. *Molecular Imprinting*, **2**, 1-17.
91. Flavin, K., Resmini, M. (2009). Imprinted nanomaterials: a new class of synthetic receptors. *Analytical and Bioanalytical Chemistry*, **393**, 437-444.
92. Vaihinger, D., Landfester, K., Krauter, I., Brunner, H., Tovar, G.E.M. (2002). Molecularly imprinted polymer nanospheres as synthetic affinity receptors obtained by miniemulsion polymerisation. *Macromolecular Chemistry and Physics*, **203**, 1965-1973.
93. Chern, C.S. (2006). Emulsion polymerization mechanisms and kinetics. *Progress in Polymer Science*, **31**, 443-486.
94. Dvorakova, G., Haschick, R., Kappler, M., Muellen, K., Biffis, A. (2013). Nonaqueous emulsion polymerisation: a practical synthetic route for the production of molecularly imprinted nanospheres. *Journal of Polymer Science Part A: Polymer Chemistry*, **51**, 267-274.
95. Slomkowski, S., Aleman, J.V., Gilbert, R.G., Hess, M., Horie, K., Jones, R.G., Kubisa, P., Meisel, I., Mormann, W., Penczek, S., Stepto, R.F.T. (2011). Terminology of polymers and polymerization processes in dispersed systems (IUPAC recommendations 2011). *Pure and Applied Chemistry*, **83**, 2229-2259.
96. Poma, A., Guerreiro, A., Whitcombe, M.J., Piletska, E.V., Turner, A.P.F., Piletsky, S.A. (2013). Solid-phase synthesis of molecularly imprinted polymer nanoparticles with a reusable template-"plastic antibodies". *Advanced Functional Materials*, **23**, 2821-2827.
97. Ambrosini, S., Beyazit, S., Haupt, K., Tse Sum Bui, B. (2013). Solid-phase synthesis of molecularly imprinted nanoparticles for protein recognition. *Chemical Communications*, **49**, 6746-6748.
98. Canfarotta, F., Poma, A., Guerreiro, A., Piletsky, S. (2016). Solid-phase synthesis of molecularly imprinted nanoparticles. *Nature Protocols*, **11**, 443-455.

99. Guerreiro, A.R., Chianella, I., Piletska, E., Whitcombe, M.J., Piletsky, S.A. (2009). Selection of imprinted nanoparticles by affinity chromatography. *Biosensors and Bioelectronics*, **24**, 2740-2743.
100. Moczko, E., Poma, A., Guerreiro, A., Perez de Vargas Sansalvador, I., Caygill, S., Canfarotta, F., Whitcombe, M.J., Piletsky, S. (2013). Surface-modified multifunctional MIP nanoparticles. *Nanoscale*, **5**, 3733-3741.
101. Xu, J., Ambrosini, S., Tamahkar, E., Rossi, C., Haupt, K., Tse Sum Bui, B. (2016). Toward a universal method for preparing molecularly imprinted polymer nanoparticles with antibody-like affinity for proteins. *Biomacromolecules*, **17**, 345-353.
102. Altintas, Z., Gittens, M., Guerreiro, A., Thompson, K.-A., Walker, J., Piletsky, S., Tothill, I.E. (2015). Detection of waterborne viruses using high affinity molecularly imprinted polymers. *Analytical Chemistry*, **87**, 6801-6807.
103. Poma, A., Guerreiro, A., Caygill, S., Moczko, E., Piletsky, S. (2014). Automatic reactor for solid-phase synthesis of molecularly imprinted polymeric nanoparticles (MIP NPs) in water. *RSC Advances*, **4**, 4203-4206.
104. Chianella, I., Guerreiro, A., Moczko, E., Caygill, J.S., Piletska, E.V., De Vargas Sansalvador, I.M.P., Whitcombe, M.J., Piletsky, S.A. (2013). Direct replacement of antibodies with molecularly imprinted polymer nanoparticles in ELISA-development of a novel assay for vancomycin. *Analytical Chemistry*, **85**, 8462-8468.
105. Caceres, C., Canfarotta, F., Chianella, I., Pereira, E., Moczko, E., Esen, C., Guerreiro, A., Piletska, E., Whitcombe, M.J., Piletsky, S.A. (2016). Does size matter? Study of performance of pseudo-ELISAs based on molecularly imprinted polymer nanoparticles prepared for analytes of different sizes. *Analyst*, **141**, 1405-1412.
106. Korposh, S., Chianella, I., Guerreiro, A., Caygill, S., Piletsky, S., James, S.W., Tatam, R.P. (2014). Selective vancomycin detection using optical fibre long period gratings

functionalised with molecularly imprinted polymer nanoparticles. *Analyst*, **139**, 2229-2236.

107. Altintas, Z., Guerreiro, A., Piletsky, S.A., Tothill, I.E. (2015). NanoMIP based optical sensor for pharmaceuticals monitoring. *Sensors and Actuators B: Chemical*, **213**, 305-313.
108. Guerreiro, A., Poma, A., Karim, K., Moczko, E., Takarada, J., de Vargas-Sansalvador, I.P., Turner, N., Piletska, E., de Magalhães, C.S., Glazova, N., Serkova, A., Omelianova, A., Piletsky, S. (2014). Influence of surface-imprinted nanoparticles on trypsin activity. *Advanced Healthcare Materials*, **3**, 1426-1429.
109. Brahmbhatt, H., Poma, A., Pendergraff, H.M., Watts, J.K., Turner, N.W. (2016). Improvement of DNA recognition through molecular imprinting: hybrid oligomer imprinted polymeric nanoparticles (oligoMIP NPs). *Biomaterials Science*, **4**, 281-287.
110. Poma, A., Brahmbhatt, H., Pendergraff, H.M., Watts, J.K., Turner, N.W. (2014). Generation of novel hybrid aptamer-molecularly imprinted polymeric nanoparticles. *Advanced Materials*, **27**, 1478-1478.
111. Poma, A., Brahmbhatt, H., Watts, J.K., Turner, N.W. (2014). Nucleoside-tailored molecularly imprinted polymeric nanoparticles (MIP NPs). *Macromolecules*, **47**, 6322-6330.
112. Uzun, L., Turner, A.P.F. (2015). Molecularly-imprinted polymer sensors: realising their potential. *Biosensors Bioelectronics*, **76**, 131-144.
113. Wackerlig, J., Lieberzeit, P.A. (2015). Molecularly imprinted polymer nanoparticles in chemical sensing: Synthesis, characterisation and application. *Sensors and Actuators B: Chemical*, **207, Part A**, 144-157.
114. Holthoff, E.L., Stratis-Cullum, D.N., Hankus, M.E. (2011). A nanosensor for TNT detection based on molecularly imprinted polymers and surface enhanced Raman scattering. *Sensors*, **11**, 2700-2714.
115. Uzun, L., Uzek, R., Senel, S., Say, R., Denizli, A. (2013). Chiral recognition of proteins having L-histidine residues on the

surface with lanthanide ion complex incorporated-molecularly imprinted fluorescent nanoparticles. *Material Science and Engineering C*, **33**, 3432-3439.

116. Chang, L., Ding, Y., Li, X. (2013). Surface molecular imprinting onto silver microspheres for surface enhanced Raman scattering applications. *Biosensors and Bioelectronics*, **50**, 106-110.
117. Cennamo, N., Dona, A., Pallavicini, P., D'Agostino, G., Dacarro, G., Zeni, L., Pesavento, M. (2015). Sensitive detection of 2,4,6-trinitrotoluene by tridimensional monitoring of molecularly imprinted polymer with optical fiber and five-branched gold nanostars. *Sensors and Actuators B: Chemical*, **208**, 291-298.
118. Wan, W., Biyikal, M., Wagner, R., Sellergren, B., Rurack, K. (2013). Fluorescent sensory microparticles that "light-up" consisting of a silica core and a molecularly imprinted polymer (MIP) shell. *Angewandte Chemie International Edition*, **52**, 7023-7027.
119. Feng, X., Gan, N., Zhou, J., Li, T., Cao, Y., Hu, F., Yu, H., Jiang, Q. (2014). A novel dual-template molecularly imprinted electrochemiluminescence immunosensor array using Ru(bpy)2+3-Silica@Poly-L-lysine-Au composite nanoparticles as labels for near-simultaneous detection of tumor markers. *Electrochimica Acta*, **139**, 127-136.
120. Liu, H., Fang, G., Wang, S. (2014). Molecularly imprinted optosensing material based on hydrophobic CdSe quantum dots via a reverse microemulsion for specific recognition of ractopamine. *Biosensors and Bioelectronics*, **55**, 127-132.
121. Liu, H., Fang, G., Zhu, H., Wang, S. (2013). Application of molecularly imprinted polymer appended onto CdSe/ZnS quantum dots for optosensing of tocopherol in rice. *Food Analytical Methods*, **7**, 1443-1450.
122. Tan, L., Huang, C., Peng, R., Tang, Y., Li, W. (2014). Development of hybrid organic-inorganic surface imprinted Mn-doped ZnS QDs and their application as a sensing material for target proteins. *Biosensors and Bioelectronics*, **61**, 506-511.

123. Tan, L., Kang, C., Xu, S., Tang, Y. (2014). Selective room temperature phosphorescence sensing of target protein using Mn-doped ZnS QDs-embedded molecularly imprinted polymer. *Biosensors and Bioelectronics*, **48**, 216-223.
124. Chen, P.-Y., Nien, P.-C., Hu, C.-W., Ho, K.-C. (2010). Detection of uric acid based on multi-walled carbon nanotubes polymerized with a layer of molecularly imprinted PMAA. *Sensors and Actuators B: Chemical*, **146**, 466-471.
125. Prasad, B.B., Madhuri, R., Tiwari, M.P., Sharma, P.S. (2010). Imprinting molecular recognition sites on multiwalled carbon nanotubes surface for electrochemical detection of insulin in real samples. *Electrochimica Acta*, **55**, 9146-9156.
126. Peeters, M., Kobben, S., Jimenez-Monroy, K.L., Modesto, L., Kraus, M., Vandenryt, T., Gaulke, A., van Grinsven, B., Ingebrandt, S., Junkers, T., Wagner, P. (2014). Thermal detection of histamine with a graphene oxide based molecularly imprinted polymer platform prepared by reversible addition-fragmentation chain transfer polymerization. *Sensors and Actuators B: Chemical*, **203**, 527-535.
127. Qiu, H., Luo, C., Sun, M., Lu, F., Fan, L., Li, X. (2012). A chemiluminescence array sensor based on graphene-magnetite-molecularly imprinted polymers for determination of benzenediol isomers. *Analytica Chimica Acta*, **744**, 75-81.
128. Qiu, H., Luo, C., Sun, M., Lu, F., Fan, L., Li, X. (2012). A chemiluminescence sensor for determination of epinephrine using graphene oxide-magnetite-molecularly imprinted polymers. *Carbon*, **50**, 4052-4060.
129. Anirudhan, T.S., Alexander, S. (2014). Multiwalled carbon nanotube based molecular imprinted polymer for trace determination of 2,4-dichlorophenoxyacetic acid in natural water samples using a potentiometric method. *Applied Surface Science*, **303**, 180-186.
130. Madrakian, T., Haryani, R., Ahmadi, M., Afkhami, A. (2016). A sensitive electrochemical sensor for rapid and selective

determination of venlafaxine in biological fluids using carbon paste electrode modified with molecularly imprinted polymer-coated magnetite nanoparticles. *Journal of Iranian Chemical Society*, **13**, 243-251.

131. Zhu, L., Cao, Y., Cao, G. (2014). Electrochemical sensor based on magnetic molecularly imprinted nanoparticles at surfactant modified magnetic electrode for determination of bisphenol A. *Biosensors and Bioelectronics*, **54**, 258-261.
132. Jin, G., Li, W., Yu, S., Peng, Y., Kong, J. (2008). Novel superparamagnetic core-shell molecular imprinting microspheres towards high selective sensing. *Analyst*, **133**, 1367-1372.
133. Zamora-Galvez, A., Ait-Lahcen, A., Mercante, L.A., Morales-Narvaez, E., Amine, A., Merkoci, A. (2016). Molecularly imprinted polymer-decorated magnetite nanoparticles for selective sulfonamide detection. *Analytical Chemistry*, **88**, 3578-3584.
134. Ahmad, R., Griffete, N., Lamouri, A., Felidj, N., Chehimi, M.M., Mangeney, C. (2015). Nanocomposites of gold nanoparticles@molecularly imprinted polymers: chemistry, processing, and applications in sensors. *Chemistry of Materials*, **27**, 5464-5478.
135. Yu, D., Zeng, Y., Qi, Y., Zhou, T., Shi, G. (2012). A novel electrochemical sensor for determination of dopamine based on AuNPs@SiO2 core-shell imprinted composite. *Biosensors and Bioelectronics*, **38**, 270-277.
136. Li, H., Wang, Z., Wu, B., Liu, X., Xue, Z., Lu, X. (2012). Rapid and sensitive detection of methyl-parathion pesticide with an electropolymerized, molecularly imprinted polymer capacitive sensor. *Electrochimica Acta*, **62**, 319-326.
137. Altintas, Z., France, B., Ortiz, J.O., Tothill, I.E. (2016). Computationally modelled receptors for drug monitoring using an optical based biomimetic SPR sensor. *Sensors and Actuators B: Chemical*, **224**, 726-737.
138. Abdin, M.J., Altintas, Z., Tothill, I.E. (2015). In silico designed nanoMIP based optical sensor for endotoxins monitoring. *Biosensors and Bioelectronics*, **67**, 177-183.

139. Shutov, R.V., Guerreiro, A., Moczko, E., de Vargas-Sansalvador, I.P., Chianella, I., Whitcombe, M.J., Piletsky, S.A. (2014). Introducing MINA - The Molecularly Imprinted Nanoparticle Assay. *Small*, **10**, 1086-1089.
140. Abu-Dalo, M.A., Al-Rawashdeh, N.A.F., Al-Mheidat, I.R., Nassory, N.S. (2016). Preparation and evaluation of new uranyl imprinted polymer electrode sensor for uranyl ion based on uranyl-carboxybezotriazole complex in PVC matrix membrane. *Sensors and Actuators B: Chemical*, **227**, 336-345.
141. Alizadeh, T., Akbari, A. (2013). A capacitive biosensor for ultra-trace level urea determination based on nano-sized urea-imprinted polymer receptors coated on graphite electrode surface. *Biosensors and Bioelectronics*, **43**, 21-327.
142. Alizadeh, T., Ganjali, M.R., Akhoundian, M., Norouzi, P. (2016). Voltammetric determination of ultratrace levels of cerium(III) using a carbon paste electrode modified with nano-sized cerium-imprinted polymer and multiwalled carbon nanotubes. *Microchimica Acta*, **183**, 1123-1130.
143. Zia, A.I., Mukhopadhyay, S.C., Yu, P.-L., Al-Bahadly, I.H., Gooneratne, C.P., Kosel, J. (2015). Rapid and molecular selective electrochemical sensing of phthalates in aqueous solution. *Biosensors and Bioelectronics*, **67**, 342-349.
144. Murugan, P., Krishnamurthy, M., Jaisankar, S.N., Samanta, D., Mandal, A.B. (2015). Controlled decoration of the surface with macromolecules: polymerization on a self-assembled monolayer (SAM). *Chemical Society Reviews*, **44**, 3212-3243.
145. Justino, C.I.L., Freitas, A.C., Pereira, R., Duarte, A.C., Rocha Santos, T.A.P. (2015). Recent developments in recognition elements for chemical sensors and biosensors. *Trends in Analytical Chemistry*, **68**, 2-17.
146. Lakshmi, D., Bossi, A., Whitcombe, M.J., Chianella, I., Fowler, S.A., Subrahmanyam, S., Piletska, E.V., Piletsky, S.A. (2009). Electrochemical sensor for catechol and dopamine based on a catalytic molecularly imprinted polymer-

conducting polymer hybrid recognition element. *Analytical Chemistry*, **81**, 3576-3584.

147. Gholivand, M.B., Karimian, N. (2015). Fabrication of a highly selective and sensitive voltammetric ganciclovir sensor based on electropolymerized molecularly imprinted polymer and gold nanoparticles on multiwall carbon nanotubes/glassy carbon electrode. *Sensors and Actuators B: Chemical*, **215**, 471-479.
148. Gholivand, M.B., Torkashvand, M. (2016). The fabrication of a new electrochemical sensor based on electropolymerization of nanocomposite gold nanoparticle-molecularly imprinted polymer for determination of valganciclovir. *Material Science and Engineering, C*, **59**, 594-603.
149. Schweiger, B., Kim, J., Kim, Y.J., Ulbricht, M. (2015). Electropolymerized molecularly imprinted polypyrrole film for sensing of clofibric acid. *Sensors*, **15**, 4870-4889.
150. Li, X., He, Y., Zhao, F., Zhang, W., Ye, Z. (2015). Molecularly imprinted polymer-based sensors for atrazine detection by electropolymerization of o-phenylenediamine. *RSC Advances*, **5**, 56534-56540.
151. Peng, Y., Wu, Z., Liu, Z. (2015). An electrochemical sensor for paracetamol based on an electropolymerized molecularly imprinted o-phenylenediamine film on a multi-walled carbon nanotube modified glassy carbon electrode. *Analytical Methods*, **6**, 5673-5681.
152. Wang, Q., Paim, L.L., Zhang, X., Wang, S., Stradiotto, N.R. (2014). An electrochemical sensor for reducing sugars based on a glassy carbon electrode modified with electropolymerized molecularly imprinted poly-o-phenylenediamine film. *Electroanalysis*, **26**, 1612-1622.
153. Pellicer, C., Gomez-Caballero, A., Unceta, N., Goicolea, M.A., Barrio, R.J. (2010). Using a portable device based on a screen-printed sensor modified with a molecularly imprinted polymer for the determination of the insecticide fenitrothion in forest samples. *Analytical Methods*, **2**, 1280-1285.

154. Gomez-Caballero, A., Ugarte, A., Sanchez-Ortega, A., Unceta, N., Goicolea, M.A., Barrio, R.J. (2010). Molecularly imprinted poly[tetra(o-aminophenyl)porphyrin] as a stable and selective coating for the development of voltammetric sensors. *Journal of Electroanalytical Chemistry*, **638**, 246-253.
155. Fu, X.-C., Chen, X., Guo, Z., Xie, C.-G., Kong, L.-T., Liu, J.-H., Huang, X.-J. (2011). Stripping voltammetric detection of mercury(II) based on a surface ion imprinting strategy in electropolymerized microporous poly(2-mercaptobenzothiazole) films modified glassy carbon electrode. *Analytica Chimica Acta*, **685**, 21-28.
156. Fu, X.-C., Wu, J., Nie, L., Xie, C.-G., Liu, J.-H., Huang, X.-J. (2012). Electropolymerized surface ion imprinting films on a gold nanoparticles/single-wall carbon nanotube nanohybrids modified glassy carbon electrode for electrochemical detection of trace mercury(II) in water. *Analytica Chimica Acta*, **720**, 29-37.
157. Riskin, M., Tel-Vered, R., Willner, I. (2007). The imprint of electropolymerized polyphenol films on electrodes by donor-acceptor interactions: selective electrochemical sensing of N,N'-dimethyl-4,4'-bipyridinium (methyl viologen). *Advanced Functional Materials*, **17**, 3858-3863.
158. Gomez-Caballero, A., Goicolea, M.A., Barrio, R.J. (2005). Paracetamol voltammetric microsensors based on electrocopolymerized-molecularly imprinted film modified carbon fiber microelectrodes. *Analyst*, **130**, 1012-1018.
159. Gomez-Caballero, A., Unceta, N., Goicolea, M.A., Barrio, R.J. (2008). Evaluation of the selective detection of 4,6-dinitro-o-cresol by a molecularly imprinted polymer based microsensor electrosynthesized in a semiorganic media. *Sensors and Actuators B: Chemical*, **130**, 713-722.
160. Gomez-Caballero, A., Unceta, N., Goicolea, M.A., Barrio, R.J. (2007). Voltammetric determination of metamitron with an electrogenerated molecularly imprinted polymer microsensor. *Electroanalysis*, **19**, 356-363.

161. Karimian, N., Gholivand, M.B., Taherkhani, F. (2015). Computational design and development of a novel voltammetric sensor for minoxidil detection based on electropolymerized molecularly imprinted polymer. *Journal of Electroanalytical Chemistry*, **740**, 45-52.
162. Yan, X., Deng, J., Xu, J., Li, H., Wang, L., Chen, D., Xie, J. (2012). A novel electrochemical sensor for isocarbophos based on a glassy carbon electrode modified with electropolymerized molecularly imprinted terpolymer. *Sensors and Actuators B: Chemical*, **171-172**, 1087-1094.
163. Apodaca, D.C., Pernites, R.B., Ponnapati, R., Del Mundo, F.R., Advincula, R.C. (2011). Electropolymerized molecularly imprinted polymer film: EIS sensing of bisphenol A. *Macromolecules*, **44**, 6669-6682.
164. Moreira, F.T.C., Dutra, R.A.F., Noronha, J.P.C., Fernandes, J.C.S., Sales, M.G.F. (2013). Novel biosensing device for point-of-care applications with plastic antibodies grown on Au-screen printed electrodes. *Sensors and Actuators B: Chemical*, **182**, 733-740.
165. Pan, G., Zhang, Y., Guo, X., Li, C., Zhang, H. (2010). An efficient approach to obtaining water-compatible and stimuli-responsive molecularly imprinted polymers by the facile surface-grafting of functional polymer brushes via RAFT polymerization. *Biosensors and Bioelectronics*, **26**, 976-982.
166. Jenkins, A.D., Jones, R.G., Moad, G. (2010). Terminology for reversible-deactivation radical polymerization previously called "controlled" radical or "living" radical polymerization (IUPAC Recommendations 2010). *Pure and Applied Chemistry*, **82**, 483-491.
167. Otsu, T., Matsumoto, A. (1998). Controlled synthesis of polymers using the iniferter technique: developments in living radical polymerisation. In *Microencapsulation/Microgels/Iniferters*, DiMari, S., Funke, W., Haralson, M.A., Hunkeler, D., Joos-Müller, B., Matsumoto, A., Okay, O., Otsu, T., Powers, A.C., Prokop, A.,

Wang, T.G. and Whitesell, R.R. (eds.) Srpinger, Heidelberg, pp. 75-139.

168. Sellergren, B., Hall, A.J. (2001). Fundamental aspects on the synthesis and characterisation of imprinted network polymers. In *Molecularly Imprinted Polymers Man-made Mimics of Antibodies and their Applications in Analytical Chemistry*, Börje, S. (ed.) Elsevier, Amsterdam, Vol. Volume 23, pp. 21-57.
169. Moad, G., Salomon, D.H. (2006). Living radical polymerisation. In *The chemistry of radical polymerisation*, Moad, G. and Salomon, D.H. (eds.) Elsevier, Oxford, pp. 451-585.
170. Lu, C.-H., Zhou, W.-H., Han, B., Yang, H.-H., Chen, X., Wang, X.-R. (2007). Surface-imprinted core-shell nanoparticles for sorbent assays. *Analytical Chemistry*, **79**, 5457-5461.
171. Zhang, H. (2013). Controlled/"living" radical precipitation polymerization: A versatile polymerization technique for advanced functional polymers. *European Polymer Journal*, **49**, 579-600.
172. Otsu, T., Matsunaga, T., Kuriyama, A., Yoshioka, M. (1989). Living radical polymerization through the use of iniferters: controlled synthesis of polymers. *European Polymer Journal*, **25**, 643-650.
173. Hawker, C.J., Bosman, A.W., Harth, E. (2001). New polymer synthesis by nitroxide mediated living radical polymerizations. *Chemical Reviews*, **101**, 3661-3688.
174. Matyjaszewski, K., Xia, J. (2001). Atom transfer radical polymerization. *Chemical Reviews*, **101**, 2921-2990.
175. Kamigaito, M., Ando, T., Sawamoto, M. (2001). Metal-catalyzed living radical polymerization. *Chemical Reviews*, **101**, 3689-3746.
176. Moad, G., Rizzardo, E., Thang, S.H. (2008). Radical additional-fragmentation chemistry in polymer synthesis. *Polymer*, **49**, 1079-1131.
177. Stuart, B.H. (2004). Polymers. In *Infrared spectroscopy. Fundamentals and applications*, Stuart, B.H. (ed.) John Wiley & Sons, Chichester, pp. 113-135.

178. Fuchs, Y., Soppera, O., Haupt, K. (2012). Photopolymerization and photostructuring of molecularly imprinted polymers for sensor applications. A review. *Analytica Chimica Acta*, **717**, 7-20.
179. Otsu, T., Yoshida, M. (1982). Role of initiator-transfer agent-terminator (iniferter) in radical polymerizations: Polymer design by organic disulfides as iniferters. *Die Makromolekulare Chemie, Rapid Communications*, **3**, 127-132.
180. Li, J., Zu, B., Zhang, Y., Guo, X., Zhang, H. (2010). One-pot synthesis of surface-functionalized molecularly imprinted polymer microspheres by iniferter-induced "living" radical precipitation polymerization. *Journal of Polymer Science Part A: Polymer Chemistry*, **48**, 3217-3228.
181. Song, R.-y., Hu, X.-l., Guan, P., Li, J., Qian, L.-w., Wang, Q.-l. (2015). Synthesis of glutathione imprinted polymer particles via controlled living radical precipitation polymerization. *Chinese Journal Polymer Science*, **33**, 404-415.
182. Martins, N., Carreiro, E.P., Simoes, M., Cabrita, M.J., Burke, A.J., Garcia, R. (2015). An emerging approach for the targeting analysis of dimethoate in olive oil: The role of molecularly imprinted polymers based on photo-iniferter induced “living” radical polymerization. *Reactive and Functional Polymers*, **86**, 37-46.
183. Gutiérrez-Climente, R., Gómez-Caballero, A., Halhalli, M., Sellergren, B., Goicolea, M.A., Barrio, R.J. (2016). Iniferter-mediated grafting of molecularly imprinted polymers on porous silica beads for the enantiomeric resolution of drugs. *Journal of Molecular Recognition*, **29**, 106-114.
184. Singh, M., Tarannum, N., Kumar, A. (2014). Selective recognition of fenbufen by surface-imprinted silica with iniferter technique. *Journal of Porous Materials*, **21**, 677-684.
185. Ruckert, B., Hall, A.J., Sellergren, B. (2002). Molecularly imprinted composite materials via iniferter-modified supports. *Journal of Materials Chemistry*, **12**, 2275-2280.

186. Ahmad, R., Felidj, N., Boubekeur-Lecaque, L., Lau-Truong, S., Gam-Derouich, S., Decorse, P., Lamouri, A., Mangeney, C. (2015). Water-soluble plasmonic nanosensors with synthetic receptors for label-free detection of folic acid. *Chemical Communications*, **51**, 9678-9681.
187. Patra, S., Roy, E., Madhuri, R., Sharma, P.K. (2015). Nano-iniferter based imprinted sensor for ultra trace level detection of prostate-specific antigen in both men and women. *Biosensors and Bioelectronics*, **66**, 1-10.
188. Liu, W., Qin, L., Yang, Y., Liu, X., Xu, B. (2014). Synthesis and characterization of dibenzothiophene imprinted polymers on the surface of iniferter-modified carbon microspheres. *Materialas Chemistry and Physics*, **148**, 605-613.
189. Bali Prasad, B., Jauhari, D., Prasad Tiwari, M. (2013). A dual-template imprinted polymer-modified carbon ceramic electrode for ultra trace simultaneous analysis of ascorbic acid and dopamine. *Biosensors and Bioelectronics*, **50**, 19-27.
190. Perrier, S., Takolpuckdee, P. (2005). Macromolecular design via reversible addition–fragmentation chain transfer (RAFT)/xanthates (MADIX) polymerization. *Journal of Polymer Science Part A: Polymer Chemistry*, **43**, 5347-5393.
191. McLeary, J.B., Klumperman, B. (2006). RAFT mediated polymerization in heterogeneous media. *Soft Matter*, **2**, 45-53.
192. Chiefari, J., Chong, Y.K., Ercole, F., Krstina, J., Jeffery, J., Le, T.P.T., Mayadunne, R.T.A., Meijs, G.F., Moad, C.L., Moad, G., Rizzardo, E., Thang, S.H. (1998). Living free-radical polymerization by reversible addition-fragmentation chain transfer: The RAFT process. *Macromolecules*, **31**, 5559-5562.
193. Niu, H., Yang, Y., Zhang, H. (2015). Efficient one-pot synthesis of hydrophilic and fluorescent molecularly imprinted polymer nanoparticles for direct drug quantification in real biological samples. *Biosensors and Bioelectronics*, **74**, 440-446.

194. Kamra, T., Zhou, T., Montelius, L., Schnadt, J., Ye, L. (2015). Implementation of molecularly imprinted polymer beads for surface enhanced Raman detection. *Analytical Chemistry*, **87**, 5056-5061.
195. Ma, Y., Zhang, Y., Zhao, M., Guo, X., Zhang, H. (2013). Narrowly dispersed molecularly imprinted polymer microspheres with photo- and thermo-responsive template binding properties in pure aqueous media by RAFT polymerization. *Molecular Imprinting*, **1**, 3-16.
196. Xie, X., Chen, L., Pan, X., Wang, S. (2015). Synthesis of magnetic molecularly imprinted polymers by reversible addition fragmentation chain transfer strategy and its application in the Sudan dyes residue analysis. *Journal of Chromatography A*, **1405**, 32-39.
197. He, Y., Huang, Y., Jin, Y., Liu, X., Liu, G., Zhao, R. (2014). Well-Defined Nanostructured Surface-Imprinted Polymers for Highly Selective Magnetic Separation of Fluoroquinolones in Human Urine. *ACS Applied Materials & Interfaces*, **6**, 9634-9642.
198. Li, Y., Zhao, X., Li, P., Huang, Y., Wang, J., Zhang, J. (2015). Highly sensitive Fe3O4 nanobeads/graphene-based molecularly imprinted electrochemical sensor for 17beta-estradiol in water. *Analytica Chimica Acta*, **884**, 106-113.
199. Halhalli, M.R., Schillinger, E., Aureliano, C.S.A., Sellergren, B. (2013). Thin walled imprinted polymer beads featuring both uniform and accessible binding sites. *Chemistry of Materials*, **24**, 2909-2919.
200. Guo, Y., Yang, Y., Zhang, L., Guo, T.Y. (2011). Core/shell molecular imprinting microparticles prepared using RAFT technology for degradation of paraoxon. *Macromolecular Research*, **19**, 1202-1209.
201. Fischer, L.M., Tenje, M., Heiskanen, A.R., Masuda, N., Castillo, J., Bentien, A., Emneus, J., Jakobsen, M.H., Boisen, A. (2009). Gold cleaning methods for electrochemical detection applications. *Microelectronic Engineering*, **86**, 1282-1285.

202. Tielens, F., Santos, E. (2010). AuS and SH Bond Formation/Breaking during the Formation of Alkanethiol SAMs on Au(111): A Theoretical Study. *Journal of Physical Chemistry C*, **114**, 9444-9452.
203. Xue, Y., Li, X., Li, H., Zhang, W. (2014). Quantifying thiol-gold interactions towards the efficient strength control. *Nature Communications*, **5**, 4348.
204. Bossi, A., Whitcombe, M.J., Uludag, Y., Fowler, S., Chianella, I., Subrahmanyam, S., Sanchez, I., Piletsky, S.A. (2010). Synthesis of controlled polymeric cross-linked coatings via iniferter polymerization in the presence of tetraethyl thiuram disulphide chain terminator. *Biosensors and Bioelectronics*, **25**, 2149-2155.
205. Monk, P.M.S. (2002). Linear sweep voltammetry and cyclic voltammetry at solid electrodes. In *Fundamentals of Electroanalytichal Chemistry*, John Whiley and Sons LTD, Chichester, pp. 156-176.
206. Wang, J. (2000). Study of electrode reactions. In *Analytical electrochemistry*, Wiley-VCH, pp. 28-44.
207. Fernandez-Sanchez, C., McNeil, C.J., Rawson, K. (2005). Electrochemical impedance spectroscopy studies of polymer degradation: application to biosensor development. *Trends in Analytical Chemistry*, **24**, 37-48.
208. Campuzano, S., Pedrero, M., Montemayor, C., Fatas, E., Pingarron, J.M. (2006). Characterization of alkanethiol-self-assembled monolayers-modified gold electrodes by electrochemical impedance spectroscopy. *Journal of Electroanalytical Chemistry*, **586**, 112-121.
209. Ahmad, A., Moore, E. (2012). Electrochemical immunosensor modified with self-assembled monolayer of 11-mercaptoundecanoic acid on gold electrodes for detection of benzo[a]pyrene in water. *Analyst*, **137**, 5839-5844.
210. Bernalte, E., Marin-Sanchez, C., Pinilla-Gil, E., Brett, C.M.A. (2013). Characterisation of screen-printed gold and gold nanoparticle-modified carbon sensors by electrochemical

impedance spectroscopy. *Journal of Electroanalytical Chemistry*, **709**, 70-76.

211. Motaghedifard, M., Ghoreishi, S.M., Behpour, M., Moghadam, Z., Salavati-Niasari, M. (2012). Electrochemical study of new self-assembled monolayer of 2-hydroxy-N'1-[(E)-1-(3-methyl-2-thienyl)methylidene] benzohydrazide on gold electrode as an epinephrine sensor element. *Journal of Electroanalytical Chemistry*, **682**, 14-22.
212. Gamry Instruments (2010). Application Note Rev. 1.0. Basics of Electrochemical Impedance Spectroscopy. *Gamry Instruments Inc. Warminster (Pensylvania)*.
213. Monk, P.M.S. (2002). Electroanalytical measurements involving impedance. In *Fundamentals of Electroanalytichal Chemistry*, John Whiley and Sons LTD, Chichester, pp. 253-270.
214. Pingarrón, J.M., Sánchez, P. (1999). Principios básicos de la electroquímica analítica. In *Química electroanalítica*, Editorial Síntesis S.A., Madrid, pp. 25-43.
215. Schmickler, W. (2012). Double layer capacity. In Bard, A.J., Inzelt, G. and Scholz, F. (eds.), *Electrochemical dictionary*. Springer, Berlin, pp. 230.
216. Autolab application note (2011). EIS Part 3, Data analysis. *Metrohm Autolab B.V. Utrecht (The Netherlands)*.
217. Raistrick, I.D., Franceschetti, D.R., Macdonald, R.J. (2005). Physical and electrochemical models. In *Impedance Spectroscopy*, Barsoukov, E. and Macdonald, R.J. (eds.) John Wiley and Sons LTD, New Jersey, pp. 80-117.
218. Lasia, A. (2014). Modeling of experimental data (Methods for finding the best parameters). In *Electrochemical Impedance Spectroscopy and its Applications*, Springer Science+Business Media, New York, pp. 311.
219. Lillethorup, M., Torbensen, K., Ceccato, M., Pedersen, S.U., Daasbjerg, K. (2013). Electron transport through a diazonium-based initiator layer to covalently attached polymer brushes of ferrocenylmethyl methacrylate. *Langmuir*, **29**, 13595-13604.

220. Chechik, V., Crooks, R.M., Stirling, C.J.M. (2000). Reactions and reactivity in self-assembled monolayers. *Advanced Materials*, **12**, 1161-1171.

Chapter 5

GENERAL CONCLUSIONS

General conclusions

Based on the objectives established previously and in compliance with the results presented along this thesis, it can be concluded that synthetic receptors based on molecular imprinting technology, have been successfully synthesised and applied to different analytical techniques. These receptors have been used for the extraction and separation of 4-ethylphenol and the compounds belonging to its metabolic pathway and for the sensing of 4-ethylphenol.

In the first part of this work, it has been developed a method based on molecularly imprinted polymers for the extraction and chromatographic separation of 4-ethylphenol and the compounds that belong to its metabolic pathway in wine samples. To this end, two different molecularly imprinted polymers have been developed. First, a 4-ethylphenol imprinted polymer has been used as sorbent for solid phase extraction of the target compounds from wine. Subsequently, the obtained eluates have been analysed using a chromatographic column with coumaric acid imprinted polymer as the solid phase in liquid chromatography with fluorescence and diode array detectors. The developed method has been proved to be applicable on the extraction, chromatographic separation and quantification of 4-ethylphenol

and the compounds that belong to its metabolic pathway in wine samples.

On the other hand the research carried out during this thesis has been also focused on the development of syntethic receptors for voltammetric sensing of 4-ethylphenol. For this purpose, different strategies based on Reversible Deactivation Radical Polymerisation have been employed for the modification of gold surfaces to be used as sensing elements. Initially, a 4-ethylphenol specific sensor has been developed by the grafting from approach, obtaining gold microelectrode surface coated with MIP films. Alternatively, imprinted nanoparticles synthesised by solid phase approach were immobilised on gold electrode surface using the grafting to approach.

Although sensors developed by both strategies showed an improvement of the selectivity comparing to the bare gold electrodes, the sensor with the grafted nanoparticles resulted more sensible and selective for 4-ethylphenol voltammetric measurements. However, analytical evaluation of the sensors demonstrated that the two development strategies, grafting from and grafting to of imprinted polymers on gold electrode surfaces, provide devices that could determine 4EP in real samples.

Annex I

VOLTAMPEROGRAMS AND NYQUIST PLOTS

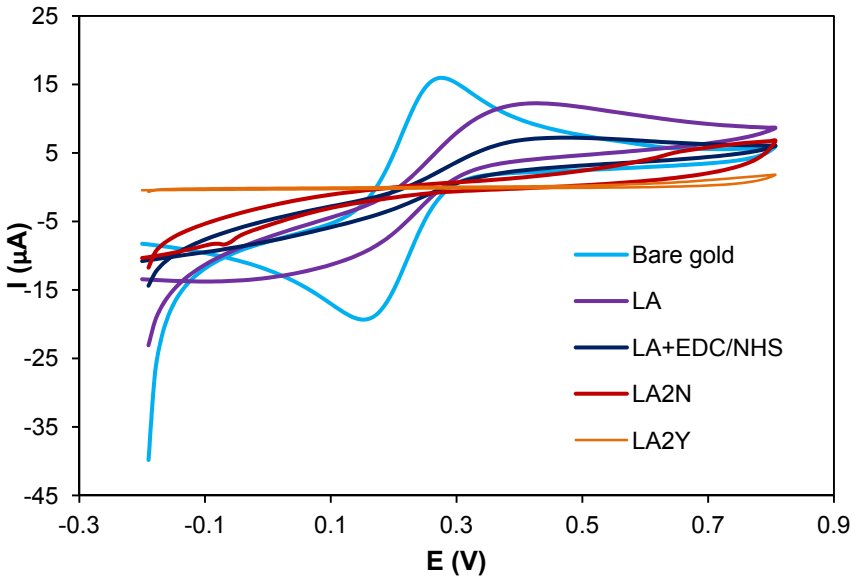

Figure A.I. 1. Cyclic voltammograms for each step on the fabrication of LA2N and LA2Y sensors.

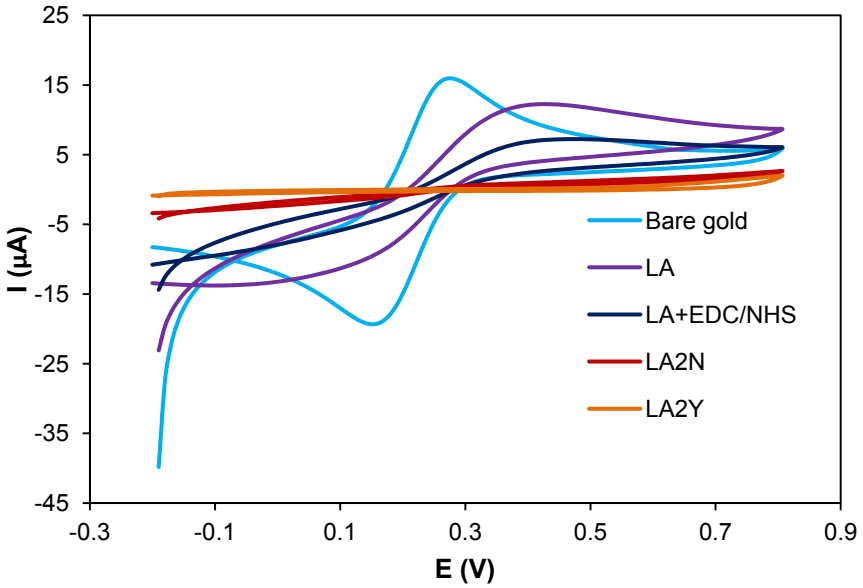

Figure A.I. 2. Cyclic voltammograms for each step on the fabrication of LA3N and LA3Y sensors.

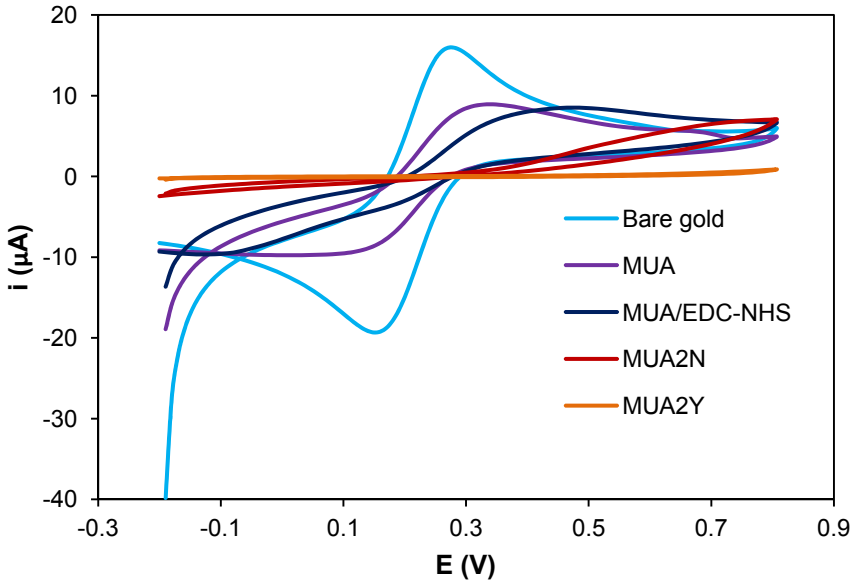

Figure A.I. 3. Cyclic voltammograms for each step on the fabrication of MUA2N and MUA2Y sensors.

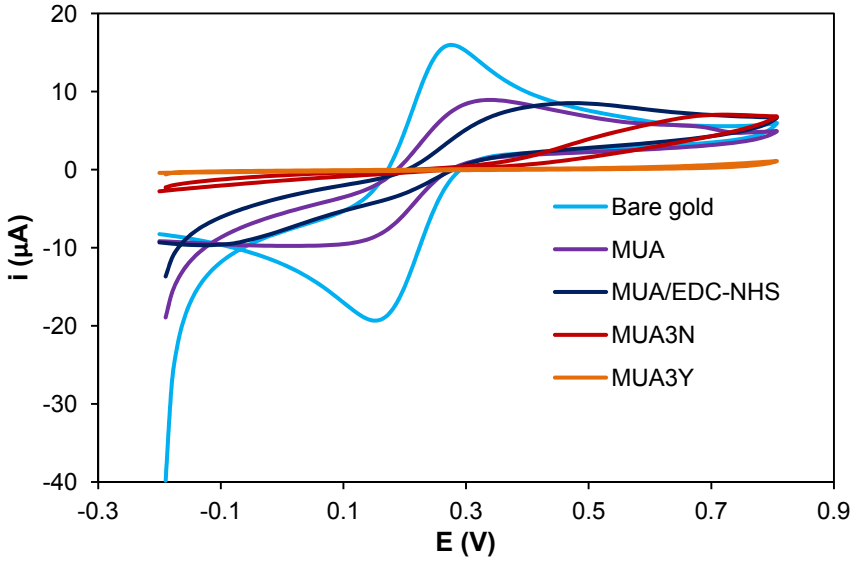

Figure A.I. 4. Cyclic voltammograms for each step on the fabrication of MUA3N and MUA3Y sensors.

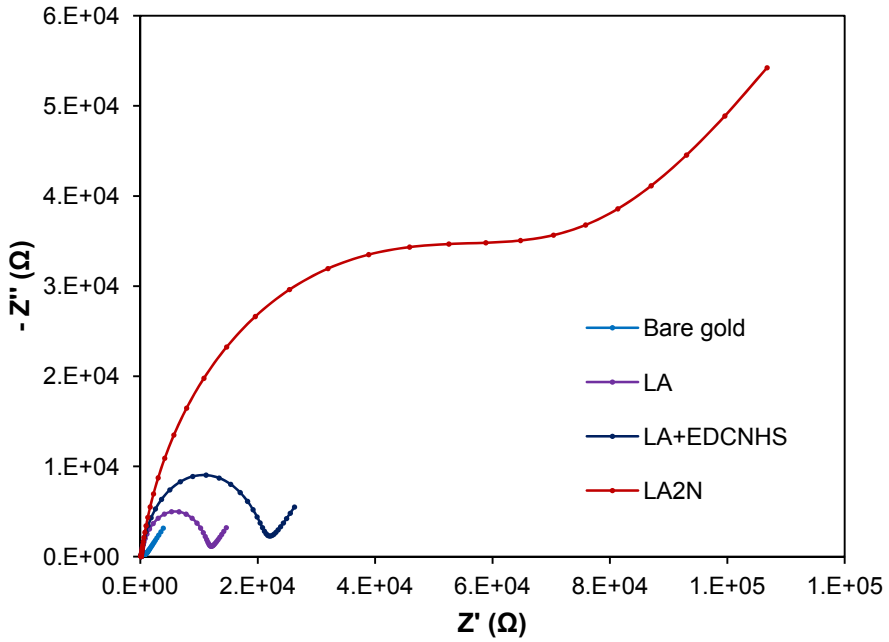

Figure A.I. 5. Nyquist plots registered with the bare gold electrode and LA based electrodes after each modification step for LA2N fabrication.

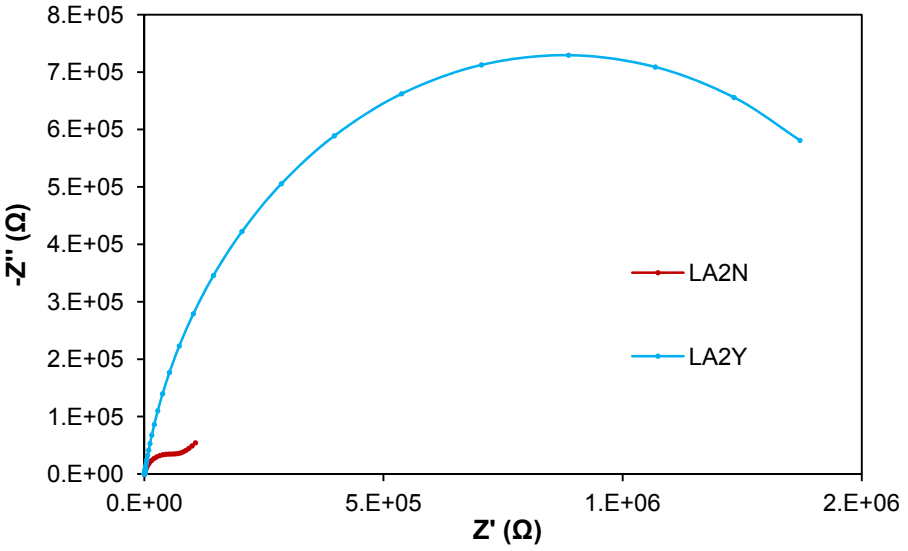

Figure A.I. 6. Nyquist plots for LA2N and LA2Y sensors.

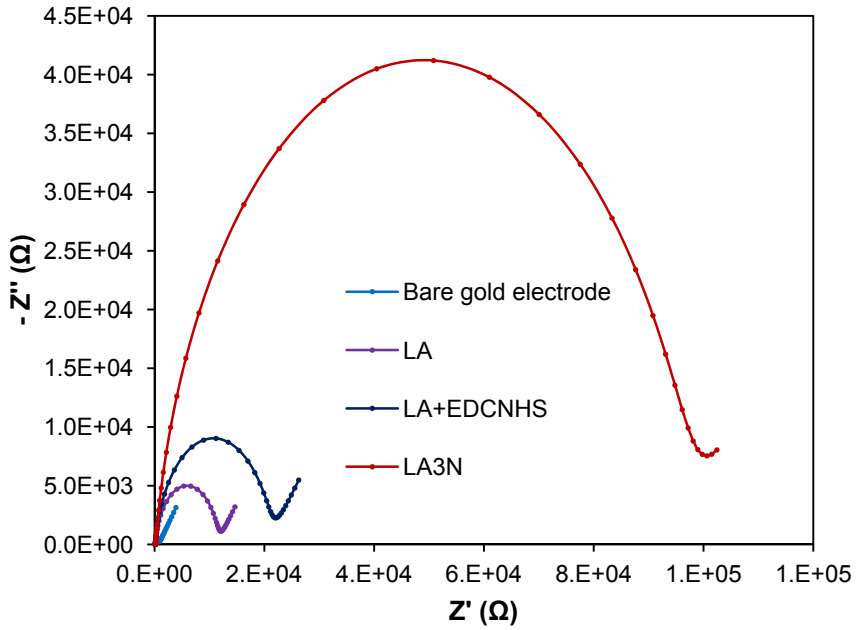

Figure A.I. 7. Nyquist plots registered with the bare gold electrode and LA based electrodes after each modification step for LA3N fabrication.

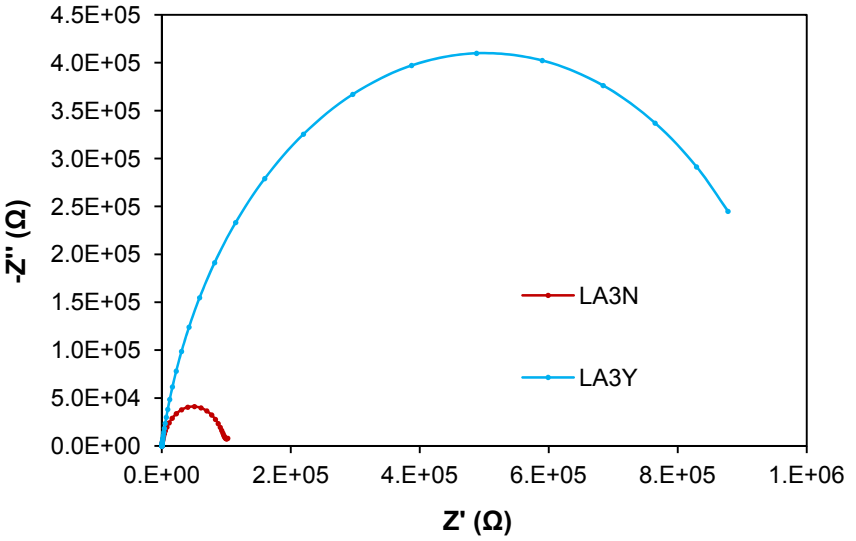

Figure A.I. 8. Nyquist plots for LA3N and LA3Y sensors.

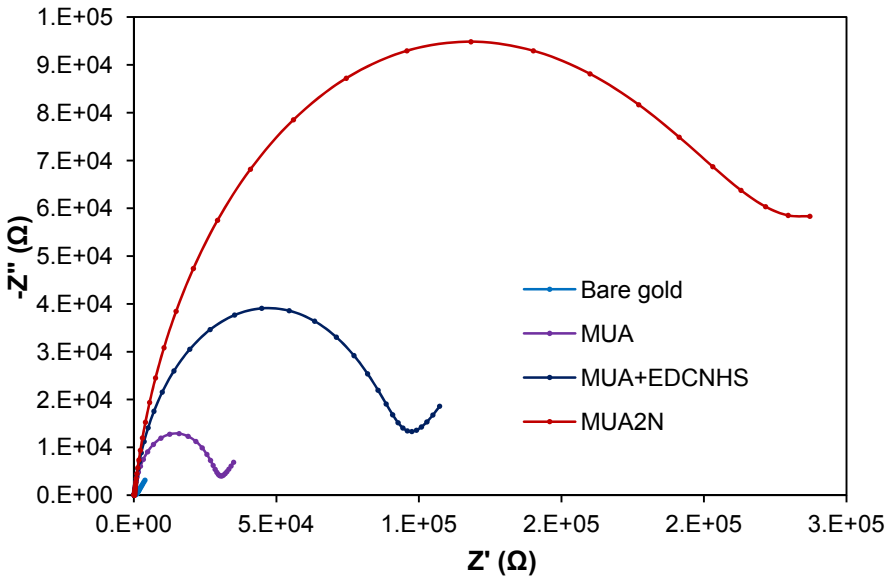

Figure A.I. 9. Nyquist plots registered with the bare gold electrode and MUA based electrodes after each modification step for MUA2N fabrication.

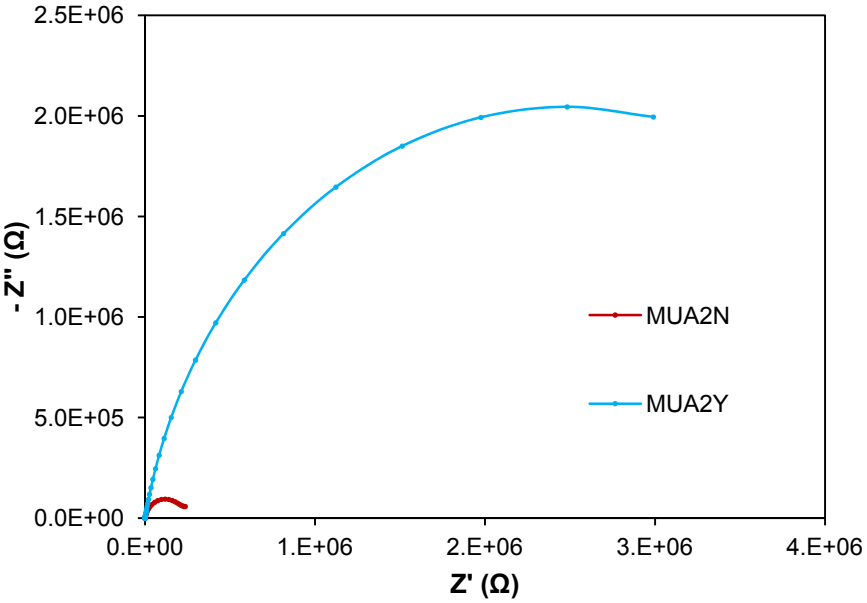

Figure A.I. 10. Nyquist plots for MUA2N and MUA2Y sensors.

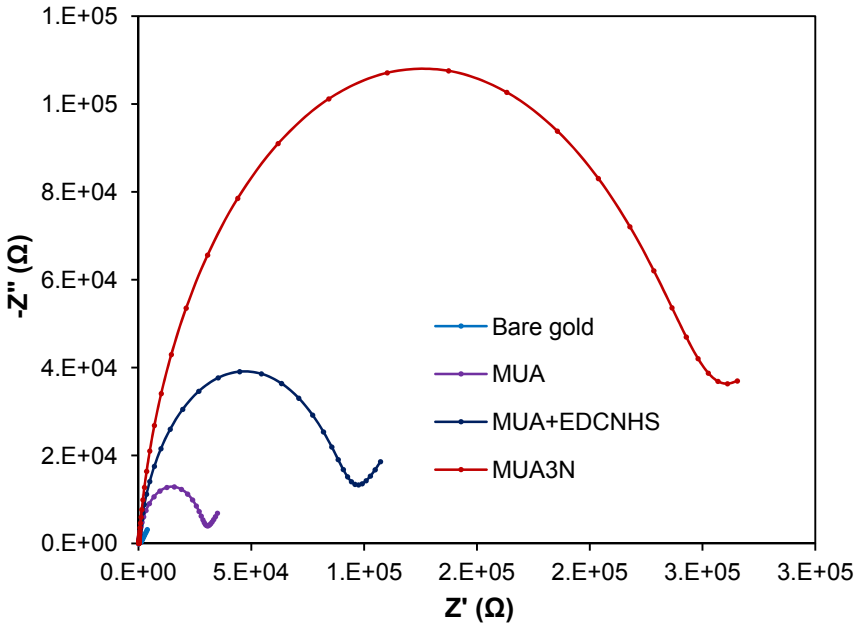

Figure A.I. 11. . Nyquist plots registered with the bare gold electrode and MUA based electrodes after each modification step for MUA3N fabrication.

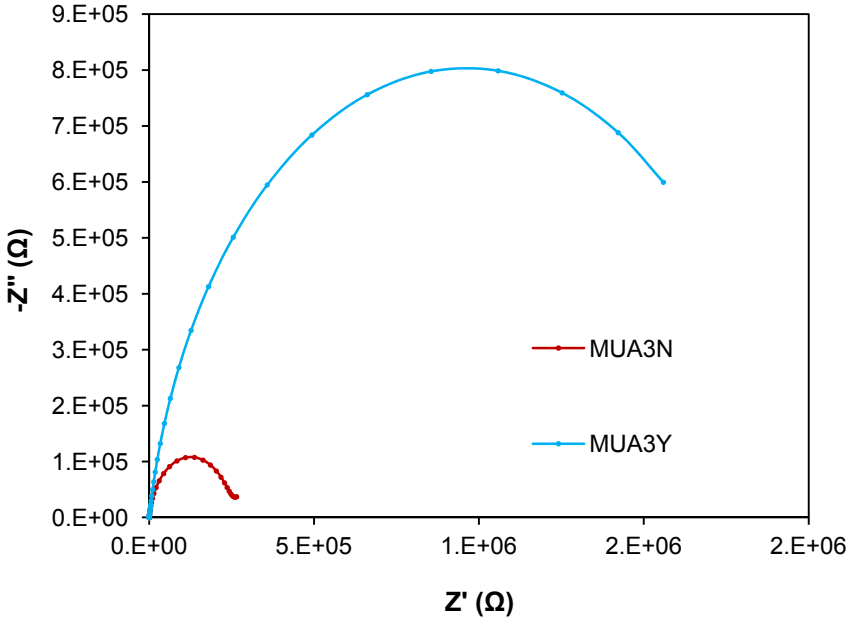

Figure A.I. 12. . Nyquist plots for MUA3N and MU3Y sensors.

Annex II

ARTICLES PUBLISHED IN

SCIENTIFIC JOURNALS

Enantioselective extraction of (+)-(S)-citalopram and its main metabolites using a tailor-made stir bar chiral imprinted polymer for their LC-ESI-MS/MS quantitation in urine samples

Talanta 116 (2013) 448–453

Contents lists available at ScienceDirect

Talanta

journal homepage: www.elsevier.com/locate/talanta

Enantioselective extraction of (+)-(*S*)-citalopram and its main metabolites using a tailor-made stir bar chiral imprinted polymer for their LC-ESI-MS/MS quantitation in urine samples

Nora Unceta [a], Alberto Gómez-Caballero [a], Deiene García [a], Goretti Díaz [a], Antonio Guerreiro [b], Sergey Piletsky [b], M. Aránzazu Goicolea [a], Ramón J. Barrio [a,*]

[a] Department of Analytical Chemistry, Faculty of Pharmacy, University of the Basque Country, Paseo de la Universidad 7, 01006 Vitoria-Gasteiz, Spain
[b] Cranfield Health, Cranfield University, Cranfield, Bedfordshire MK43 0AL, United Kingdom

ARTICLE INFO

Article history:
Received 24 April 2013
Received in revised form
2 July 2013
Accepted 4 July 2013
Available online 10 July 2013

Keywords:
S-citalopram
S-desmethylcitalopram
S-didesmethylcitalopram: chiral imprinted polymer (CIP)-coated stir bar
LC-ESI-ITMS
Urine

ABSTRACT

This paper reports the application of a chiral imprinted polymer (CIP)-coated stir bar for the selective extraction of (+)-(*S*)-citalopram (SCIT) and its main metabolites, (+)-(*S*)-desmethylcitalopram (SDCIT) and (+)-(*S*)-didesmethylcitalopram (SDDCIT), from urine samples. The developed device has been demonstrated to be capable of selectively extracting the three target analytes from urine samples without saturating the imprinted sites. A CIP-coated stir bar sorptive extraction procedure (CIP-SBSE) is proposed for the isolation of SCIT, SDCIT and SDDCIT followed by their subsequent analysis using liquid chromatography ion trap mass spectrometry (LC-ITMS). Deuterated SCIT-d6 was used as an internal standard. The method was validated using a standard procedure, which revealed that a quantification of 5 ng mL^{-1} was obtained in urine samples and that the accuracy and precision were within the established values while no matrix effect was observed.

1. Introduction

The antidepressant citalopram (CIT) is a potent and highly selective serotonin reuptake inhibitor (SSRI) that is primarily prescribed for the treatment of depression and other central nervous system diseases, such as anxiety disorder, panic disorder, obsessive–compulsive disorder, social phobia or post-traumatic stress disorder [1]. CIT was first introduced into therapy as a racemic drug because it has one chiral centre and therefore exists in the (−)-(*R*) and (+)-(*S*) forms. However, in vitro studies in rat brains have shown that the pharmacological effect of citalopram primarily lies on the (+)-(*S*)–CIT (SCIT) enantiomer, whereas the (−)-(*R*)–CIT (RCIT) enantiomer is considered to be pharmacologically inactive and could counteract the activity of the (*S*)-enantiomer [2]. Additionally, compared to the racemate, preclinical studies have postulated that the SCIT is more efficacious [3] and even 150-times more potent than the RCIT [4], which was initially assumed to be pharmacologically inactive but is currently known to counteract the action of the SCIT without causing pharmacokinetic interactions [5,6]. Based on these premises and on the growing trend to develop drugs that comprise a single enantiomer rather than a mixture of them [4], SCIT has begun to be marketed as a single-enantiomer drug.

SCIT is metabolised by partial N-demethylation to (+)-(*S*)-demethylcitalopram (SDCIT) and (+)-(*S*)-didemethylcitalopram (SDDCIT) by hepatic metabolism [7]. These compounds are primarily eliminated by the kidneys, and approximately 35% of the dose is excreted in urine [8]. From the literature available, it seems that mainly the *S*-enantiomer of DCIT is responsible for the clinically relevant 5-HT reuptake inhibiting properties of the drug [9]

In clinical practice, the determination of SCIT and its metabolites in urine samples could be useful for defining an efficient and safe dose and for detecting the adherence and compliance to the treatment.

To date, the separation of the *R* and *S* enantiomers of CIT and their metabolites has been based on chromatographic and electrophoretic methods [10]. With regard to chromatographic methods, the majority of the developed liquid chromatography methods are based on the use of cyclodextrin, macrocyclic glucopeptide or protein-based chiral stationary phases [11–19]. It is also possible to resolve both enantiomers by adding chiral selectors to the background electrolyte, such as carboxymethyl-gamma-cyclodextrin [20], beta-cyclodextrin [21,22] or macrocyclic antibiotics [23]. Another option for resolving the enantiomers has been to derivitise

* Corresponding author. Tel.: +34 945013055; fax: +34 945014351.
E-mail address: r.barrio@ehu.es (R.J. Barrio).

0039-9140/$ - see front matter © 2013 Elsevier B.V. All rights reserved.
http://dx.doi.org/10.1016/j.talanta.2013.07.004

Table 1
Data acquisition parameters for the smart parameter setting (SPS) used in the LC/ITMS for detecting the analytes. Compound stability and trap drive level are fixed at 100% for all compounds, and the fragmentation width was 10.0 (*m/z*).

Compound name	Retention time (min)	Precursor ion $[M+H]^+$	MRM transition (*m/z*)	Fragmentation amplitude (V)	Cut-off (*m/z*)
SDDCIT	7.1	297.0	297.0→261.9	88	0.48
SDCIT	7.8	311.0	311.0→261.9	84	0.60
SCIT	8.6	325.0	325.0→261.9	80	0.51
SCIT-d6	8.6	331.0	331.0→261.9	89	0.50

the analytes with a chiral reagent to form diastereoisomeric derivatives followed by their chromatographic separation in an achiral column [24].

Within the field of methodologies for synthesising host-guest systems, there are numerous works that appear in the literature related to the generation of molecularly imprinted polymers (MIPs) for its application to stereoselective separation processes [25–27], which are primarily used as stationary phases in chromatography [28] and electrophoresis[29,30]. The interaction between the template molecule and the imprinted cavity plays a crucial role in chiral separation, and the MIPs synthesised using the non-covalent approach are suggested by most authors for chiral recognition [31,32].

Recently, imprinted polymer based stir bar coating with high affinity towards drugs of biological significance [33,34], triazine herbicides [35] or minor constituents in food samples [36] have been developed.

The purpose of this study was to evaluate the applicability of this CIP-coated stir bar for the enantiospecific biological sample preconcentration and clean-up before the subsequent analysis of the selected target compounds. The capability of the developed CIP coating for the simultaneous extraction of SCIT and its metabolites SDCIT and SDDCIT was also investigated, and the influence of their presence in the same matrix was evaluated. The proposed method could be beneficial in selective and simple urine sample treatment as a valuable tool from the analytical point of view.

2. Materials and methods

2.1. Chemicals and reagents

All the chemicals and reagents used in this work were analytical grade. Ammonium formate (99%) and HPLC-MS grade acetonitrile, which were used as the mobile phase, were supplied by Acros Organics (New Jersey, USA) and Scharlab (Barcelona, Spain), respectively. Dry toluene was purchased from Panreac (Barcelona, Spain), and HPLC grade methanol and dichloromethane were obtained from Scharlab (Barcelona, Spain). Sodium carbonate and sodium chloride were obtained from Merck (Darmstadt, Germany). All solutions were prepared using ultra-high purity water (UHP) prepared from tap water that was pre-treated using Elix reverse osmosis cartridges before filtration by a Milli-Q system from Millipore (Bedford, MA, USA).

(+)-(*S*)-citalopram oxalate was purchased from Trademax (Shangai, China). Optically pure (+)-(*S*)-enantiomers of DCIT and DDCIT were kindly donated by Lundbeck A/S (Copenhagen, Denmark). The deuterated internal standard *S*-citalopram-d6 oxalate (SCIT-d6) with a purity greater than 98% was obtained from LGC Standards (East Greenwich, Rhode Island, USA).

2.2. LC-ITMS analysis

Chromatographic separation was performed on an Agilent 1100-series binary pump system. A Zorbax Eclipse XDB-CN column ($150 \times 4.6\ mm^2$, 5 μm) from Agilent Technologies (Palo Alto, CA, USA) was used, and the mobile phase consisted of a mixture of ammonium formate (30 mM) and acetonitrile (30:70, v/v) with a flow rate of 0.6 mL min^{-1} at a constant temperature of 25 °C.

The ion trap mass spectrometer was a MSD Trap XCT Plus equipped with a G1948A electrospray ionisation source operating in the positive ion mode (ESI +). The operating conditions of the ESI interface were as follows: drying gas (N_2) temperature of 350 °C, drying gas (N_2) flow rate of 11.0 L min^{-1}, nebuliser gas (N_2) pressure of 60 psi and a capillary voltage of −3200 V. Full-scan MS and MS/MS spectra were obtained by scanning over mass ranges from 100 to 500. The multiple-reaction monitoring (MRM) transitions, using the protonated molecular ions $[M+H]^+$ as precursor ions, and the MRM parameters are also summarised in Table 1.

2.3. Urine samples

Urine samples were collected from a volunteer who was treated daily with Esertia® (10 mg escitalopram). The urine samples were collected in sterile containers (Deltalab Eurotubo, Barcelona, Spain) 0 h, 6 h and 12 h after administering the unique dose of the day and maintained at −42 °C until analysis. Control urine samples were collected before the volunteer donor was treated. Before extraction, the urine sample was centrifuged at 2500 rpm for 10 min at room temperature. The supernatant was diluted 1:10 in a 20 mM carbonate buffer solution (pH of 10.5) that contained 9% (w/v) sodium chloride.

2.4. Standards and quality control (QC) samples

Stock solutions that contained 1 mg mL^{-1} of the individual analytes and the deuterated internal standard were prepared in methanol. All solutions were maintained in the dark at −42 °C in a freezer. From the standard stock solution of each analyte, aqueous working standard solutions that contained each compound at a final concentration of 10 mg L^{-1} were prepared and stored in a refrigerator at 4 °C during use. The stock solution of the deuterated internal standard was also diluted in water to obtain a stock solution that contained 10 mg L^{-1} of the standard and was stored at 4 °C.

Calibration standards were freshly prepared in triplicate on the day of analysis by adding the appropriate volume of the working standard solutions to 10 mL of the blank urine samples to yield the following concentrations: 5, 20, 50, 200, 400, 1000, and 2000 ng mL^{-1}.

QC samples were prepared at the lower limit of quantification of 5 ng mL^{-1} (LLOQ), 15 ng mL^{-1} (low QC, three times the LLOQ), 150 ng mL^{-1} (middle QC) and 1600 ng mL^{-1} (high QC, 80% of the ULOQ) in blank urine.

2.5. CIP-SBSE procedure

CIP-coated stir bars were synthesised as previously reported [33]. Once the stir bar was prepared, the extraction of the analytes from the sample was performed by directly immersing a CIP-coated stir bar into 9 mL of a urine sample that was diluted in a 20 mM

carbonate buffer solution (pH of 10.5) that contained 9% NaCl (w/v) for 300 min while stirring at 300 rpm. The CIP-coated stir bars were subsequently cleaned with MilliQ water, dried under nitrogen and stirred in a dichloromethane:toluene (1:3, v/v) mixture for 15 min. Finally, the stir bars were dried and immersed in 3 mL of methanol at 55 °C under stirring at 300 rpm for 90 min to desorb the analytes. The methanol extract was evaporated to dryness under nitrogen, and the residue was reconstituted with 1 mL of the mobile phase. Subsequently, 10 μL of a stock solution that contained 10 mg L^{-1} of the deuterated analogue, SCIT-d6, was added.

3. Results and discussion

3.1. LC–MS/MS conditions

During method development, the first step was to optimise the chromatographic and detection conditions to enhance sensitivity with a good separation of the analytes. With this objective, different experiments were conducted using different mobile phase compositions on Zorbax Eclipse XDB-CN and Zorbax Eclipse XDB-C8 columns with dimensions of 150 × 4.6 mm^2 and a 5 μm particle size. The use of the Zorbax Eclipse XDB-CN column with a mobile phase that contained an aqueous phase of 30 mM ammonium formate (pH of 3) and acetonitrile as an organic modifier in isocratic elution (30:70, v/v) with a flow rate of 0.6 mL min^{-1} allowed a satisfactory separation of the compounds to be obtained in less than 10 min (Fig. 1). No additional equilibration time was required for the sample injection. To reduce the variability in the assay, the deuterated analogue of *S*-citalopram, SCIT-d6, was used. The retention times obtained under the described conditions are presented in Table 1.

The optimisation of the ion trap mass spectrometer parameters was conducted by infusing 20 μg mL^{-1} of each standard in a control urine sample that was previously extracted following the sample preparation procedure presented above. The precursor ions of the analytes resulted from the protonation of the molecular ion $[M+H]^+$ and were selected to generate the MS/MS spectra. The optimum fragmentation amplitude for each analyte was determined by increasing this parameter until the precursor ion intensity was reduced to 5–20% of its major product ion response. Improved sensitivity for these analytes was obtained using manual fragmentation cut-off values rather than the default value (27% from the *m/z* ratio of the precursor ions).

The multiple reaction monitoring mode (MRM) with an isolation width of 4 *m/z* for each analyte was used for data acquisition.

The mass transitions were selected according to their stabilities and intensities. The detection of the ions was performed by monitoring the transitions shown in Table 1. The LC–MS/MS ion trap chromatogram and the product ion spectra generated from the precursor ions at the expected retention time are shown in Fig. 1. As precursor ions, the protonated molecular ions $[M+H]^+$ were selected at 325.0 *m/z* for SCIT, at 311.0 *m/z* for SDCIT, at 297.0 *m/z* for SDDCIT and at 331.0 *m/z* for SCIT-d6. No ion-source fragmentation was observed. The most characteristic fragmentation route involved the loss of H_2O then yielding to an ion at 306.9 *m/z* for SCIT, 292.9 *m/z* for SDCIT and 279.9 *m/z* for SDDCIT, which was followed by loss of the end-of-chain amine towards the 261.9 *m/z* fragment. The formation of the 108.9 *m/z* ion observed for all the analytes could be due to the 1-fluoro-4-methylbenzene unit [37]. An alternative pathway yielded a 279.9 *m/z* ion, which was due to the loss of $HN(CH_3)_2$ from the precursor ion $[M+H]^+$ [38].

3.2. Sample preparation and CIP-SBSE procedure

The evaluation of the influence of the matrix on this method in comparison with standards prepared in water was conducted by

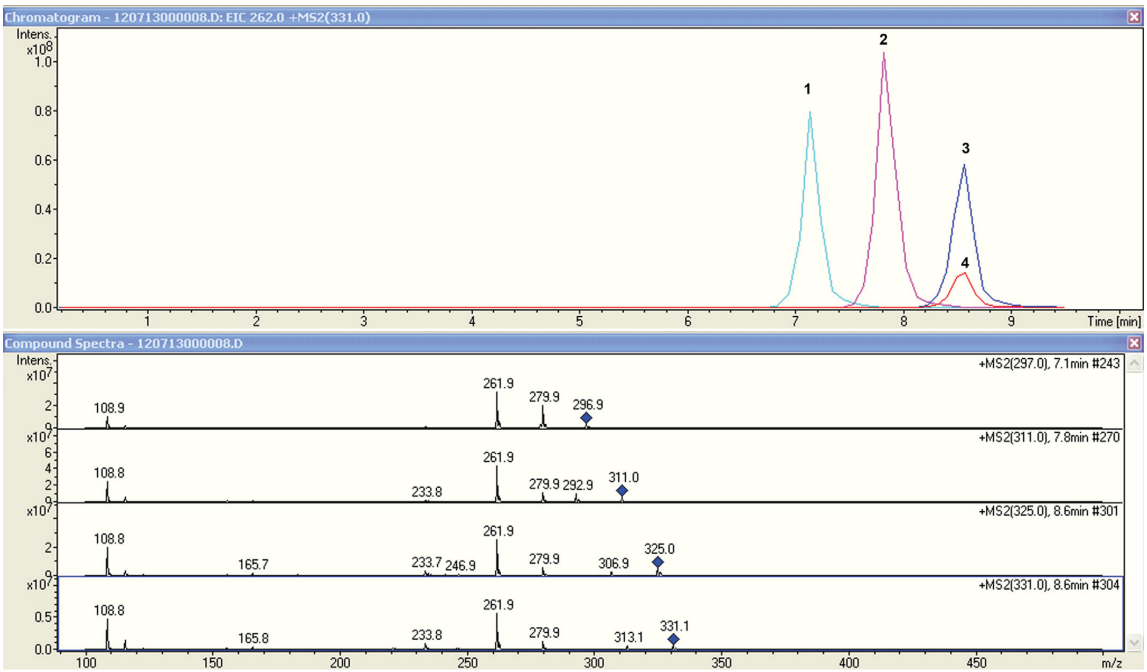

Fig. 1. LC–MS/MS ion trap segmented chromatogram (MRM) and MS/MS spectra of 500 ng mL^{-1} of each analyte and 100 ng/mL of the deuterated IS. 1: (+)-(*S*)–DDCIT, 2: (+)-(*S*)–DCIT, 3: (+)-(*S*)–CIT, and 4: (+)-(*S*)-CIT-d6.

doping the control urine samples with different concentrations of the analytes before applying the developed procedure. The urine samples were centrifuged at 2500 rpm for 10 min at room temperature to precipitate the urinary sediment. Initially, the supernatant was directly extracted using the developed CIP-SBSE procedure, but a considerable loss of sensitivity was observed due to an important matrix effect. Therefore, several trials were conducted using urine samples that were diluted in water in different proportions; the trials revealed that a 1:10 dilution allowed a satisfactory suppression of the matrix effect to be obtained. The 1:10 dilution of the samples should not be problematic for the quantification of SCIT, SDDCIT and SDDCIT in urine because their excreted levels are usually at the mg L^{-1} levels [39]. Note that the extraction and desorption processes were not influenced by passing from the aqueous solutions to urine samples and no interfering peak was observed in any chromatogram obtained after the extraction of the blank urine samples.

The CIP-SBSE procedure was described and justified by Gómez-Caballero et al. [33]. However, this procedure was only validated for the selective extraction of SCIT. Therefore, in the present work, the suitability of this procedure for a reproducible extraction of SDCIT and SDDCIT was also verified. Note that to improve the limit of quantification of the method, a final step was added that consisted of evaporating the methanol used in the desorption step. Then, the dry residue was reconstituted with 1 mL of the mobile phase.

3.3. Study of the selective recognition capability

The MIP-stir bar chiral recognition capability for different concentration levels of the metabolites SDCIT and SDDCIT was initially tested. This was performed comparing the signal of *S* enantiomers with the signal of the racemic mixtures at a concentration that ranged from 5 to 2000 ng mL^{-1}. A comparison study was carried out from the slope data of the linear regressions. In this sense, the slope of the calibration of each *S* metabolite was compared with the calibration slope of the racemic mixture. It was found that the residual standard deviations of each straight line do not differ significantly. This assumption was based on lower *F* experimental values than tabulated, i.e, experimental values of 1.94 for SDCIT and 2.80 for SDDCIT versus a tabulated *F* value of 7.39. Consequently it can be stated that data come from the same population[40].

In addition a two sided *t*-test was performed comparing the experimental *t* value with the tabulated one considering (n_1+n_2-4) degrees of freedom and a confidence level of 95% ($n_1=n_2=5$ calibration levels). The t experimental values were 1.36 for SDCIT and 0.94 for SDDCIT, lower than the tabulated *t* value 2.45. This results indicate that the MIP-stir bar presents enantioselective recognition capability for the metabolites SDCIT and SDDCIT.

Previous studies conducted by our research group have demonstrated that the CIP-coated stir bar was capable of recognising the target SCIT enantiomer with a high specificity [33]. In addition, in this work, this good selectivity was corroborated through by extending this study to the extraction of SCIT in the presence of SDCIT and SDDCIT. As shown in the chromatogram in Fig. 1, these metabolites are also extracted by the enantiospecific coating.

Moreover, the effect of the presence of SDCIT and SDDCIT on the recognition capability of this stir bar towards SCIT was also evaluated at different concentration ratios according to the relationship between the excreted urine levels of CIT, DCIT and DDCIT during the day in patients under a daily dose of CIT: between 0 and 6 h after the ingestion of the drug, CIT:DCIT:DDCIT relationship was 1:1:1; 6–12 h after the ingestion, the ratio was 2:1:1; and 12–24 h after, it was 1:2:2 [39]. Considering these ratios, individual stock solutions that contained 10 mg L^{-1} of SCIT, SDCIT or SDDCIT were prepared. In addition, three stock solutions were prepared as follows: solution A contained 10 mg L^{-1} of SCIT, SDCIT and SDDCIT; solution B contained 10 mg L^{-1} of SCIT, 5 mg L^{-1} of SDCIT and 5 mg L^{-1} of SDDCIT; and solution C contained 10 mg L^{-1} of SCIT, 20 mg L^{-1} of SDCIT and 20 mg L^{-1} of SDDCIT.

Different aliquots of the urine samples ($n=3$) were doped with the individual solution of 10 mg L^{-1} SCIT, SDCIT or SDDCIT to obtain a final concentration of 5, 20, 50, 200, 400, 1000 or 2000 μg L^{-1}. The procedure was repeated with solutions A, B and C in an attempt to obtain final SCIT concentrations of 5, 20, 50, 200, 400, 1000 or 2000 μg L^{-1}.

The CIP-coated stir bars were immersed in the doped urine control samples that were previously diluted 1:10 in a 20 mM carbonate buffer solution (pH 10.5) that contained 9% (w/v) NaCl, and the extraction procedure was conducted as described above. In this manner, the calibration curves were constructed applying a weighting factor of $1/x^2$ to the data. As shown in Table 2, the correlation coefficients (r^2) were greater than 0.987 in all the cases.

The agreement between the slopes of the calibrated straight lines was calculated according to the Student's *t*-test ($p<0.05$). This statistical test revealed no significant difference ($t_{calculated} < t_{tabulated}$) between the slopes of the calibration curve of SCIT in the absence of these metabolites and in the presence of different ratios of SDCIT and SDDCIT. Therefore, it was concluded that at these concentration levels, the presence of the metabolites did not alter the extraction capability of SCIT, and it was consequently assumed that the metabolites did not cause saturation of the imprinted sites with the subsequent significant decrease of the retention capacity. In the same manner, the extraction capability of SDCIT and SDDCIT was not altered in the presence of the remainder of the analytes because there was not a statistically significant difference between the slopes (Table 3).

As a conclusion, it can be stated that the CIP-coated stir bar is enantioselective towards SCIT, SDCIT and SDDCIT. Although these

Table 2
Summary of the linearity, detection limits and quantification limits of SCIT, SDCIT and SDDCIT in urine samples in the absence and presence of the remainder of the compounds.

Compound	Individual calibrations	SCIT:SDCIT:SDDCIT (1:1:1)	SCIT:SDCIT:SDDCIT (2:1:1)	SCIT:SDCIT:SDDCIT (1:2:2)	LOD (ng mL^{-1})	LOQ (ng mL^{-1})
SCIT	$y=0.0020x+0.0587$ $r^2=0.9877$[a]	$y=0.0023x-0.0634$ $r^2=0.9959$	$y=0.0020x+0.114$ $r^2=0.9922$	$y=0.0022x+0.1290$ $r^2=0.9870$	2	5
SDCIT	$y=0.0054x+0.0080$ $r^2=0.9941$[b]	$y=0.0053x+0.0032$ $r^2=0.9911$	$y=0.0061x+0.0058$ $r^2=0.9993$	$y=0.0056x+0.0030$ $r^2=0.9958$	2	5
SDDCIT	$y=0.0055x+0.0105$ $r^2=0.9891$[c]	$y=0.0051-1.322$ $r^2=0.9969$	$y=0.0053+0.0133$ $r^2=0.9967$	$y=0.0051x+0.0086$ $r^2=0.9883$	2	5

[a] Calibration prepared from individual solution of SCIT.
[b] Calibration prepared from individual solution of SDCIT.
[c] Calibration prepared from individual solution of SDDCIT.

Table 3
Experimental Student's *t*-test values for comparing the slopes of the regression lines. The tabulated Student's *t*-value was 2.45 ($p=0.05$).

	SCIT	SDCIT	SDDCIT
SCIT:SDCIT:SDDCIT (1:1:1)	1.37	0.20	0.47
SCIT:SDCIT:SDDCIT (2:1:1)	0.22	1.44	0.32
SCIT:SDCIT:SDDCIT (1:2:2)	1.23	0.32	0.75

main metabolites are simultaneously extracted by the CIP-coated stir bar, their presence did not affect the extraction of the parent drug in the investigated concentration range. Therefore, the developed CIP-coated stir bar procedure is suitable for the enantiospecific sample pre-concentration of SCIT, SDCIT and SDDCIT in urine samples and their subsequent analysis by LC-ITMS.

3.4. Method validation

The developed method for the quantification of SCIT, SDCIT and SDDCIT in urine samples was validated using the standard procedure to ensure adequate selectivity, linearity, sensitivity, accuracy, precision, carry-over and matrix effects of the assay and the stability of the analytes [41].

The selectivity of the method was confirmed by the analysis of blank urine samples from ten different lots. No interfering signals were observed at the retention time and with the same m/z ratio of the compounds of interest.

As previously reported, the linearity of the method was validated for concentrations of SCIT, SDCIT and SDDCIT in urine between 5 and 2000 ng mL^{-1}. The LOD, which was 2 ng mL^{-1} for all the analytes, was defined as the lowest concentration that presented acceptable chromatography and with the presence of precursor and product ions with the ion ratios within $\pm 20\%$ of standards. The LLOQ, which was defined as the lowest concentration used in the calibration with a trueness and precision of 100% $\pm$ 20%, was validated as 5 ng mL^{-1} in urine for all the analytes (Table 2).

The method accuracy was evaluated in terms of precision and trueness[42] by analysing ten replicates ($n=10$) of the QC samples at the four different spiking levels including at LLOQ, low QC, middle QC and high QC under within-laboratory reproducibility conditions. Five MIP-stir bars were used for each spiking level. Precision was calculated in terms of global inter-day precision and estimated as RSD (%) of 10 determinations. Trueness was calculated in terms of recovery. Measurement uncertainty was assessed at the four different spiking levels covering the whole dynamic range, with a confidence interval of 95%. For each level, the uncertainty (U) was evaluated using the within-laboratory reproducibility relative standard deviation (Table 4).

As shown in Table 4, the measured concentration of the analytes fell within the acceptable range of recovery of 89–107%. The precision determined at each concentration level did not exceed an RSD of 12% at the LLOQ level.

Sample carry-over was assessed by injection blank samples after calibration standard at the upper limit of quantification (2000 ng mL^{-1}). The carry-over signal in the blank sample was below the LOD ($n=10$) for all the analytes. In this way, it can be stated that the carry-over effect was not detected and at least 20 cycles of extraction could be performed without loss of effectiveness of stir bar.

The matrix effect was determined in the control urine samples from ten different lots of blank urine samples that were spiked with the analytes at concentrations of 15 and 500 ng mL^{-1}. The matrix effect was measured by comparing the responses from the post-extraction spiked samples with those from the standard solutions. Because the calculated ratios varied from 86 to 91% and 89 to 96% respectively, it could be concluded that there is no matrix effect. In addition, when the calibration curves based in the aqueous standards and the calibration curves of the diluted urine samples were compared, the slope of the equation did not significantly vary and the recoveries of the analytes were minimally affected by the matrix effect.

Table 4
Summary of the trueness and precision results for the LC/MS/MS method in urine samples ($n=10$) for the analysed quality control samples.

Compound	Concentration level	Recovery (%)	Uncertainty (U) (%)	Global inter-day precision (RSD) (%)
(+)-(*S*)–CIT	LLOQ	104.4	4.2	8.9
	Low	100.0	4.2	9.2
	Middle	89.5	3.1	7.7
	High	102.9	4.0	8.5
(+)-(*S*)–DCIT	LLOQ	103.4	4.3	9.1
	Low	105.5	4.3	9.0
	Middle	100.7	4.6	10.0
	High	101.2	5.3	11.6
(+)-(*S*)–DDCIT	LLOQ	106.6	5.2	10.8
	Low	101.4	4.4	9.6
	Middle	97.3	5.0	11.3
	High	98.9	1.3	2.9

Table 5
Concentrations of the detected target analytical compounds in urine samples from depressed patients.

Sampling interval	(+)-(*S*)–CIT (ng mL^{-1})	(+)-(*S*)–DCIT (ng mL^{-1})	(+)-(*S*)–DCIT (ng mL^{-1})
0–6 h	1095 $\pm$ 44	907 $\pm$ 41	481 $\pm$ 22
6–12 h	476 $\pm$ 63	713 $\pm$ 91	468 $\pm$ 23
12–24 h	91 $\pm$ 13	116 $\pm$ 11	302 $\pm$ 7

*Mean $\pm$ SD.

Finally, the stability of the analytes and of the deuterated internal standards was evaluated. The stability results revealed that the stock solutions were stable after 1 month at 4 °C (97–106%) and 3 months at −42 °C (96–105%). The stability of the analytes in the urine samples was verified by analysing the QC samples after storage for 6, 12 and 24 h at room temperature (103–108%), after long-term storage for 60 days at −42 °C (92–102%) and after going through freeze and thaw cycles (refrozen for 12 h when completely thawed) (87–99%).

3.5. Application to real samples

The effectiveness of the proposed method for the determination of SCIT, SDCIT and SDDCIT in real samples was investigated by performing analyses of urine samples from a patient diagnosed with depression. This patient was under daily treatment with Esertia® (10 mg escitalopram). Urine samples were collected 0 h, 6 h and 12 h after the administration of the first dose of the day and were monitored. With regard to the mean concentrations found in these urine samples (Table 5), it can be concluded that this method is suitable for a reliable quantification of analytes at clinical levels and therefore, it could be useful in the detection of non-adherence to treatment, which is commonly observed in long-term treatments and results in suboptimal medication and poor disease control.

4. Conclusions

This study demonstrates the suitability of a recently developed enantioselective molecularly imprinted polymer (CIP)-based stir-bar coating SBSE for the selective extraction of SCIT and its main active metabolites SDCIT and SDDCIT from urine samples. No saturation of the binding sites occurred when SCIT was simultaneously extracted with its main metabolites at concentrations close to the ones expected in real samples. Moreover, the absence of a matrix effect has also been demonstrated, which can be attributed to the highly specific CIP devices. The developed SBSE-CIP method meets the current requirements of bioanalytical method validation and has been successfully applied for the quantification of the analytes in real urine samples.

Acknowledgements

This work was supported by the Spanish Ministry of Science Innovation (Project CTQ2008-00651/BQU). The technical and human support provided by the Central Service of Analysis of Alava, SGIker (UPV/EHU, MICINN, GV/EJ, ESF) is gratefully acknowledged.

References

[1] M. Vaswani, F.K. Linda, S. Ramesh, Prog. Neuropsychopharmacol. Biol. Psychiatry 27 (2003) 85–102.
[2] A. Mork, M. Kreilgaard, C. Sanchez, Neuropharmacology 45 (2003) 167–173.
[3] H. Zhong, N. Haddjeri, C. Sanchez, Psychopharmacology 219 (2012) 1–13.
[4] B. Leonard, D. Taylor, J. Psychopharmacol. 24 (2010) 1143–1152.
[5] O. Mnie-Filali, C. Faure, M. El Mansari, L. Lambas-Senas, A. Berod, L. Zimmer, C. Sanchez, N. Haddjeri, NeuroReport 18 (2007) 1553–1556.
[6] B. Waldeck, Pharmacol. Toxicol. 93 (2003) 203–210.
[7] J. van Harten, Clin. Pharmacokinet. 24 (1993) 203–220.
[8] L. Dalgaard, C. Larsen, Xenobiotica 29 (1999) 1033–1041.
[9] F.C. Kugelberg, Br. J. Pharmacol. 132 (2001) 1683–1690.
[10] N. Unceta, M.A. Goicolea, R.J. Barrio, Biomed. Chromatogr. 25 (2011) 238–257.
[11] B. Rochat, M. Amey, P. Baumann, Ther. Drug Monit. 17 (1995) 273–279.
[12] B. Carlsson, B. Norlander, Chromatographia 53 (2001) 266–272.
[13] M. Kosel, C.B. Eap, M. Amey, P. Baumann, J. Chromatogr. B 719 (1998) 234–238.
[14] Z.C. Zheng, M. Jamour, U. Klotz, Ther. Drug Monit. 22 (2000) 219–224.
[15] A. Rocha, M.P. Marques, E.B. Coelho, V.L. Lanchote, Chirality 19 (2007) 793–801.
[16] P. Holmgren, B. Carlsson, A.L. Zackrisson, B. Lindblom, M.L. Dahl, M.G. Scordo, H. Druid, J. Ahlner, J. Anal. Toxicol. 28 (2004) 94–104.
[17] R. Wimal, H. Perera, W.J. Lough, J. Chromatogr. A 1218 (2011) 8655–8663.
[18] T. Michishita, P. Franco, T. Zhang, J. Sep. Sci. 33 (2010) 3627–3637.
[19] N.M. Maier, P. Franco, W. Lindner, J. Chromatogr. A 906 (2001) 3–33.
[20] J.J. Berzas Nevado, C. Guiberteau Cabanillas, M.J. Villasenor Llerena, V. Rodriguez Robledo, J. Chromatogr. A 1072 (2005) 249–257.
[21] R. Mandrioli, S. Fanali, V. Pucci, M.A. Raggi, Electrophoresis 24 (2003) 2608–2616.
[22] A. El-Gindy, S. Emara, M.K. Mesbah, G.M. Hadad, J. AOAC Int. 89 (2006) 65–70.
[23] A.P. Kumar, J.H. Park, J. Chromatogr. A 1218 (2011) 1314–1317.
[24] S. Millan, M.A. Goicolea, A. Sanchez, A. Gomez-Caballero, M.C. Sampedro, N. Unceta, R.J. Barrio, Biomed. Chromatogr. 22 (2008) 265–271.
[25] M. Kempe, K. Mosbach., J. Chromatogr. A 694 (1995) 3–13.
[26] W.J. Cheong, F. Ali, J.H. Choi, J.O. Lee, K.Yune Sung, Talanta 106 (2013) 45–59.
[27] K. Sreenivasan, Talanta 68 (2006) 1037–1039.
[28] Q. Zhou, J. He, Y. Tang, Z. Xu, H. Li, C. Kang, J. Jiang, J. Chromatogr. A 1238 (2012) 60–67.
[29] Z.-H. Wei, L.-N. Mu, Y.-P. Huang, Z.-S. Liu, J. Chromatogr. A 1237 (2012) 115–121.
[30] Z.-H. Wei, L.-N. Mu, Q.-Q. Pang, Y.-P. Huang, Z.-S. Liu, Electrophoresis 33 (2012) 3021–3027.
[31] L.I. Andersson, K. Mosbach, J, Chromatography 516 (1990) 313–322.
[32] B. Sellergren, Chirality 1 (2004) 63.
[33] A. Gómez-Caballero, A. Guerreiro, K. Karim, S. Piletsky, M.A. Goicolea, R. J. Barrio, Biosens. Bioelectron. 28 (2011) 25–32.
[34] Z. Xu, C. Song, Y. Hu, G. Li, Talanta 85 (2011) 97–103.
[35] Y. Hu, J. Li, G. Li, Talanta 82 (2010) 464–470.
[36] M. Kawaguchi, A. Takatsu, R. Ito, H. Nakazawa, TrAC, Trends Anal. Chem. 45 (2013) 280–293.
[37] C. Sun, H. Xu, Y. Pan, Z. Shen, D. Wang, Rapid Commun. Mass Spectrom. 21 (2007) 2889–2894.
[38] W.F. Smyth, J.C. Leslie, S. McClean, B. Hannigan, H.P. McKenna, B. Doherty, C. Joyce, E. O'Kane, Rapid Commun. Mass Spectrom. 20 (2006) 1637–1642.
[39] N. Unceta, A. Gómez-Caballero, A. Sánchez, S. Millán, M.C. Sampedro, M. A. Goicolea, J. Sallés, R.J. Barrio, J. Pharm. Biomed. Anal. 46 (2008) 763–770.
[40] J. Coello, S. Maspoch, Regresión lineal por mínimos cuadrados. Calibrado univariable, in: M. Blanco, V. Cerdá (Eds.) Advanced Topics in Chemometrics, Universitat de les Illes Balears, Illes Balears, 2007, pp. 189–232.
[41] Committee for Medicinal Products for Human Use (CHMP), European Medicines Agency, Guideline on Bioanalytical Method Validation, London, 2011, pp. 22.
[42] A.G. Gonzalez, M.A. Herrador, A.G. Asuero, Talanta 82 (2010) 1995–1998.

Molecularly imprinted polymers as a tool for the study of the 4-ethylphenol metabolic pathway in red wines

Journal of Chromatography A, 1410 (2015) 164–172

Contents lists available at ScienceDirect

Journal of Chromatography A

journal homepage: www.elsevier.com/locate/chroma

Molecularly imprinted polymers as a tool for the study of the 4-ethylphenol metabolic pathway in red wines

Deiene Garcia[a], Alberto Gomez-Caballero[a], Antonio Guerreiro[b], M. Aranzazu Goicolea[a], Ramon J. Barrio[a,*]

[a] Department of Analytical Chemistry, Faculty of Pharmacy, University of the Basque Country UPV/EHU, 01006 Vitoria-Gasteiz, Spain
[b] Department of Chemistry, University of Leicester, LE1 7RH, United Kingdom

ARTICLE INFO

Article history:
Received 26 May 2015
Received in revised form 6 July 2015
Accepted 29 July 2015
Available online 1 August 2015

Keywords:
Molecularly imprinted polymer
4-Ethylphenol
Wine
Solid phase extraction
Molecularly imprinted stationary phase

ABSTRACT

A molecularly imprinted polymer (MIP) based methodology is described here for the determination of compounds that belong to the 4-ethylphenol (4EP) metabolic pathway in red wines. To this end, two MIP materials have been developed: a 4EP MIP as a class-selective material to extract phenols that belong to the 4EP metabolic pathway and a coumaric acid (CA) imprinted polymer as a MIP-based stationary phase capable of selectively separating these phenols on HPLC analysis, obtaining clean chromatograms. 4-vinyl pyridine and ethylene glycol dimethacrylate were respectively used as functional monomer and cross-linker for both MIPs. Once polymer compositions were optimised, the 4EP MIP was packed into SPE cartridges for wine sample clean-up and CA MIP was packed into HPLC columns to chromatographically separate the compounds present in the eluates obtained after SPE extraction. The accuracy of the proposed method was tested spiking wine samples with known concentrations of target compounds and subsequently, analytes were quantified by the standard addition method. Registered mean recoveries ranged from 95.2 to 109.2% and RSD values were below 10% in most cases. The described methodology was found to be suitable for the selective extraction and quantification of the compounds that belong to the 4EP metabolic pathway in red wines with minimal matrix effects and could be undoubtedly exploited to monitor 4EP and its precursors in wines.

1. Introduction

Volatile phenols (VP) are aromatic compounds that, at low levels, contribute positively to wine aroma. They provide spice, leather and smoke aromas as well as different sensory attributes such as bitterness and astringency [1]. In contrast, high concentrations of these compounds are responsible for organoleptic changes in wines, also known as "Brett character" or "phenolic character" [2], and in some instances they can lead to wine spoilage [3]. The principal VP contributing to this effect is 4-ethylphenol (4EP) and 4-ethylguaiacol (4EG) and when their total concentration exceeds 600 μg L^{-1} the "Brett character" becomes unacceptable [4]. The indicative sensory threshold values range from 230 μg L^{-1} to 440 μg L^{-1} for 4EP, and from 33 μg L^{-1} to 47 μg L^{-1} for 4EG [1,2,5–8]. Wines containing higher concentrations of these VP have unpleasant odours or off-flavours which have been described as spicy, smoky, mousy, leather, tar, burnt rubber, medicine, horse sweat, stable, barnyard and manure [1,2].

VP are present in wines as a result of decarboxylation of hydroxycinnamic acids (HCA), such as p-coumaric acid and ferulic acid, principally by enzymatic activities in the yeasts of the genus *Brettanomyces* and its teleomorph form *Dekkera* [5]. Decarboxylation of *p*-coumaric and ferulic acid is carried out by the enzyme hydroxycinnamate decarboxylase and it leads to the formation of 4-vinylphenol (4VPh) and 4-vinylguaiacol (4VG) respectively. These compounds are transformed into 4EP and 4EG by the enzyme vinylphenol reductase [5,9]. The principal reaction in terms of quantity and efficiency is considered to be the biotransformation of *p*-coumaric acid into 4VPh and 4EP which is specific of *Brettanomyces* yeast [1]. These reactions mainly occur during wine maturation, due to the fact that the porous structure of wood casks permits diffusion of small amounts of oxygen which favours the growth of *Brettanomyces* yeasts during wine aging [1,10]. Besides, this growth coincides with the hydrolysis of tartaric esters of HCA, which are considered as the predominant form of HCA in grapes and musts. These esters are slowly hydrolysed during barrel aging thanks to the acidic polar environment of wine

* Corresponding author. Tel.: +34 945013055; fax: +34 945014351.
E-mail address: r.barrio@ehu.es (R.J. Barrio).

http://dx.doi.org/10.1016/j.chroma.2015.07.103
0021-9673/

and it makes the levels of free HCA increase and, consequently, the final concentration of VP raises [9]. VP production can also take place via an alternative pathway thanks to the esterase activity of *Brettanomyces/Dekkera* yeast. It has recently been reported that these yeast can hydrolyse ethyl coumarate and therefore they contribute in increasing the final 4EP concentration [11].

4VPh and 4VG are the main VP in white wines, whereas 4EP and 4EG are the principal in red ones [12,13]. Although all these compounds can be determined by direct sample analysis [4], sample pretreatment is highly desirable not only to reduce intereferences originating from the complexity of wine matrices but also for analyte preconcentration [7,14] which plays a key role due to the low levels of these targets in wines. In this sense, different sample treatments such as solid phase extraction (SPE) [15,16] or solid phase microextraction (SPME) [17,18] have been widely employed. As an alternative to these methods, more recently, new strategies have been reported including liquid-liquid microextraction [7,14] and stir bar sorptive extraction (SBSE) [19]. Moreover, the QuEChERS methodology has also been applied to the extraction of these targets in different beverages such as beer, wine or fruit juices [4]. Research into new sorbent materials focused on selective extraction of the abovementioned targets would be highly desirable in order to obtain more concentrated and cleaner sample extracts [20] and thereby simplifying to a great extent the subsequent analysis step. In this regard, molecular imprinting [21] could serve as a useful tool to develop selective sorbent materials with high retention capacity [20,22,23].

The main objective of the present work was to develop a new type of class-selective materials based on Molecularly Imprinted Polymers (MIP), suitable for monitorisation of compounds of the 4EP metabolic pathway in wine samples. To this end, two strategies are presented here one of which is focused on the development of a class selective sorbent to extract 4EP and its precursors from wine samples and another one that deals with the synthesis of a new stationary phase material for the separation of the extracted compounds by affinity chromatography. The proposed analytical method consists of two steps: the first one where selective extraction/preconcentration on the target compounds is performed by solid-phase extraction using the class selective MIP, and a second step where separation and quantification of 4EP and its precursors is performed via HPLC with minimal interferences and background noise. The combined Molecularly Imprinted Solid Phase (MISPE) protocol with subsequent MIP-based chromatographic separation allows the targeted study of the metabolic pathway of 4EP in a simple and reliable way.

2. Experimental

2.1. Chemical and reagents

4-ethylphenol (4EP) (99.7%) and 4-ethylguaiacol (≥98%) were obtained from Sigma–Aldrich (Madrid, Spain), coumaric acid ethyl ester (CAEE) (≥90%) was purchased from LGC Standards (Barcelona, Spain) and 4-vinylphenol (4VPh) (10% in ethylene glycol) and 4-coumaric acid (CA) (≥90%) from Cymit Química (Barcelona, Spain). The cross-linkers trimethylpropane trimethacrylate (TRIM), divinylbenzene (DVB) and ethylene dimethacrylate (EDMA), the initiator 1,1'-azobis(cyclohexanecarbonitrile) (ABCN) and the functional monomer 4-vinylpyridine (4VP) were acquired from Sigma–Aldrich. Prior to use, 4VP was purified by distillation under vacuum obtaining a colorless liquid which was stored below −20 °C and under nitrogen atmosphere. Mass Spectrometry grade ammonium formate > 99% and formic acid ≥98% were acquired from Sigma-Aldrich. Acetonitrile (ACN), methanol (MeOH), dichloromethane (DCM), toluene (TLN) and dimethyl sulfoxide (DMSO) were HPLC grade and were acquired from Scharlab (Barcelona, Spain). Every buffer solution was prepared with ultra-pure water obtained from Elix20 reverse osmosis and Milli-Q water purification systems. All other reagents were analytical grade and used as received.

2.2. Synthesis of 4-ethylphenol and coumaric acid imprinted polymers

4EP imprinted polymers (MIP_{4EP}) were prepared dissolving 0.41 g of 4EP (3.3 mmol), 0.70 g of 4VP (6.7 mmol) and 4 g of EDMA (20 mmol) in 5.11 g of ACN previously degassed with pure nitrogen (1:2:6 template:functional monomer:cross-linker molar ratio). Then, 0.076 g of ABCN was added and the mixture was purged again with pure nitrogen for 1 min.

To synthesise CA imprinted polymers (MIP_{CA}), 0.27 g of CA (1.68 mmol), 0.53 g of 4VP (5.04 mmol) and 4 g of EDMA (20 mmol) were dissolved in 4.80 g of previously degassed MeOH (1:3:12) template:functional monomer:cross-linker molar ratio). 0.076 g of ABCN was then added and, finally, the solution was purged with nitrogen for 1 min. Polymerisation of these mixtures was performed using an UVAcube 100 UV lamp (100 W) purchased from Dr. Hönle UV-technology (Gräfelfing, Germany). The solutions were placed in an ice bath and irradiated with UV for 120 min. The resulting polymer monoliths were ground using a Pulverisette 14 mill from Fritsch (Idar-Oberstein, Germany) and wet-sieved in MeOH through 50 and 25 μm sieves. Obtained polymers particles (≈2 g) were finally dried in an oven at 50 °C overnight. Template was removed once the polymer was packed on SPE cartridges or HPLC columns with a 2–4 mL min^{-1} MeOH flow until no template could be detected on the eluate by HPLC. The non-imprinted (control) polymers (NIP_{4EP} and NIP_{CA}) were synthesised using the same procedures but in the absence of the template.

2.3. Packing of SPE cartridges and HPLC columns

Dry MIP_{4EP} polymer powders were manually packed in 6 ml empty SPE propylene tubes containing polyethylene frits (Sigma–Aldrich). A total polymer mass of 500 mg was packed in each tube.

For HPLC experiments, stainless steel columns of 100 and 250 mm in length and 4.6 mm in diameter were packed using a Pack in a Box column packing system from Restek (Bellefonte, USA) comprised of a dual piston pump and a 20 mL reservoir. Column packing was performed at a constant flow of 20 mL min^{-1} until a stable pressure was observed. Then the flow was decreased to 1 mL min^{-1} which was maintained constant for another 30 min.

2.4. Chromatographic evaluation of polymers

Liquid chromatography was initially used for imprinting factor (IF) determination and specificity testing of polymers. These experiments were carried out using an Agilent 1200 series HPLC system comprised of a Agilent 1260 infinity binary pump, vacuum degasser and a Rheodyne manual sample injector with a loop of 20 μL. The liquid chromatograph was coupled to a diode array detector (DAD) and a fluorescence detector (FD) connected in series. System control and data analysis were provided by the Agilent LC ChemStation software (Agilent Technologies, USA). To evaluate the specificity of the MIP column towards target compounds, the retention factor and the IF of the polymers were calculated.

The imprinted factor (IF) was calculated as: $IF = K_{MIP}/K_{NIP}$ where K_{MIP} and K_{NIP} are the retention factors of the analyte in the MIP and the NIP column, respectively. The corresponding retention factors were calculated using the equation, $K = (t - t_o)/t_o$ where (t) and (t_0)

are the retention time of the analyte and the void volume marker, respectively.

2.5. Molecularly imprinted solid phase extraction

A vacuum manifold from Varian (Palo Alto, USA), connected to a vacuum pump was used for molecularly imprinted solid phase extraction experiments (MISPE). First, each cartridge packed with MIP_{4EP} was washed by percolating 200 mL of MeOH to extract the template from the polymer matrix. Cartridges were then left to dry until use.

Before analysis, dry cartridges were first conditioned by percolating 5 mL of MeOH, followed by 5 mL of water containing 12% of ethanol. 5 mL of sample were subsequently loaded and cartridges were then washed with 5 mL of water/ethanol (12%). Then, the sorbent was dried under vacuum (15 mm Hg) for 15 min. Once the cartridges were dry, 4 mL of DCM was percolated for interference clean-up and finally, target compounds were recovered eluting the columns with 5 mL of ACN:MeOH (8:2). Obtained eluates were directly injected in a liquid chromatograph (see Section 2.4) using a MIP_{CA} packed column as stationary phase.

Binding capacity of imprinted materials was determined by frontal chromatography. Different solutions of 5 mg L^{-1} 4EP were prepared in DCM, MeOH and ACN. These solutions were percolated at a constant flow of 1 mL min^{-1} through stainless steel columns packed with the MIP_{4EP} particles. To calculate binding capacities, the following expression was employed: BC (mg analyte/g polymer) = RV(mL) × conc. (mg/mL)/polymer mass (g), as described elsewhere [24–26]. The retention volume (RV) was calculated from the inflection points of the sigmoidal curves observed in experimental frontal chromatograms.

2.6. MIP-based chromatographic separation

The final eluates obtained after MISPE were injected in the Agilent 1200 series HPLC-DAD-FD equipment detailed in Section 2.4. Analytes were separated using a stainless steel column of 250 mm in length and 4.6 mm in diameter packed with the MIP_{CA}. Gradient mode separation was applied using ultra-pure water and ACN as the aqueous and the organic solvents respectively. At the beginning of the analysis, the mobile phase consisted of 100% ACN and it was kept constant up to 5 min. Then the organic percentage of the mobile phase was decreased gradually to 98% over 15 min and then, changed to 90% until the end of analysis. DAD signals were registered at 225 nm for 4EP, at 260 nm for 4VPh and at 310 for CAEE and CA. Fluorescence signals were recorded also for 4EP and 4VPh working in multi-excitation mode. Excitation wavelength was 230 nm for 4EP and 260 nm for 4VPh whereas the emission wavelength was set to 320 nm for both compounds.

The retention factors (K) of MIP and NIP columns were calculated using the equation, $K = (t - t_0)/t_0$ where (t) and (t_0) are the retention times of the analyte and void volume marker, i.e. acetone, respectively. The separation factor (α) was calculated by the following equation: $\alpha = K_2/K_1$ where K_2 and K_1 are the retention factors of two consecutive chromatographic peaks.

3. Results and discussion

3.1. Development of 4-ethylphenol imprinted polymers

Two different MIPs were synthesised in this work in order to develop a MIP-based methodology to determine compounds that belong to the 4EP metabolic pathway in wines. The MIP_{4EP} was developed first in order to obtain a class-selective material capable of selectively extracting these phenols from wine matrices. To achieve this goal, a material that could recognise the phenolic group of every target compound was desirable; 4EP was therefore used as template. Different synthesis-related variables that influence final MIP performance were assessed first with the objective of developing a MIP with optimal binding behaviour. In this regard, the type of porogen, the cross-linker, and the template:functional monomer:cross-linker molar ratios were optimised.

4VP was selected as functional monomer based on preliminary HPLC experiments carried out with stationary phases made with non-imprinted polymers using 4VP, EGMP, acrylamide, methacrylic acid and itaconic acid as functional monomers and EDMA as cross-linker. It was found that columns packed with 4VP polymers showed higher retention times for 4EP in comparison with other polymers (Fig. S1) in different aprotic solvents tested as mobile phases. Taking into account these results, it was hypothesised that this monomer could establish strong hydrogen-bonding interactions between 4VP and 4EP hydroxyl moieties as well as complementary π–π stacking between aromatic rings. In addition, pyridine monomers have been proven to provide good results when used for imprinting of other phenolic compounds, as reported before [27–35].

3.2. Porogen selection

The effect of porogen polarity on MIP behaviour was evaluated by HPLC using columns packed with MIPs synthesised in ACN, TLN and DCM. Different solvents were employed as mobile phases to test every MIP column. The template:functional monomer:cross-linker (4EP, 4VP and EDMA) molar ratio was set to 1:4:20. As depicted in Fig. 1, MIP columns synthesised in DCM were the ones showing best imprinting factors (IF). The MIP synthesised in TLN behaved similarly to the one synthesised in DCM if rebinding was performed using DCM or MeOH as mobile phase, however, IF was not as good when working in ACN. As it can be deduced from the observed low IF values (Fig. 1a), the most polar solvent, ACN, is the one that led to MIPs with worst binding behaviour towards the template since MIPs synthesised in ACN behaved similarly to the NIP column. Based on the obtained results DCM was chosen as solvent for further experiments.

3.3. Optimisation of the polymer composition

In first instance, the template:functional monomer molar ratio was optimised in order to maximise the MIP performance. Keeping the functional monomer:cross-linker molar ratio constant at 1:3, different imprinted and non-imprinted polymers were synthesised at different template:functional monomer ratios. Resultant materials were evaluated by HPLC using DCM as mobile phase. Best results were obtained using a 1:2 template:functional monomer molar ratio; under these conditions an IF close to 2 was registered (Fig. S2).

The cross-linker monomer also plays an important role on MIP performance. It influences the recognition ability of the MIP and physicochemical properties of imprinted materials strongly depend on the cross-linking degree [36]. Depending on the cross-linker nature, it can impart the final polymer with a polar or non-polar character [37] and it is also known to be responsible for a large proportion of the non-specific hydrophobic interactions that are usually present in MIP systems.

In this part of the work, different amounts of DVB, TRIM and EDMA were employed to cross-link the adduct formed between 4VP and 4EP. MIPs synthesised in DCM using different functional monomer:cross-linker molar ratios were packed in HPLC columns and evaluated chromatographically. The retentions times and IF were compared with the ones registered using non-imprinted materials. The results are illustrated in Fig. 2 Imprinting factors observed using DVB and EDMA were higher than the ones for TRIM

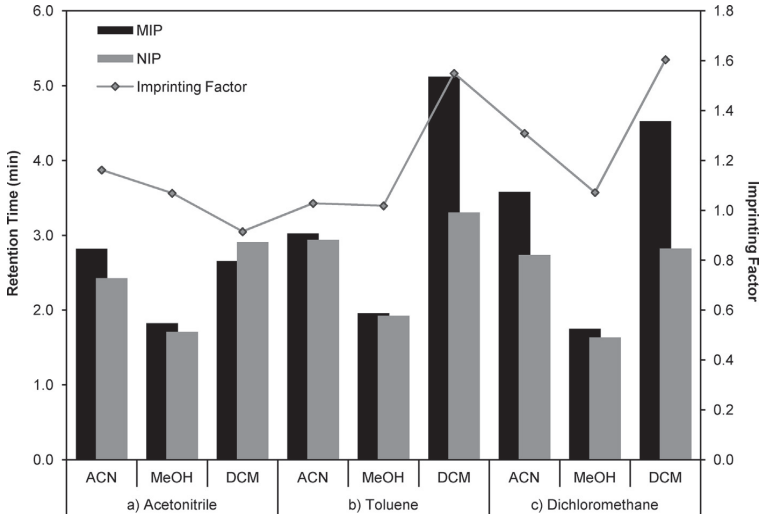

Fig. 1. Retention times and imprinting factors of 4EP using acetonitrile, methanol and dichloromethane as mobile phases. Columns packed with imprinted and non-imprinted polymers synthesised in (a) acetonitrile, (b) toluene and (c) dichloromethane were used as stationary phase.

which was discarded for further experimental due to the very low IF obtained. Despite all the optimisation steps, the highest imprinting factors were still around 2, a relatively modest value for a MIP. This can undoubtedly be attributed to the low number of functionalities suitable for imprinting present on the template molecule (a single hydroxyl group) and its weak acidity. Regardless, an IF of 2 can be considered sufficient not only to demonstrate the imprinting effect but also to fulfil the goal of developing a sorbent that successfully extracts the target from the sample matrix. Both DVB and EDMA led to materials with similar IF, however, retention times observed using EDMA were higher, probably due the higher polarity of this cross-linker. Between the two, EDMA was selected as the cross-linker in order to minimise possible unspecific hydrophobic interactions and to make the polymer more 'water compatible' considering that the final application of the material was to be carried out in wine samples. As IF was highest at this point, a template:functional monomer: cross-linker ratio 1:2:6 was chosen as optimum.

3.4. Selectivity of the 4-ethylphenol imprinted polymer

In order to evaluate the capacity of the developed material to extract compounds belonging to the metabolic pathway of 4EP, the retention of this target and its precursors 4VPh, CA and CAEE was assessed by the MIP_{4EP}. In addition, a compound structurally related to 4EP, was also used to check the capacity of the material to discriminate between the targets and possible interferences. 4-ethylguaiacol (4EG) was selected as a potential interfering

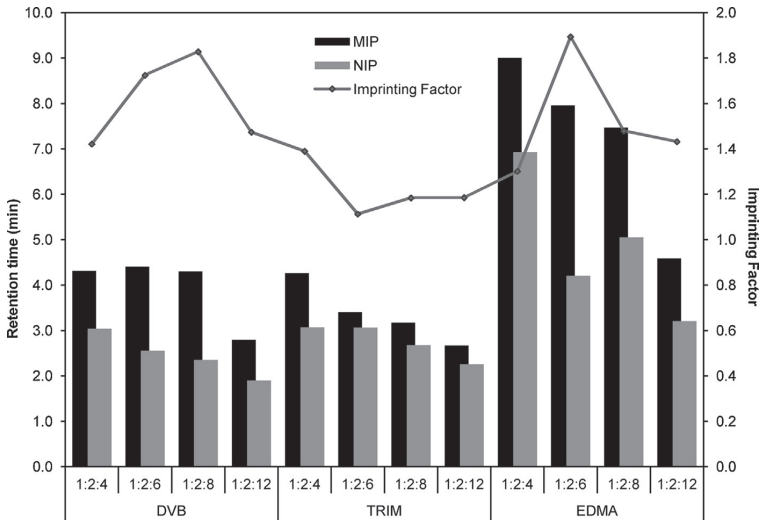

Fig. 2. Retention times and the corresponding IF of 4EP registered with columns packed with MIP and NIP materials synthesised using different template: functional monomer: cross-linker ratios. ACN was used as mobile phase in all cases.

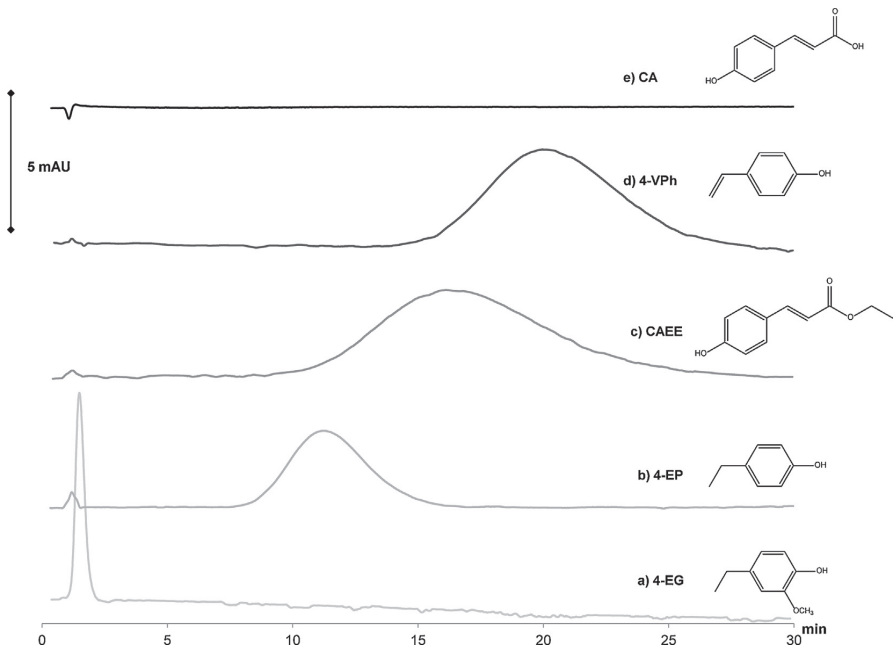

Fig. 3. Chromatograms registered after the injection of stock solutions of 10 mg L^{-1} of (a) 4EG, (b) 4EP, (c) CAEE, d) 4VPh and (e) CA. In all cases, a column packed with the MIP_{4EP} material was used as stationary phase and 100% dichloromethane as mobile phase (225 nm).

compound due to the fact that it is a phenolic compound that does not belong to the 4EP pathway, its structure is similar to 4EP and also because it can be naturally present in wine.

The chromatograms shown in Fig. 3 depict the retention times registered using the optimised MIP material as stationary phase and DCM as mobile phase. 4EP was the first to elute (11.1 min). Obtained retention times for 4VPh and CAEE were 16.6 and 19.8 min respectively. 4EP is a smaller and less functionalised molecule than CA, 4VP or CAEE. 4EP has only a hydroxyl polar group, whereas precursors have other polar groups that may be interacting non-specifically with the polymer. The reason for observing slightly longer retention times with precursors may be attributed to non-specific hydrogen bonding with randomly distributed functional monomers that may be present in the polymer, outside binding sites. No retention was observed in the MIP column for 4EG and full retention was observed for CA. Even working in 100% ACN as mobile phase, full retention of this compound was observed. Based on the presented results it can be stated that the developed material was successful in retaining selectively target analytes in comparison with a structurally related compound.

3.5. Development of coumaric acid imprinted polymers

As 4EP is a small and poorly functionalised template molecule, resulting MIP was not capable of separating the different compounds of its metabolic pathway chromatographically. Probably, during the synthesis of the MIP, template-monomer adducts were very weak and that was leading to poor imprinting effect with heterogeneous binding site distribution. In this sense, even if the MIP_{4EP} worked successfully for the extraction of 4EP, 4VPh, CAEE and CA, the developed material could not be also used as stationary phase to separate and determine these targets in wine extracts. It would be of great interest to have selective materials that allow for the quantification of these phenolic compounds in wine matrices, since it would help monitoring the levels of 4EP precursors, and thereby taking special actions to avoid its formation during wine ageing. Based on this, a second class-selective MIP was developed in order to make a MIP-based stationary phase for HPLC capable of separating target analytes mentioned above. For this purpose, CA was used as template. It was expected that this template could be capable of establishing stronger adducts with 4VP since CA has an additional carboxylic group to interact with the functional monomer. Also, as demonstrated during chromatographic evaluation (Section 3.1.3), this compound can interact strongly with 4VP polymers. As described in Section 3.1, different parameters that could affect the final outcome were again optimised in order to produce an imprinted material with the best possible characteristics.

3.6. Porogen selection

DMSO and MeOH were tested as solvents to carry out the polymer synthesis. Due to template solubility limitations, other solvents like ACN or DCM could not be employed. Two imprinted polymers and the corresponding non-imprinted ones were synthesised for this study using MeOH or DMSO as porogens. In all cases, CA was used as the template, 4VP as the functional monomer and EDMA as the cross-linker (1:3:12 molar ratio). The polymers were packed in HPLC columns and evaluated by liquid chromatography using ACN as mobile phase. Fig. 4 shows the chromatograms registered with MIP_{CA} materials synthesised using different porogens. Full retention of CA was observed in both MIP_{CA}, in consequence, 15 min after the injection, the mobile phase was changed to 95% of ACN and 5% of MeOH in order to favour the elution of CA.

The IF of the DMSO MIP_{CA} was remarkably higher than the one observed for the MeOH MIP_{CA}, 31.05 and 7.89 respectively for CA, what clearly denotes that the binding strength is higher in the DMSO MIP. However, separation of target phenolic compounds

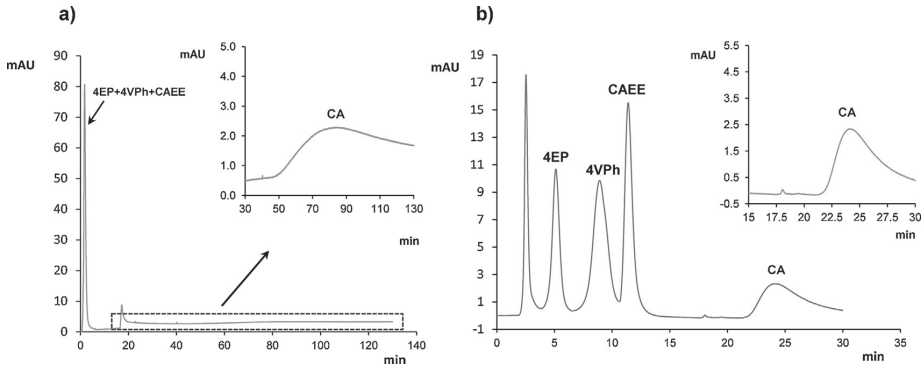

Fig. 4. Chromatograms registered after the injection of stock solutions of 5 mg L^{-1} of 4EP, 4VPh, CAEE, and CA. Columns packed with the MIP_{CA} synthesised in (A) DMSO and (B) MeOH as porogen were used as stationary phase (225 nm).

took place better using the MIP_{CA} polymer synthesised in MeOH. Probably, when using DMSO as porogen, the prepolymerisation template-functional monomer adduct was more stable and consequently, resulting binding site distribution was more homogeneous which resulted in a more selective MIP_{CA} for the target compound and less specific for other phenolic compounds. It was concluded that the MIP prepared in DMSO was less class-specific than the one synthesised with MeOH, therefore, considering that the purpose of imprinting CA was to obtain a polymer capable of separating the different compounds involved in the 4EP metabolic pathway, MeOH was chosen as porogen for further research.

3.7. Optimisation of the polymer composition

In order to determine the best template:functional monomer:cross-linker molar ratio, a series of polymers were synthesised using 4VP as the functional monomer, EDMA as the cross-linker and CA as the template. First, four MIPs, synthesised using 1:2, 1:3, 1:4 and 1:6 template:functional monomer molar ratios, were tested. All these MIPs were synthesised with a constant functional monomer:cross-linker ratio of 1:4. All synthesised imprinted and non-imprinted polymers were chromatographically evaluated using ACN:MeOH 95:5 as mobile phase. Obtained retention times and IF are depicted in Fig. 5a. Best imprinting effect was observed at 1:3 molar ratio.

Once selected the template:functional monomer molar ratio, different functional monomer:cross-linker ratios were tested, in this regard, MIPs and NIPs were synthesised using 1:3, 1:4 and 1:5 ratios and they were evaluated by HPLC as described previously. As can be deduced from Fig. 5b, best results were obtained using 1:4 functional monomer:cross-linker molar ratio (1:3:12 template:functional monomer:cross-linker).

Once the polymer composition was optimised, the developed material was employed as stationary phase to separate the phenolic compounds that belong to the 4EP metabolic pathway in wines. As illustrated in Fig. 6, baseline separation of all analytes was observed using the MIP column employing conditions detailed in Section 2.6. However, the NIP column was not able to separate target analytes. In order to compare the efficiencies of both columns, retention and separation factors were calculated as described in Section 2.6. From the results illustrated in Table S1, it can be deduced the NIP column practically does not retain 4EP, 4VPh or CAEE, since retention factors were below 1 in all cases. In addition, the retention of CA in the MIP column was higher than in the NIP column. As regards the separation factors, it can be observed in Table S1 that the MIP column provided higher values than the NIP column, thereby demonstrating the goodness of the MIP to separate the target compounds.

3.8. Optimisation of the MISPE procedure

Based on the obtained results in Section 3.2, it might be expected that the MIP_{CA} could serve not only for chromatographic separation of target phenols but also for MISPE of wine samples. However, it was observed that the binding capacity of the MIP_{4EP} was remarkably higher than the one observed for the MIP_{CA} (Fig. S3). Consequently, MIP_{4EP} was used in SPE cartridges for MISPE of

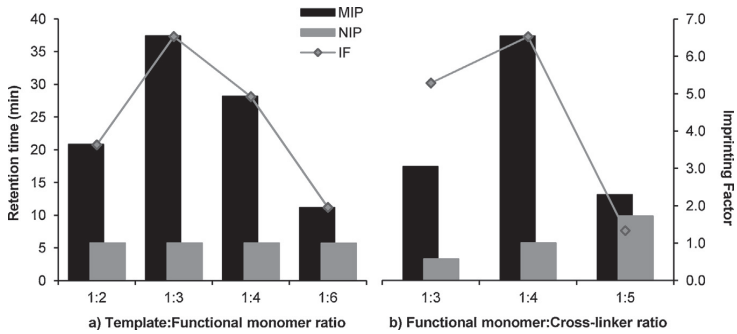

Fig. 5. Retention times and imprinting factors of CA using acetonitrile as mobile phase. Columns packed with imprinted and non-imprinted polymers synthesised using different (A) template: functional monomer and (B) functional monomer: cross-linker ratios were employed.

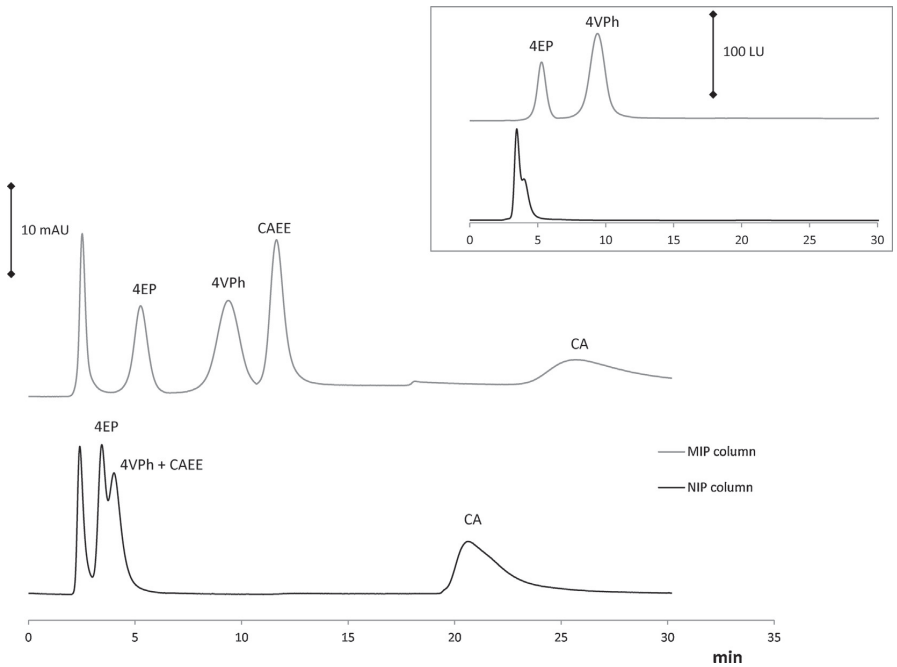

Fig. 6. Chromatograms registered with the DAD detector after the injection of stock solutions of 5 mg L^{-1} of 4EP, 4VPh, CAEE and CA using a MIP_{CA} and a NIP_{CA} column. In the inset, the signal registered in the fluorescence detector using the same conditions is depicted.

target analytes as described in Section 2.5 whereas the MIP_{CA} was employed only for HPLC experiments.

Initially, the washing and elution steps were optimised in order to minimise non-specific interactions of interfering compounds as well as to obtain maximum analyte recovery. After cartridge activation, 5 mL of a solution of 10 mg mL^{-1} of 4EP, 4VPh, CAEE and CA prepared in water containing 12% ethanol were percolated through it at constant flow. Next, 5 mL of water containing 12% of ethanol was percolated and then cartridges were washed with different amounts of DCM. Finally, analyte elution was carried out using 5 mL of MeOH. Since the cartridges were to be employed to extract target analytes from red wine samples, the cartridges were washed first with 5 mL of water with 12% ethanol in order to remove wine matrix components from the sorbent bed, thereby removing non-adsorbed or weakly adsorbed polar compounds that may be present in the wine samples. DCM was selected as the washing solvent because among the tested ones, it was the one with lower elution strength for 4EP. Other solvents like ACN or MeOH were also tested for washing, however, as previously stated, poorly functionalised 4EP binds quite weakly to the MIP_{4EP} and consequently polar solvents favour faster elution of the target without properly allowing the removal of interfering compounds. This effect was corroborated measuring the binding capacity of the sorbents by frontal chromatography employing DCM and ACN. It was empirically observed that the capacity of the MIP material was higher in DCM (97.9 mg g^{-1}) than in ACN (31.4 mg g^{-1}) or MeOH (18.8 mg g^{-1}). In order

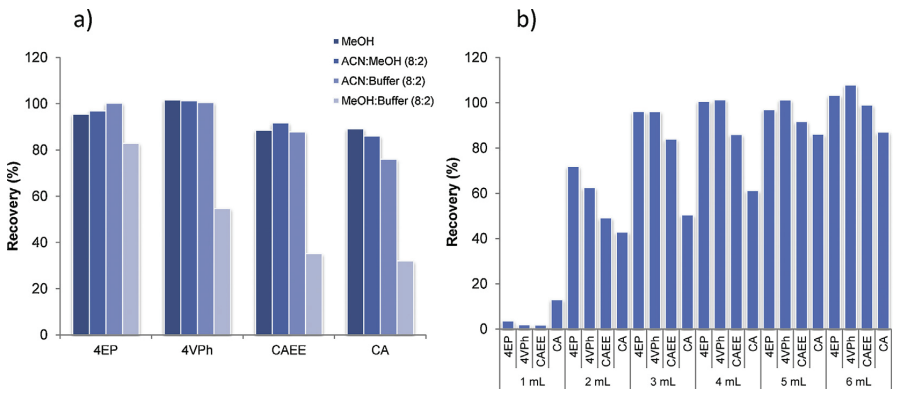

Fig. 7. Recoveries (%) obtained for 4EP, 4VPh, CAEE and CA after eluting the MIP_{4EP} SPE cartridges with (a) 5 mL of different solvents and (b) different volumes of the selected solvent (ACN:MeOH 8:2).

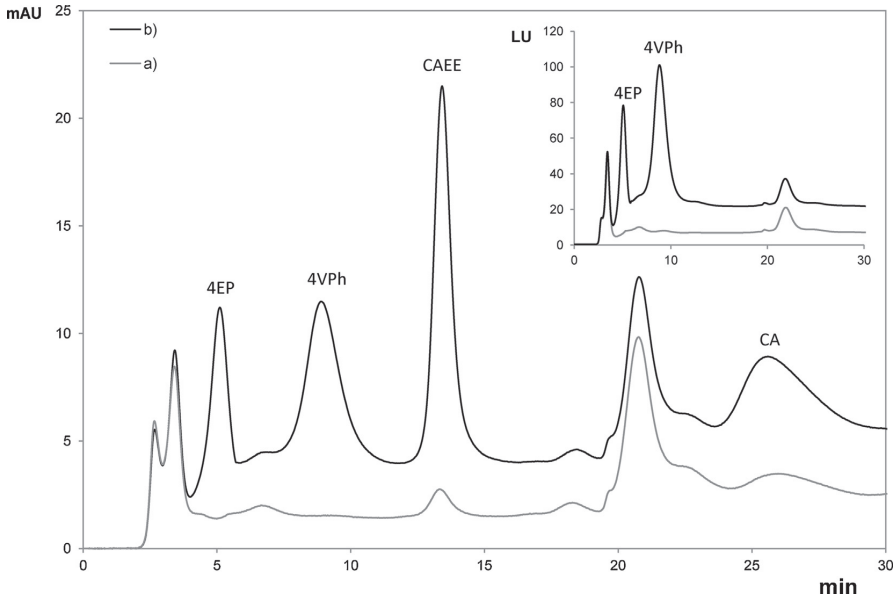

Fig. 8. HPLC-DAD chromatograms registered with final eluates obtained after percolating through MISPE cartridges (a) a red wine sample or (b) a red wine sample spiked with 5 mg L^{-1} of 4EP, 4VPh, CAEE and CA. The MIP_{CA} material was used as stationary phase in chromatographic experiments. Figure inset shows the chromatograms of the same eluates registered in the FD.

to know the maximum solvent amount that could be employed without analyte loss, a series of experiments were carried out percolating increasing volumes of the washing solvent and measuring the recovery in the final eluates. Recovery percentages recorded with MIP and NIP cartridges after washing them with increasing volumes of DCM are depicted in Fig. S4. Best results comparing MIP to NIP recoveries were observed using 4 mL DCM in the washing step.

Concerning the analyte elution step, different solvents like MeOH, ACN and formate buffer (10 mM, pH:3) were tested in order to get maximum analyte recovery. Furthermore, the required solvent volume to get complete analyte elution was also studied. When 100% ACN was used, CA could not be eluted, moreover, 100% aqueous solutions did not show enough elution strength for target analytes. Hence, different ACN:MeOH and ACN:Buffer mixtures were also tested as SPE eluents. Fig. 7a details recovery values for each target analyte after eluting the MISPE cartridges with different solvents. MeOH and ACN:MeOH 8:2 or ACN:buffer (8:2) mixtures were the eluents leading to highest recoveries. ACN:MeOH was chosen for further experiments since final SPE extracts were cleaner using this solvent mixture, probably due to a more selective behaviour of the MIP sorbent in the elution step. Different amounts of this mixture were employed for analyte elution. Calculated recoveries in final eluates are depicted in Fig. 7b. It can be deduced from the figure that 3 mL of eluent are enough to almost completely elute 4EP, 4VPh and CAEE. However, a higher volume is required for a quantitative elution of CA, thus, 5 mL of ACN:MeOH (8:2) were chosen.

3.9. Method application to red wine samples

The effectiveness of the developed method, based on MISPE coupled to MIP-based chromatographic separation of compounds from the 4EP metabolic pathway, was finally investigated in real matrices.

Since target compounds can be, to a greater or lesser extent, naturally present in wines, standard addition method was required to quantify these compounds in wine samples. Initially, analytical data were obtained using standard solutions of target compounds. Method dependence to concentration was evaluated loading the MISPE cartridges with stock solutions of 4EP, 4VP, CAEE and CA that ranged from 0.010 to 10 mg L^{-1} prepared in water containing 12% of ethanol. The final eluates were analysed by HPLC obtaining a linear dependence of the peak area with concentration in the whole tested range (R_{4EP}^2: 0.9923 and R_{4VP}^2: 0.9901) except for CAEE and CA, whose linearities were comprised between 0.025 and 10 mg L^{-1} (R^2: 0.9956) and 0.25–10 mg L^{-1} (R^2: 0.9865) respectively. The instrumental limit of detection (LOD) and limit of quantification (LOQ) were calculated based on the $3\sigma/S$ and $10\sigma/S$ criterion [38] where σ is the value of the standard deviation of the blank signal and S the sensitivity value obtained from the calibration slope. The LOD and LOQ were found to be 2.63 μg L^{-1} and 8.77 μg L^{-1} respectively for 4EP, 2.82 μg L^{-1} and 9.42 μg L^{-1} for 4VPh, 6.81 μg L^{-1} and 22.7 μg L^{-1} for CAEE and 66.1 μg L^{-1} and 220 μg L^{-1} for CA.

The standard addition method was designed based on previously observed signal dependence with concentration in stock solutions of target analytes. Initially, 5 mL of red wine were percolated through a MIP_{4EP} cartridge as detailed in Section 2.5. Fig. 8a depicts the chromatogram corresponding to the final eluate obtained after MISPE of wine and Fig. 8b shows a chromatogram corresponding to a wine sample spiked with 5 mg L^{-1} of each target compound. As can be deduced from the figure, only signals attributable to CA and CAEE were found in the wine sample. Next, in order to quantify found analytes, 3 wine aliquots were spiked with 1, 2 and 3 mg L^{-1} of CAEE and 10, 20 and 30 mg L^{-1} of CA respectively. MISPE was performed and final eluates were injected in the HPLC. CA and CAEE concentrations in the tested wine sample were found to be 7.07 ± 0.56 mg L^{-1} and 0.63 ± 0.09 mg L^{-1} respectively, expressed as mean ± SD ($n = 3$).

In order to test method accuracy, control wine samples were prepared at different concentration levels spiking wine samples

Table 1
Summary of validation parameters in non-spiked and spiked wine.

Spiked (mg L^{-1})				Measured (mg L^{-1})				Recovery (%)				RSD (%)			
4EP	4VPh	CAEE	CA	4EP	4VPh	CAEE	CA	4EP	4VPh	CAEE	CA	4EP	4VPh	CAEE	CA
ns	ns	Ns	ns	<LOD	<LOD	0.63 ± 0.09	7.07 ± 0.56	–	–	–	–	–	–	14.3	7.9
0.1	0.1	0.1	1.0	0.095 ± 0.005	0.099 ± 0.007	0.72 ± 0.04	8.28 ± 0.54	95.2 ± 5.1	99.2 ± 7.0	98.0 ± 6.2	102.6 ± 6.7	5.3	7.1	5.5	6.5
0.5	0.5	0.5	5.0	0.52 ± 0.01	0.51 ± 0.02	1.23 ± 0.05	12.35 ± 0.45	104.6 ± 3.6	102.5 ± 4.1	109.2 ± 8.4	102.4 ± 5.0	1.9	3.9	4.1	3.6

Measured values expressed as mean ± SD of $n = 3$ measurements of different wine aliquots.
ns: non-spiked wine.

with known amounts of 4EP, 4VP, CAEE and CA. Then, target compounds were determined in control samples following the developed analytical method. Obtained results are summarised in Table 1. Mean recovery ranged from 95.2 to 109.2% and the RSD% were below 10% in most cases confirming the suitability of the method for the quantification of 4EP, 4VPh, CAEE and CA in red wine samples.

4. Conclusions

A new MIP-based methodology is presented here to determine the levels of compounds that belong to the 4EP metabolic pathway in red wines. Two MIP based materials have been successfully synthesised using 4EP and CA respectively as templates. By subsequent optimisation of the conditions for polymer synthesis, a MIP_{4EP} was obtained which could rebind target compounds from red wine samples. Concurrently, a class-selective MIP_{CA} was also obtained capable of separating target phenols by HPLC. Both materials have been employed to develop an analytical methodology that allows for the simple, accurate and selective determination of 4EP, 4VPh, CAEE and CA in red wine matrices with minimal matrix effect.

Acknowledgments

This work was supported by The Spanish Ministry of Economy and Competitiveness (project CTQ2013-47921-P) and the University of The Basque Country UPV/EHU (project US13/10).

Appendix A. Supplementary data

Supplementary data associated with this article can be found, in the online version, at http://dx.doi.org/10.1016/j.chroma.2015.07.103

References

[1] J. Kheir, D. Salameh, P. Strehaiano, C. Brandam, R. Lteif, Eur. Food Res. Technol. 237 (2013) 655–671.
[2] M. Petrozziello, A. Asproudi, M. Guaita, D. Borsa, S. Motta, L. Panero, A. Bosso, Food Chem. 149 (2014) 197–202.
[3] M.P. Sangorrin, V. Garcia, C.A. Lopes, J.S. Saez, C. Martinez, M.A. Ganga, J. Appl. Microbiol. 114 (2013) 1066–1074.
[4] I.M. Valente, C.M. Santos, M.M. Moreira, J.A. Rodrigues, J. Chromatogr. A 1271 (2013) 27–32.
[5] R. Suarez, J.A. Suarez-Lepe, A. Morata, F. Calderon, Food Chem. 102 (2007) 10–21.
[6] M.P. Nikfardjam, B. May, C. Tschiersch, Eur. Food Res. Technol. 230 (2009) 333–341.
[7] I. Carpinteiro, B. Abuin, I. Rodriguez, M. Ramil, R. Cela, J. Chromatogr. A 1229 (2012) 79–85.
[8] S. Benito, F. Palomero, A. Morata, F. Calderon, J.A. Suarez-Lepe, J. Appl. Microbiol. 106 (2009) 1743–1751.
[9] A. Morata, R. Vejarano, G. Ridolfi, S. Benito, F. Palomero, C. Uthurry, W. Tesfaye, C. Gonzalez, J.A. Suarez-Lepe, Enzyme Microb. Technol. 52 (2013) 99–104.
[10] R. Nieto-Rojo, C. Ancin-Azpilicueta, J.J. Garrido, Food Chem. 152 (2014) 399–406.
[11] J.L. Hixson, N.R. Sleep, D.L. Capone, G.M. Elsey, C.D. Curtin, M.A. Sefton, D.K. Taylor, J. Agric. Food. Chem. 60 (2012) 2293–2298.
[12] P. Chatonnet, D. Dubourdieu, J.N. Boidron, M. Pons, J. Sci. Food Agric. 60 (1992) 165–178.
[13] L. Dias, S. Dias, T. Sancho, H. Stender, A. Querol, M. Malfeito-Ferreira, V. Loureiro, Food Microbiol. 20 (2003) 567–574.
[14] C. Pizarro, C. Saenz-Gonzalez, N. Perez-del-Notario, J.M. Gonzalez-Saiz, J. Chromatogr. A 1218 (2011) 1576–1584.
[15] D. Allen, A.D. Bui, N. Cain, G. Rose, M. Downey, Anal. Bioanal. Chem. 405 (2013) 9869–9877.
[16] B.T. Weldegergis, A.M. Crouch, T. Gorecki, A. de Villiers, Anal. Chim. Acta 701 (2011) 98–111.
[17] M.-C. Monje, C. Privat, V. Gastine, F. Nepveu, Anal. Chim. Acta 458 (2002) 111–117.
[18] B. Mendes, J. Goncalves, J.S. Camara, Talanta 88 (2012) 79–94.
[19] C. Franc, F. David, G. de Revel, J. Chromatogr. A 1216 (2009) 3318–3327.
[20] I. Basozabal, A. Gomez-Caballero, G. Diaz-Diaz, A. Guerreiro, S. Gilby, M.A. Goicolea, R.J. Barrio, J. Chromatogr. A 1308 (2013) 45–51.
[21] M.J. Whitcombe, N. Kirsch, I.A. Nicholls, J. Mol. Recognit. 27 (2013) 297–401.
[22] A. Gomez-Caballero, A. Guerreiro, K. Karim, S. Piletsky, M.A. Goicolea, R.J. Barrio, Biosens. Bioelectron. 28 (2013) 25–32.
[23] N. Unceta, A. Gomez-Caballero, D. Garcia, G. Diaz, A. Guerreiro, S. Piletsky, M. Aranzazu Goicolea, R.J. Barrio, Talanta 116 (2013) 448–453.
[24] M. Yan, O. Ramström, Molecularly Imprinted Materials: Science and Technology, Marcel Dekker, New York, 2005.
[25] I. Chianella, K. Karim, E.V. Piletska, C. Preston, S.A. Piletsky, Anal. Chim. Acta 559 (2006) 73–78.
[26] T. Muhammad, L. Cui, W. Jide, E.V. Piletska, A.R. Guerreiro, S.A. Piletsky, Anal. Chim. Acta 709 (2012) 98–104.
[27] C. Baggiani, L. Anfossi, C. Giovannoli, Anal. Chim. Acta 591 (2007) 29–39.
[28] E. Caro, R.M. Marce, P.A.G. Cormack, D.C. Sherrington, F. Borrull, J. Chromatogr. A 995 (2003) 233–238.
[29] T. Garde-Cerdan, A. Zalacain, C. Lorenzo, J.L. Alonso, M.R. Salinas, Am. J. Enol. Vitic. 59 (2008) 396–400.
[30] E. Herrero-Hernandez, R. Carabias-Martinez, E. Rodriguez-Gonzalo, Anal. Chim. Acta 650 (2009) 195–201.
[31] N.M. Maier, G. Buttinger, S. Welhartizki, E. Gavioli, W. Lindner, J. Chromatogr. B 804 (2004) 103–111.
[32] N. Masque, R.M. Marce, F. Borrull, P.A. Cormack, D.C. Sherrington, Anal. Chem. 72 (2000) 4122–4126.
[33] B. San Vicente, F. Navarro Villoslada, M. Moreno-Bondi, Anal. Bioanal. Chem. 380 (2004) 115–122.
[34] H. Sanbe, J. Haginaka, J. Pharm. Biomed. Anal. 30 (2003) 1835–1844.
[35] L.J. Schwarz, B. Danylec, S.J. Harris, R.I. Boysen, M.T.W. Hearn, J. Chromatogr. A 1218 (2011) 2189–2195.
[36] T. Muhammad, Z. Nur, E.V. Piletska, O. Yimit, S.A. Piletsky, Analyst (Cambridge, United Kingdom) 137 (2012) 2623–2628.
[37] F. Horemans, A. Weustenraed, D. Spivak, T.J. Cleij, J. Mol. Recognit. 25 (2012) 344–351.
[38] M. Valcárcel, Principles of Analytical Chemistry, first ed., Springer, Berlin, 2000.

Molecularly imprinted high affinity nanoparticles for 4-ethylphenol sensing

Available online at www.sciencedirect.com

ScienceDirect

Procedia Engineering 120 (2015) 1132 – 1136

Procedia Engineering

www.elsevier.com/locate/procedia

EUROSENSORS 2015

Molecularly imprinted high affinity nanoparticles for 4-ethylphenol sensing

D. Garcia-Mutio[a], A. Guerreiro[b], A. Gomez-Caballero[a], R. Gutierrez-Climente[a], S. Piletsky[b], M.A. Goicolea[a], R.J. Barrio[a]*

[a]*Department of Analytical Chemistry, Faculty of Pharmacy, University of the Basque Country UPV/EHU, Paseo de la Universidad 7, 01006, Vitoria-Gasteiz, Spain.*

[b]*Department of Chemistry, University of Leicester, Leicester, LE1 7RH, UK*

Abstract

A novel sensor for 4-ethylphenol (4EP) was developed based on molecularly imprinted nanoparticles produced via the solid phase imprinting method. The nanoparticles were immobilised on the surface of a gold electrode previously modified with a self assembled monolayer of lipoic acid coupled to EDC/NHS ((1-ethyl-3-[dimethylaminopropyl]carbodiimide)/N-hydroxysuccinimide). Each step of the process was characterised by electrochemical impedance spectroscopy and cyclic voltammetry. The electrode was used to selectively determine 4EP by differential pulse voltammetry; a quite remarkable sensitivity improvement was observed in the nanoparticle-modified electrode in reference to the non modified bare gold electrode.

Peer-review under responsibility of the organizing committee of EUROSENSORS 2015

Keywords: 4-ethylphenol, electrochemical sensor, molecularly imprinted nanoparticles, solid phase synthesis.

1. Introduction

Natural receptors such as antibodies or enzymes have been widely employed as selective and sensitive recognition elements in the field of Analytical Chemistry in order to develop analytical methods targeted to a certain compound or a group of compounds [1]. Inspired by those that can be found in nature, biological receptors can be mimicked to synthesise smart materials for chemical sensing [2], to this end, the Molecular Imprinting Technology

* Corresponding author. Tel.: 0034 945013055; fax: 0034 945014351
E-mail address: r.barrio@ehu.eus.

Peer-review under responsibility of the organizing committee of EUROSENSORS 2015
doi:10.1016/j.proeng.2015.08.821

offers a versatile approach to develop artificial receptors based on organic polymers. These artificial receptors are synthesised by thermal or photochemical polymerisation that takes place in a mixture containing a template and a functional monomer which previously establish a prepolymerisation adduct in a non-protic solvent known as porogen. This adduct is cross-linked by radical polymerisation employing a cross-linking monomer which will favour the spatial immobilisation of the template-functional monomer complex thanks to the generation of a polymer network around them. Once the polymerisation is complete, the template is removed from the polymer and imprinted sites are released for the latter rebinding or recognition of the target compound.

Usually, Molecularly Imprinted Polymers (MIP) are synthesised in bulk format and they are subsequently ground to obtain irregular microsized imprinted particles [1]. One of the main drawbacks of the bulk polymerisation technique is that ground particles need to be sieved obtaining very low yields [3]. Nanosized MIP has constituted a step forward in Imprinting Technology since they overcome most of the drawbacks related with traditional MIP synthesis. On one hand, much higher surface-to-volume ratios are obtained using Molecularly Imprinted Nanoparticles (MIN), and on the other hand, they provide better accessibility to recognition sites and lower mass transfer resistance. Different strategies have been used to obtain MIN such as precipitation polymerisation, emulsion polymerisation or template synthesis approach [1].

Recently, a new method for the synthesis of nanoparticles has been developed, the solid phase synthesis approach. According to this protocol, the template relies immobilised on a solid phase during the synthesis of the polymer instead of being free in a solution; after nanoparticle polymerisation the imprinted particles are purified based on the affinity for the template [4]. Due to the final affinity-based purification step, the number of binding sites is maximised as particles with low or no affinity are removed, lowering non-specific interactions on the final application. Basozabal et al. employed MIN synthesised by solid phase imprinting to develop a potentiometric sensor. The use of high affinity and specifity nanoparticles allowed label-free detection and quantification of histamine in wine and fish samples [5].

In this work, 4-ethylphenol (4EP) specific MIN synthesised using the solid phase approach have been immobilised on a gold electrode surface to improve the performance of the electrode upon 4EP measurement by differential pulse voltammetry (DPV). Electrochemical Impedance Spectroscopy (EIS) and Cyclic Voltammetry (CV) were used for the characterisation of each step of the process.

2. Experimental

2.1. Nanoparticle synthesis

The protocol for the solid-phase synthesis with immobilised 4EP was adapted from Moczko et al. [6]. In this work, the 4EP analogue tyramine (TY) was used as template immobilised to the solid phase (glass beads). Immobilisation was carried out through the amino group of TY leaving the phenolic group unbound in order to favour the latter complexation of this hydroxyl group with the functional monomer. The composition of the polymerisation mixture was adapted from [4, 7]. Briefly, the functional monomer 4-vinylpyiridine (4ViPy), the cross-linkers ethylene glycol dimethacrylate (EGDMA) and trimethyloylpropane trimethacrylate (TRIM), the iniferter N,N-diethyldithiocarbamic acid benzyl ester, the chain transfer agent pentaerythritol-tetrakis-(3-mercaptopropionate) and the monomer N-(3-aminopropyl) methacrylamide hydrochloride (APMA) were dissolved in acetonitrile (ACN). APMA was used to provide the nanoparticles with amino groups in order to facilitate the subsequent immobilisation on the gold surface. Then the TY derivatised glass beads were added to this mixture and it was left polymerise for 2.5 min under UV energy. After polymerisation, the glass beads were placed in a empty SPE cartridge in order to perform the temperature-based affinity separation of MIN.

2.2. Assembly of the MIN on the Gold surface

Prior to immobilisation reactions, the surface of bare gold electrodes was cleaned as describe elsewhere [8]. Then, they were immediately immersed in an ethanol solution of 0.5 mg mL^{-1} of lipoic acid, for 24 h at room temperature in order to coat the electrode surface with a self-assembled monolayer (SAM). The carboxylic group of the immobilised LA was linked to EDC/NHS to get a stable active ester. Finally, the electrodes were immersed MIN suspension in phosphate buffer pH 7 for 24 h.

2.3. Electrochemical measurements

All electrochemical measurements were performed using a classical three-electrode system, where the MIN modified electrode was used as working electrode, a Ag/AgCl (KCl 3M) as reference electrode and a platinum-wire as counter electrode. All electrochemical measurements were conducted at room temperature using a PGSTAT12 potentiostat/galvanostat controlled by the NOVA 1.8.17 software (Metrohm Autolab B.V., Utrecht, The Netherlands). EIS behaviour of the electrode is determined by analysing the AC voltage and current response at the frequencies ranging from 0.1 Hz to 1 MHz, at an applied potential of 200 mV with an amplitude of 10 mV. CV measurements were carried out from -200 mV to 600 mV on a 10 mV step potential and 100 mVs^{-1} scan rate. Characterisation measurements were carried out using an equimolar mixture of $[Fe(CN)_6^{4-}]/[Fe(CN)_6^{3-}]$ (2 mM) in a KCl 0.1 M solution. 4EP measurements were carried out using Britton-Robinson buffer, modified with NaOH 0.5 M to pH 10, DPV measurements were performed scanning the potential between 0 and 0.5 V, at a scan rate of 10 mVs^{-1}.

3. Results and discussion

3.1. Electrochemical characterisation

Characterisation of the gold electrode after each surface modification step was carried out by CV and EIS. EIS was used to corroborate surface functionalisation of gold electrodes through the evaluation of changes in charge transfer resistance (R_{CT}) before and after surface modification. The Nyquist diagrams of the bare gold electrode, gold/LA, gold/LA/EDC-NHS and gold/LA/EDC-NHS/MIN electrodes are presented in Fig 1a. As despicted the monolayer assembly on the electrode surface led to an increase of R_{CT}. The surface of the gold electrode covered with SAM blocks almost all faradaic current from penetrating to the surface. The Randles circuit (included in Figure 1a) was used as equivalent circuit for the modelling of the electric properties of the modified electrodes were R_Ω is the dynamic solution resistance or cell resistance which describes the resistance measured between the working and reference electrodes, R_{CT} is the charge transfer resistance, which describes the insulation of the electrode, CPE the constant phase element, modelling non-ideal capacitors and W the finite Warburg element describing the time dependence of mass transport [9].

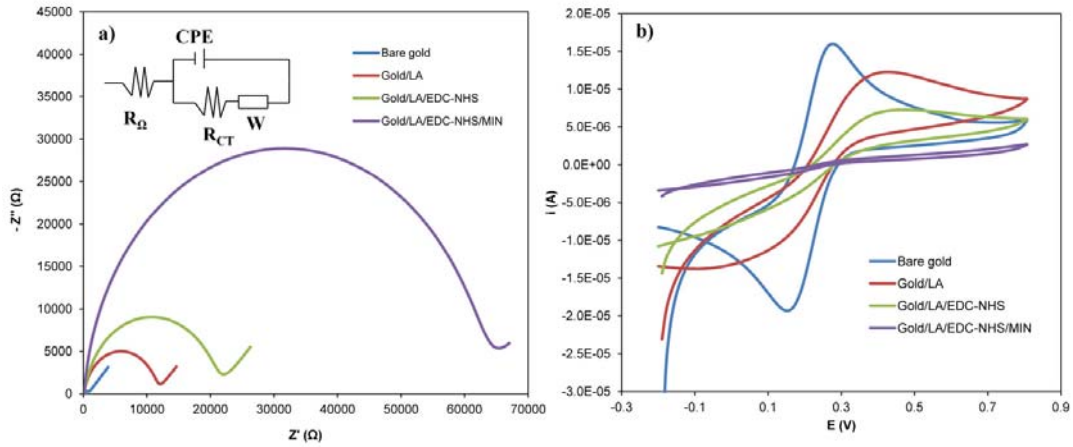

Fig. 1. Nyquist plots (a) and cyclic voltammograms (b) measured after each electrode modification step. Measurements recorded using 2 mM $[Fe(CN)_6^{4-}]/[Fe(CN)_6^{3}]$ prepared in KCl 0.1 M as supporting electrolyte.

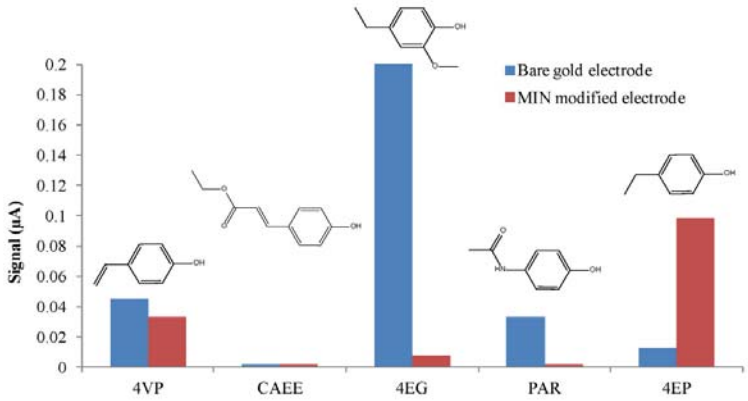

Fig. 2. DPV signals (µA) corresponding to the bare gold electrode and MIN modified electrode in 1 mg L^{-1} of 4EP and different analogues: 4-vinylphenol (4VP), coumaric acid ethyl ester (CAEE), 4-ethylguaiacol (4EG), and paracetamol (PAR).

EIS observations were confirmed by CV following the ferricyanide/ferrocyanide redox pair. Fig. 1b shows the cyclic voltammograms before and after modification of the gold electrode with the LA, EDC/NHS and finally nanoparticle immobilisation. It can be deduced from the figure that the peak current of [$Fe(CN)_6^{4-}$]/[$Fe(CN)_6^{3-}$] decreased after each modification step, what clearly denotes the electrical insulating property in every coating.

3.2. 4EP measurements

4EP was quantified by DPV using the bare gold and the MIN modified sensor as working electrodes. As it can be observed, the linearity of the MIN modified electrode was noticeably higher than the one obtained with the bare gold electrode, results are summarised in table 1. The detection limit (LOD) of the developed sensor was around 10 times lower than the limit of the non modified electrode. It can be therefore concluded that modifying the gold electrode with high affinity MIP nanoparticles represents a promising approach to increase sensitivity of metallic electrodes, and it may constitute an alternative to other existing commercial nanomaterials.

Table 1. Results obtained after measuring 4EP with different electrodes.

Electrode	LOD (mg L^{-1})	Linear range (mg L^{-1})	R^2
Bare gold electrode	0.29	0.96-5	0.9951
MIN modified electrode	0.07	0.24-5	0.9987

To determine the selectivity of the MIN modified electrode, four analogues were measured and compared to the results obtained with the bare gold electrode under the same experimental conditions (Fig. 2). In all cases, the signals corresponding to the structural analogues were lower than the 4EP signal using the MIN modified electrode. Besides, the MIN sensor provided lower responses to analogues but higher for the target compound, thereby demonstrating sensor selectivity towards 4EP.

Acknowledgements

This work was supported by the Spanish Ministry of Economy and Competitiveness (project CTQ2013-47921-P) and the University of The Basque Country UPV/EHU (project US13/10).

4. References

[1] Wackerlig J, Lieberzeit PA. Molecularly imprinted polymer nanoparticles in chemical sensing: Synthesis, characterisation and application. Sensors and Actuators B: Chemical. 2015;207, Part A(0):144-57.
[2] Martinez-Manez R, Sancenon F, Biyikal M, Hecht M, Rurack K. Mimicking tricks from nature with sensory organic-inorganic hybrid materials. J Mater Chem. 2011;21(34):12588-604.
[3] Ye L, Weiss R, Mosbach K. Synthesis and Characterization of Molecularly Imprinted Microspheres. Macromolecules. 2000;33(22):8239-45.
[4] Poma A, Guerreiro A, Whitcombe MJ, Piletska EV, Turner APF, Piletsky SA. Solid-Phase Synthesis of Molecularly Imprinted Polymer Nanoparticles with a Reusable Template-"Plastic Antibodies". Adv Funct Mater. 2013;23(22):2821-7.
[5] Basozabal I, Guerreiro A, Gomez-Caballero A, Aranzazu Goicolea M, Barrio RJ. Direct potentiometric quantification of histamine using solid-phase imprinted nanoparticles as recognition elements. Biosens Bioelectron. 2014;58:138-44.
[6] Moczko E, Guerreiro A, Piletska E, Piletsky S. PEG-Stabilized Core-Shell Surface-Imprinted Nanoparticles. Langmuir. 2013;29(31):9891-6.
[7] Guerreiro AR, Chianella I, Piletska E, Whitcombe MJ, Piletsky SA. Selection of imprinted nanoparticles by affinity chromatography. Biosens Bioelectron. 2009;24(8):2740-3.
[8] Heiskanen AR, Spegel CF, Kostesha N, Ruzgas T, Emneus J. Monitoring of Saccharomyces cerevisiae Cell Proliferation on Thiol-Modified Planar Gold Microelectrodes Using Impedance Spectroscopy. Langmuir. 2008;24(16):9066-73.
[9] Ahmad A, Moore E. Electrochemical immunosensor modified with self-assembled monolayer of 11-mercaptoundecanoic acid on gold electrodes for detection of benzo[a]pyrene in water. Analyst (Cambridge, U K). 2012;137(24):5839-44.

Solid-phase synthesis of imprinted nanoparticles grafted on gold substrates for voltammetric sensing of 4-ethylphenol

Sensors and Actuators B xxx (2016) xxx–xxx

Contents lists available at ScienceDirect

Sensors and Actuators B: Chemical

journal homepage: www.elsevier.com/locate/snb

Solid-phase synthesis of imprinted nanoparticles grafted on gold substrates for voltammetric sensing of 4-ethylphenol

D. Garcia-Mutio[a], A. Gomez-Caballero[a,*], A. Guerreiro[b], S. Piletsky[b], M.A. Goicolea[a], R.J. Barrio[a]

[a] Department of Analytical Chemistry, Faculty of Pharmacy, University of the Basque Country UPV/EHU, 01006 Vitoria-Gasteiz, Spain
[b] Department of Chemistry, University of Leicester, Leicester LE1 7RH, UK

ARTICLE INFO

Article history:
Received 27 November 2015
Received in revised form 29 January 2016
Accepted 5 February 2016
Available online xxx

Keywords:
Solid-phase synthesis
Molecularly imprinted nanoparticles
4-Ethylphenol
Voltammetric sensor

ABSTRACT

A voltammetric sensor based on molecularly imprinted high affinity nanoparticles has been developed for the direct, selective, and label-free detection of 4-ethylphenol (4EP). The poorly functionalised template 4EP, was successfully imprinted by the recently developed method of solid-phase synthesis of molecularly imprinted nanoparticles. These nanoparticles were grafted to the surface of gold electrodes allowing for selective and sensitive detection of 4EP. Each step of the electrode modification process was characterised by cyclic voltammetry and electrochemical impedance spectroscopy. The electrochemical response of the developed sensor was evaluated and a linear range between 0.24 and 5 mg L^{-1} was obtained, together with good repeatability (RSD < 10%). The sensor was proven to recognise specifically the target compound over structural analogues, including compounds that belong to the same metabolic pathway such as coumaric acid ethyl ester, coumaric acid and 4-vinylphenol, or other phenolic compounds such as 4-ethylguaiacol or paracetamol.

1. Introduction

Over the last decades, chemical and biochemical sensors have attracted great scientific interest as these open the possibility to perform online and real-time measurements, as opposed to off-site or laboratory-based analysis [1]. The major challenge involved on the development of these sensors is the development of a suitable selective recognition material [2]. The molecular imprinting technique offers the possibility of developing artificial receptors that can be used as recognition elements in sensors, in a fast and straightforward way. This technique consists on the synthesis of a highly cross-linked polymer in the presence of a target molecule known as template. This molecule is responsible for generating molecular imprints (the binding sites) in the polymer network which are complementary in size, shape and chemical functionality to the template itself, in the polymer network. Molecularly imprinted polymers (MIP) possess, in numerous instances, binding affinities comparable to biological receptors. Also, due to their chemical composition (stable cross-linked polymer) MIPs can overcome many of the stability limitations commonly associated with protein-based natural receptors, which normally can only be used in a narrow range of physicochemical conditions. MIPs, also known as plastic antibodies [3], have been successfully applied to a wide range of sensing platforms in recent years, including electrochemical, mass-sensitive and optical/surface plasmon resonance (SPR) sensors [4–14].

Molecularly imprinted nanoparticles (MIN), in comparison with conventional bulk imprinted polymers, possess higher surface-to-volume ratio and larger total surface area per weight unit of polymer, providing better accessibility for the template to recognition sites and lowering mass-transfer resistance. For these reasons, MIP nanomaterials demonstrate improved binding performance when compared to conventional MIPs [12]. Traditionally, precipitation polymerisation [15–18] and emulsion polymerisation [19–22] have commonly been used for MIN synthesis, but, recently, a new synthesis method has emerged [23], the solid-phase imprinting approach. MINs synthesised by solid-phase imprinting have already been applied to potentiometric sensing using PVC membranes [4] or even to SPR sensors through self-assembled monolayers (SAM) [8,9]. In this synthesis approach, the template

* Corresponding author. Fax: +34 945014351.
E-mail address: a.gomez@ehu.eus (A. Gomez-Caballero).

http://dx.doi.org/10.1016/j.snb.2016.02.018
0925-4005/

is immobilised on a solid support (glass beads) instead of being free in solution and nanoparticles are generated around it, through UV irradiation in the presence of an iniferter (initiator, chain transfer agent and terminator) in solution. These nanoparticles remain bound to the glass beads until an affinity-based purification of the imprinted particles is performed. This way, high affinity MINs with a monodisperse distribution of binding sites [23–26] are obtained in a short time. Thanks to the affinity-based purification step, the number of nanoparticles having high-affinity binding sites is maximised in the final product removing nanoparticles with low or no affinity. This allows reducing non-specific interactions when the MIN product is in use, what would enhance sensor selectivity when these nanoparticles are employed as recognition elements, as previously demonstrated [4]. Additionally, unlike in conventional imprinted nanoparticles, binding sites in nanoparticles synthesised by solid-phase imprinting are located at the surface of the nanoparticles. This has the potential to minimise diffusion effects and so allow for faster association–dissociation kinetics in the rebinding step what may contribute to faster sensor response.

SAMs are organic assemblies formed by the adsorption of organic molecules from a solution onto a surface that organise spontaneously into crystalline structures [27]. They have attracted great interest for sensor modification as these can be used to prevent random orientation of components on the surface, provide good surface coverage and allow for preparation of combined layers to avoid nonspecific binding effects [28]. Commonly, gold surfaces are used for sensing; gold interaction with thiol or disulphide-terminated molecules has been widely studied as this method yields good quality SAMs [27]. SAMs can be produced with a variety of heterobifunctional reagents, resulting in monolayers terminated with specific end-groups. These include carboxylic acids which can then be activated via carbodiimide chemistry to immobilise ligands (such as those containing primary amines) at the sensor surface. This coupling method can be adapted for the immobilisation of MINs containing amine groups to carboxyl-terminated SAM on gold substrates [29,30].

SAM are commonly characterised by electrochemical techniques such as electrochemical impedance spectroscopy (EIS), and cyclic voltammetry (CV). Information on the surface coverage, distribution of defects/holes, properties of the linked molecules/particles and kinetics and mechanism of the monolayer formation process can be obtained by these techniques [31]. The measurement of electron transfer between a compound and the electrode substrate provides information about the SAM integrity and impedance analysis can be used to detect the presence and distribution of the regions occupied by the SAM [32].

In this work, MIN synthesised using the solid-phase imprinting approach were immobilised on a gold electrode surface modified with SAMs in order to develop a selective voltammetric sensor for the determination of 4-ethylphenol (4EP) by differential pulse voltammetry (DPV). 4EP is a volatile phenol that at high levels is responsible for providing beverages, such as wine or beer, with undesirable organoleptic attributes. It is considered to be one of the principal compounds that contributes to “Brett character” in wines [33]. Therefore, sensors capable of selective determination of this target would be highly desirable, for instance, for its quick monitoring during wine ageing. As a target molecule for preparation of MIPs, 4EP is a small and poorly functionalised molecule, and can be considered to be particularly challenging. As an alternative to traditional imprinting approaches, in this work, imprinted nanoparticles have been synthesised by the solid-phase approach in order to obtain high affinity recognition elements for 4EP sensing. Results demonstrate that solid-phase synthesis can successfully be employed for imprinting small molecules providing high affinity MIN easily integrated with electrochemical sensors.

2. Materials and methods

2.1. Reagents

4-Ethylphenol (4EP) (99.7%), tyramine (≥98.5%), 4-ethylguaiacol (4EG) (≥98%) and paracetamol hydrochloride were obtained from Sigma–Aldrich (Madrid, Spain), coumaric acid ethyl ester (CAEE) (≥90%) was purchased from LGC Standards (Barcelona, Spain) and 4-vinylphenol (4VPh) (10% in ethylene glycol) from Cymit Química (Barcelona, Spain). Trimethylolpropane trimethacrylate (TRIM), ethylene dimethacrylate (EDMA), 4-vinylpyridine (4VP), ferrocenylmethyl methacrylate (FER), pentaerythritol tetrakis (3-mercaptopropionate) (95%), *N*-[3-(trimethoxysilyl)propyl]ethylenediamine, glutaraldehyde (50% in water), lipoic acid (LA), mercaptoundecanoic acid (MUA), ethanolamine and phosphate buffered saline (PBS) tablets (pH 7.4) were acquired from Sigma–Aldrich. Prior to be used, 4VP was purified by distillation under vacuum obtaining a colourless liquid which was stored below −20 °C and under nitrogen atmosphere. *N*-(3-aminopropyl) methacrylamide hydrochloride was acquired from Polysciences Europe GmbH, (Eppelheim, Germany). *N*,*N*,-Diethyldithiocarbamic acid benzyl ester was obtained from TCI Europe (Zwijndrecht, Belgium). 1-ethyl-3-[dimethylaminopropyl]carbodiimide (EDC) and *N*-hydroxysuccinimide (NHS) were purchased from Thermo Fischer Scientific (Waltham, USA).

Acetonitrile, dry toluene, tetrahydrofuran and isopropanol were HPLC grade and they were acquired from Scharlab (Barcelona, Spain). Every buffer solution was prepared with ultra-pure water obtained from Elix20 reverse osmosis and Milli-Q water purification systems. All other reagents were analytical grade and they were used as received. Glass beads (Spheriglass® 53 μm < diameter < 106 μm) were from Blagden Chemicals (Westerham, UK).

2.2. Synthesis of molecularly imprinted nanoparticles

2.2.1. Preparation of tyramine derivatised glass beads

Prior to MIN synthesis, the template analogue tyramine was immobilised on the solid support (glass beads) [23] through the amino group, leaving the phenolic group free to interact with the functional monomer.

Glass beads (300 mL) were mixed with ceramic beads and next, they were shaken for 5 h on 45 μm sieves using a Vibratory Sieve Shaker model AS 200 basic from Retsch (Hope Valley, UK) in order to abrade the surface coating and expose fresh surface. Then, the glass beads were activated by boiling in 1 M NaOH for 10 min and afterwards, rinsed with deionised water, then with acetone and finally they were dried in an oven at 80 °C. Subsequently, dry glass beads were incubated overnight in 2% *N*-[3-(trimethoxysilyl)propyl]ethylenediamine in dry toluene. Next, in a sintered funnel, beads were extensively rinsed with acetone and dried under vacuum before being incubated in a 5% glutaraldehyde solution in PBS (pH 7.4) for 2 h. Finally, glass beads were rinsed with water and placed overnight in a solution of 0.5 mg mL^{-1} of tyramine in PBS in order to immobilise it. A schematic representation of this process is depicted in Fig. 1a.

Once tyramine was immobilised, 12 μL of ethanolamine was added to the glass bead/tyramine solution for 15 min to cap any unreacted aldehyde group on the glass beads, to prevent reaction with the monomer containing a primary amine. This was followed by the addition of 1 mg mL^{-1} of sodium cyanoborohydride to reduce the Schiff's base formed between tyramine and glutaraldehyde to a stable amine. Finally, glass beads were rinsed with deionised water under vacuum and stored at 4 °C.

Please cite this article in press as: D. Garcia-Mutio, et al., Solid-phase synthesis of imprinted nanoparticles grafted on gold substrates for voltammetric sensing of 4-ethylphenol, Sens. Actuators B: Chem. (2016), http://dx.doi.org/10.1016/j.snb.2016.02.018

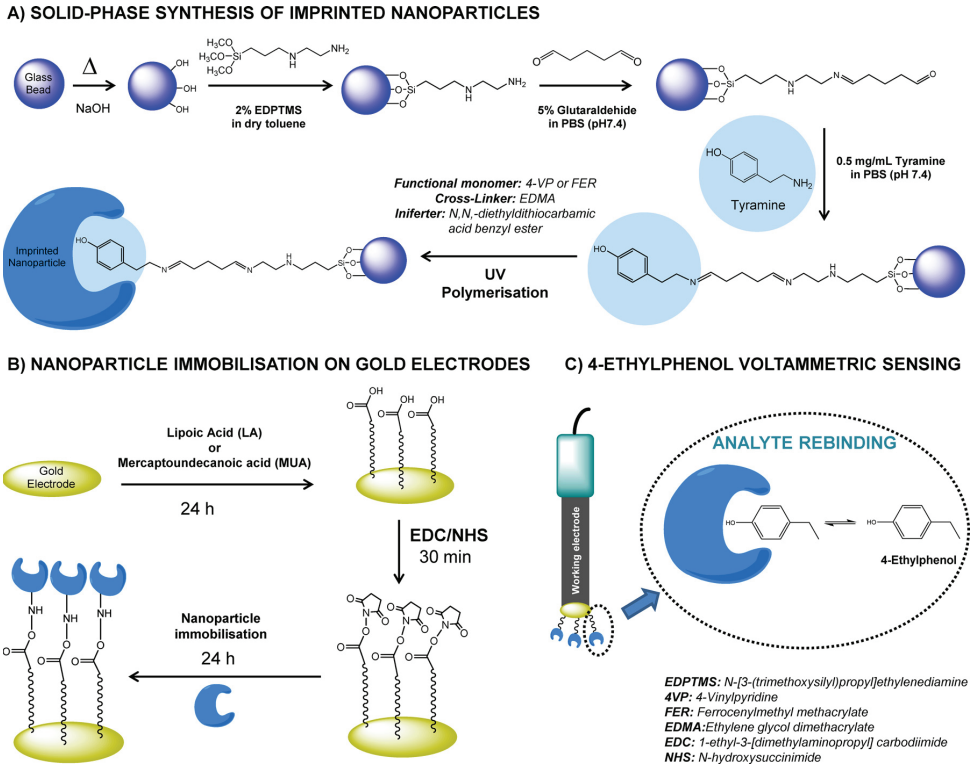

Fig. 1. Schematic representation of (a) template immobilisation on glass beads and solid-phase synthesis of nanoparticles, (b) immobilisation of nanoparticles on the surface of gold electrodes and (c) voltammetric sensing of the target analyte.

2.2.2. Nanoparticle synthesis on tyramine derivatised glass beads

The composition of 4EP MIN was adapted from previous works [4,33]. Three types of nanoparticles were synthesised, MIN1 were prepared using 16.7 mM 4VP (1.759 g) as functional monomer and acetonitrile as porogen. MIN2 were synthesised using FER (0.24 g) as functional monomer, due to solubility limitations, only 5% of the molarity used for 4VP was used (0.835 mM) in tetrahydrofuran as porogen. Finally, for MIN3 synthesis, a mixture of the previous two monomers was used, 4VP 15.9 mM (1.67 g) and FER 0.835 mM (0.237 g) employing tetrahydrofuran as porogen. The other components for the polymerisation mixture were the same for the three types of nanoparticles to be synthesised. Briefly, EDMA 8.42 mM (1.62 g) and TRIM 4.79 mM (1.62 g) were used as cross-linkers, *N,N,*-diethyldithiocarbamic acid benzyl ester (0.37 g) as iniferter (initiator), pentaerythritol tetrakis (3-mercaptopropionate) (0.09 g) as chain transfer agent and the monomer *N*-(3-aminopropyl) methacrylamide hydrochloride 0.0167 mM (2.98 mg) as amine group containing monomer. All components were dissolved in the corresponding abovementioned porogen (5.26 g). Once prepared, the mixture was then bubbled with high purity N_2 for 10 min to remove dissolved oxygen.

Tyramine-derivatised glass beads (25 g), were placed in a 200 mL flat-bottomed glass beaker (with a flat glass cover) and degassed under vacuum for 20 min, then the atmosphere inside the beaker was replaced with N_2. The polymerisation mixture was poured onto the solid-phase (under a N_2 stream) and the vessel then placed between two UV light sources (one above and one below the beaker). A Philips UV device, model HB/171/A, each fitted with 4 × 15 W lamps was employed to this end for 2.5 min (Fig. 1a). After polymerisation, the content of the beaker was transferred into an empty SPE cartridge fitted with a polyethylene frit (20 μm porosity) in order to perform a temperature-based affinity separation of MIN. In the first instance, cold cartridge washing was performed with 8 bed volumes of acetonitrile (relative to the volume of the solid-phase, 20 mL) in order to remove non polymerised monomers and low affinity nanoparticles. Secondly, the cartridge was conditioned at 60 °C and 5 bed volumes of acetonitrile were used in order to elute high-affinity nanoparticles. This temperature is capable of disrupting the non-covalent binding interactions between the MIN and the template (increasing temperature increases the rate of exchange and reduces the strength of association between the nanoparticles and the template immobilised on the solid glass beads) [34], and consequently nanoparticles are eluted from the cartridge with the solvent [4,9].

2.3. Size analysis by dynamic light scattering

For dynamic light scattering measurements, nanoparticle suspensions in acetonitrile were sonicated for 5 min and then analysed at room temperature in a 3 cm^3 glass cuvette using a Zetasizer Nano (Nano-S) from Malvern Instruments Ltd. (UK). The values are reported as an average of at least 3 measurements.

2.4. Gold electrode modification

Gold electrodes of 2 mm in diameter purchased from Metrohm (Utrecht, The Netherlands) were used for surface modification. Proper cleaning of the gold surface is required prior to

Please cite this article in press as: D. Garcia-Mutio, et al., Solid-phase synthesis of imprinted nanoparticles grafted on gold substrates for voltammetric sensing of 4-ethylphenol, Sens. Actuators B: Chem. (2016), http://dx.doi.org/10.1016/j.snb.2016.02.018

Table 1
Components employed for surface modification of gold electrodes.

Sensor	Linker	Nanoparticles		Ethanolamine capping
		Type	Functional monomer	
MUA1N	MUA	MIN1	4VP	No
MUA1Y	MUA	MIN1	4VP	Yes
LA1N	LA	MIN1	4VP	No
LA1Y	LA	MIN1	4VP	Yes
MUA2N	MUA	MIN2	FER	No
MUA2Y	MUA	MIN2	FER	Yes
LA2N	LA	MIN2	FER	No
LA2Y	LA	MIN2	FER	Yes
MUA3N	MUA	MIN3	4VP/FER	No
MUA3Y	MUA	MIN3	4VP/FER	Yes
LA3N	LA	MIN3	4VP/FER	No
LA3Y	LA	MIN3	4VP/FER	Yes

MUA: mercaptoundecanoic acid, LA: lipoic acid, 4VP: 4-vinylpyridine, FER: ferrocenylmethyl methacrylate.

organosulfur-based SAM assembly. This was conducted immersing the bare gold electrode in a 50 mM KOH (in 25% H_2O_2) solution for 10 min. Then, the electrode was rinsed with water and it was placed in an aqueous 50 mM solution of KOH to perform an electrochemical cleaning step. To this end, the potential was scanned from −2000 to 1200 mV by linear sweep voltammetry (vs. Ag/AgCl), at a scan rate of 50 mV s^{-1}, then the electrode was rinsed with water and ethanol and finally it was left to air dry prior to SAM formation [35].

SAM formation was carried out immersing the gold electrodes in solutions of 0.5 mg mL^{-1} of LA or MUA in ethanol for 24 h. Next, gold electrodes were immersed in a 2 mL mixture of 200 mM EDC and 50 mM NHS in PBS (modified to pH 6 with HCl 0.1 M) for 1 h, this way a stable active ester is obtained. The activated surface was rinsed with PBS and immersed in a 1 mL stirring MIN suspension in PBS for 24 h. Finally, the electrodes were rinsed with water and isopropanol to remove all the physically adsorbed MIN particles. Finally, certain electrodes were immersed in an ethanolamine (1 mM) solution in order to cap any unreacted group and to prevent non-specific binding (Table 1). The electrode modification process is schematically represented in Fig. 1b.

2.5. Characterisation of the modified electrodes

The surface of the modified electrode was characterised by scanning electron microscopy (SEM). SEM images were obtained using a Schottky-type field emission scanning electron microscope model JSM-7000F (JEOL, Tokyo, Japan).

Surface modification of gold electrodes was confirmed by EIS and CV. Impedance spectra were acquired at frequencies that ranged from 0.1 Hz to 1 MHz, applying a potential of 200 mV and amplitude of 10 mV. An equimolar mixture of $[Fe(CN)_6^{4-}]/[Fe(CN)_6^{3-}]$ (2 mM) in a KCl 0.1 M solution was used as supporting electrolyte. CV measurements were carried out from −200 mV to 600 mV at a step potential of 10 mV and a scan rate of 100 mV s^{-1}.

All electrochemical measurements were performed using a classical three-electrode system, where the MIN modified electrode was used as the working electrode, a Ag/AgCl (KCl 3 M) as the reference electrode and a platinum-wire as the counter electrode, all of them, acquired from Metrohm (Utrecht, The Netherlands). All electrochemical measurements were conducted at room temperature using a PGSTAT12 potentiostat/galvanostat controlled by the NOVA 1.8.17 software (Metrohm Autolab B.V, Utrecht, The Netherlands).

Table 2
Mean and standard deviation of the diameter and PDI readings obtained by dynamic light scattering for each type of nanoparticle synthesised in different batch ($n = 3$ syntheses for each type).

Type	Particle size (nm)	PDI
MIN1	128.58 ± 4.97	0.233 ± 0.01
MIN2	160.71 ± 11.60	0.360 ± 0.02
MIN3	163.18 ± 8.22	0.313 ± 0.03

2.6. Electrochemical measurements

Electrochemical determination of 4EP and structural analogues was carried out by DPV between 0 and 0.5 V, at a scan rate of 10 mV s^{-1}, step potential of 0.01 V, modulation amplitude of 0.1 V, interval time of 1 s and modulation time of 0.01 s. A Britton–Robinson buffer solution modified with NaOH 0.5 M to pH 10 was employed as supporting electrolyte in these measurements. The potentiostat and the reference and auxiliary electrodes employed for these measurements are the same as those described in Section 2.5.

3. Results and discussion

3.1. Synthesis and size analysis of molecularly imprinted nanoparticles

For the synthesis of 4EP imprinted nanoparticles, tyramine was used as a template analogue. This was done as 4EP does not possess any additional functional groups which permit its covalent immobilisation onto the solid-phase. Accordingly, the primary amine of tyramine was used for coupling to the amine-derivatised solid-phase, exposing the phenolic moiety for imprinting. Three different types of nanoparticles were synthesised using different functional monomers. For MIN1 nanoparticles, 4VP was chosen as functional monomer due to the fact that it was found to be the one that led to polymers with best imprinting behaviour for 4-EP recognition, as described in a previous work [33]. On the other hand, as developed nanoparticles were to be applied on gold electrodes, other functional monomers with apparently higher electrical conductivity were also tested as potential monomers for imprinting 4EP. In this regard, another type of nanoparticles, MIN2, was synthesised using FER as functional monomer [36]. Finally, a mixture of 4VP and FER was also used (MIN3 nanoparticles) to determine whether the combination of both monomers provided polymers with better performance. All nanoparticle types were synthesised using EDMA and TRIM as cross-linkers, since they were the ones providing the right balance of flexibility/rigidity which is crucial for molecular recognition [37]. Additionally, the monomer *N*-(3-aminopropyl)methacrylamide hydrochloride was also included in the polymerisation mixture to provide all developed nanoparticles

Please cite this article in press as: D. Garcia-Mutio, et al., Solid-phase synthesis of imprinted nanoparticles grafted on gold substrates for voltammetric sensing of 4-ethylphenol, Sens. Actuators B: Chem. (2016), http://dx.doi.org/10.1016/j.snb.2016.02.018

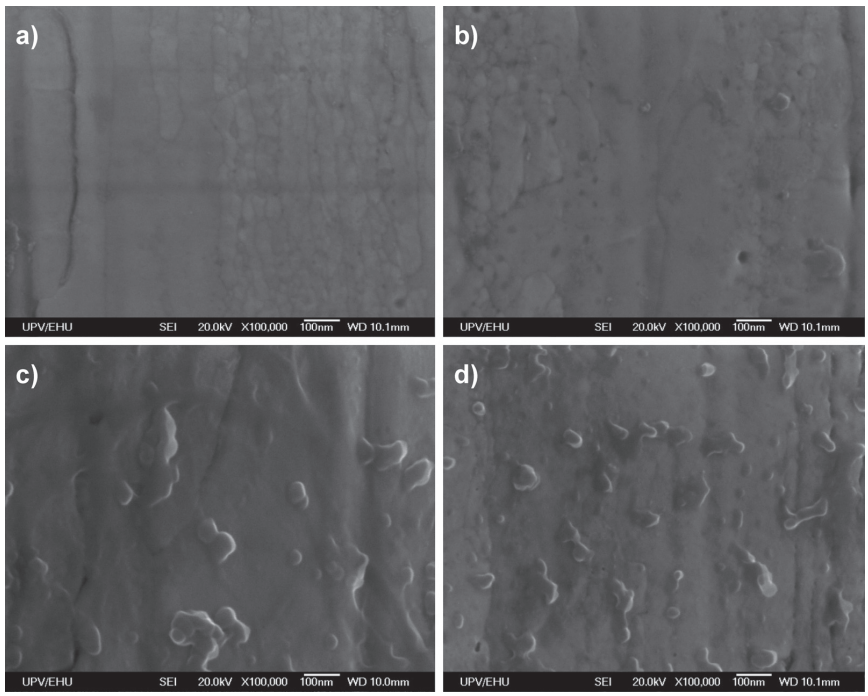

Fig. 2. SEM pictures of (a) the bare gold electrode, (b) the gold electrode coated with lipoic acid and (c–d) different gold electrodes modified with MIN1 nanoparticles.

with amine groups, in order to allow for their subsequent grafting to the gold electrode surface.

Nanoparticles were synthesised by the solid-phase approach through reversible deactivation radical polymerisation initiated by an iniferter. This polymerisation strategy provides polymers of controlled composition, architecture and molecular weight distribution [38] since the polymer chains grow at a more constant rate than in traditional polymerisation, achieving similar chain lengths and low polydispersity index. Moreover, the short irradiation time reduces any significant temperature increase that could disrupt the interactions between template and functional monomer during polymerisation, instead, small homogeneous high affinity nanoparticles are obtained [9,25]. The solid-phase synthesis of nanoparticles allows for the generation of more accessible binding sites (due to the surface imprinting) and also for the subsequent temperature based affinity separation of high-affinity MIN from polymer nanoparticles with poor binding characteristics.

The hydrodynamic diameter of the synthesised MIN was measured by dynamic light scattering, which measures Brownian motion of particles in suspension and correlates this measurement to particle size [8]. In Table 2 the average size of the developed MIN as well as their polydispersity index (PDI) are illustrated ($n = 3$). PDI values close to 0 indicate a monodisperse suspension. From registered values, the nano-size of the particles was confirmed, as they ranged between 128 and 163 nm, being the smallest the MIN synthesised with 4VP as functional monomer (MIN1). All PDI values were around 0.3, indicating a monodisperse nanoparticle population [9].

3.2. Gold electrode modification and characterisation

Surface modification of the electrodes was confirmed by SEM. Fig. 2 depicts different SEM micrographs corresponding to the bare gold electrode (Fig. 2a), the LA coated electrode (Fig. 2b) and gold electrodes modified with MIN1 nanoparticles (Fig. 2c and d). As expected, no significant difference could be observed after the immobilisation of a thin LA self-assembled monolayer on the surface of the electrode. In contrast, Fig. 2c and d clearly demonstrate the successful immobilisation of the imprinted nanoparticles on the surface of the gold substrate.

Electrochemical characterisation of gold electrodes after each surface modification step was carried out both by EIS and CV. The electrode was modified by a resistive monolayer that passivates the surface and in consequence, changes the AC response [39] which can be measured by EIS. The frequency responses from the EIS measurements were fit to the Randles equivalent circuit as shown in Fig. 3a. The simplest equivalent circuit for describing an electrochemical cell, where a single-step Faradaic process in the presence of diffusion may take place, is the Randles circuit [40]. In this circuit three components are combined: R_Ω represents the dynamic solution resistance or cell resistance, namely, the electrolyte resistance between working and reference electrodes, this element is not affected by electrode modification. Constant phase element (CPE) represents the double layer capacitance measured between the gold electrode and electrolyte. CPE is modelling a non-ideal capacitor, the CPE exponent α represents the roughness and non-uniformity of the electrode surface, an α value of 1 corresponding to a perfectly smooth surface (ideal capacitor) and of 0.5 to a porous electrode. Finally Z_f, which is the Faradaic impedance due to the charge transfer process, is subdivided into a charge transfer resistance of the immobilised layer (R_{ct}), and the Warburg impedance (Z_W), describing the frequency dependence of mass transport. For the diffusion-limited processes, Z_W is dominant, on the other hand, in charge transfer-controlled processes, Z_f is just R_{ct} [40].

A typical way of presenting EIS data is the complex plane or Nyquist plot, in which the real (Z') versus the imaginary (Z'') com-

Please cite this article in press as: D. Garcia-Mutio, et al., Solid-phase synthesis of imprinted nanoparticles grafted on gold substrates for voltammetric sensing of 4-ethylphenol, Sens. Actuators B: Chem. (2016), http://dx.doi.org/10.1016/j.snb.2016.02.018

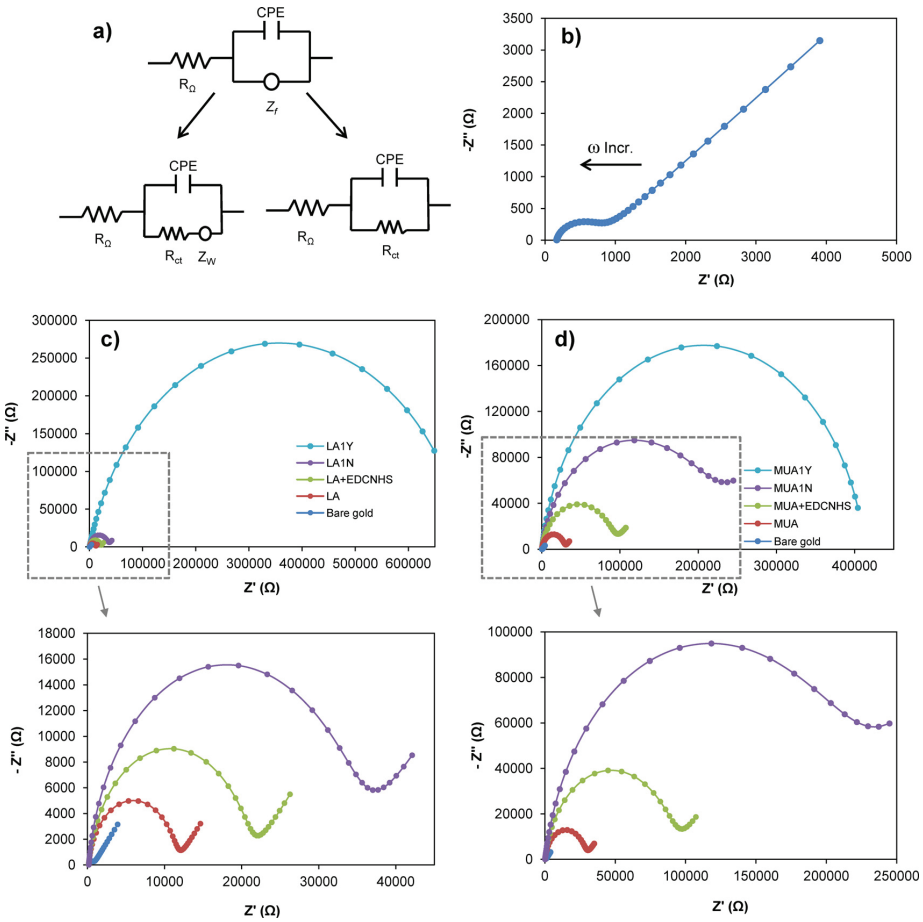

Fig. 3. (a) Equivalent circuits employed to fit impedance spectra. Nyquist plots registered with (b) a bare gold electrode, (c) LA1N and LA1Y modified electrodes and (d) MUA1Y and MUA1N modified electrodes after each surface modification step.

ponents of the impedance are plotted. The Nyquist plots include a semicircle region at high frequencies indicating a charge transfer controlled process followed by a linear range on lower frequencies showing diffusion-controlled process from mass-transfer, the diameter of the semicircle is proportional to R_{ct} while the linear range is due to Z_W [3,40].

EIS spectra registered with a bare gold electrode and with MIN1 electrodes after performing each of the modification steps are depicted in Fig. 3. As it is shown, the plot corresponding to the bare gold electrode shows a small semicircle at high frequencies due to fast charge transfer processes with a diffusion-limited step (Fig. 3b). All electrode modification steps, including LA or MUA attachment, activation with EDC/NHS, nanoparticle grafting and ethanolamine capping, increased the insulation layer on the electrode surface, what made the charge transfer process speed decrease. Consequently, R_{ct} increased and also the semicircle of the plot (Fig. 3c and d), while the Z_W disappears as the electrode coverage increases after each modification step.

All Nyquist plots registered after each electrode modification step were fitted to the equivalent circuit (see Fig. 3a) that provided minimum fitting error. R_Ω, R_{ct} and Z_W values obtained from these fittings are summarised in Table 3. As it can be deduced, electrodes modified with MUA and non-capped with ethanolamine, showed higher R_{ct} values comparing to those modified with LA due to the fact that long chain alkanethiols, such as MUA, form very well ordered defect-free monolayers, forming a barrier for the electron-transfer process [39]. The use of ethanolamine for capping non reacted EDC/NHS groups resulted in higher charge transfer resis-

Table 3
Parameters resulting from fitting the experimental plots, registered with different sensors, to a Randles circuit.

Electrode	R_Ω (Ω)	CPE (nS sα)	α	R_{ct} (KΩ)	Z_W (μS $s^{1/2}$)
Bare gold electrode	164.0	2458.6	0.86	0.63	283.32
MUA1N	170.1	495.56	0.89	214.63	21.36
MUA1Y	160.7	3369.8	0.90	412.53	–
LA1N	171.3	5942.5	0.92	34.38	112.86
LA1Y	149.3	444.4	0.82	712.78	–
MUA2N	137.4	447.22	0.85	89.22	81.40
MUA2Y	84.0	236.4	0.88	4976.80	–
LA2N	134.2	1121.0	0.88	67.74	18.31
LA2Y	163.9	401.9	0.88	1755.30	–
MUA3N	163.2	244.4	0.91	243.33	34.07
MUA3Y	136.5	329.5	0.89	1923.50	–
LA3N	174.3	259.3	0.90	96.47	140.90
LA3Y	133.5	451.3	0.87	1002.90	–

MUA: mercaptoundecanoic acid, LA: lipoic acid, CPE: constant phase element.

Please cite this article in press as: D. Garcia-Mutio, et al., Solid-phase synthesis of imprinted nanoparticles grafted on gold substrates for voltammetric sensing of 4-ethylphenol, Sens. Actuators B: Chem. (2016), http://dx.doi.org/10.1016/j.snb.2016.02.018

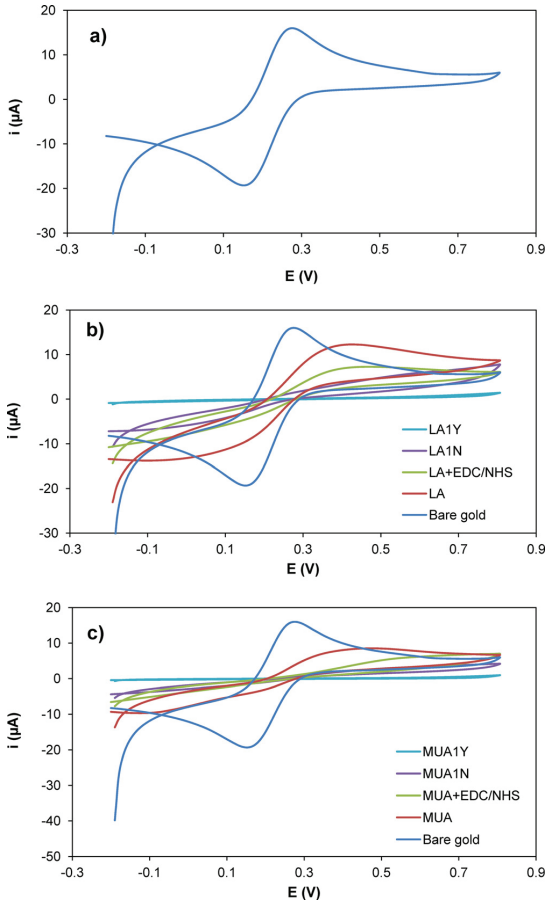

Fig. 4. Cyclic voltammograms recorded with (a) a bare gold electrode, (b) LA1N and LA1Y modified electrodes and c) MUA1Y and MUA1N modified electrodes after each surface modification step.

tance. In all ethanolamine modified electrodes the charge transfer resistance is much higher than the one obtained without capping. In this regard, the insulation of the gold surface is higher in these modified electrodes. Concerning the CPE exponent α, all modified electrodes including the bare gold electrode have values higher than 0.8, indicating a rather smooth surface than a porous surface (Table 3).

The results obtained with EIS were confirmed by CV (Fig. 4). As the electrode is modified by the different steps of the process, the cathodic and anodic peak potentials are more separated due to the increased charge transfer resistance. While the cathodic peak current decreases with each modification of the gold surface, the anodic peak tends to disappear, what may be attributed to the irreversibility of the reaction of the redox probe once the surface is modified. Both SAM assembly (LA and MUA) and EDC/NHS attachment increase the coverage of the surface, leading to a decrease in peak current intensity. Similarly, nanoparticle immobilisation on the surface also influences the current, leading to even lower cathodic peaks. Finally, ethanolamine coated electrodes did not show any current signal (LA1Y and MUA1Y in Fig. 4b and c), probably due to its high surface coverage, hindering electron transfer.

3.3. Evaluation of the electrochemical response of the developed sensors

4EP was measured with the different sensors, developed as detailed in Section 2.4, in order to determine which of them showed best electrochemical response.

In the first instance, electrochemical signals provided by electrodes prepared with different linkers were examined. Peak current signals corresponding to the electrochemical oxidation of 4EP by DPV are depicted in Fig. 5a. The electrodes modified with MUA showed lower peak currents in comparison with the electrodes modified with LA. These results are in accordance with previously described EIS and CV data, obtaining higher R_{ct} values for MUA modified electrodes than for LA modified ones. The same was observed for ethanolamine capped electrodes. In most cases, lower 4EP current signals (Fig. 5b) were recorded with these electrodes in comparison with non capped ones, attributable to their higher resistance to electron transfer. However, all the electrodes that were modified with LA but without being capped with ethanolamine, showed higher responses for 4EP than the bare gold electrode, despite their higher R_{ct} and consequently their higher surface insulation. In this regard, it could be stated that nanoparticles may be responsible for this voltammetric signal improvement, which could be explained as a result of 4EP binding to imprinted sites. Based on all these findings, electrodes modified with LA as linker and without being capped with ethanolamine were chosen for further experiments.

The response of sensors developed using different nanoparticles (LA1N, LA2N and LA3N in Table 1) was assessed next, in order to determine which imprinted nanoparticles led to best sensor performance concerning current intensity and selectivity against structural analogues. For this, the three modified electrodes and, for comparison, a bare gold electrode were used to measure 4EP by DPV. Additionally, 4 structural analogues to 4EP (4-vinylphenol, coumaric acid ethyl ester and 4-ethylguaiacol) were also tested in order to determine MIN selectivity (Fig. 6). MIN1 and MIN3 modified electrodes improved peak current intensity of 4EP at 1 mg L^{-1}, but the signal recorded with the MIN1 modified electrode was remarkably higher. On the other hand, at 5 mg L^{-1}, MIN1 and

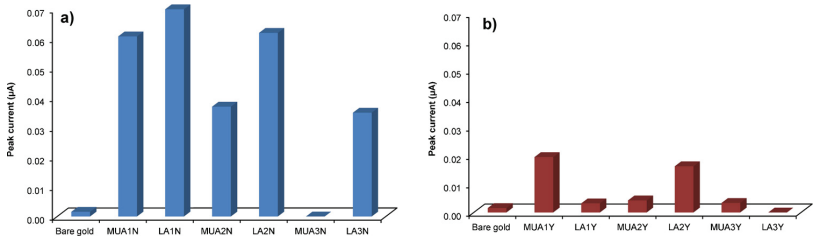

Fig. 5. Peak current signals corresponding to the oxidation of 1 mg L^{-1} of 4EP in Britton–Robinson buffer using a bare gold electrode and different modified electrodes (a) without ethanolamine capping and (b) with ethanolamine capping.

Please cite this article in press as: D. Garcia-Mutio, et al., Solid-phase synthesis of imprinted nanoparticles grafted on gold substrates for voltammetric sensing of 4-ethylphenol, Sens. Actuators B: Chem. (2016), http://dx.doi.org/10.1016/j.snb.2016.02.018

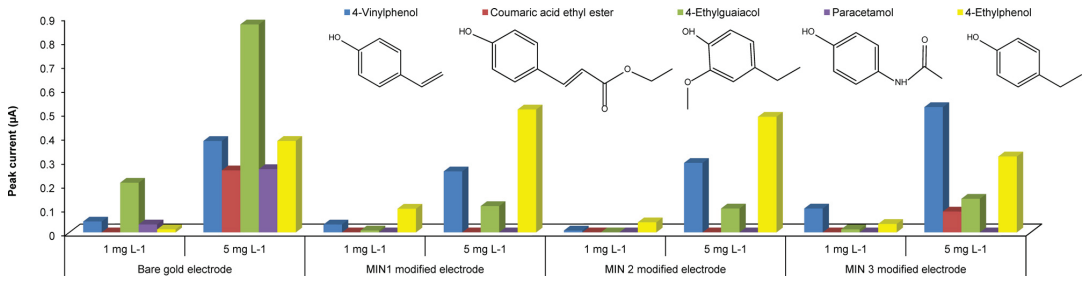

Fig. 6. Peak current signals, registered with the bare gold electrode and the different modified electrodes. Depicted values correspond to the oxidation of 1 mg L^{-1} and 5 mg L^{-1} of 4EP and different structural analogues in Britton–Robinson buffer. Gold electrodes were modified with MIN made with 4-vinylpiridine (MIN1) and ferrocenylmethyl methacrylate as functional monomers (MIN2) or both (MIN3).

MIN2 electrodes provided the best results; however, the difference between these electrodes and the bare gold electrode was minimal at this concentration level, probably due to the saturation of the MIN sensor.

Concerning the measurements of the structural analogues, no signal was observed for paracetamol with any of the modified electrodes. For 4EG and CAEE the signal is lower with all the modified electrodes, especially for MIN1 and MIN2 modified ones. As regards 4VPh, lower electrochemical signals where recorded with the MIN1 and MIN2 modified electrodes in comparison with 4EP. However, 4VPh signal was higher than the ones obtained with the rest of compounds, probably due to its higher structural similarity to 4EP.

As MIN1 provided lower responses for all analogues and higher responses for 4EP, compared to the bare gold electrode (Figs. 6 and 7), LA1N was selected for 4EP sensing.

3.4. Analytical evaluation of the sensor

The electrochemical DPV response of the LA1N sensor towards increasing concentrations of 4EP was determined next using Britton–Robinson buffer (adjusted to pH 10 with 0.5 M NaOH) as supporting electrolyte. From registered voltammograms, current intensities of anodic peaks corresponding to 4EP oxidation were measured at every tested concentration. Well-defined concentration dependence of the analytical signal towards 4EP concentration was observed at concentrations that ranged from 0.20 mg L^{-1} to 5 mg L^{-1} (R^2 = 0.9981) with a sensitivity of 0.118 ± 0.002 μA L mg^{-1} and an intercept of −0.013 ± 0.003 μA. The detection limit, calculated as LOD = $3S_b$/slope, where S_b is the standard deviation of the blank signal [41], was found to be 0.068 mg L^{-1}. Comparatively, a bare gold electrode was also tested as working electrode to measure increasing levels of the target compound by DPV, using the same experimental conditions as those employed for the LA1N sensor. With the bare gold electrode, a linear dependence of the electrochemical signal was observed in a concentration range comprised between 1 and 5 mg L^{-1} (R^2 = 0.9947) with a sensitivity of 0.100 ± 0.004 μA L mg^{-1} and an intercept of −0.095 ± 0.013 μA. The detection limit was found to be 0.33 mg L^{-1}. Based on these results, it was concluded that grafting MIN to the gold electrode resulted in higher method linearity and sensitivity, with consequent lower detection limit.

Subsequently, 4EP and every structural analogue were measured by DPV, employing the MIN modified electrode LA1N and, comparatively, a bare gold electrode. Obtained voltammograms are depicted in Fig. 7. As it can be observed, all compounds are capable of being electrochemically oxidised between 0 and 0.6 V using a gold electrode (Fig. 7a), being the current signal of 4EP the lowest one. In contrast, using the developed LA1N sensor, most of the compounds did not present any electrochemical response, except for 4VPh and 4EG (Fig. 7b). These two compounds possess more structural similarities with the target molecule and consequently, they are capable of interacting to some extent with the monomers present at the binding sites. Accordingly, 4VPh, being nearly identical to the target compound (4EP), led to higher peak current than 4EG, the latter giving rise to very low signals. Considering that 4EG is one of the compounds that presents higher oxidation signal on gold surfaces (Fig. 7a), the values obtained with the LA1N sensor may be regarded as negligible. In any case, the improvement in selectivity achieved by nanoparticles immobilised on the gold electrode is very clear when Fig. 7a and b are compared. If the potential of the anodic peaks are compared in these figures, the existence of a little potential shift towards more positive values can be observed in Fig. 7b, what may be attributed to the surface of the modified gold electrode. Diffusion of compounds towards the surface of the mod-

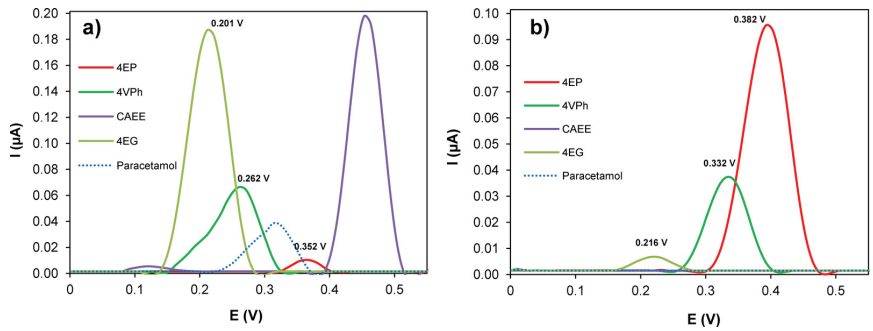

Fig. 7. Differential pulse voltammograms for 4EP (1 mg L^{-1}) and the structural analogues 4VPh (1 mg L^{-1}), CAEE (5 mg L^{-1}), 4EG (1 mg L^{-1}) and paracetamol (1 mg L^{-1}) using (a) a bare gold electrode and (b) the developed LA1N sensor.

Please cite this article in press as: D. Garcia-Mutio, et al., Solid-phase synthesis of imprinted nanoparticles grafted on gold substrates for voltammetric sensing of 4-ethylphenol, Sens. Actuators B: Chem. (2016), http://dx.doi.org/10.1016/j.snb.2016.02.018

ified gold electrode may be more hindered what may contribute to this potential shift.

Finally, repeatability of the sensor response was evaluated through consecutive measurements of 4EP at different concentrations levels (1 mg L^{-1} and 5 mg L^{-1}) (n = 5). Additionally, 4EP was also measured at these levels employing different sensors fabricated under the same conditions (n = 5), in order to test the repeatability of the electrode modification process. Obtained RSD (%) values were 6.63% and 7.76% for 1 and 5 mg L^{-1} respectively when the same sensor was used consecutively, and 11.15% and 17.36% using different sensors. The observed RSD values are clearly lower when the same sensor was employed for 4EP measurements, being adequate for 4EP determination (<10%). Nevertheless, RSD values obtained with different sensors (<20%) can also be considered to be satisfactory considering the large number of variables that may influence on the sensor manufacturing process, all of them contributing to signal variability.

4. Conclusions

In the present work, molecularly imprinted nanoparticles have been successfully produced by solid-phase imprinting in order to be used as recognition elements in voltammetric sensors. Nanoparticles synthesised using 4-vinyl pyridine as functional monomer (as opposed to those prepared with ferrocenylmethyl methacrylate) possessed the best selectivity and were used for further sensor development and testing. For sensor fabrication, imprinted nanoparticles were immobilised at the surface of gold electrodes derivatised with lipoic acid via carbodiimide chemistry. Obtained sensors demonstrated higher sensitivity, as compared with bare gold electrodes, and excellent selectivity, with minimal cross-reactivity. Based on the obtained results, it can be stated that the immobilisation of imprinted nanoparticles as recognition elements on gold electrodes is an effective and straightforward strategy that can be exploited for selective sensing of electroactive compounds.

Acknowledgements

The authors would like to acknowledge the Spanish Ministry of Economy and Competitiveness (project CTQ2013-47921-P) and the University of The Basque Country UPV/EHU (project US13/10) for the financial support. Technical and human support provided by SGIker (UPV/EHU, MICINN, GV/EJ, ESF) is also gratefully acknowledged.

References

[1] K. Kotova, M. Hussain, G. Mustafa, P.A. Lieberzeit, MIP sensors on the way to biotech applications: targeting selectivity, Sens. Actuators B 189 (2013) 199–202.
[2] S.Z. Bajwa, G. Mustafa, R. Samardzic, T. Wangchareansak, P.A. Lieberzeit, Nanostructured materials with biomimetic recognition abilities for chemical sensing, Nanoscale Res. Lett. 7 (328) (2012) 327.
[3] F.T.C. Moreira, R.A.F. Dutra, J.P.C. Noronha, J.C.S. Fernandes, M.G.F. Sales, Novel biosensing device for point-of-care applications with plastic antibodies grown on Au-screen printed electrodes, Sens. Actuators B 182 (2013) 733–740.
[4] I. Basozabal, A. Guerreiro, A. Gomez-Caballero, M. Aranzazu Goicolea, R.J. Barrio, Direct potentiometric quantification of histamine using solid-phase imprinted nanoparticles as recognition elements, Biosens. Bioelectron. 58 (2014) 138–144.
[5] A. Gomez-Caballero, M.A. Goicolea, R.J. Barrio, Paracetamol voltammetric microsensors based on electrocopolymerized-molecularly imprinted film modified carbon fiber microelectrodes, Analyst (Cambridge, U. K.) 130 (2005) 1012–1018.
[6] A. Gomez-Caballero, N. Unceta, M. Aranzazu Goicolea, R.J. Barrio, Evaluation of the selective detection of 4,6-dinitro-*o*-cresol by a molecularly imprinted polymer based microsensor electrosynthesized in a semiorganic media, Sens. Actuators B 130 (2008) 713–722.
[7] F.R.F. Leite, W. de Jesus Rodrigues Santos, L.T. Kubota, Selective determination of caffeic acid in wines with electrochemical sensor based on molecularly imprinted siloxanes, Sens. Actuators B 193 (2014) 238–246.
[8] Z. Altintas, M. Gittens, A. Guerreiro, K.-A. Thompson, J. Walker, S. Piletsky, et al., Detection of waterborne viruses using high affinity molecularly imprinted polymers, Anal. Chem. 87 (2015) 6801–6807.
[9] Z. Altintas, A. Guerreiro, S.A. Piletsky, I.E. Tothill, NanoMIP based optical sensor for pharmaceuticals monitoring, Sens. Actuators B 213 (2015) 305–313.
[10] A. Gomez-Caballero, A. Ugarte, A. Sanchez-Ortega, N. Unceta, M.A. Goicolea, R.J. Barrio, Molecularly imprinted poly[tetra(*o*-aminophenyl)porphyrin] as a stable and selective coating for the development of voltammetric sensors, J. Electroanal. Chem. 638 (2010) 246–253.
[11] M. Motaghedifard, S.M. Ghoreishi, M. Behpour, Z. Moghadam, M. Salavati-Niasari, Electrochemical study of new self-assembled monolayer of 2-hydroxy-*N*′1-[(*E*)-1-(3-methyl-2-thienyl)methylidene]benzohydrazide on gold electrode as an epinephrine sensor element, J. Electroanal. Chem. 682 (2012) 14–22.
[12] J. Wackerlig, P.A. Lieberzeit, Molecularly imprinted polymer nanoparticles in chemical sensing: synthesis, characterisation and application, Sens. Actuators B 207 (2015) 144–157.
[13] Z. Guo, A. Florea, C. Cristea, F. Bessueille, F. Vocanson, F. Goutaland, et al., 1,3,5-Trinitrotoluene detection by a molecularly imprinted polymer sensor based on electropolymerization of a microporous-metal-organic framework, Sens. Actuators B 207 (2015) 960–966.
[14] F.T.C. Moreira, M.J.M.S. Ferreira, J.R.T. Puga, M.G.F. Sales, Screen-printed electrode produced by printed-circuit board technology. Application to cancer biomarker detection by means of plastic antibody as sensing material, Sens. Actuators B 223 (2016) 927–935.
[15] Z. Chen, L. Ye, Controlling size and uniformity of molecularly imprinted nanoparticles using auxiliary template, J. Mol. Recognit. 25 (2012) 370–376.
[16] K. Yoshimatsu, K. Reimhult, A. Krozer, K. Mosbach, K. Sode, L. Ye, Uniform molecularly imprinted microspheres and nanoparticles prepared by precipitation polymerization: the control of particle size suitable for different analytical applications, Anal. Chim. Acta 584 (2007) 112–121.
[17] E. Asadi, S. Azodi-Deilami, M. Abdouss, S. Khaghani, Cyproterone synthesis, recognition and controlled release by molecularly imprinted nanoparticle, Appl. Biochem. Biotechnol. 167 (2012) 2076–2087.
[18] M. Seifi, M. Hassanpour Moghadam, F. Hadizadeh, S. Ali-Asgari, J. Aboli, S.A. Mohajeri, Preparation and study of tramadol imprinted micro-and nanoparticles by precipitation polymerization: microwave irradiation and conventional heating method, Int. J. Pharm. 471 (2014) 37–44.
[19] D. Vaihinger, K. Landfester, I. Krauter, H. Brunner, G.E.M. Tovar, Molecularly imprinted polymer nanospheres as synthetic affinity receptors obtained by miniemulsion polymerisation, Macromol. Chem. Phys. 203 (2002) 1965–1973.
[20] G. Sener, L. Uzun, R. Say, A. Denizli, Use of molecular imprinted nanoparticles as biorecognition element on surface plasmon resonance sensor, Sens. Actuators B 160 (2011) 791–799.
[21] H. Liu, G. Fang, S. Wang, Molecularly imprinted optosensing material based on hydrophobic CdSe quantum dots via a reverse microemulsion for specific recognition of ractopamine, Biosens. Bioelectron. 55 (2014) 127–132.
[22] T. Alizadeh, M.R. Ganjali, M. Akhoundian, Synthesis and application of different nano-sized imprinted polymers for the preparation of promethazine membrane electrodes and comparison of their efficiencies, Int. J. Electrochem. Sci. 7 (2012) 7655–7674.
[23] A. Poma, A. Guerreiro, M.J. Whitcombe, E.V. Piletska, A.P.F. Turner, S.A. Piletsky, Solid-phase synthesis of molecularly imprinted polymer nanoparticles with a reusable template-plastic antibodies, Adv. Funct. Mater. 23 (2013) 2821–2827.
[24] S. Ambrosini, S. Beyazit, K. Haupt, B. Tse Sum Bui, Solid-phase synthesis of molecularly imprinted nanoparticles for protein recognition, Chem. Commun. (Cambridge, U. K.) 49 (2013) 6746–6748.
[25] E. Moczko, A. Guerreiro, E. Piletska, S. Piletsky, PEG-stabilized core–shell surface-imprinted nanoparticles, Langmuir 29 (2013) 9891–9896.
[26] E. Moczko, A. Poma, A. Guerreiro, I. Perez de Vargas Sansalvador, S. Caygill, F. Canfarotta, et al., Surface-modified multifunctional MIP nanoparticles, Nanoscale 5 (2013) 3733–3741.
[27] J.C. Love, L.A. Estroff, J.K. Kriebel, R.G. Nuzzo, G.M. Whitesides, Self-assembled monolayers of thiolates on metals as a form of nanotechnology, Chem. Rev. 105 (2005) 1103–1169.
[28] S.B. Dulay, R. Gransee, S. Julich, H. Tomaso, C.K. O'Sullivan, Automated microfluidically controlled electrochemical biosensor for the rapid and highly sensitive detection of Francisella tularensis, Biosens. Bioelectron. 59 (2014) 342–349.
[29] T. Kamra, S. Chaudhary, C. Xu, L. Montelius, J. Schnadt, L. Ye, Covalent immobilization of molecularly imprinted polymer nanoparticles on a gold surface using carbodiimide coupling for chemical sensing, J. Colloid Interface Sci. 461 (2016) 1–8.
[30] W.C. Mak, R. Georgieva, R. Renneberg, H. Baeumler, Protein particles formed by protein activation and spontaneous self-assembly, Adv. Funct. Mater. 20 (2010) 4139–4144.
[31] N.K. Chaki, M. Aslam, J. Sharma, K. Vijayamohanan, Applications of self-assembled monolayers in materials chemistry, Proc. Indian Natl. Sci. Acad. 113 (2001) 659–670.

Please cite this article in press as: D. Garcia-Mutio, et al., Solid-phase synthesis of imprinted nanoparticles grafted on gold substrates for voltammetric sensing of 4-ethylphenol, Sens. Actuators B: Chem. (2016), http://dx.doi.org/10.1016/j.snb.2016.02.018

[32] B. Liedberg, J.M. Cooper, Bioanalytical applications of self assembled monolayers, in: T.C.F.S. Ligler (Ed.), Immobilized Biomolecules in Analysis: A Practical Approach, Kluwer Academic Publishers–Plenum Publishers, 2000, pp. 55–78.
[33] D. Garcia, A. Gomez-Caballero, A. Guerreiro, M.A. Goicolea, R.J. Barrio, Molecularly imprinted polymers as a tool for the study of the 4-ethylphenol metabolic pathway in red wines, J. Chromatogr. A 1410 (2015) 164–172.
[34] A. Poma, A. Guerreiro, M.J. Whitcombe, E.V. Piletska, A.P.F. Turner, S.A. Piletsky, Solid-phase synthesis of molecularly imprinted polymer nanoparticles with a reusable template-plastic antibodies, Adv. Funct. Mater. 23 (220) (2013) 2821–2827.
[35] L.M. Fischer, M. Tenje, A.R. Heiskanen, N. Masuda, J. Castillo, A. Bentien, et al., Gold cleaning methods for electrochemical detection applications, Microelectron. Eng. 86 (2009) 1282–1285.
[36] M. Lillethorup, K. Torbensen, M. Ceccato, S.U. Pedersen, K. Daasbjerg, Electron transport through a diazonium-based initiator layer to covalently attached polymer brushes of ferrocenylmethyl methacrylate, Langmuir 29 (2013) 13595–13604.
[37] A.R. Guerreiro, I. Chianella, E. Piletska, M.J. Whitcombe, S.A. Piletsky, Selection of imprinted nanoparticles by affinity chromatography, Biosens. Bioelectron. 24 (2009) 2740–2743.
[38] A.R. Kannurpatti, S. Lu, G.M. Bunker, C.N. Bowman, Kinetic and mechanistic studies of iniferter photopolymerizations, Macromolecules 29 (1996) 7310–7315.
[39] S. Campuzano, M. Pedrero, C. Montemayor, E. Fatas, J.M. Pingarron, Characterization of alkanethiol-self-assembled monolayers-modified gold electrodes by electrochemical impedance spectroscopy, J. Electroanal. Chem. 586 (2006) 112–121.
[40] C. Fernandez-Sanchez, C.J. McNeil, K. Rawson, Electrochemical impedance spectroscopy studies of polymer degradation: application to biosensor development, Trends Anal. Chem. 24 (2005) 37–48.
[41] M. Valcárcel, Principles of Analytical Chemistry, first ed., Springer, Berlin, 2000.

Biographies

Deiene Garcia-Mutio obtained her Bachelor degree in Environmental Sciences in 2008 and a Master degree in Forensic Analysis in 2011 from the University of the Basque Country. Since January of 2012 Ms. Deiene is a full time PhD Student at the Analytical Chemistry Department on the Faculty of Pharmacy of the University of the Basque Country. Her current research interests focus on the developments of different analytical applications based on molecularly imprinted polymers.

Alberto Gómez-Caballero (PhD) was awarded the PhD degree in Analytical Chemistry at the University of the Basque Country in 2007, and currently he is a lecturer in Analytical Chemistry at the same university. He undertook his doctoral studies in electrochemistry and his PhD thesis focused on the electrochemical synthesis of MIP based sensors. His current research interests include the development of new imprinted micro and nanomaterials for sensor development, the application of novel imprinted polymers to miniaturised sample treatment devices and imprinted materials in chiral separation.

Antonio Guerreiro (PhD) is a senior research fellow. He received his BSc and MSc degrees from Universidade do Algarve (Portugal). He did his PhD in the area of Supramolecular Chemistry in Cranfield University (UK) before starting as research fellow in the same university. His current research is focused on applied polymer science and molecular recognition, in addition to the design of processes for the manufacture of nano-materials.

Sergey A. Piletsky (PhD) is a professor in Bioanalytical Chemistry. Piletsky supervised work of numerous MSc and PhD students and published over 250 peer-reviewed papers and patent applications. Prof. Piletsky is visiting Professor in Jinan and Huazhong Universities, China, member of Editorial Board of ACS Combinatorial Sciences, Scientific Board of Society of Molecular Imprinting, Fellow of the Society of Biology, and Vice-President of the International Union of Advanced Materials.

M.A. Goicolea (PhD) received her PhD in chemistry from the University of The Basque Country in 1987. She is currently a professor of analytical chemistry of the University of the Basque Country and manager of various national and international scientific projects carried out in Analytical Chemistry Department. Her current research interests concern the synthesis and characterisation of new imprinted materials for chromatographic separation and sensor development.

Ramón J. Barrio (PhD) received his PhD in analytical chemistry from the University of Valladolid in 1984. He is currently a professor of analytical chemistry at the University of the Basque Country and the leader of scientific pesticide and metabolites group. He is the Head of the Central Service of Analysis of the University of the Basque Country at the Campus of Alava (Vitoria–Gasteiz). His present research interests focus on new sensors, microsystems and new amperometric detection systems in chromatography related to pesticides.

Please cite this article in press as: D. Garcia-Mutio, et al., Solid-phase synthesis of imprinted nanoparticles grafted on gold substrates for voltammetric sensing of 4-ethylphenol, Sens. Actuators B: Chem. (2016), http://dx.doi.org/10.1016/j.snb.2016.02.018